

Dissertation presented to the Instituto Tecnológico de Aeronáutica, in partial fulfillment of the requirements for the degree of Master of Science in the Graduate Program of Physics, Field of Atomic and Molecular Physics.

**João Víctor Moreira Pimentel**

**ASSESSING PROSPECTIVE SINGLET FISSION AND  
THERMALLY ACTIVATED DELAYED  
FLUORESCENCE CANDIDATES IN  
B,N-SUBSTITUTED 5,12-DIPHENYLTETRACENE**

Dissertation approved in its final version by the signatories below:

Prof. Dr. Francisco Bolivar Correto Machado

Advisor

Campo Montenegro  
São José dos Campos, SP - Brazil  
2024

**Cataloging-in Publication Data**  
**Documentation and Information Division**

Pimentel, João Vítor Moreira

Assessing prospective singlet fission and thermally activated delayed fluorescence candidates in B,N-substituted 5,12-diphenyltetracene / João Vítor Moreira Pimentel.

São José dos Campos, 2024.

155f.

Dissertation of Master of Science – Course of Physics. Area of Atomic and Molecular Physics – Instituto Tecnológico de Aeronáutica, 2024. Advisor: Prof. Dr. Francisco Bolivar Correto Machado.

1. Excited states. 2. Acenes. 3. Polycyclic aromatic hydrocarbons. 4. Multireference methods. I. Instituto Tecnológico de Aeronáutica. II. Title.

**BIBLIOGRAPHIC REFERENCE**

PIMENTEL, João Vítor Moreira. **Assessing prospective singlet fission and thermally activated delayed fluorescence candidates in B,N-substituted 5,12-diphenyltetracene.** 2024. 155f. Dissertation of Master of Science – Instituto Tecnológico de Aeronáutica, São José dos Campos.

**CESSION OF RIGHTS**

AUTHOR'S NAME: João Vítor Moreira Pimentel

PUBLICATION TITLE: Assessing prospective singlet fission and thermally activated delayed fluorescence candidates in B,N-substituted 5,12-diphenyltetracene.

PUBLICATION KIND/YEAR: Dissertation / 2024

The Instituto Tecnológico de Aeronáutica is granted permission to reproduce copies of this dissertation and to loan or sell copies for academic and scientific purposes only. The author reserves all other publication rights and no part of this dissertation can be reproduced without the authorization of the author.



---

João Vítor Moreira Pimentel

Rua H8A, Ap. 114

12.228-460 – São José dos Campos–SP

**ASSESSING PROSPECTIVE SINGLET FISSION AND  
THERMALLY ACTIVATED DELAYED  
FLUORESCENCE CANDIDATES IN  
B,N-SUBSTITUTED 5,12-DIPHENYLTETRACENE**

**João Vítor Moreira Pimentel**

Thesis Committee Composition:

Prof. Dr.	Luiz Fernando de Araújo Ferrão	President	-	ITA
Prof. Dr.	Francisco Bolivar Correto Machado	Advisor	-	ITA
Prof. Dr.	Leonardo Tsuyoshi Ueno	Internal Member	-	ITA
Dr.	Alejandro López Castillo	External Member	-	UFSCar

To quantum decoherence, for Schrödinger's cat can be in a superposition of being alive and dead, but a thesis cannot be both complete and incomplete.

# Acknowledgments

I would like to express my gratitude to Prof. Dr. Francisco Machado, my advisor, for his support and guidance from my third year of undergraduate studies up to the completion of my MSc degree. His advice and constructive feedback were invaluable in shaping my research and my future.

I owe a special debt of gratitude to my parents, who have been a constant source of encouragement and inspiration since I was a child. Dad, thank you for always challenging me to aim higher and strive for excellence. I would also like to thank the rest of my family, especially my godmother and my sister, for their love.

My passion for chemistry was sparked by Dr. Antonino Fontenelle and Sérgio Matos, MS, who helped me develop a deep appreciation for the subject and taught me how to solve difficult problems. I am grateful for their mentorship and friendship.

Lastly, I would like to express my esteem to my fellow students, especially Nacib and Julio, for their help and support in debugging the countless issues that arose during my research. Their willingness to lend a hand and share their expertise made this journey less daunting.

To everyone who played a part in making this thesis possible, I extend my gratitude. Thank you.

*"[O]n n'est peut-être pas éloigné de l'époque à laquelle on pourra soumettre au calcul la plupart des phénomènes chimiques."*

— JOSEPH LOUIS GAY-LUSSAC  
(MÉMOIRES DE PHYSIQUE ET DE CHIMIE,  
DE LA SOCIÉTÉ D'ARCUEIL, 1808)

# Resumo

Em acenos, a substituição de um par de átomos de carbono por um par isoeletrônico boro-nitrogênio permite a modulação do caráter dirradicaloide do aceno B,N-substituído, possibilitando o ajuste fino das propriedades químicas, ópticas e eletrônicas. Este estudo teórico investiga as propriedades de fissão de singleto (SF) e fluorescência atrasada termicamente ativada (TADF) de 34 moléculas específicas de 5,12-difeniltetraceno (DPT) B,N-substituídas, identificadas como candidatas promissoras através de uma busca sistemática feita anteriormente em derivados de tetraceno. Utilizando métodos de química quântica computacional, analisamos a estrutura eletrônica e as propriedades excitônicas dessas moléculas de DPT B,N-substituído para entender seu potencial de aplicação em células solares orgânicas (OSC) e diodos emissores de luz orgânicos (OLEDs). Foram encontradas 22 moléculas que provavelmente apresentam TADF. O DPT foi escolhido por sua semelhança com o rubreno, que, por sua vez, possui propriedades mais interessantes em comparação com o tetraceno puro, como a maior mobilidade de buracos.

# Abstract

In acenes, substituting a pair of carbon atoms with a boron-nitrogen isoelectronic pair allows for the modulation of the diradical character of the B,N-substituted acene, enabling fine-tuning of chemical, optical, and electronic properties. This theoretical study investigated the singlet fission (SF) and thermally activated delayed fluorescence (TADF) properties of 34 specific B,N-substituted 5,12-diphenyltetracene (DPT) molecules, identified as promising candidates through a previous systematic computational search in tetracene derivatives. Using computational quantum chemistry methods, we analyzed the electronic structure and excitonic properties of these B,N-substituted DPT molecules to understand their potential for application in organic solar cell (OSC) and organic light-emitting diode (OLED) technology. 22 molecules likely to undergo TADF were found. DPT was chosen for its similarity with rubrene, which has more interesting properties, such as enhanced hole mobility, compared to pristine tetracene.

# List of Figures

FIGURE 1.1 – Structure of an acene. For tetracene, $n = 4$ . . . . .	21
FIGURE 1.2 – Structures of DPT (left) and rubrene (right). . . . .	22
FIGURE 2.1 – Losses in a single-junction silicon (band gap = 1.1 eV) solar cell. <i>Note.</i> From “Quantum dots for next-generation photovoltaics,” by O. Semonin, J. Luther and M. Beard, 2012, <i>Materials Today</i> , 15(11), 508-515 (SEMONIN <i>et al.</i> , 2012). . . . .	27
FIGURE 2.2 – Singlet-fission solar cell devised by Einzinger <i>et al.</i> <i>Note.</i> From “An exciting boost for solar cells,” by J. Luther and J. Johnson, 2019, <i>Nature</i> , 571, 38-39 (LUTHER; JOHNSON, 2019). . . . .	27
FIGURE 2.3 – Jablonski diagram illustrating singlet fission. <i>Note.</i> From “Recent Advances in Singlet Fission,” by M. Smith and J. Michl, 2013, <i>Annu.</i> <i>Rev. Phys. Chem.</i> , 64, 361-86 (SMITH; MICHL, 2013). . . . .	29
FIGURE 2.4 – Scheme of a white OLED. <i>Note.</i> In a screen, the white light is then passed through an RGB color filter. From <a href="http://www.futaba.co.jp/en/product/oled_backup/about">www.futaba.co.jp/en/ product/oled_backup/about</a> . . . . .	30
FIGURE 2.5 – Jablonski diagram depicting radiative (straight arrows) and nonra- diative (squiggly arrows) transitions. <i>Note.</i> This diagram does not differentiate between intersystem crossing (singlet to triplet) and re- verse intersystem crossing (triplet to singlet). From <a href="http://www.edinst.com">www.edinst.com</a> . . . . .	31
FIGURE 2.6 – Comparison of FOLEDs, PhOLEDs and TADF OLEDs. <i>Note.</i> From <a href="http://www.edinst.com">www.edinst.com</a> . . . . .	32
FIGURE 3.1 – Atom labeling scheme within the structure of tetracene. . . . .	38
FIGURE 3.2 – Each B,N-tetracene molecule (except 7,16) corresponds to two B,N- DPT molecules. 4,1-left (left) and 4,1-right (right) are shown as examples. . . . .	38

- FIGURE 3.3 – Figure illustrating the MRAQCC orbitals. The reference space of configurations incorporates the excitations depicted by green arrows, which involve transitions between active orbitals. The external configurations for the MRAQCC method encompass the single and double excitations denoted by yellow arrows. These excitations involve transitions from closed-shell orbitals that are not frozen to active orbitals, from closed-shell orbitals that are not frozen to virtual orbitals that are not frozen, or from active orbitals to virtual orbitals that are not frozen. These external configurations account for the correlated behavior of the non-frozen orbitals. Transitions from the frozen core or to the frozen virtual orbitals are excluded. . . . . 43
- FIGURE 4.1 – Vertical  $E(S_1)$  of pristine DPT and the 34 B,N-doped molecules calculated using the CASPT2(8,8)/6-31G\* method. . . . . 46
- FIGURE 4.2 –  $\Delta E_{ST} = E(S_1) - E(T_1)$  of pristine DPT and the 34 B,N-doped molecules calculated using the CASPT2(8,8)/6-31G\* method. . . . . 47
- FIGURE 4.3 – Color map for the HOMA index of each ring in pristine DPT and the 34 B,N-doped SF and TADF precandidate molecules with the wB97XD/def2-TZVP optimized geometries. . . . . 49
- FIGURE 4.4 – Bar chart of the maximum HOMA value in pristine DPT and the 34 B,N-doped SF and TADF precandidate molecules with the wB97XD/def2-TZVP optimized geometries. . . . . 49
- FIGURE 4.5 – Bar chart of the minimum HOMA value in pristine DPT and the 34 B,N-doped SF and TADF precandidate molecules with the wB97XD/def2-TZVP optimized geometries. . . . . 50
- FIGURE 4.6 – Bar chart of the mean HOMA value in pristine DPT and the 34 B,N-doped SF and TADF precandidate molecules with the wB97XD/def2-TZVP optimized geometries. . . . . 50
- FIGURE 4.7 – Density of effectively unpaired electrons plotted with isovalue  $5 \times 10^{-4} e a_0^{-3}$  (where  $a_0$  is the Bohr radius) and the number of effectively unpaired electrons given in parentheses for each molecule. . . . . 52
- FIGURE 4.8 – Linear regression of  $N_U$  values for twelve selected B,N-DPT molecules compared with the corresponding counterparts (the B,N-tetracene TADF candidates): (left subplot) B,N-DPT-(left) molecules versus B,N-tetracene, (right subplot) B,N-DPT-(right) molecules versus B,N-tetracene. . . . . 53

---

FIGURE D.1 –wB97XD/def2-TZVP optimized geometries of pristine DPT and the 34 B,N-DPT precandidates for SF and TADF. . . . .	150
FIGURE D.2 –Vertical $E(T_1)$ of pristine DPT and the 34 B,N-doped molecules calculated by using the CASPT2(8,8)/6-31G* method. . . . .	151

# List of Tables

TABLE 3.1 – HOMA parameters . . . . .	40
TABLE D.1 – $E(S_1)$ , $E(T_1)$ and $\Delta E_{ST} = E(S_1) - E(T_1)$ for each of the 34 B,N-doped (10 SF precandidates and 24 TADF precandidates) and pristine DPT molecules calculated with the CASPT2(8,8) method. TADF candidates are highlighted in red. . . . .	152
TABLE D.2 – HOMA values for each ring of the 34 B,N-doped (10 SF precandidates and 24 TADF precandidates) and pristine DPT molecules calculated at the wB97XD optimized geometries. TADF candidates are highlighted in red. . . . .	153
TABLE D.3 – Summary of energy values obtained by various methods for tetracene.	154
TABLE D.4 – Summary of energy values obtained by various methods for DPT. .	155

# List of Abbreviations and Acronyms

1-RDM	one-particle reduced density matrix
ACID	anisotropy of the induced current density
CAS	complete active space
CASCI	complete active space configuration interaction
CASPT2	complete active space second-order perturbation theory
CC	coupled cluster
CCSD	coupled cluster including single and double excitations
CASSCF	complete active space self-consistent field
CI	configuration interaction
CISD	configuration interaction including single and double excitations
CSF	configuration state function
CT	charge transfer
DFT	density functional theory
DPT	5,12-diphenyltetracene
EQE	external quantum efficiency
FET	field-effect transistor
FOLED	fluorescent organic light-emitting diode
HF	Hartree-Fock
HOMA	harmonic oscillator model of aromaticity
HOMO	highest occupied molecular orbital
IC	integrated circuit
IQE	internal quantum efficiency
ISC	intersystem crossing
LCD	liquid-crystal display
LED	light-emitting diode
LUMO	lowest unoccupied molecular orbital
MC	multiconfigurational
MCI	multicenter bond indices
MCSCF	multiconfigurational self-consistent field

---

MP2	second-order Møller–Plesset perturbation theory
MR	multireference
MRAQCC	multireference averaged quadratic coupled cluster
MRCI	multireference configuration interaction
MRCISD	multireference configuration interaction including single and double excitations
NEVPT2	second-order n-electron valence state perturbation theory
NICS	nucleus independent chemical shifts
NO	natural orbital
OFET	organic field-effect transistor
OLED	organic light-emitting diode
OPV	organic photovoltaic
PAH	polycyclic aromatic hydrocarbon
PhOLED	phosphorescent organic light-emitting diode
PT	perturbation theory
+P	Pople correction in MRCI
RAS	restricted active space
RASSCF	restricted active space self-consistent field
RI	resolution of identity approximation
RISC	reverse intersystem crossing
SC	strongly contracted
SCF	self-consistent field
SF	singlet fission
TADF	thermally activated delayed fluorescence
TDDFT	time-dependent density functional theory

# List of Symbols

$a_0$	Bohr radius
$e$	elementary charge
$e$	Euler's number
$E$	energy
$E_{\text{corr}}$	correlation energy
$E_{\text{HF}}$	HF limit energy
$N$	number of electrons in a molecule
$K$	number of spatial functions in a basis
$\epsilon_0$	permittivity of free space
$\gamma(\mathbf{x}_1, \mathbf{x}'_1)$	1-RDM
$\hbar$	reduced Planck constant
$k_B$	Boltzmann constant
$\hat{a}^\dagger$	creation operator
$\hat{a}$	annihilation operator
$\hat{F}$	Fock operator
$\hat{H}$	Hamiltonian operator
$\hat{V}$	perturbation to the Hamiltonian operator
$\hat{J}$	Coulomb operator
$\hat{K}$	exchange operator
$\hat{T}$	cluster operator
$\hat{S}^2$	total spin operator squared
$\hat{S}_z$	spin operator along the $z$ -axis
$S$	total spin quantum number
$2S + 1$	spin multiplicity
$M_S$	spin quantum number for the $z$ -axis component
$h_{aa}$	one-electron contribution to the energy
$J_{ab}$	Coulomb integral
$K_{ab}$	exchange integral
$m_e$	electron mass
$\mathbf{C}$	coefficient matrix

---

$\mathbf{F}$	Fock matrix
$\mathbf{k}$	wave vector
$\mathbf{p}$	crystal momentum
$\mathbf{r}$	position vector
$\mathbf{r}_i$	position of the electron $i$
$\mathbf{R}_A$	position of the nucleus $A$
$\mathbf{S}$	overlap matrix
$\mathbf{x}$	vector containing both position and spin
$\nabla_i$	gradient operator in the coordinates of $i$
$\nabla_i^2$	Laplacian operator in the coordinates of $i$
$\Psi$ or $\Phi$	wavefunction
$\Psi_{ijk}^{abc}$ or $\Phi_{ijk}^{abc}$	excited configuration obtained by promoting electrons from occupied orbitals $\chi_i, \chi_j, \chi_k$ to virtual orbitals $\chi_a, \chi_b, \chi_c$
$ \chi_1\chi_2 \dots \chi_N\rangle$	Slater determinant
$\psi_i(\mathbf{r})$	spatial orbital
$\chi_i(\mathbf{x})$	spin orbital
$\rho(\mathbf{r})$	electron density function
$S_0$	singlet ground state
$S_n, n \geq 1$	$n^{\text{th}}$ excited singlet state
$T$	absolute temperature
$T_n, n \geq 1$	$n^{\text{th}}$ excited triplet state
$Z_A$	atomic number of the nucleus $A$
$\Delta E_{ST}$	$E(S_1) - E(T_1)$

# Contents

1	INTRODUCTION . . . . .	19
1.1	Objective . . . . .	19
1.2	Motivation . . . . .	19
1.3	Literature Review . . . . .	22
1.4	Outline of the Work . . . . .	23
2	THEORETICAL BACKGROUND . . . . .	25
2.1	Singlet Fission . . . . .	25
2.2	Thermally Activated Delayed Fluorescence . . . . .	29
2.3	Density Functional Theory Overview . . . . .	32
2.4	wB97XD . . . . .	33
2.5	Complete Active Space Perturbation Theory Second Order (CASPT2) . . . . .	34
2.6	Coupled Cluster Method . . . . .	34
3	METHOD AND MODELS . . . . .	37
3.1	Selection of the B,N-substituted DPT Molecules . . . . .	37
3.2	Nomenclature of the B,N-substituted DPT Molecules . . . . .	37
3.3	Geometry Optimization . . . . .	39
3.4	Harmonic Oscillator Model of Aromaticity . . . . .	39
3.5	Choice of the Method . . . . .	39
3.6	CASPT2 Calculations . . . . .	40
3.7	Selection of Candidates for TADF . . . . .	41
3.8	Effectively Unpaired Electrons . . . . .	41
3.9	MRAQCC Calculations . . . . .	41

---

4	RESULTS . . . . .	44
4.1	Choice of Method, Basis, and Active Space . . . . .	45
4.2	Energies . . . . .	46
4.3	HOMA . . . . .	48
4.4	Spin Density . . . . .	51
5	CONCLUSION . . . . .	54
5.1	Summary of Findings . . . . .	54
5.2	Implications and Future Work . . . . .	55
5.3	Concluding Remarks . . . . .	55
	BIBLIOGRAPHY . . . . .	57
	APPENDIX A – ADDITIONAL THEORETICAL BACKGROUND . . . . .	71
	APPENDIX B – “EXPLORING THERMALLY ACTIVATED DELAYED FLUORESCENCE IN B,N-SUBSTITUTED TETRACENE DERIVATIVES: TOWARDS ENHANCED OLED MATERIALS” . . . . .	105
	APPENDIX C – CARTESIAN COORDINATES FOR THE WB97XD OPTIMIZED GEOMETRIES . . . . .	130
	APPENDIX D – SUPPORTING INFORMATION: TABLES AND FIGURES	149

# 1 Introduction

## 1.1 Objective

This work investigates the potential application of B,N-substituted derivatives of 5,12-diphenyltetracene (DPT), which is itself a polycyclic aromatic hydrocarbon (PAH) derivative of the acene tetracene, in organic electronics such as organic photovoltaic (OPV) solar cells and organic light-emitting diodes (OLEDs).

The research examines B,N-DPT analogues of specific B,N-tetracene candidates that were previously identified for their potential to exhibit singlet fission (SF) and/or thermally activated delayed fluorescence (TADF). These candidates were discovered in earlier research and a systematic analysis of the 77 B,N-substituted derivatives of tetracene (PIMENTEL, 2023a; PIMENTEL, 2023b; PIMENTEL *et al.*, 2024). Multiconfigurational computational quantum chemistry methods are employed to analyze the chemical, optical, and electronic properties of these molecules. Through this analysis, the study seeks to identify promising candidates for future OPV and OLED technologies.

This work builds upon prior research (PINHEIRO *et al.*, 2017; PINHEIRO *et al.*, 2020a) that explored the impact of polarization and the modulation of diradical character in acenes through the substitution of a pair of carbon atoms with a B,N pair. Additionally, this work provides an abridged summary of the previous research to offer context for the systematic search and subsequent analysis of B,N-substituted derivatives.

## 1.2 Motivation

### SF-based Organic Photovoltaics

In 1965, Singh *et al.* first reported the phenomenon of singlet fission in anthracene crystals (SINGH *et al.*, 1965). Later, Nozik and Hanna's 2006 paper demonstrated that SF could increase solar cell efficiency by approximately one-third beyond the Shockley-Queisser limit (HANNA; NOZIK, 2006; SHOCKLEY; QUEISSER, 1961), providing a significant

impetus to the field.

Since then, the exploration of SF materials has grown significantly, with notable advancements in identifying molecules that exhibit SF capabilities. Despite these advances, the number of SF materials remains relatively limited. Some molecules that are known to exhibit SF include anthracene derivatives (BAE *et al.*, 2018), tetracene and its derivatives (MERRIFIELD *et al.*, 1969; TOMKIEWICZ *et al.*, 1971; THORSMØLLE *et al.*, 2009; GRUMSTRUP *et al.*, 2010; BURDETT *et al.*, 2010; CHAN *et al.*, 2013; MÜLLER *et al.*, 2007; PILAND *et al.*, 2013; CHEN *et al.*, 2014; KOROVINA *et al.*, 2016; THOMPSON *et al.*, 2015; ROBERTS *et al.*, 2012; MA *et al.*, 2012; WU *et al.*, 2021; MA *et al.*, 2013), and pentacene and its derivatives (THORSMØLLE *et al.*, 2009; CHAN *et al.*, 2013; WILSON *et al.*, 2011; JUNDT *et al.*, 1995; RAO *et al.*, 2010; CHEN *et al.*, 2014; BUDDEN *et al.*, 2021; WALKER *et al.*, 2013; SANDERS *et al.*, 2015; SAKAI *et al.*, 2018; BASEL *et al.*, 2017; FUEMMELE *et al.*, 2016; BUDDEN *et al.*, 2021). Acenes and their derivatives are a flagship class of materials in this field (LI *et al.*, 2022).

## TADF-based Organic Light-Emitting Diodes

Unlike traditional light-emitting diodes (LEDs) made from inorganic materials such as gallium nitride (GaN), OLEDs utilize organic compounds as the emissive layer. This organic layer can consist of polymers or small molecules that exhibit electroluminescent properties. In 2014, the Nobel Prize in Physics was awarded to Isamu Akasaki, Hiroshi Amano, and Shuji Nakamura for their groundbreaking work on efficient blue LEDs (NOBEL FOUNDATION, Stockholm: Nobel Prize Outreach, 2023; NAKAMURA *et al.*, 1996; NAKAMURA *et al.*, 1995; AMANO *et al.*, 1989; SAWAKI *et al.*, 1986), marking a major milestone in LED technology and energy-efficient lighting.

The development of practical OLED devices began in the early 1980s, with notable contributions from researchers Ching Wan Tang and Steven Van Slyke at Eastman Kodak Company (TANG; VANSLYKE, 1987; TANG, 1986; SLYKE *et al.*, 1996; TANG *et al.*, 1989). OLEDs offer several advantages over traditional liquid-crystal display (LCD) screens, including the ability to achieve perfect black levels, higher contrast ratios, more accurate colors, and faster refresh rates (WONG; ZYSMAN-COLMAN, 2017; HONG *et al.*, 2021). Additionally, OLED displays are thinner and lighter due to the absence of a separate backlight layer and support flexible and curved displays, enabling innovative form factors such as curved smartphones and rollable screens.

The key challenge in OLED development lies in selecting and designing organic materials with optimal photophysical properties, including efficient light emission and charge transport characteristics (BALDO *et al.*, 1998).

## DPT

PAHs have garnered significant interest in recent years due to their interesting properties and potential applications in various fields, including optoelectronics. Among the PAHs, acenes have emerged as a promising class of compounds for electronic device fabrication. Acenes, characterized by their linear arrangement of fused aromatic rings, possess unique electronic structures that make them attractive for use in organic semiconductor technologies (ANTHONY, 2008). Figure 1.1 shows the structure of an acene.

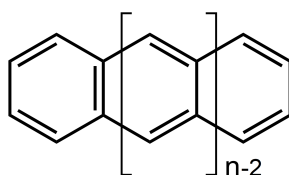


FIGURE 1.1 – Structure of an acene. For tetracene,  $n = 4$ .

This study investigates the potential of B,N-substituted analogues of the acene derivative DPT. Rubrene (5,6,11,12-tetraphenyltetracene), a tetracene derivative with two additional phenyl rings compared to DPT, is renowned for its exceptional hole mobility, making it a prominent candidate for applications in OLEDs, OPVs (CHAN *et al.*, 2007), organic field effect transistors (OFETs) (SUNDAR *et al.*, 2004; MCGARRY *et al.*, 2013; MATSUOKA *et al.*, 2023; HASEGAWA; TAKEYA, 2009), and other electronic devices. The molecular structures of DPT and rubrene are depicted in Figure 1.2. The superior charge carrier mobility exhibited by acenes such as rubrene (HASEGAWA; TAKEYA, 2009) enables efficient charge generation, transport, and electroluminescence in these devices.

DPT was selected for this study due to its ability to undergo SF in disordered films (ROBERTS *et al.*, 2012; SUTTON *et al.*, 2017) and colloidal nanoparticles (MASTRON *et al.*, 2013). Additionally, its smaller size relative to rubrene reduces the computational cost, making it a more practical choice for in-depth analysis.

## Our Work

A previous paper (PINHEIRO *et al.*, 2020a) investigated 60 out of the 77 possible B,N-substituted tetracene derivatives and identified four candidates that showed promise for SF. This research highlighted how replacing a pair of carbon atoms with one boron and one nitrogen atom could effectively alter the diradicaloid nature of the derivatives. This replacement led to significant changes in the excitonic and energetic properties of the molecules.

In subsequent work (PIMENTEL, 2023a; PIMENTEL, 2023b; PIMENTEL *et al.*, 2024), we systematically explored all 77 possible B,N-substituted tetracene derivatives to identify

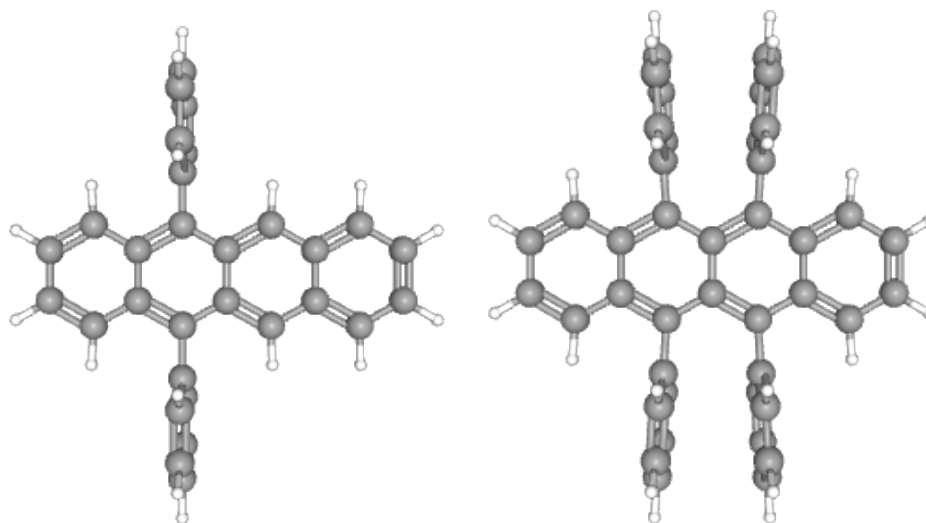


FIGURE 1.2 – Structures of DPT (left) and rubrene (right).

patterns of B,N substitution that offered favorable properties for SF and/or TADF while maintaining chemical stability. The research pinpointed five B,N-tetracene candidates with promising SF characteristics and twelve candidates with potential for TADF.

Building on these findings, the present work extends the examination to B,N-DPT analogues of B,N-tetracene candidates that show potential for SF and TADF. In this study, the focus shifts to treating the corresponding B,N-DPT analogues as precandidates and assessing whether they can exhibit the SF and/or TADF properties seen in their B,N-tetracene counterparts.

### 1.3 Literature Review

Some research groups have reported significant advancements in the synthesis and application of B,N-substituted organic semiconductors as SF chromophores in OPVs and TADF emitters in OLEDs. These materials show great promise for making new optoelectronic devices.

In their study, Matsui *et al.* demonstrated the synthesis of B,N-doped nanographenes through a one-shot multiple borylation reaction. The researchers successfully employed a B,N-doped nanographene as an emitter in an OLED device, which exhibited deep pure-blue emission at 460 nm with an external quantum efficiency (EQE) of 18.3% (MATSUI *et al.*, 2018).

Suresh *et al.* designed and synthesized an easily accessible B,N-doped heptacene with high thermal stability. The compound exhibited TADF at ambient temperature. As aimed to be reproduced in the present study, significant changes in the optoelectronic

properties of a molecule have been predicted by Suresh *et al.* when altering the positions of the boron and nitrogen atoms in the molecule (SURESH *et al.*, 2020).

Earlier, Ishibashi *et al.* managed to synthesize for the first time a B,N-substituted tetracene and found that it exhibits a slightly larger gap between the highest occupied molecular orbital and the lowest unoccupied molecular orbital (HOMO-LUMO) and a lower-lying HOMO and is less prone to photodecomposition when compared to the pristine tetracene molecule. They also predicted changes in the HOMO and LUMO energies as a function of the position of the boron and nitrogen atoms (ISHIBASHI *et al.*, 2017).

In addition, several studies have focused on SF chromophores. Zeng *et al.* identified three potential chromophores (a benzene, a naphthalene, and an azulene), in which four carbon atoms were replaced by a pair of boron and a pair of nitrogen atoms, as candidates for SF using multireference calculations for excited states (ZENG *et al.*, 2014). Nagami *et al.* investigated phenanthrenes with similar replacements of carbon with boron and nitrogen, identifying potential candidates for SF through quantum chemical calculations (NAGAMI *et al.*, 2020).

Walia and Yang performed a systematic computational analysis of B,N-doped perylenes, finding four SF chromophore candidates (WALIA; YANG, 2022). Singh *et al.* analyzed various perylene derivatives doped with one or two B,N pairs and identified the most suitable isomer for singlet fission using TDDFT and CASPT2 calculations (SINGH *et al.*, 2021). Lastly, Zeng *et al.* found a previously synthesized pyrene with two B,N pairs to be a viable singlet fission chromophore (ZENG *et al.*, 2018). Their theoretical calculations indicated that it met the thermodynamic criteria for singlet fission.

In conclusion, SF-based OPVs and TADF-based OLEDs utilizing B,N-substituted acene derivatives have shown promise in achieving efficient and stable devices. Novel molecular designs and material synthesis strategies are expanding the range of suitable molecules for these applications.

## 1.4 Outline of the Work

- **Chapter 1:** Introduces the research by presenting its objectives and motivations, along with a literature review. This chapter establishes the necessary context for the study.
- **Chapter 2:** Provides the theoretical foundation required to understand the study. This chapter outlines fundamental concepts and refers the reader to Appendix A for more detailed explanations. It aims to equip the reader with the theoretical background necessary for understanding the subsequent chapters.

- **Chapter 3:** Describes the methodologies and models employed in the research. It details the specific procedures used in the chemical calculations.
- **Chapter 4:** Presents the results from the computational quantum chemistry calculations. The focus is on the 34 B,N-substituted derivatives of DPT analyzed as potential precandidates. This chapter discusses the calculated properties of these molecules, evaluating their potential as candidates for exhibiting SF for OPV devices and/or TADF for OLEDs. It serves as a showcase of the research findings.
- **Chapter 5:** Concludes the study by summarizing the main findings and their implications. It discusses any limitations or challenges encountered during the research and suggests future research directions.

## Appendices

- **Appendix A:** Provides a copy of Chapter 2 from my senior thesis (PIMENTEL, 2023b), offering a comprehensive overview of the theoretical aspects of computational quantum chemistry necessary for understanding this study. For further reference, readers may consult “Modern Quantum Chemistry: Introduction to Advanced Electronic Structure Theory” by Szabo and Ostlund (SZABO; OSTLUND, 1996).
- **Appendix B:** Contains the paper “Exploring Thermally Activated Delayed Fluorescence in B,N-Substituted Tetracene Derivatives: Towards Enhanced OLED Materials” by Pimentel, Pinheiro Jr., Aquino, Lischka, and Machado (PIMENTEL *et al.*, 2024). This paper, prepared for submission to the Journal of Physical Chemistry A, is relevant to the current work.
- **Appendix C:** Includes the Cartesian coordinates of the 34 B,N-DPT molecules analyzed in the study.
- **Appendix D:** Contains relevant tables and figures presenting energies and descriptors that, while important, are secondary in relevance and therefore not included in Chapter 4.

## 2 Theoretical Background

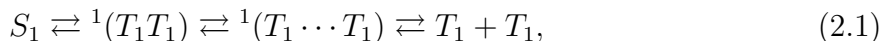
In this chapter, we present the theoretical background essential for understanding the methods employed in this study. For a comprehensive overview of fundamental theoretical concepts, the reader can refer to Appendix A, which is a chapter of my senior thesis (PIMENTEL, 2023b). Additionally, Szabo and Ostlund’s “Modern Quantum Chemistry” (SZABO; OSTLUND, 1996) offers a broader context on quantum chemistry methods discussed here.

The focus of this chapter is on the theory underlying SF and TADF, as well as methods used here and not covered in my senior thesis, namely wB97XD and CASPT2.

### 2.1 Singlet Fission

Smith and Michl’s 2010 review (SMITH; MICHL, 2010) provided a comprehensive summary of previous knowledge on SF and emphasized the potential of this phenomenon in the development of high-efficiency solar cells. This review was later updated in 2013 (SMITH; MICHL, 2013), further solidifying the foundation for future SF research.

The simplified mechanism of SF can be represented by a three-step process:



where  $S_1$  represents the first (*i.e.*, the lowest energy) excited singlet (total spin  $S = 0$ ) state previously generated by the absorption of a photon ( $S_0 \xrightarrow{h\nu} S_1$ ), while  $T_1$  represents the first triplet (total spin  $S = 1$ ) state. In the first step,  $S_1$  is converted to a spin-entangled triplet pair  ${}^1(T_1T_1)$  (WANG *et al.*, 2015; CHAN *et al.*, 2011; TEMPELAAR; REICHMAN, 2017b; TEMPELAAR; REICHMAN, 2017a; STERN *et al.*, 2015; ZIMMERMAN *et al.*, 2010; KIM; ZIMMERMAN, 2018; SANDERS *et al.*, 2019). Subsequently, the  ${}^1(T_1T_1)$  separates spatially to  ${}^1(T_1 \cdots T_1)$ , while still preserving its spin-entanglement. Finally, the two triplets that compose the  ${}^1(T_1 \cdots T_1)$  state undergo quantum decoherence, splitting into two triplets with independent spins, denoted as  $T_1 + T_1$ . While the isolated system of triplets appears to change its total spin during decoherence, the interaction with the

environment ensures that angular momentum conservation laws are not violated when the system and its environment are considered together.

Processes involving intersystem crossing (ISC), that is spin-forbidden, such as phosphorescence, are usually very slow, with time scales of up to milliseconds. In contrast, SF is a spin-allowed process, which means it can be extremely fast, frequently happening in the timescale of picosecond or subpicosecond (RAO *et al.*, 2010; THORSMØLLE *et al.*, 2009; LANZANI *et al.*, 2001; WANG; TAUBER, 2010; BURDETT *et al.*, 2010; WILSON *et al.*, 2011; KOROVINA *et al.*, 2016; MA *et al.*, 2012; WU *et al.*, 2021; MA *et al.*, 2013; SCHULTZ *et al.*, 2021).

Moreover, the generated triplet excitons generally have a very long lifetime and after dissociation to separated electrons and holes can be used as charge carriers in practical applications, such as solar cells. It also can generate up to two excitons per absorbed photon, *i.e.*, it can reach 200% internal quantum efficiency (IQE) (WANG; TAUBER, 2010; BAE *et al.*, 2018; BHATTACHARYYA; DATTA, 2017; LEE *et al.*, 2009; BUSBY *et al.*, 2015; SANDERS *et al.*, 2015; WALKER *et al.*, 2013). This efficiency is achieved through a process called downconversion, in which one high-energy photon splits into two lower-energy excitons. In photovoltaic cells, this helps to reduce thermalization losses (RAO; FRIEND, 2017), which occur when the excess energy of a photon in relation to the semiconductor's band gap is converted to kinetic energy of the exciton and dissipated as heat. They are the most significant losses in solar cells besides below band gap losses, that come from the inability of the semiconductor to absorb photons of energy below its band gap. Together, they make up a total loss greater than 55% for single junction solar cell with a band gap of 1.3 eV (NELSON *et al.*, 2013). Indeed, they are responsible for most of the limitation of the power conversion efficiency of a photovoltaic cell, as expressed by the Shockley-Queisser limit.

Figure 2.1 shows the solar spectrum and the main losses for a single-junction solar cell. Figure 2.2 shows the diagram for an SF solar cell described by Einzinger *et al.* (EINZINGER *et al.*, 2019). In order to allow the tunneling of charge carriers from tetracene into the silicon cell, they used a thin hafnium oxynitride ( $\text{HfO}_x\text{N}_y$ ) passivation layer keeping in mind that the tunneling probability decreases exponentially with the layer's width. This layer prevents the recombination of electrons and holes in silicon. However, not only the  $T_1$  triplets, but also some of the  $S_1$  singlets are transferred through the passivation layer, causing an efficiency loss.

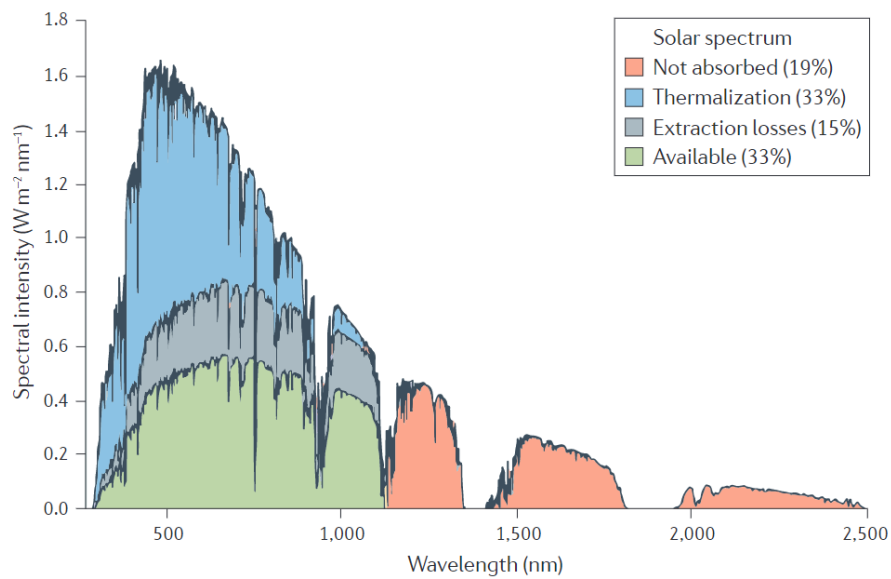


FIGURE 2.1 – Losses in a single-junction silicon (band gap = 1.1 eV) solar cell. *Note.* From “Quantum dots for next-generation photovoltaics,” by O. Semonin, J. Luther and M. Beard, 2012, *Materials Today*, 15(11), 508-515 (SEMONIN *et al.*, 2012).

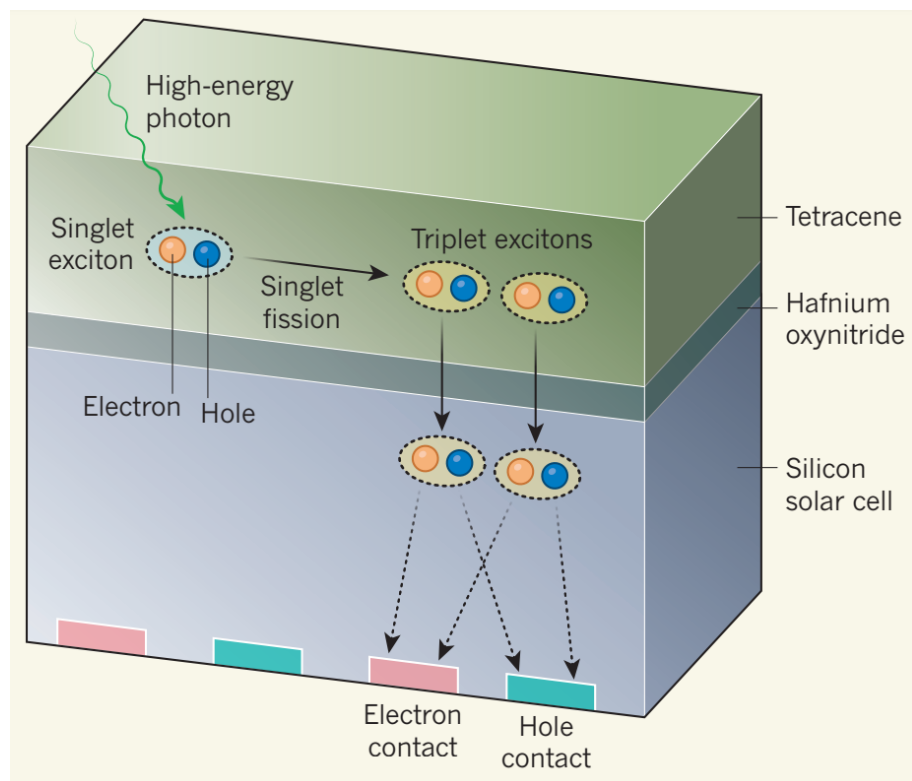


FIGURE 2.2 – Singlet-fission solar cell devised by Einzinger *et al.* *Note.* From “An exciting boost for solar cells,” by J. Luther and J. Johnson, 2019, *Nature*, 571, 38-39 (LUTHER; JOHNSON, 2019).

As previously said, SF uses the excess energy that would be wasted as heat to produce another electron-hole pair, thereby increasing (up to doubling) photocurrent. However, it also halves the open circuit voltage of the cell (LEE *et al.*, 2013). Thus, in order to achieve

a high efficiency, an SF solar cell must have not only SF chromophores that absorb high energy photons, but also chromophores that absorb lower energy photons.

Although singlet fission (SF) offers several advantages, certain criteria must be met for it to be efficient. These include outcompeting triplet-triplet annihilation (TTA, it's inverse process) (BURDETT *et al.*, 2010; WANG *et al.*, 2020; BASEL *et al.*, 2017), exhibiting adequate vibronic coupling (GRUMSTRUP *et al.*, 2010; FINTON *et al.*, 2019; SCHULTZ *et al.*, 2021; TAKAHASHI *et al.*, 2019; RENAUD; GROZEMA, 2015; FUEMMELEER *et al.*, 2016; TEMPELAAR; REICHMAN, 2017b; TEMPELAAR; REICHMAN, 2017a; TEMPELAAR; REICHMAN, 2018; MORRISON; HERBERT, 2017) and coupling between  $S_1$  and  $^1(T_1T_1)$  (BURDETT; BARDEEN, 2012; ZHANG *et al.*, 2014; PENSACK *et al.*, 2018; MORRISON; HERBERT, 2017; CHAN *et al.*, 2012). The coupling must be strong enough to ensure fast SF and weak enough to allow the triplets to diffuse away. Certain vibrational modes that break molecular symmetry can sometimes activate coupling (MIYATA *et al.*, 2017; ALVERTIS *et al.*, 2019). The appropriate packing, crystal size and morphology (THORSMØLLE *et al.*, 2009; RAMANAN *et al.*, 2012; BURDETT *et al.*, 2010; BHATTACHARYYA; DATTA, 2017; MASTRON *et al.*, 2013; MARGULIES *et al.*, 2017; BAYLISS *et al.*, 2015; FINTON *et al.*, 2019; ARIAS *et al.*, 2016; MIRJANI *et al.*, 2014; DAIBER *et al.*, 2020) (due to, *e.g.*, Davydov splitting and entropic gain (KOLOMEISKY *et al.*, 2014; CHAN *et al.*, 2012)) are also relevant, but occupational disorder does not always affect SF as expected (BROCH *et al.*, 2018).  $\pi$ - $\pi$  interactions in solids, films and molecular dimers also seem to play an important role in SF (BASEL *et al.*, 2017; KOROVINA *et al.*, 2016; ROBERTS *et al.*, 2012; BASEL *et al.*, 2019; FOLIE *et al.*, 2018; KOROVINA *et al.*, 2018; SAKAI *et al.*, 2018; ZHANG *et al.*, 2020; LUKMAN *et al.*, 2016). Fundamentally, the most important criteria that must be fulfilled are two thermodynamic ones:

$$E(S_1) \geq 2E(T_1), \quad (2.2)$$

$$E(T_2) \geq 2E(T_1). \quad (2.3)$$

All energies corresponding to excited states, denoted as  $E(T_n)$  or  $E(S_n)$ , are calculated with respect to the ground singlet state ( $S_0$ ), which serves as the reference energy. Therefore, the energy of the  $S_0$  state is considered as 0, and the energy of a triplet state  $T_n$ , for example, should be interpreted as  $E(T_n) - E(S_0)$ .

Equation (2.2) is required by conservation of energy in order for two  $T_1$  excitons be formed from one  $S_1$  exciton. Equation (2.3) avoids that two  $T_1$  excitons recombine to form one  $T_2$  exciton that undergoes internal conversion to the  $T_1$  triplet according to Kasha's rule (KASHA, 1950), and results in the loss of one of the two initial triplet excitons (WANG *et al.*, 2020). In order to be more rigorous, we must consider a third thermodynamic constraint, namely  $E(Q_1) \geq 2E(T_1)$ , *i.e.*, the energy of the first quintet  $Q_1$  must be greater than that of the  $T_1$  pair. However, this constraint is typically satisfied

and therefore we will not further discuss it.

Figure 2.5 shows the extended Jablonski diagram for SF. Smith and Michl categorize SF chromophores' parent hydrocarbons in three classes, depending on the nature of the  $S_0 \rightarrow S_1$  transition: class I, if it corresponds to a HOMO  $\rightarrow$  LUMO transition; class II, if it is a linear combination of a HOMO-1  $\rightarrow$  LUMO and a HOMO  $\rightarrow$  LUMO+1 transition; class III, if it has a significant contribution of the double excitation HOMO,HOMO  $\rightarrow$  LUMO,LUMO.

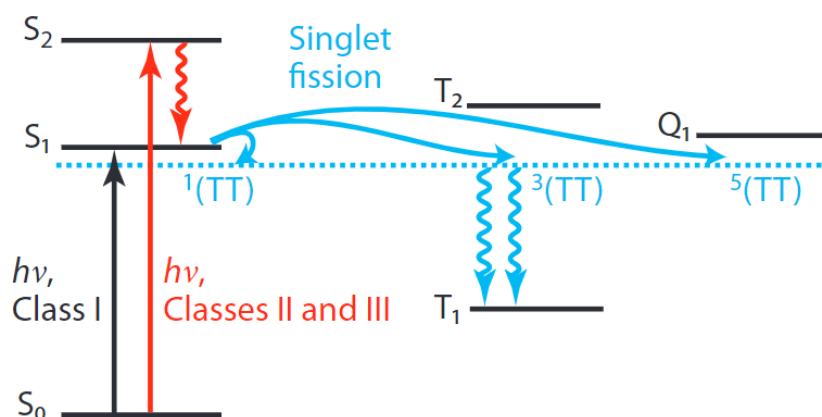


FIGURE 2.3 – Jablonski diagram illustrating singlet fission. *Note.* From “Recent Advances in Singlet Fission,” by M. Smith and J. Michl, 2013, *Annu. Rev. Phys. Chem.*, 64, 361-86 (SMITH; MICHL, 2013).

## 2.2 Thermally Activated Delayed Fluorescence

Figure 2.4 shows the diagram of a white OLED.

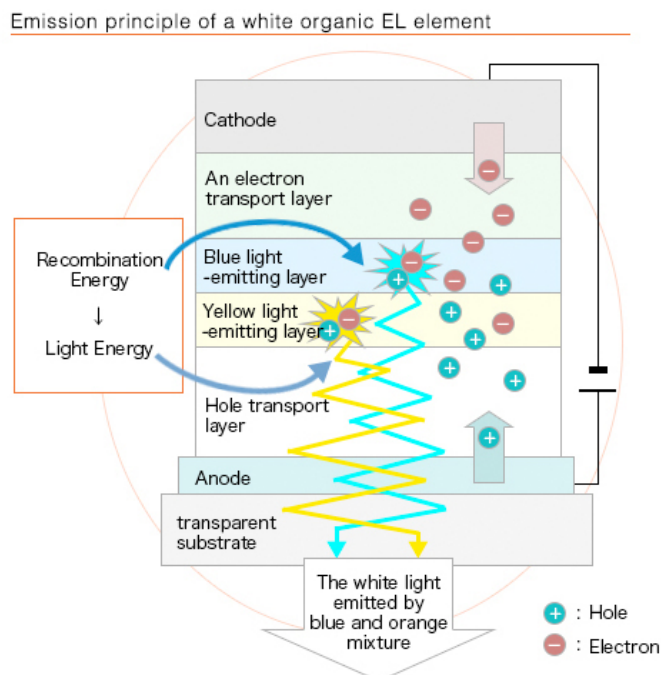


FIGURE 2.4 – Scheme of a white OLED. *Note.* In a screen, the white light is then passed through an RGB color filter. From [www.futaba.co.jp/en/product/oled\\_backup/about](http://www.futaba.co.jp/en/product/oled_backup/about).

In small-molecule OLEDs, organic molecules like anthracene and tetracene are used as the emissive layer (SHAH *et al.*, 2006). Polymer-based OLEDs, also known as PLEDs or P-OLEDs, emerged as another significant milestone, offering advantages such as flexibility and compatibility with large-scale manufacturing processes (BHARATHAN; YANG, 1998; HEBNER *et al.*, 1998).

OLEDs operate based on the phenomenon of electroluminescence in an organic semiconductor layer when an electric current is applied. The operation begins with the injection of electrons and holes into the organic layer from the electrodes. When an electron and a hole combine within the organic layer, they form an exciton, a quasiparticle which can be defined as a bound electron-hole pair. These excitons can exist in two possible states: singlet and triplet. Statistically, there is a 25% probability of forming a singlet state and a 75% probability of forming a triplet state (BROWN *et al.*, 1993; BALDO *et al.*, 1999b). As the excitons decay, they release energy in the form of light through spontaneous emission. The emitted light corresponds to a specific wavelength determined by the energy difference between the excited state and the ground state  $S_0$  of the organic material. Figure 2.5 shows a Jablonski diagram containing possible radiative and nonradiative transitions and their timescales.

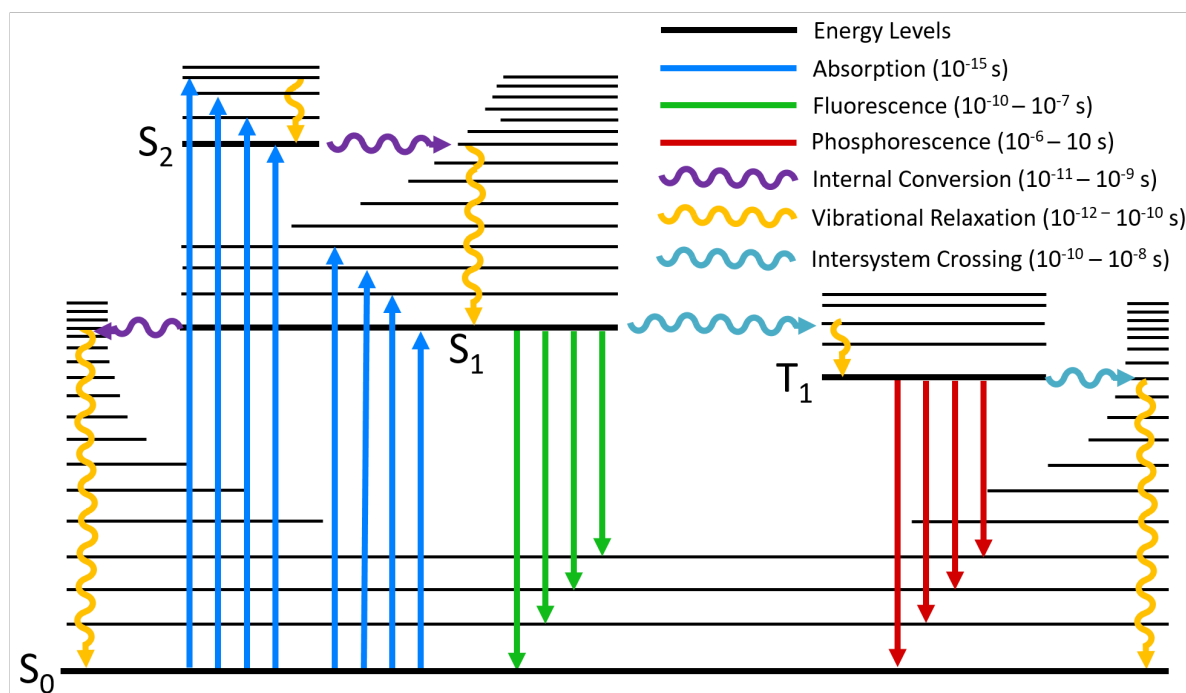


FIGURE 2.5 – Jablonski diagram depicting radiative (straight arrows) and nonradiative (squiggly arrows) transitions. *Note.* This diagram does not differentiate between intersystem crossing (singlet to triplet) and reverse intersystem crossing (triplet to singlet). From [www.edinst.com](http://www.edinst.com).

Different types of OLEDs have been explored, such as fluorescent OLEDs (FOLEDs) and phosphorescent OLEDs (PhOLEDs). While PhOLEDs have demonstrated high efficiency due to the utilization of triplet excitons, they often require expensive and scarce heavy metal complexes as emitter materials. As an alternative, TADF has emerged as a promising mechanism for achieving high-efficiency OLEDs without relying on heavy metals (UOYAMA *et al.*, 2012).

First-generation OLEDs, the FOLEDs, utilize organic dyes as emitters. These dyes primarily undergo the transition of singlet excitons to the singlet ground state ( $S_1 \rightarrow S_0$ ) for fluorescence. However, the ISC decay of the triplet excitons to the ground state is forbidden by selection rules, limiting the efficiency of fluorescence OLEDs. Only around 25% of singlet excitons can be harvested for luminescence, resulting in an upper limit of 5% EQE without additional optical outcoupling (HONG *et al.*, 2021).

To make use of the triplet excitons, that make up 75% of the total, and improve OLED efficiency, phosphorescent heavy-metal complexes have been developed as emitters for the second generation of OLEDs (BALDO *et al.*, 2000). The metal atoms in these complexes enhance the spin-orbit coupling, which reduces the lifetime of the lowest-lying triplet state  $T_1$  (BALDO *et al.*, 1999a; O'BRIEN *et al.*, 1999). This prompts phosphorescence as  $T_1$  decays to the ground state  $S_0$ . ISC from the lowest-lying singlet state  $S_1$  to  $T_1$  is also facilitated. This triplet-using strategy enables phosphorescent emitters to achieve IQE of nearly 100%, resulting in high EQEs (MINAEV *et al.*, 2014; BALDO *et al.*, 1998).

To address the limitations of heavy-metal-based phosphorescent emitters, the development of emitters that avoid the usage of high-cost and environmentally detrimental elements has gained momentum (VOLZ *et al.*, 2015). One promising solution is TADF emitters. The energetic criteria for achieving efficient TADF are of utmost importance. The energy gap between the lowest singlet and triplet excited states,  $\Delta E_{ST} = E(S_1) - E(T_1)$ , should be small to facilitate efficient reverse intersystem crossing (RISC) in order for a molecule to exhibit TADF. When the  $T_1$  excitons have a sufficiently long lifetime, the RISC process is thermally activated, though it is formally spin-forbidden. This allows the  $T_1$  triplet excitons to undergo upconversion into the  $S_1$  state, followed by radiative relaxation to the ground state  $S_0$ , resulting in a theoretical IQE of 100% (YANG *et al.*, 2017; ZHANG *et al.*, 2012).

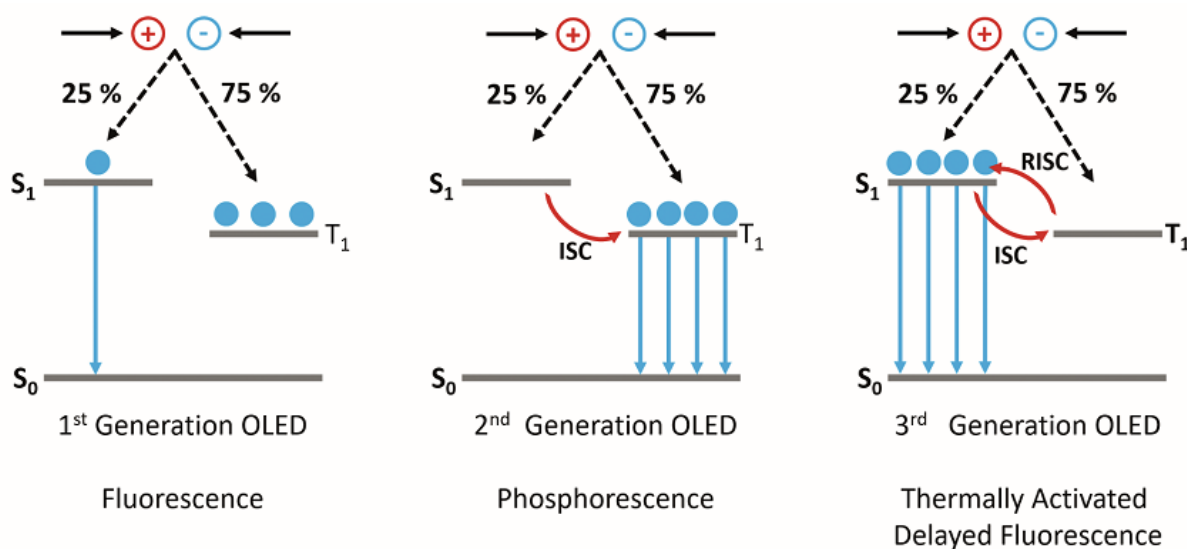


FIGURE 2.6 – Comparison of FOLEDs, PhOLEDs and TADF OLEDs. *Note.* From [www.edinst.com](http://www.edinst.com)

## 2.3 Density Functional Theory Overview

The quantum mechanical description of molecular systems is often based on the wavefunction, a complex function that depends on the spatial and spin coordinates of all the electrons in a molecule. However, the wavefunction is not easy to calculate or store, and it encodes more information than is typically required to determine physical properties such as energies and dipole moments. A conceptually simpler approach would involve the electron density  $\rho(\mathbf{r})$ .

In 1964, Pierre Hohenberg and Walter Kohn introduced two pivotal theorems that laid the foundation for Density Functional Theory (DFT), which has since become a powerful and popular approach in condensed matter physics and quantum chemistry. DFT has seen remarkable growth in usage and development, offering an alternative to

wavefunction-based methods.

## Hohenberg-Kohn Theorems

The first Hohenberg-Kohn theorem established that there is a one-to-one correspondence between the external potential (due to the atomic nuclei)  $V_{\text{ext}}(\mathbf{r})$  (within a constant) and the ground-state electron density  $\rho(\mathbf{r})$ . Since  $V_{\text{ext}}(\mathbf{r})$  fixes the hamiltonian  $\hat{H}$ , the ground state energy and all other ground-state (and excited state) properties of a molecular system can be expressed as functionals of  $\rho(\mathbf{r})$ .

The second theorem is a variational principle: given any trial electron density  $\rho(\mathbf{r})$  different from the exact ground-state density  $\rho_0(\mathbf{r})$ , the corresponding energy calculated with the external potential  $V_{\text{ext}}(\mathbf{r})$  corresponding to  $\rho_0(\mathbf{r})$  will always be greater than or equal to the exact ground state energy.

The primary challenge with DFT arises from the need to express the total energy as a sum of two components: one that depends on the external potential (the interaction between the electrons and this potential) and another that encompasses the kinetic energy and electron-electron interactions. This second term, which combines the kinetic energy and electron-electron interactions, must be represented as a functional of the electron density  $\rho(\mathbf{r})$ . This functional must be universal, meaning it should map any possible electron density function to its corresponding energy contribution from kinetic energy and electron-electron interactions. However, the precise form of this universal functional is unknown. Consequently, practical applications of DFT rely on approximations, both empirical and derived from physical insights, which often work well in specific cases.

## 2.4 wB97XD

The wB97XD functional is a range-separated hybrid density functional that includes an empirical dispersion correction (CHAI; HEAD-GORDON, 2008), distinguishing it from its predecessors wB97 and wB97X, which lack such a correction.

### wB97XD for Geometry Optimization

The wB97XD functional, though not ideal for excited state geometry determinations, offers a cost-effective and accurate approach for optimizing ground state geometries (WANG; DURBEEJ, 2020). In this work, we apply wB97XD to optimize the ground state geometries of B,N-substituted 5,12-diphenyltetracene derivatives. These optimized geometries serve as a basis for further analyses, including calculations related to excited

states.

## wB97XD with TDDFT for Excited State Calculations

Time-dependent density functional theory (TDDFT) (RUNGE; GROSS, 1984; DREUW; HEAD-GORDON, 2005; STRATMANN *et al.*, 1998; BAUERNSCHMITT; AHLRICHS, 1996; PETERSILKA *et al.*, 1996) combined with the wB97XD functional allows for the calculation of excited state energies in molecular systems. The TDDFT method is employed to simulate electronic transitions and excited states.

However, while wB97XD with TDDFT is a valuable tool, it may not provide the most accurate energy predictions for excited states, particularly in systems with significant charge-transfer effects (HERBERT, 2024). In this study, the more accurate CASPT2 method is used for final energy calculations of excited states to address this limitation.

## 2.5 Complete Active Space Perturbation Theory Second Order (CASPT2)

The second-order complete active space perturbation theory (CASPT2) approach combines complete active space self-consistent field (CASSCF) calculations with second-order perturbation theory to account for electron correlation within a chosen active space (ROOS *et al.*, 2007).

In the CASPT2 method, the active space consists of a selection of orbitals that are energetically important for the system being studied. The method can offer accurate energy predictions and descriptions of excited states, which are crucial for evaluating the potential of SF and TADF candidates.

For a more detailed discussion on many-body perturbation theory, particularly focusing on second order Møller-Plesset perturbation theory (MP2), readers can refer to Appendix A. While MP2 calculates dynamic correlation energy as a second-order perturbation correction to the Hartree-Fock energy, CASPT2 accounts for dynamic correlation energy by perturbing a CASSCF approximation, which inherently captures static correlation.

## 2.6 Coupled Cluster Method

The coupled cluster (CC) method excels at capturing dynamical correlation. This dynamic electron correlation is systematically treated by CC methods using different

levels of excitations. The key idea of the CC method is to express the wavefunction of the electronic ground state as an exponential transformation of a reference state, typically the Hartree-Fock ground state  $|\Phi_0\rangle$ . The CC wavefunction  $|\Psi_0\rangle$  is expressed as:

$$|\Psi_0\rangle = e^{\hat{T}} |\Phi_0\rangle, \quad (2.4)$$

where  $\hat{T}$  is the cluster operator. This exponential ansatz makes CC size extensive. The operator  $\hat{T}$  is expanded as a sum of terms representing different levels of excitations:

$$\hat{T} = \hat{T}_1 + \hat{T}_2 + \hat{T}_3 + \dots, \quad (2.5)$$

where  $\hat{T}_n$  denotes the  $n$ -electron excitations from the reference state. For instance,  $\hat{T}_1$  represents single excitations,  $\hat{T}_2$  represents double excitations, and so on. Each term  $\hat{T}_n$  can be expressed as:

$$\hat{T}_n = \frac{1}{(n!)^2} \sum_{i_1, i_2, \dots, i_n} \sum_{a_1, a_2, \dots, a_n} t_{a_1, a_2, \dots, a_n}^{i_1, i_2, \dots, i_n} \hat{a}_{a_1}^\dagger \hat{a}_{a_2}^\dagger \dots \hat{a}_{a_n}^\dagger \hat{a}_{i_1} \hat{a}_{i_2} \dots \hat{a}_{i_n}, \quad (2.6)$$

where  $i_1, \dots, i_n$  and  $a_1, \dots, a_n$  denote occupied and virtual orbitals, respectively. The creation and annihilation operators,  $\hat{a}_{a_k}^\dagger$  and  $\hat{a}_{i_k}$ , refer to the operators responsible for adding an electron to the virtual orbital  $a_k$  and removing an electron from the occupied orbital  $i_k$ , respectively. The  $t_{a_1, \dots, a_n}^{i_1, \dots, i_n}$  coefficients are the cluster amplitudes that need to be determined. For an  $N$ -electron wavefunction, if the operators up to  $\hat{T}_N$  are included in  $\hat{T}$ , then  $\hat{T}$  coincides with the full CI operator (see Appendix A).

The Schrödinger equation can be written as:

$$\hat{H}|\Psi_0\rangle = \hat{H}e^{\hat{T}}|\Phi_0\rangle = Ee^{\hat{T}}|\Phi_0\rangle. \quad (2.7)$$

Then, due to the orthogonality of the excited determinants with respect to the reference wave function, the energy and the cluster amplitudes can be determined by solving a set of nonlinear coupled equations:

$$\begin{aligned} \langle \Phi_0 | e^{-\hat{T}} \hat{H} e^{\hat{T}} | \Phi_0 \rangle &= E, \\ \langle \Phi_{i_1}^{a_1} | e^{-\hat{T}} \hat{H} e^{\hat{T}} | \Phi_0 \rangle &= 0, \\ \langle \Phi_{i_1, i_2}^{a_1, a_2} | e^{-\hat{T}} \hat{H} e^{\hat{T}} | \Phi_0 \rangle &= 0, \\ &\vdots \\ \langle \Phi_{i_1, i_2, \dots, i_n}^{a_1, a_2, \dots, a_n} | e^{-\hat{T}} \hat{H} e^{\hat{T}} | \Phi_0 \rangle &= 0. \end{aligned}$$

## Multireference Averaged Quadratic Coupled-Cluster (MRAQCC)

There are several variants of the CC method, with different levels of electron excitations. For instance, CCSD (coupled cluster with single and double excitations) and CCSD(T) (CCSD with perturbative triple excitations) are commonly used due to their balance between accuracy and computational cost.

To extend the CC method's ability to account for static correlation, which occurs in systems with multiple near-degenerate electronic states, multireference approaches such as multireference averaged quadratic coupled cluster (MRAQCC) have been developed. MRAQCC uses a reference wavefunction that combines multiple electronic configurations, allowing the method to capture static correlation effectively while maintaining the CC method's strength in handling dynamical correlation. In the current work, we employ the MRAQCC method with single and double excitations to describe the spin density in the B,N-DPT molecules.

## 3 Method and Models

### 3.1 Selection of the B,N-substituted DPT Molecules

Only one B,N pair is used for doping in each B,N-DPT molecule analyzed in this work. The B,N-substitution was only done in the tetracene core, never in the phenyl rings attached to it. Since the DPT molecule ( $C_{30}H_{20}$ ) contains 20 more atoms than tetracene ( $C_{18}H_{12}$ ), the computational expense associated with performing quantum chemistry calculations for every possible B,N-substituted DPT was prohibitive. Additionally, there are nearly twice as many potential ways to B,N-substitute the tetracene core of a DPT molecule compared to tetracene, owing to the presence of phenyl rings attached to the tetracene core.

As a result, this study pre-selected molecules based on prior research involving the simpler tetracene molecule. Pinheiro Jr. *et al.* identified four B,N-substituted tetracene candidates for SF, and our work expanded upon theirs by identifying an additional SF candidate, along with twelve potential B,N-substituted tetracene candidates for TADF (PINHEIRO *et al.*, 2020a; PIMENTEL, 2023a; PIMENTEL, 2023b). The 34 molecules examined in this study were based on these 17 pre-screened molecules. The reason why there are 34 B,N-DPT molecules corresponding to the 17 B,N-tetracene counterparts will be explained in Section 3.2.

Subsequently, the corresponding DPT molecules for tetracene were investigated to ascertain if, akin to their simpler counterparts, they exhibit promising SF and/or TADF properties.

### 3.2 Nomenclature of the B,N-substituted DPT Molecules

The notation for atom positioning within the tetracene moiety, introduced by Pinheiro Jr. *et al.*, is adopted, as illustrated in Figure 3.1. This numbering scheme differs from the IUPAC standard.<sup>1</sup> Each B,N-tetracene molecule is denoted by (B atom position),(N atom

---

<sup>1</sup>For instance, when we refer to 5,12-diphenyltetracene (the IUPAC nomenclature for DPT), it does not imply that the phenyl groups are attached to the carbons numbered 5 and 12 according to our labeling

position). To address potential symmetry-related ambiguities, two rules are established: (i) assign the lowest possible number to the B atom position, and (ii) subsequently, assign the lowest possible number to the N atom position. A detailed explanation can be found in my senior thesis (PIMENTEL, 2023b).

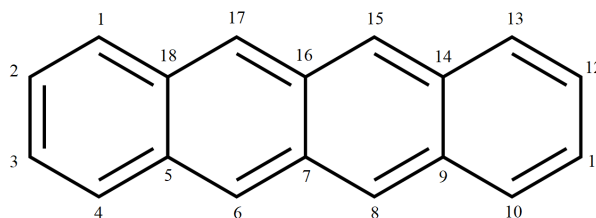


FIGURE 3.1 – Atom labeling scheme within the structure of tetracene.

Chakraborty *et al.* enumerated 77 possible B,N-tetracene molecules (CHAKRABORTY *et al.*, 2019). Among these, 76 exhibit  $C_s$  symmetry, possessing only the plane of the paper as a plane of symmetry. The remaining molecule, 7,16, demonstrates  $C_{2v}$  symmetry. Consequently, for each of the 76 B,N-tetracene molecules with  $C_s$  symmetry, there exist two corresponding B,N-DPT molecules. An example is depicted in Figure 3.2.

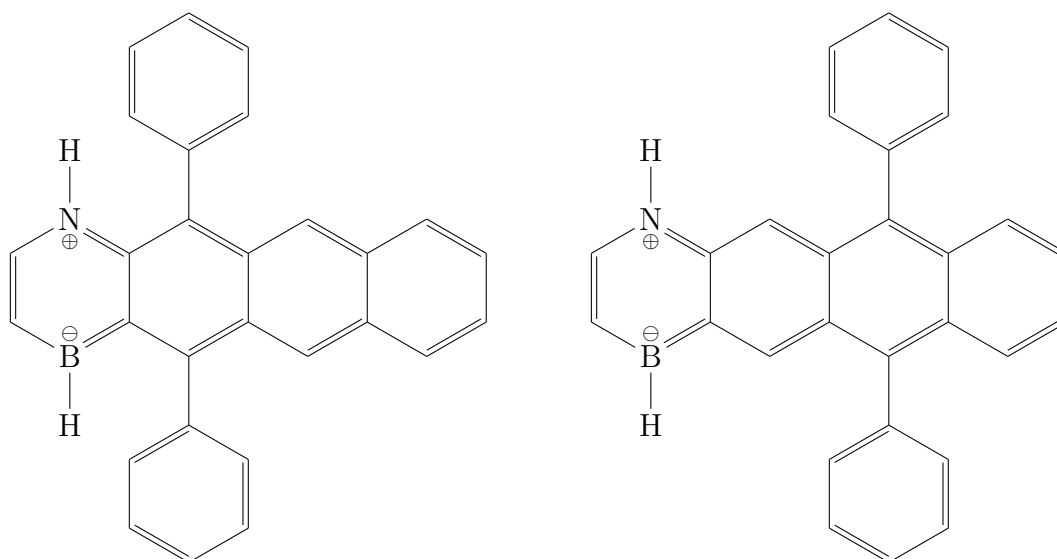


FIGURE 3.2 – Each B,N-tetracene molecule (except 7,16) corresponds to two B,N-DPT molecules. 4,1-left (left) and 4,1-right (right) are shown as examples.

Therefore, each B,N-DPT molecule (except 7,16) is named (B atom position),(N atom position)-(left or right), where “left” indicates attachment of phenyl groups to the second leftmost ring of the tetracene core, and “right” indicates attachment to the third leftmost ring of the tetracene core.

---

system.

### 3.3 Geometry Optimization

The geometry optimizations of all molecules were carried out using the def2-TZVP basis set (Ahlich's triple- $\zeta$  valence (TZV) plus (1p) polarization for H and (2d1f) polarization for B, C, and N) (WEIGEND; AHLRICH, 2005) with the DFT functional wB97XD (CHAI; HEAD-GORDON, 2008) on Gaussian software (FRISCH *et al.*, ).

The B,N-DPT molecules were optimized in  $C_s$  symmetry. Some molecules were with imaginary frequencies were found, but none of them exceeded  $50\text{ cm}^{-1}$ . This indicates deformations that cause the molecule to deviate from the molecular plane. A future improvement of this work could be reoptimizing those molecules with imaginary frequencies in  $C_1$  symmetry. The pristine DPT molecule was optimized in  $C_{2v}$  symmetry.

The optimized geometries are available in Appendix C. They are displayed in Figure D.1 in Appendix D.

### 3.4 Harmonic Oscillator Model of Aromaticity

To evaluate and quantify the aromaticity of each ring in each B,N-DPT precandidate structure at the wB97XD/def2-TZVP geometry, the descriptor harmonic oscillator model of aromaticity (HOMA) index (KRUSZEWSKI; KRYGOWSKI, 1972; KRYGOWSKI, 1993) was chosen, which is based on bond lengths and given by Equation (3.1):

$$\text{HOMA} = 1 - \frac{1}{n} \sum_{a,b} \alpha(a,b) (R_{\text{opt}}(a,b) - R_i(a,b))^2. \quad (3.1)$$

Here, the sum is taken over all pairs  $(a,b)$  of adjacent atoms (*i.e.*, that share a bond) in the ring,  $n$  is the number of atoms in the ring (6 in this study, since it is about acenes), and  $R_i(a,b)$  is the bond length of the bond between atoms  $a$  and  $b$ . The empirical parameters  $\alpha(a,b)$  and  $R_{\text{opt}}(a,b)$  depend on the atoms and are such that the following conditions are satisfied: (i) in an ideal aromatic ring, HOMA should be 1, so  $R_{\text{opt}}(a,b)$  is equal to the value  $R_i(a,b)$ ; (ii) in a non-aromatic ring, *i.e.*, that lacks resonance and has marked alternating bond lengths between the single and double bonds, HOMA should be 0.

The parameters used in this study are shown in Table 3.1.

### 3.5 Choice of the Method

Pristine tetracene and pristine DPT had their excited states calculated under various methods and bases. The results were compared to experimental results to choose the

TABLE 3.1 – HOMA parameters

Atom Pair	$R_i$ (Å)	$\alpha$ (Å <sup>-2</sup> )
C–C <sup>a</sup>	1.388	257.7
C–N <sup>a</sup>	1.334	93.52
C–B <sup>b</sup>	1.4235	104.507
B–N <sup>c</sup>	1.402	72.03

<sup>a</sup> Reference: (KRYGOWSKI; CYRAŃSKI, 2001)

<sup>b</sup> Reference: (ZBOROWSKI *et al.*, 2012)

<sup>c</sup> Reference: (MADURA *et al.*, 1998)

appropriate methodology to evaluate the TADF and SF B,N-precandidates. This choice is detailed in Section 4.1. The chosen methods were CASPT2(8,8)/6-31G\* for the excited state energies and MRAQCC/6-31G\* for the unpaired electron density (detailed in Section 3.8).

## 3.6 CASPT2 Calculations

Initially, complete active space self-consistent field (CASSCF) calculations (ROOS *et al.*, 1980) were performed to construct the reference wave function, capturing the static correlation inherent in singlet systems with open-shell character. The resulting molecular orbitals and configuration state functions (CSFs) from the CASSCF calculations were then utilized in the subsequent multireference (MR) calculations. The active space for the CASSCF procedure included 8 electrons in 8  $\pi$  orbitals, denoted as CAS(8,8). The orbitals were reordered to exclude the ones that lie on the phenyl rings attached to the tetracene core from the active space, as they are not relevant in excitations, which will be discussed in Chapter 4. Thus, the  $\pi$  orbitals that make up the active space pertain to the tetracene core. Specifically, for the precandidates, orbital 22 $a''$  (on the phenyl rings) was swapped with 20 $a''$ , and orbital 29 $a''$  (also on the phenyl rings) was swapped with 31 $a''$ .

The singlet ground state and the two lowest  $A'$  excited singlets were analyzed together, while the two lowest  $A'$  triplets were analyzed together, but separately from the singlets. The CASPT2 calculations were performed with the 6-31G\* basis (PETERSSON *et al.*, 1988) using MOLPRO software (WERNER *et al.*, ; WERNER *et al.*, 2012).

The geometries utilized were those of the ground state obtained from wB97XD/def2-TZVP calculations. Notably, the molecular geometries of the excited states themselves were not optimized, rendering the calculated energies vertical rather than adiabatic. For molecule 6,15-left, the level shift (ROOS; ANDERSSON, 1995) to avoid intruder state problems had to be adjusted to 0.25 to ensure convergence.

### 3.7 Selection of Candidates for TADF

For the selection of Thermally Activated Delayed Fluorescence (TADF) candidates, a criterion of  $\Delta E_{ST} < 0.25$  eV is applied. This criterion ensures that the energy difference between the singlet and triplet states is less than  $10k_B T$  at room temperature ( $T = 300$  K). By employing it, the TADF candidates thus identified have  $T_1$  triplet excitons capable of undergoing upconversion to the  $S_1$  state by thermal activation.

### 3.8 Effectively Unpaired Electrons

A nonlinear formula provides a useful approach for computing the total number of effectively unpaired electrons in molecules.<sup>2</sup>

The formula (HEAD-GORDON, 2003) can be expressed as:

$$N_U = \sum_i n_i^2 (2 - n_i)^2, \quad (3.2)$$

where  $n_i$  is the occupation number of the  $i^{\text{th}}$  natural orbital (NO).

The density of effectively unpaired electrons (or spin density) is:

$$\rho_U(\mathbf{r}) = \sum_i n_i^2 (2 - n_i)^2 |\psi_i(\mathbf{r})|^2, \quad (3.3)$$

where  $\psi_i(\mathbf{r})$  is the normalized  $i^{\text{th}}$  NO.

The number of effectively unpaired electrons provides a quantitative measure of the diradical character of a molecule. A significant diradical character suggests the presence of one unpaired electron in each of two degenerate or nearly degenerate molecular orbitals. Conversely, a low diradical character indicates the occupation of all occupied molecular orbitals by electron pairs, resulting in a closed-shell configuration.

### 3.9 MRAQCC Calculations

At the wB97XD/def2-TZVP geometries, the excited states were calculated using MRAQCC with the same active space used in the CASPT2 calculations (including the reordering to exclude the orbitals on the phenyl rings attached to the tetracene core). We

---

<sup>2</sup>*Erratum:* In two prior works (PIMENTEL, 2023a; PIMENTEL, 2023b) I incorrectly stated that the formula for computing the total number of effectively unpaired electrons cannot yield a value that exceeds the total number of electrons in the system. However, the formula that exhibits this property is actually  $\sum_i \min(n_i, 2 - n_i)$ .

utilized the COLUMBUS software, making efficient use of the available parallel algorithm (LISCHKA *et al.*, 2001; LISCHKA *et al.*, 2011). Additionally, the COLUMBUS software was employed to compute the unpaired electron density. Finally, post-processing of the MRAQCC results to determine the effective number of unpaired electrons was performed using the TheoDORE program (PLASSER, 2020).

An intruder state with more than 3% contribution was found in the molecules 1,14 (both 1,14-left and 1,14-right), 2,9 (both), and 6,9 (both). It was added to the reference by changing the active space with additional group restrictions. It corresponded to the excitation  $25a''(\text{HOMO}) \rightarrow 33a''$ . Other intruder states were found in molecules 1,11-left, 1,15 (both) and 6,15-right. They were added to the reference by following the same procedure.

We employed an active space of eight electrons in eight  $\pi$  orbitals, referred to as CAS(8,8), for both CASSCF and the MRAQCC reference space. The initial active orbitals were obtained from a prior Hartree-Fock calculation by selecting the four highest occupied and four lowest unoccupied  $\pi$  orbitals. No orbitals were kept frozen. In the MRAQCC calculations, correlation was introduced for all  $\pi$  orbitals.  $\sigma$  orbitals were not correlated, all of them were frozen. The reference CSFs were generated from the aforementioned CAS(8,8). The MRAQCC external configurations encompassed all permissible single and double electron excitations as per the generalized interacting space restrictions (LIU; MCLEAN, 1973; BUNGE, 1970). The MRAQCC calculations were performed for the ground state only and employed the Pople 6-31G\* basis set (FRANCL *et al.*, 1982). Figure 3.3 shows the orbitals and transitions taken into account in the MRAQCC calculations.

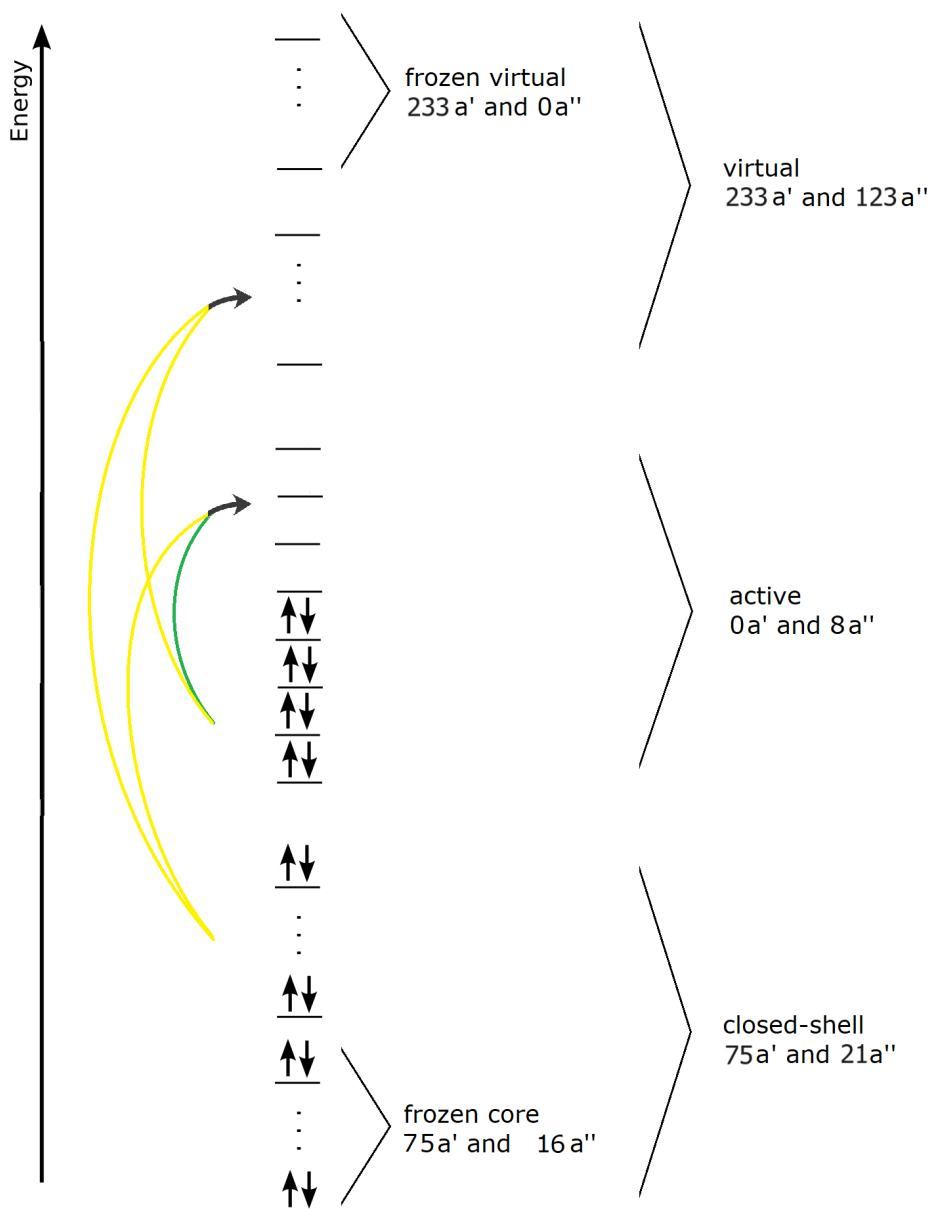


FIGURE 3.3 – Figure illustrating the MRAQCC orbitals. The reference space of configurations incorporates the excitations depicted by green arrows, which involve transitions between active orbitals. The external configurations for the MRAQCC method encompass the single and double excitations denoted by yellow arrows. These excitations involve transitions from closed-shell orbitals that are not frozen to active orbitals, from closed-shell orbitals that are not frozen to virtual orbitals that are not frozen, or from active orbitals to virtual orbitals that are not frozen. These external configurations account for the correlated behavior of the non-frozen orbitals. Transitions from the frozen core or to the frozen virtual orbitals are excluded.

# 4 Results

## Preamble: Summary of the Previous Results on B,N-tetracene

In the previous works of our research group (PINHEIRO *et al.*, 2020b; PIMENTEL, 2023a; PIMENTEL *et al.*, 2024), it was found that by B,N-doping an acene and changing the positions of the boron and nitrogen atoms, the diradicaloid character and the excitonic properties of the resulting molecule can be modulated. We explored this fact to try to find suitable candidates for SF and TADF.

Within a set of 60 B,N-doped structures, Pinheiro Jr. *et al.* found that four distinct molecules satisfied  $E(S_1) \geq 2E(T_1)$  and  $E(T_2) \geq 2E(T_1)$  (Equations (2.2) and (2.3)) for singlet fission (SF) according to SC-NEVPT2(12,12)/def2-TZVP calculations. Additionally, eleven other doping configurations nearly met these conditions, exhibiting a small endoergicity with  $2E(T_1) - E(S_1) < 0.3$  eV (PINHEIRO *et al.*, 2020b). In that study, the chemical stability of the molecules was analyzed by computing their diradicaloid character, aromaticity changes, charge transfer effects, and exciton properties. The effectiveness of chemical doping in tetracene with nitrogen and boron atoms as a promising strategy for developing efficient singlet fission sensitizers was thus demonstrated. By considering 60 BN-tetracene molecules with various doping configurations, they investigated the effects of different B and N positions on the excitation energies relevant for SF.

Inspired by that previous work, we then employed multireference quantum chemistry methods to scrutinize each of the 77 possible B,N-tetracene molecules by inspecting properties such as the energy of the first triplet state, the unpaired electron density, and the HOMA index in order to assess chemical stability and proneness to singlet fission, thereby finding five SF candidates among those molecules (PIMENTEL, 2023a). Specifically, they were: 1,10; 1,13; 2,3; 5,2; and 5,4. The 5,4 molecule had not been found in the previous work by Pinheiro Jr. *et al.*

Our subsequent work was to search for TADF candidates among the 77 B,N-tetracene molecules (PIMENTEL *et al.*, 2024). The primary objective was to identify and select prospective molecules for the fabrication of OLEDs. Based on our calculations, we identified a set of twelve B,N-tetracene candidates for TADF, namely 1,11; 1,14; 1,15; 2,9; 2,14; 2,16; 5,8; 5,12; 6,1; 6,9; 6,11; and 6,15, which exhibit potential for TADF. Five of these

are likely to emit in the visible range — 2,16; 5,8; 6,1; 6,9; 6,15. To assess the stability and aromaticity of the molecules, we employed several descriptors, such as HOMA, unpaired electron density, multicenter bond indices (MCI), Nucleus Independent Chemical Shifts (NICS), and Anisotropy of the Induced Current Density (ACID). The results regarding B,N-tetracene in this chapter can be found in that paper, available in its entirety in Appendix B.

For this work we made some changes to the methodology, which will be discussed subsequently. Hereafter, unless otherwise specified, we will discuss B,N-DPT instead of B,N-tetracene.

## 4.1 Choice of Method, Basis, and Active Space

Tetracene, possessing  $D_{2h}$  symmetry, exhibits specific orbital symmetries in its active space, with ground and excited states displaying distinct symmetries. The ground state has  $A_g$  symmetry, while the first two excited singlet states possess  $B_{2u}$  and  $B_{3u}$  symmetries, respectively. The first excited triplet state exhibits  $B_{2u}$  symmetry.

In the case of tetracene, classified as a class I SF chromophore, the  $S_0 \rightarrow S_1$  transition corresponds to a HOMO  $\rightarrow$  LUMO excitation, polarized along the molecular short axis ( $L_a$ ), resulting in the  $B_{2u}$  symmetry of the  $S_1$  state. Additionally, the  $B_{3u}$  symmetry of the  $S_2$  state arises from the  $S_0 \rightarrow S_2$  transition, a linear combination of a HOMO-1  $\rightarrow$  LUMO and a HOMO  $\rightarrow$  LUMO+1 excitation, polarized along the molecular long axis ( $L_b$ ) (YANG *et al.*, 2016). The  $L_a$  state exhibits ionic character, being sensitive to the freezing scheme of the  $\sigma$ -orbitals but not requiring an extended active space. Conversely, the covalent  $L_b$  state demands a large active space but is not sensitive to the freezing scheme within the  $\sigma$ -space, *i.e.*, to the extent of dynamic correlation (BETTANIN *et al.*, 2017).

Similarly, by analyzing the wave function of DPT (with  $C_{2v}$  symmetry), it was found that the  $S_0 \rightarrow S_1$  transition is a HOMO  $\rightarrow$  LUMO transition, with  $S_1$  having  $B_1$  symmetry. The  $S_0 \rightarrow S_2$  transition is a linear combination of a HOMO-1  $\rightarrow$  LUMO and a HOMO  $\rightarrow$  LUMO+1 transition, with  $S_2$  possessing  $A_1$  symmetry. Considering the essentially planar nature of the tetracene core in DPT, with the side phenyl rings being almost perpendicular to that plane (SUTTON *et al.*, 2017; CASANOVA, 2014), the  $C_{2v}$  symmetry choice is justified. This choice was supported by the absence of imaginary frequencies.

In contrast to the MRCISD calculations for B,N-tetracene in our previous work, where  $\sigma$  orbitals were correlated, no such correlation was applied in the MRAQCC calculations for the B,N-DPT precandidates.

The energies obtained from the tested methods and some experimental energies are presented in Tables D.3 and D.4 in Appendix D. Based on a cost-benefit analysis and considerations of accuracy, CASPT2(8,8)/6-31G\* was selected for evaluating excited state energies, while MRAQCC/6-31G\* was chosen for determining the unpaired electron density.

## 4.2 Energies

The values for  $E(S_1)$ ,  $E(T_1)$ , and  $\Delta E_{ST}$  are shown in Table D.1 in Appendix D. These results can also be seen in Figures 4.1, 4.2, and D.2.

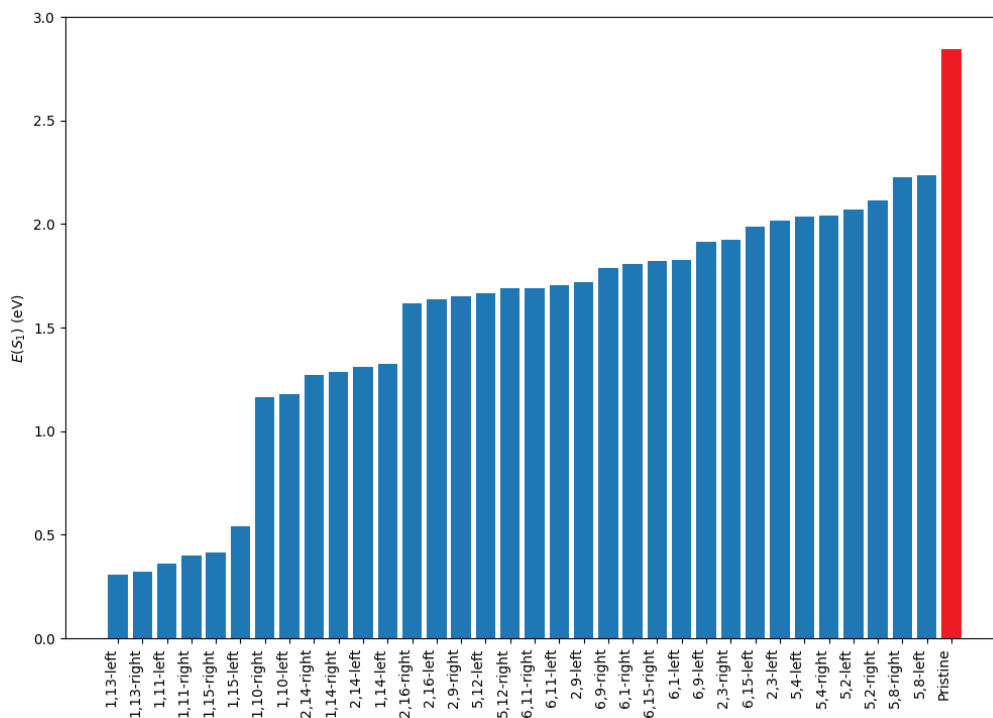


FIGURE 4.1 – Vertical  $E(S_1)$  of pristine DPT and the 34 B,N-doped molecules calculated using the CASPT2(8,8)/6-31G\* method.

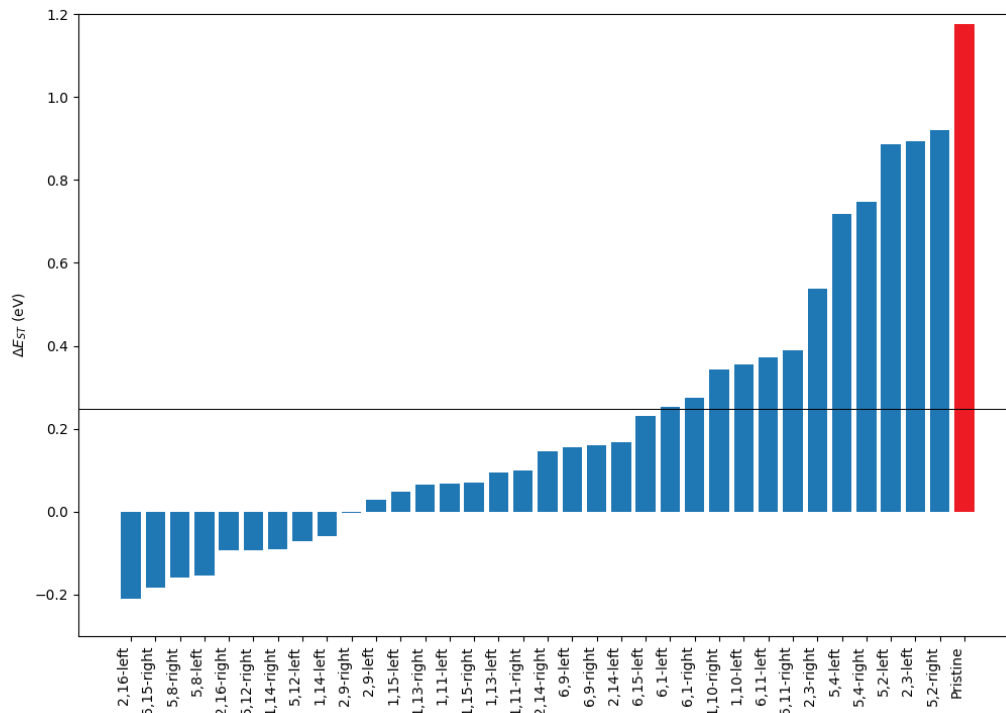


FIGURE 4.2 –  $\Delta E_{ST} = E(S_1) - E(T_1)$  of pristine DPT and the 34 B,N-doped molecules calculated using the CASPT2(8,8)/6-31G\* method.

Pristine DPT has  $E(S_1) = 2.84$  eV and  $\Delta E_{ST} = 1.18$  eV. Its  $E(S_1)$  and  $\Delta E_{ST}$  values are significantly higher than those of the precandidates. In our previous work, this phenomenon was observed in pristine tetracene compared to the B,N-substituted tetracene molecules calculated at MRCISD+P(8,8) (where +P indicates Pople’s correction), but it was absent when we used NEVPT2(12,12). This may suggest that CASPT2(8,8), which we are currently using for DPT and the precandidates, could overestimate  $E(S_1)$ . Regarding  $E(T_1)$ , there are B,N-doped precandidates with both higher and lower  $E(T_1)$  than pristine DPT.

Molecules 2,16 (both), 6,15 (both), 5,8 (both), 5,12 (both), and 1,14 (both) show a negative  $\Delta E_{ST}$ , indicating a violation of Hund’s rule. This inversion is likely an artifact of the CASPT2 calculations, but a deeper analysis is required since there are reports of this phenomenon in the context of OLEDs (AIZAWA *et al.*, 2022). Molecules 2,9 (both), 1,15 (both), 1,13 (both), and 1,11 (both) have a  $\Delta E_{ST}$  close to zero (less than 0.1 eV).

The energy values of left and right corresponding candidates are very close. The  $E(S_1)$  between them, as well as  $E(T_1)$ , generally differs by less than 0.15 eV. There are two exceptions: 2,3-left has  $E(T_1) = 1.12$  eV, while 2,3-right has  $E(T_1) = 1.38$  eV; and 6,15-left has  $E(T_1) = 1.76$  eV, while 6,15-right has  $E(T_1) = 2.01$  eV.

## SF

No SF candidates were found among the B,N-DPT precandidates. None of the analyzed precandidates fulfill  $E(S_1) \geq 2E(T_1)$  (Equation (2.2)).

## TADF

According to the CASPT2 calculations, all B,N-DPT molecules corresponding to the B,N-tetracene TADF candidates are TADF candidates themselves, except for 6,1 (both 6,1-left and 6,1-right) and 6,11 (both). Notably, 1,13 (both) is an extra pair of molecules whose corresponding B,N-tetracene was not a TADF candidate. Instead, it was an SF candidate. In summary, 1,11 (both), 1,13 (both), 1,14 (both), 1,15 (both), 2,9 (both), 2,14 (both), 2,16 (both), 5,8 (both), 5,12 (both), 6,9 (both), and 6,15 (both) were found to be TADF candidates. Among these, 2,9 (both), 2,16 (both), 5,8 (both), 5,12 (both), 6,9 (both), and 6,15 (both) emit visible light (have  $E(S_1)$  between 1.6 eV and 3.2 eV), making them suitable for displays.

## 4.3 HOMA

All the HOMA values can be seen numerically in Table D.2 in Appendix D. Figure 4.3 displays the HOMA index for each ring in the investigated molecules as a color map. The impact of the heteroatoms' position on the HOMA values is clear. The position of the phenyl rings attached to the tetracene core (left or right) does not change the trend of aromaticity in the rings of the molecules.

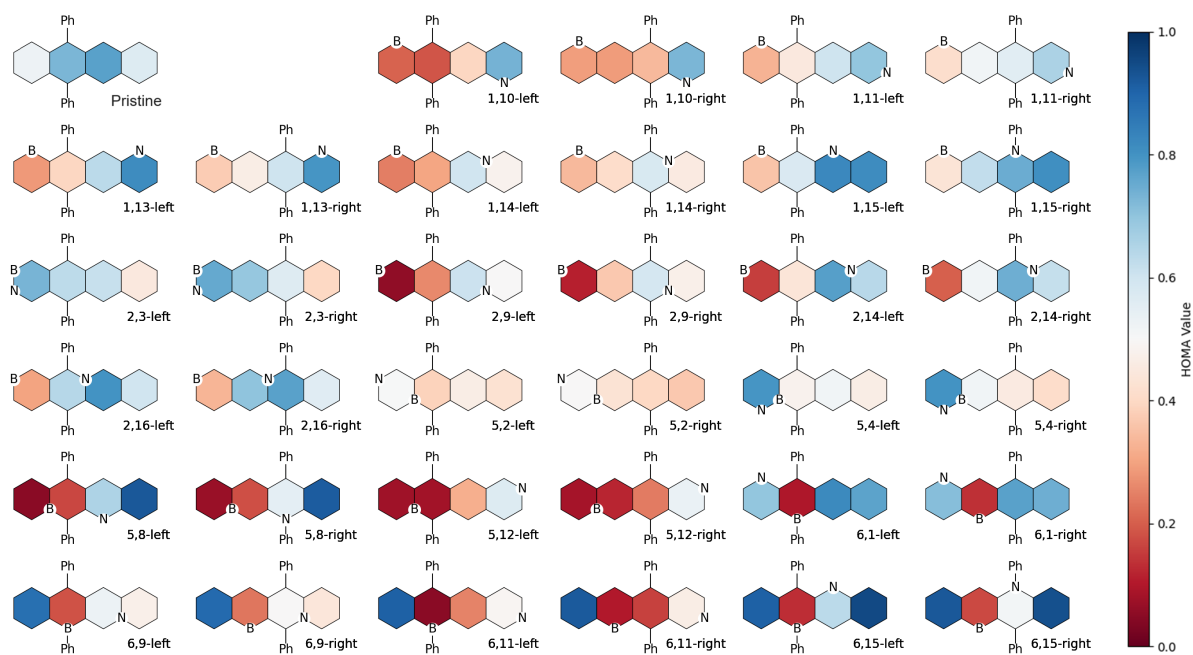


FIGURE 4.3 – Color map for the HOMA index of each ring in pristine DPT and the 34 B,N-doped SF and TADF precandidate molecules with the wB97XD/def2-TZVP optimized geometries.

Figures 4.4, 4.5, and 4.6 show bar plots of the maximum, minimum, and mean HOMA values for all rings of each analyzed molecule.

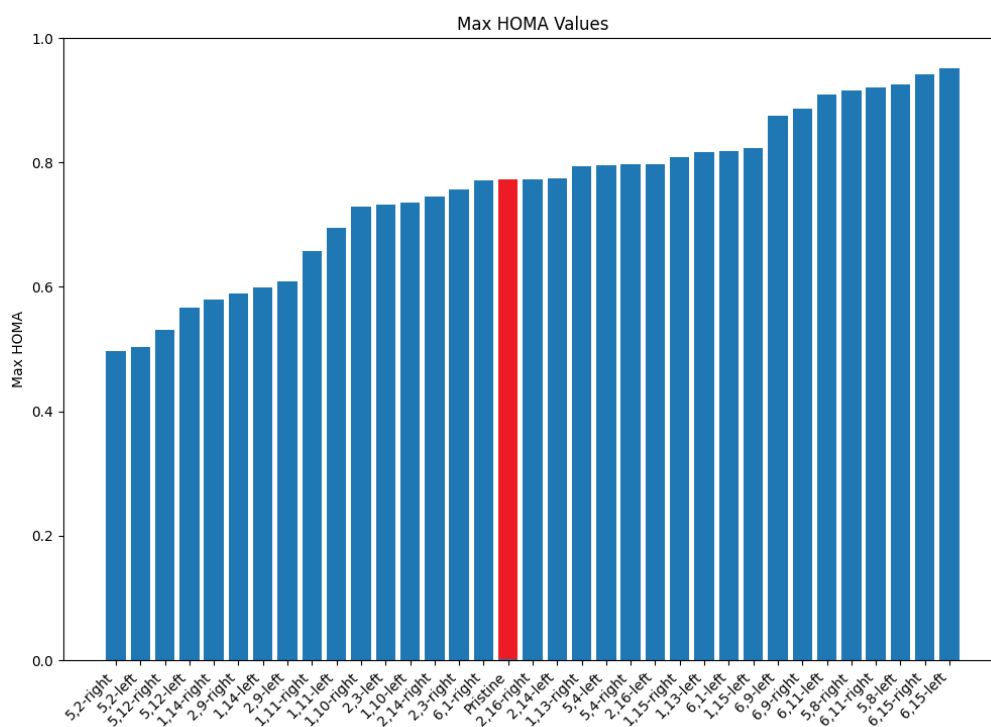


FIGURE 4.4 – Bar chart of the maximum HOMA value in pristine DPT and the 34 B,N-doped SF and TADF precandidate molecules with the wB97XD/def2-TZVP optimized geometries.

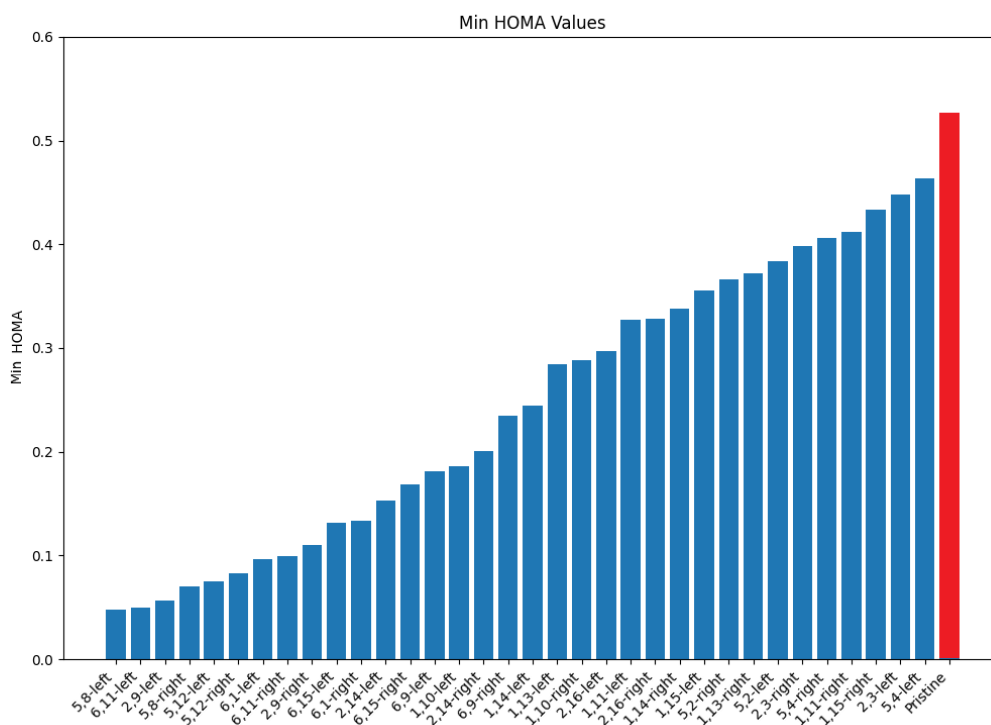


FIGURE 4.5 – Bar chart of the minimum HOMA value in pristine DPT and the 34 B,N-doped SF and TADF precandidate molecules with the wB97XD/def2-TZVP optimized geometries.

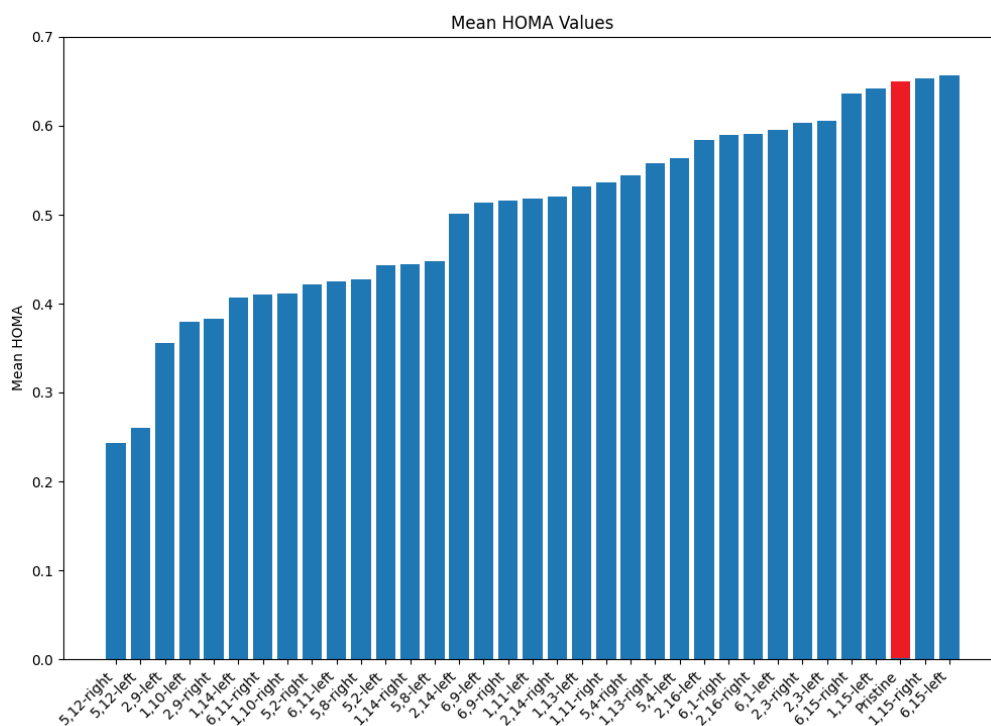


FIGURE 4.6 – Bar chart of the mean HOMA value in pristine DPT and the 34 B,N-doped SF and TADF precandidate molecules with the wB97XD/def2-TZVP optimized geometries.

Introducing the B,N pair modulates the aromaticity of the tetracene core. In each molecule that contains boron and nitrogen in different rings, the ring with the lowest HOMA contains the boron atom. Every precandidate has at least one ring with HOMA less than 0.53 (the minimum HOMA value found in pristine DPT, occurring in its leftmost ring). However, about half of the precandidates have at least one ring with HOMA greater than 0.77 (the maximum HOMA value found in pristine DPT, occurring in its third ring from left to right). All molecules have a mean HOMA smaller than pristine DPT, except for 6,15-left and 1,15-right, which have essentially the same value as pristine DPT.

## 4.4 Spin Density

Figure 4.7 shows the unpaired electron density in the rings and how the boron and nitrogen atoms affect it.

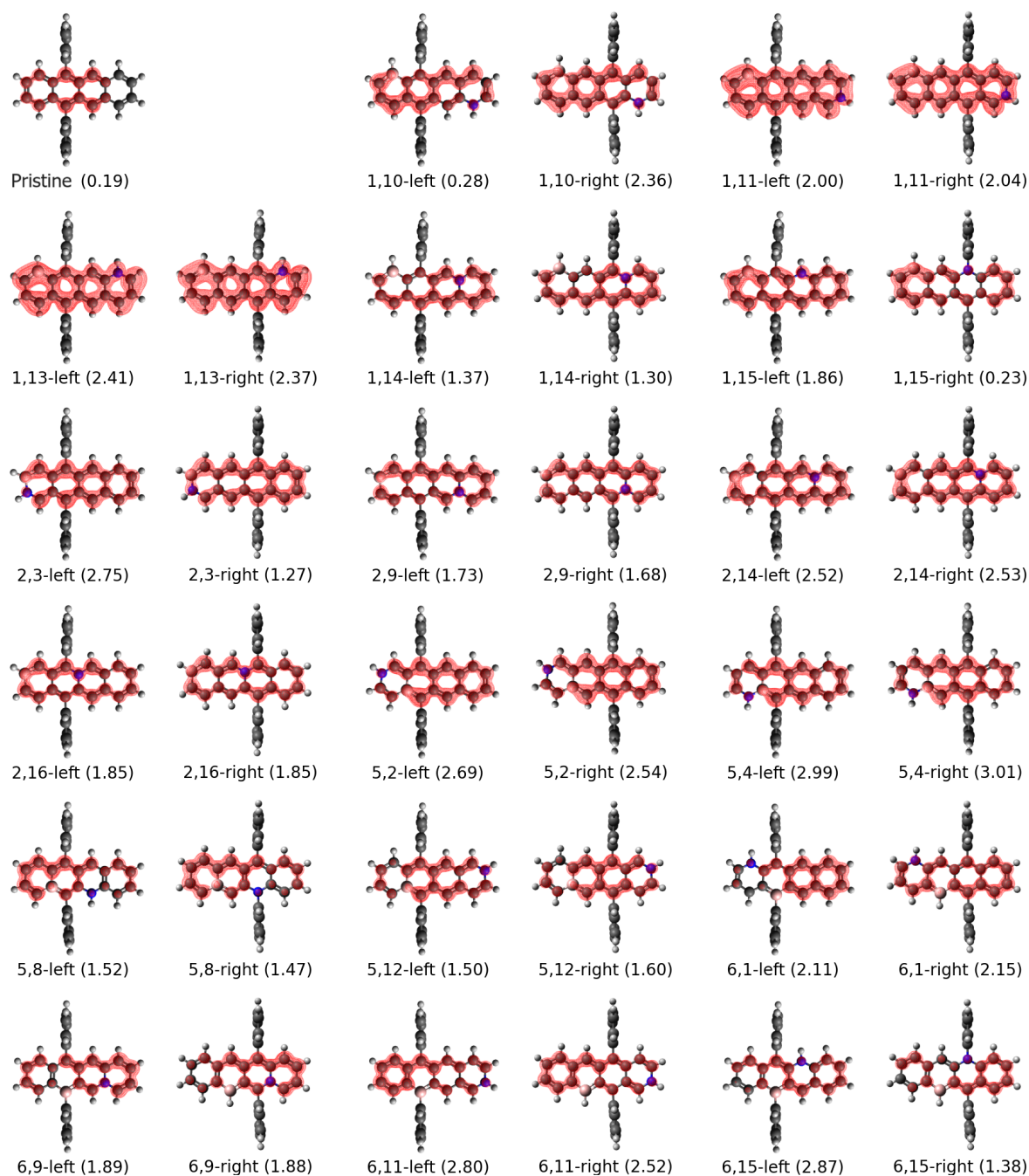


FIGURE 4.7 – Density of effectively unpaired electrons plotted with isovalue  $5 \times 10^{-4} e a_0^{-3}$  (where  $a_0$  is the Bohr radius) and the number of effectively unpaired electrons given in parentheses for each molecule.

A significant correlation can be seen between  $N_U$  values in B,N-DPT-left and the corresponding B,N-DPT-right. There are only four outlier pairs, namely 1,10 (left and right), 1,15 (left and right), 2,3 (left and right), and 6,15 (left and right), where the  $N_U$  values vary significantly when the position of the phenyl rings attached to the tetracene core is changed.

An interesting result is that no analyzed B,N-DPT molecule has a lower  $N_U$  than pristine DPT. This differs from the results in our previous work on B,N-tetracene. There

were TADF candidates with  $N_U$  both higher and lower than pristine tetracene.

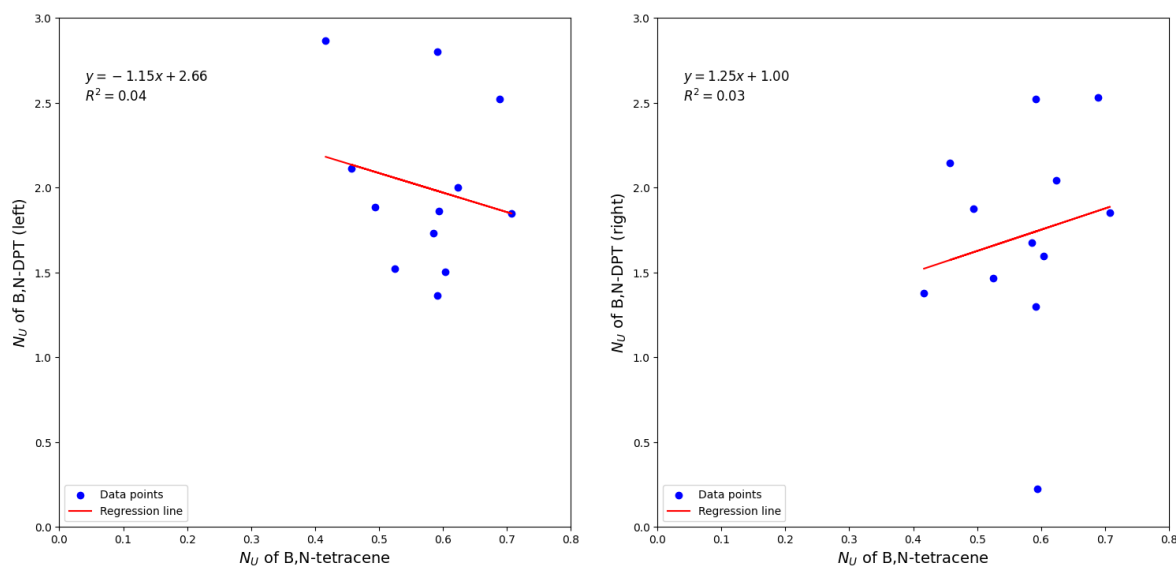


FIGURE 4.8 – Linear regression of  $N_U$  values for twelve selected B,N-DPT molecules compared with the corresponding counterparts (the B,N-tetracene TADF candidates): (left subplot) B,N-DPT-(left) molecules versus B,N-tetracene, (right subplot) B,N-DPT-(right) molecules versus B,N-tetracene.

Figure 4.8 shows, through linear regressions, how the  $N_U$  values in selected B,N-DPT molecules (that correspond to the twelve B,N-tetracene TADF candidates) are correlated to the corresponding values in the B,N-tetracene counterparts. It can be seen that there is no correlation, as indicated by the  $R^2$  values close to zero in the two subplots. Thus, the sequence of chemical stability in the B,N-DPT molecules is likely to be different from the sequence in the B,N-tetracene candidates, due to the difference in the diradicaloid characters. Even so, only one B,N-DPT molecule (1,15-right) was indicated to have a lower  $N_U$  value than its B,N-tetracene counterpart.

# 5 Conclusion

This dissertation aimed to assess the prospective candidates for SF and TADF in B,N-substituted 5,12-diphenyltetracene (DPT). The primary objective was to explore the potential of these substituted acene derivatives as advanced materials for organic electronics, particularly in OLEDs and solar cells. Through a combination of computational methods, including CASPT2 and MRAQCC, we systematically investigated the electronic properties, aromaticity, and stability of these compounds.

## 5.1 Summary of Findings

Our previous research on B,N-doped tetracenes and their derivatives has been focused on exploring the modulation of diradicaloid character and excitonic properties to identify promising candidates for SF and TADF. Building upon the foundational work by Pinheiro Jr. *et al.* and subsequent studies by our research group, we aimed to scrutinize a comprehensive set of B,N-DPT molecules using multireference quantum chemistry methods.

Previous studies identified five B,N-tetracene molecules meeting the criteria for SF. For TADF, twelve candidates were identified, five of which were likely to emit in the visible range.

In our current work, used CASPT2(8,8) and MRAQCC(8,8) methods. The primary findings from our B,N-DPT studies are as follows:

1. Energies and Excited States: Pristine DPT exhibited significantly higher  $E(S_1)$  and  $\Delta E_{ST}$  values compared to B,N-doped precandidates. Notably, no B,N-DPT molecules fulfilled the SF criteria, with  $E(S_1) \geq 2E(T_1)$ . However, our calculations showed that several B,N-substituted derivatives have  $\Delta E_{ST}$  values leading to efficient reverse intersystem crossing, thus supporting their potential as TADF candidates. Specifically, 11 pairs of molecules were identified as promising TADF candidates, six of which are likely to emit visible light.

2. HOMA Index and Aromaticity: The introduction of B and N atoms modulated the

aromaticity of the tetracene core, as evidenced by the HOMA index values. Most B,N-DPT molecules displayed lower mean HOMA values compared to pristine DPT, indicating changes in aromatic stability and electronic distribution due to doping.

3. Spin Density and Diradicaloid Character: The density of effectively unpaired electrons ( $N_U$ ) in B,N-DPT molecules was generally higher than in pristine DPT. This contrasted with the previous B,N-tetracene results, where some TADF candidates exhibited lower  $N_U$  values than pristine tetracene. Linear regression analysis showed low correlation between  $N_U$  values in B,N-DPT and B,N-tetracene, suggesting different sequences of chemical stability and diradicaloid character.

## 5.2 Implications and Future Work

The identification of TADF candidates among B,N-DPT molecules, particularly those emitting in the visible range, is promising for the development of efficient OLEDs.

Future work should focus on the following directions:

1. Extended Computational Studies: Employing larger active spaces and higher-level quantum chemical methods could provide more accurate predictions and insights into the electronic properties of potential candidates.

2. Experimental Validation: Synthesis and experimental testing of the identified TADF candidates will be crucial to validate the theoretical predictions and assess their practical applicability in OLEDs and other optoelectronic devices.

3. Alternative Doping Strategies: Beyond the specific B,N-substituted DPT molecules investigated here, the principles and methodologies developed can be applied to a broader range of polycyclic aromatic hydrocarbons. Exploring different substitution patterns and heteroatoms could yield a diverse array of compounds with tailored electronic properties for various applications. The exploration of B,N-doping in other acenes and larger PAHs could also reveal new candidates for SF and TADF.

4. Structure-Property Relationships: Developing a deeper understanding of the relationship between molecular structure and electronic properties will aid in the rational design of future candidates with tailored properties for specific applications.

## 5.3 Concluding Remarks

In conclusion, this dissertation has successfully identified and characterized a set of promising candidates for TADF in B,N-substituted 5,12-diphenyltetracene. Although no

suitable SF candidates were found among the B,N-DPT derivatives, the study's findings underscore the potential of these compounds to advance the field of organic electronics.

Future research should focus on the experimental validation of these computational predictions, as well as the exploration of additional molecular architectures to fully realize the potential of these findings. The continued development and refinement of computational methods will be essential in guiding the design of next-generation organic semiconductors.

# Bibliography

AIZAWA, N.; PU, Y.-J.; HARABUCHI, Y.; NIHONYANAGI, A.; IBUKA, R.; INUZUKA, H.; DHARA, B.; KOYAMA, Y.; NAKAYAMA, K.-I.; MAEDA, S.; ARAOKA, F.; MIYAJIMA, D. Delayed fluorescence from inverted singlet and triplet excited states. **Nature**, v. 609, n. 7927, p. 502–506, Sept. 2022.

ALVERTIS, A. M.; LUKMAN, S.; HELE, T. J. H.; FUEMMELER, E. G.; FENG, J.; WU, J.; GREENHAM, N. C.; CHIN, A. W.; MUSSER, A. J. Switching between coherent and incoherent singlet fission via Solvent-Induced symmetry breaking. **J. Am. Chem. Soc.**, v. 141, n. 44, p. 17558–17570, Nov. 2019.

AMANO, H.; KITO, M.; HIRAMATSU, K.; AKASAKI, I. P-Type conduction in Mg-Doped GaN treated with Low-Energy electron beam irradiation (LEEBI). **Jpn. J. Appl. Phys.**, v. 28, n. 12A, p. L2112, Dec. 1989.

ANTHONY, J. E. The larger acenes: versatile organic semiconductors. **Angew. Chem. Int. Ed Engl.**, v. 47, n. 3, p. 452–483, 2008.

ARIAS, D. H.; RYERSON, J. L.; COOK, J. D.; DAMRAUER, N. H.; JOHNSON, J. C. Polymorphism influences singlet fission rates in tetracene thin films. **Chem. Sci.**, v. 7, n. 2, p. 1185–1191, Feb. 2016.

BAE, Y. J.; KANG, G.; MALLIAKAS, C. D.; NELSON, J. N.; ZHOU, J.; YOUNG, R. M.; WU, Y.-L.; DUYNNE, R. P. V.; SCHATZ, G. C.; WASIELEWSKI, M. R. Singlet fission in 9,10-bis(phenylethynyl)anthracene thin films. **J. Am. Chem. Soc.**, v. 140, n. 45, p. 15140–15144, Nov. 2018.

BALDO, M. A.; LAMANSKY, S.; BURROWS, P. E.; THOMPSON, M. E.; FORREST, S. R. Very high-efficiency green organic light-emitting devices based on electrophosphorescence. **Appl. Phys. Lett.**, v. 75, n. 1, p. 4–6, July 1999.

BALDO, M. A.; O'BRIEN, D. F.; THOMPSON, M. E.; FORREST, S. R. Excitonic singlet-triplet ratio in a semiconducting organic thin film. **Phys. Rev. B Condens. Matter**, v. 60, n. 20, p. 14422–14428, Nov. 1999.

BALDO, M. A.; O'BRIEN, D. F.; YOU, Y.; SHOUSTIKOV, A.; SIBLEY, S.; THOMPSON, M. E.; FORREST, S. R. Highly efficient phosphorescent emission from organic electroluminescent devices. **Nature**, v. 395, p. 151–154, Sept. 1998.

- BALDO, M. A.; THOMPSON, M. E.; FORREST, S. R. High-efficiency fluorescent organic light-emitting devices using a phosphorescent sensitizer. **Nature**, v. 403, n. 6771, p. 750–753, Feb. 2000.
- BASEL, B. S.; HETZER, C.; ZIRZLMEIER, J.; THIEL, D.; GULDI, R.; HAMPEL, F.; KAHNT, A.; CLARK, T.; GULDI, D. M.; TYKWINSKI, R. R. Davydov splitting and singlet fission in excitonically coupled pentacene dimers. **Chem. Sci.**, v. 10, n. 13, p. 3854–3863, Apr. 2019.
- BASEL, B. S.; ZIRZLMEIER, J.; HETZER, C.; PHELAN, B. T.; KRZYANIAK, M. D.; REDDY, S. R.; COTO, P. B.; HORWITZ, N. E.; YOUNG, R. M.; WHITE, F. J.; HAMPEL, F.; CLARK, T.; THOSS, M.; TYKWINSKI, R. R.; WASIELEWSKI, M. R.; GULDI, D. M. Unified model for singlet fission within a non-conjugated covalent pentacene dimer. **Nat. Commun.**, v. 8, p. 15171, May 2017.
- BAUERNSCHMITT, R.; AHLRICHS, R. Treatment of electronic excitations within the adiabatic approximation of time dependent density functional theory. **Chem. Phys. Lett.**, v. 256, n. 4, p. 454–464, July 1996.
- BAYLISS, S. L.; THORLEY, K. J.; ANTHONY, J. E.; BOUCHIAT, H.; GREENHAM, N. C.; CHEPELIANSKII, A. D. Localization length scales of triplet excitons in singlet fission materials. **Phys. Rev. B Condens. Matter**, v. 92, n. 11, p. 115432, Sept. 2015.
- BETTANIN, F.; FERRÃO, L. F. A.; PINHEIRO JR, M.; AQUINO, A. J. A.; LISCHKA, H.; MACHADO, F. B. C.; NACHTIGALLOVA, D. Singlet  $1a$  and  $1b$  bands for N-Acenes ( $n = 2-7$ ): A CASSCF/CASPT2 study. **J. Chem. Theory Comput.**, v. 13, n. 9, p. 4297–4306, Sept. 2017.
- BHARATHAN, J.; YANG, Y. Polymer electroluminescent devices processed by inkjet printing: I. polymer light-emitting logo. **Appl. Phys. Lett.**, v. 72, p. 2660, May 1998.
- BHATTACHARYYA, K.; DATTA, A. Polymorphism controlled singlet fission in TIPS-Anthracene: Role of stacking orientation. **J. Phys. Chem. C**, v. 121, n. 3, p. 1412–1420, Jan. 2017.
- BIERMANN, D.; SCHMIDT, W. Diels-Alder reactivity of polycyclic aromatic hydrocarbons. 1. acenes and benzologs. **J. Am. Chem. Soc.**, v. 102, n. 9, p. 3163–3173, Apr. 1980.
- BROCH, K.; DIETERLE, J.; BRANCHI, F.; HESTAND, N. J.; OLIVIER, Y.; TAMURA, H.; CRUZ, C.; NICHOLS, V. M.; HINDERHOFER, A.; BELJONNE, D.; SPANO, F. C.; CERULLO, G.; BARDEEN, C. J.; SCHREIBER, F. Robust singlet fission in pentacene thin films with tuned charge transfer interactions. **Nat. Commun.**, v. 9, n. 1, p. 954, Mar. 2018.
- BROWN, A. R.; PICHLER, K.; GREENHAM, N. C.; BRADLEY, D. D. C.; FRIEND, R. H.; HOLMES, A. B. Optical spectroscopy of triplet excitons and charged excitations in poly(p-phenylenevinylene) light-emitting diodes. **Chem. Phys. Lett.**, v. 210, n. 1, p. 61–66, July 1993.

- BUDDEN, P. J.; WEISS, L. R.; MÜLLER, M.; PANJWANI, N. A.; DOWLAND, S.; ALLARDICE, J. R.; GANSCHOW, M.; FREUDENBERG, J.; BEHREND, J.; BUNZ, U. H. F.; FRIEND, R. H. Singlet exciton fission in a modified acene with improved stability and high photoluminescence yield. **Nat. Commun.**, v. 12, n. 1, p. 1527, Mar. 2021.
- BUNGE, A. Electronic wavefunctions for atoms. III. partition of degenerate spaces and ground state of C. **J. Chem. Phys.**, v. 53, n. 1, p. 20–28, July 1970.
- BURDETT, J. J.; BARDEEN, C. J. Quantum beats in crystalline tetracene delayed fluorescence due to triplet pair coherences produced by direct singlet fission. **J. Am. Chem. Soc.**, v. 134, n. 20, p. 8597–8607, May 2012.
- BURDETT, J. J.; MÜLLER, A. M.; GOSZTOLA, D.; BARDEEN, C. J. Excited state dynamics in solid and monomeric tetracene: The roles of superradiance and exciton fission. **J. Chem. Phys.**, v. 133, n. 14, p. 144506, Oct. 2010.
- BUSBY, E.; XIA, J.; WU, Q.; LOW, J. Z.; SONG, R.; MILLER, J. R.; ZHU, X.-Y.; CAMPOS, L. M.; SFEIR, M. Y. A design strategy for intramolecular singlet fission mediated by charge-transfer states in donor-acceptor organic materials. **Nat. Mater.**, v. 14, n. 4, p. 426–433, Apr. 2015.
- CASANOVA, D. Electronic structure study of singlet fission in tetracene derivatives. **J. Chem. Theory Comput.**, v. 10, n. 1, p. 324–334, Jan. 2014.
- CHAI, J.-D.; HEAD-GORDON, M. Long-range corrected hybrid density functionals with damped atom–atom dispersion corrections. **Phys. Chem. Chem. Phys.**, v. 10, n. 44, p. 6615–6620, Nov. 2008.
- CHAKRABORTY, S.; KAYASTHA, P.; RAMAKRISHNAN, R. The chemical space of b, n-substituted polycyclic aromatic hydrocarbons: Combinatorial enumeration and high-throughput first-principles modeling. **J. Chem. Phys.**, v. 150, n. 11, p. 114106, Mar. 2019.
- CHAN, M. Y.; LAI, S. L.; FUNG, M. K.; LEE, C. S.; LEE, S. T. Doping-induced efficiency enhancement in organic photovoltaic devices. **Appl. Phys. Lett.**, v. 90, n. 2, p. 023504, Jan. 2007.
- CHAN, W.-L.; BERKELBACH, T. C.; PROVORSE, M. R.; MONAHAN, N. R.; TRITSCH, J. R.; HYBERTSEN, M. S.; REICHMAN, D. R.; GAO, J.; ZHU, X.-Y. The quantum coherent mechanism for singlet fission: experiment and theory. **Acc. Chem. Res.**, v. 46, n. 6, p. 1321–1329, June 2013.
- CHAN, W.-L.; LIGGES, M.; JAILAUBEKOV, A.; KAAKE, L.; MIAJA-AVILA, L.; ZHU, X.-Y. Observing the multiexciton state in singlet fission and ensuing ultrafast multielectron transfer. **Science**, v. 334, n. 6062, p. 1541–1545, 2011.
- CHAN, W.-L.; LIGGES, M.; ZHU, X.-Y. The energy barrier in singlet fission can be overcome through coherent coupling and entropic gain. **Nat. Chem.**, v. 4, n. 10, p. 840–845, Oct. 2012.

CHEN, Y.; SHEN, L.; LI, X. Effects of heteroatoms of tetracene and pentacene derivatives on their stability and singlet fission. **J. Phys. Chem. A**, v. 118, n. 30, p. 5700–5708, July 2014.

DAIBER, B.; MAITI, S.; FERRO, S. M.; BODIN, J.; BOOM, A. F. J. van den; LUXEMBOURG, S. L.; KINGE, S.; PUJARI, S. P.; ZUILHOF, H.; SIEBBELES, L. D. A.; EHRLER, B. Change in tetracene polymorphism facilitates triplet transfer in singlet Fission-Sensitized silicon solar cells. **J. Phys. Chem. Lett.**, v. 11, n. 20, p. 8703–8709, Oct. 2020.

DREUW, A.; HEAD-GORDON, M. Single-Reference ab initio methods for the calculation of excited states of large molecules. **Chem. Rev.**, v. 105, n. 11, p. 4009–4037, Nov. 2005.

EINZINGER, M.; WU, T.; KOMPALLA, J. F.; SMITH, H. L.; PERKINSON, C. F.; NIENHAUS, L.; WIEGHOLD, S.; CONGREVE, D. N.; KAHN, A.; BAWENDI, M. G.; BALDO, M. A. Sensitization of silicon by singlet exciton fission in tetracene. **Nature**, v. 571, n. 7763, p. 90–94, July 2019.

FINTON, D. M.; WOLF, E. A.; ZOUTENBIER, V. S.; WARD, K. A.; BIAGGIO, I. Routes to singlet exciton fission in rubrene crystals and amorphous films. **AIP Adv.**, v. 9, n. 9, p. 095027, Sept. 2019.

FOLIE, B. D.; HABER, J. B.; REFAELY-ABRAMSON, S.; NEATON, J. B.; GINSBERG, N. S. Long-Lived correlated triplet pairs in a  $\pi$ -Stacked crystalline pentacene derivative. **J. Am. Chem. Soc.**, v. 140, n. 6, p. 2326–2335, Feb. 2018.

FRANCL, M. M.; PIETRO, W. J.; HEHRE, W. J.; BINKLEY, J. S.; GORDON, M. S.; DEFREES, D. J.; POPLE, J. A. Self-consistent molecular orbital methods. XXIII. a polarization-type basis set for second-row elements. **J. Chem. Phys.**, v. 77, n. 7, p. 3654–3665, Oct. 1982.

FRISCH, M. J.; TRUCKS, G. W.; SCHLEGEL, H. B.; SCUSERIA, G. E.; ROBB, M. A.; CHEESEMAN, J. R.; SCALMANI, G.; BARONE, V.; PETERSSON, G. A.; NAKATSUJI, H.; LI, X.; CARICATO, M.; MARENICH, A. V.; BLOINO, J.; JANESKO, B. G.; GOMPERS, R.; MENNUECCI, B.; HRATCHIAN, H. P.; ORTIZ, J. V.; IZMAYLOV, A. F.; SONNENBERG, J. L.; WILLIAMS-YOUNG, D.; DING, F.; LIPPARINI, F.; EGIDI, F.; GOINGS, J.; PENG, B.; PETRONE, A.; HENDERSON, T.; RANASINGHE, D.; ZAKRZEWSKI, V. G.; GAO, J.; REGA, N.; ZHENG, G.; LIANG, W.; HADA, M.; EHARA, M.; TOYOTA, K.; FUKUDA, R.; HASEGAWA, J.; ISHIDA, M.; NAKAJIMA, T.; HONDA, Y.; KITAO, O.; NAKAI, H.; VREVEN, T.; THROSELL, K.; MONTGOMERY Jr., J. A.; PERALTA, J. E.; OGLIARO, F.; BEARPARK, M. J.; HEYD, J. J.; BROTHERS, E. N.; KUDIN, K. N.; STAROVEROV, V. N.; KEITH, T. A.; KOBAYASHI, R.; NORMAND, J.; RAGHAVACHARI, K.; RENDELL, A. P.; BURANT, J. C.; IYENGAR, S. S.; TOMASI, J.; COSSI, M.; MILLAM, J. M.; KLENE, M.; ADAMO, C.; CAMMI, R.; OCHTERSKI, J. W.; MARTIN, R. L.; MOROKUMA, K.; FARKAS, O.; FORESMAN, J. B.; FOX, D. J. **Gaussian 09 Revision A.02**. Wallingford, CT: Gaussian, 2016.

FUEMMELE, E. G.; SANDERS, S. N.; PUN, A. B.; KUMARASAMY, E.; ZENG, T.; MIYATA, K.; STEIGERWALD, M. L.; ZHU, X.-Y.; SFEIR, M. Y.; CAMPOS, L. M.;

ANANTH, N. A direct mechanism of ultrafast intramolecular singlet fission in pentacene dimers. **ACS Cent Sci**, v. 2, n. 5, p. 316–324, May 2016.

GRIMME, S.; PARAC, M. Substantial errors from time-dependent density functional theory for the calculation of excited states of large pi systems. **Chemphyschem**, v. 4, n. 3, p. 292–295, Mar. 2003.

GRUMSTRUP, E. M.; JOHNSON, J. C.; DAMRAUER, N. H. Enhanced triplet formation in polycrystalline tetracene films by femtosecond optical-pulse shaping. **Phys. Rev. Lett.**, v. 105, n. 25, p. 257403, Dec. 2010.

HANNA, M. C.; NOZIK, A. J. Solar conversion efficiency of photovoltaic and photoelectrolysis cells with carrier multiplication absorbers. **J. Appl. Phys.**, v. 100, n. 7, p. 074510, Oct. 2006.

HASEGAWA, T.; TAKEYA, J. Organic field-effect transistors using single crystals. **Sci. Technol. Adv. Mater.**, v. 10, n. 2, p. 024314, Apr. 2009.

HEAD-GORDON, M. Characterizing unpaired electrons from the one-particle density matrix. **Chem. Phys. Lett.**, v. 372, n. 3, p. 508–511, Apr. 2003.

HEBNER, T. R.; WU, C. C.; MARCY, D.; LU, M. H.; STURM, J. C. Ink-jet printing of doped polymers for organic light emitting devices. **Appl. Phys. Lett.**, v. 72, n. 5, p. 519–521, Feb. 1998.

HERBERT, J. M. Visualizing and characterizing excited states from time-dependent density functional theory. **Phys. Chem. Chem. Phys.**, v. 26, n. 5, p. 3755–3794, Jan. 2024.

HONG, G.; GAN, X.; LEONHARDT, C.; ZHANG, Z.; SEIBERT, J.; BUSCH, J. M.; BRÄSE, S. A brief history of OLEDs-Emitter development and industry milestones. **Adv. Mater.**, v. 33, n. 9, 2005630, Mar. 2021.

ISHIBASHI, J. S. A.; DARGELOS, A.; DARRIGAN, C.; CHROSTOWSKA, A.; LIU, S.-Y. BN tetracene: Extending the reach of BN/CC isosterism in acenes. **Organometallics**, v. 36, n. 14, p. 2494–2497, July 2017.

JUNDT, C.; KLEIN, G.; SIPP, B.; MOIGNE, J. L.; JOUCLA, M.; VILLAEYS, A. A. Exciton dynamics in pentacene thin films studied by pump-probe spectroscopy. **Chem. Phys. Lett.**, v. 241, n. 1, p. 84–88, July 1995.

KASHA, M. Characterization of electronic transitions in complex molecules. **Discuss. Faraday Soc.**, v. 9, n. 0, p. 14–19, Jan. 1950.

KIM, H.; ZIMMERMAN, P. M. Coupled double triplet state in singlet fission. **Phys. Chem. Chem. Phys.**, v. 20, n. 48, p. 30083–30094, Dec. 2018.

KOLOMEISKY, A. B.; FENG, X.; KRYLOV, A. I. A simple kinetic model for singlet fission: A role of electronic and entropic contributions to macroscopic rates. **J. Phys. Chem. C**, v. 118, n. 10, p. 5188–5195, Mar. 2014.

KOROVINA, N. V.; DAS, S.; NETT, Z.; FENG, X.; JOY, J.; HAIGES, R.; KRYLOV, A. I.; BRADFORTH, S. E.; THOMPSON, M. E. Singlet fission in a covalently linked cofacial alkynyltetracene dimer. **J. Am. Chem. Soc.**, v. 138, n. 2, p. 617–627, Jan. 2016.

- KOROVINA, N. V.; JOY, J.; FENG, X.; FELTENBERGER, C.; KRYLOV, A. I.; BRADFORTH, S. E.; THOMPSON, M. E. Linker-Dependent singlet fission in tetracene dimers. **J. Am. Chem. Soc.**, v. 140, n. 32, p. 10179–10190, Aug. 2018.
- KRUSZEWSKI, J.; KRYGOWSKI, T. M. Definition of aromaticity basing on the harmonic oscillator model. **Tetrahedron Lett.**, v. 13, n. 36, p. 3839–3842, 1972.
- KRYGOWSKI, T. M. Crystallographic studies of inter- and intramolecular interactions reflected in aromatic character of  $\pi$ -electron systems. **J. Chem. Inf. Comput. Sci.**, v. 33, n. 1, p. 70–78, Jan. 1993.
- KRYGOWSKI, T. M.; CYRAŃSKI, M. K. Structural aspects of aromaticity. **Chem. Rev.**, v. 101, n. 5, p. 1385–1419, May 2001.
- LANZANI, G.; CERULLO, G.; ZAVELANI-ROSSI, M.; SILVESTRI, S. D.; COMORETTO, D.; MUSSO, G.; DELLEPIANE, G. Triplet-Exciton generation mechanism in a new soluble (Red-Phase) polydiacetylene. **Phys. Rev. Lett.**, v. 87, n. 18, p. 187402, Oct. 2001.
- LEE, J.; JADHAV, P.; BALDO, M. A. High efficiency organic multilayer photodetectors based on singlet exciton fission. **Appl. Phys. Lett.**, v. 95, n. 3, p. 033301, July 2009.
- LEE, J.; JADHAV, P.; REUSSWIG, P. D.; YOST, S. R.; THOMPSON, N. J.; CONGREVE, D. N.; HONTZ, E.; VOORHIS, T. V.; BALDO, M. A. Singlet exciton fission photovoltaics. **Acc. Chem. Res.**, v. 46, n. 6, p. 1300–1311, June 2013.
- LI, J.; CAO, H.; ZHANG, Z.; LIU, S.; XIA, Y. Research progress on singlet fission in acenes and their derivatives. **Photonics**, v. 9, n. 10, p. 689, Sept. 2022.
- LISCHKA, H.; MÜLLER, T.; SZALAY, P. G.; SHAVITT, I.; PITZER, R. M.; SHEPARD, R. Columbus—a program system for advanced multireference theory calculations. **Wiley Interdiscip. Rev. Comput. Mol. Sci.**, v. 1, n. 2, p. 191–199, Mar. 2011.
- LISCHKA, H.; SHEPARD, R.; PITZER, R. M.; SHAVITT, I.; DALLOS, M.; MÜLLER, T.; SZALAY, P. G.; SETH, M.; KEDZIORA, G. S.; YABUSHITA, S.; ZHANG, Z. High-level multireference methods in the quantum-chemistry program system COLUMBUS: Analytic MR-CISD and MR-AQCC gradients and MR-AQCC-LRT for excited states, GUGA spin-orbit CI and parallel CI density. **Phys. Chem. Chem. Phys.**, v. 3, n. 5, p. 664–673, Jan. 2001.
- LIU, B.; MCLEAN, A. D. Accurate calculation of the attractive interaction of two ground state helium atoms. **J. Chem. Phys.**, v. 59, n. 8, p. 4557–4558, Oct. 1973.
- LUKMAN, S.; CHEN, K.; HODGKISS, J. M.; TURBAN, D. H. P.; HINE, N. D. M.; DONG, S.; WU, J.; GREENHAM, N. C.; MUSSER, A. J. Tuning the role of charge-transfer states in intramolecular singlet exciton fission through side-group engineering. **Nat. Commun.**, v. 7, p. 13622, Dec. 2016.
- LUTHER, J. M.; JOHNSON, J. C. An exciting boost for solar cells. **Nature**, v. 571, p. 38–39, July 2019.

MA, L.; ZHANG, K.; KLOC, C.; SUN, H.; MICHEL-BEYERLE, M. E.; GURZADYAN, G. G. Singlet fission in rubrene single crystal: direct observation by femtosecond pump-probe spectroscopy. **Phys. Chem. Chem. Phys.**, v. 14, n. 23, p. 8307–8312, June 2012.

MA, L.; ZHANG, K.; KLOC, C.; SUN, H.; SOCI, C.; MICHEL-BEYERLE, M. E.; GURZADYAN, G. G. Fluorescence from rubrene single crystals: Interplay of singlet fission and energy trapping. **Phys. Rev. B Condens. Matter**, v. 87, n. 20, p. 201203, May 2013.

MADURA, I. D.; KRYGOWSKI, T. M.; CYRAŃSKI, M. K. Structural aspects of the aromaticity of cyclic  $\pi$ -electron systems with BN bonds. **Tetrahedron**, v. 54, n. 49, p. 14913–14918, Dec. 1998.

MARGULIES, E. A.; LOGSDON, J. L.; MILLER, C. E.; MA, L.; SIMONOFF, E.; YOUNG, R. M.; SCHATZ, G. C.; WASIELEWSKI, M. R. Direct observation of a Charge-Transfer state preceding High-Yield singlet fission in terrylenediimide thin films. **J. Am. Chem. Soc.**, v. 139, n. 2, p. 663–671, Jan. 2017.

MASTRON, J. N.; ROBERTS, S. T.; MCANALLY, R. E.; THOMPSON, M. E.; BRADFORTH, S. E. Aqueous colloidal acene nanoparticles: a new platform for studying singlet fission. **J. Phys. Chem. B**, v. 117, n. 49, p. 15519–15526, Dec. 2013.

MATSUI, K.; ODA, S.; YOSHIURA, K.; NAKAJIMA, K.; YASUDA, N.; HATAKEYAMA, T. One-Shot multiple borylation toward BN-Doped nanographenes. **J. Am. Chem. Soc.**, v. 140, n. 4, p. 1195–1198, Jan. 2018.

MATSUOKA, W.; KAWAHARA, K. P.; ITO, H.; SARLAH, D.; ITAMI, K.  $\pi$ -Extended rubrenes via dearomative annulative  $\pi$ -Extension reaction. **J. Am. Chem. Soc.**, v. 145, n. 1, p. 658–666, Jan. 2023.

MCGARRY, K. A.; XIE, W.; SUTTON, C.; RISKO, C.; WU, Y.; YOUNG JR, V. G.; BRÉDAS, J.-L.; FRISBIE, C. D.; DOUGLAS, C. J. Rubrene-Based Single-Crystal organic semiconductors: Synthesis, electronic structure, and Charge-Transport properties. **Chem. Mater.**, v. 25, n. 11, p. 2254–2263, June 2013.

MERRIFIELD, R. E.; AVAKIAN, P.; GROFF, R. P. Fission of singlet excitons into pairs of triplet excitons in tetracene crystals. **Chem. Phys. Lett.**, v. 3, n. 3, p. 155–157, Mar. 1969.

MINAEV, B.; BARYSHNIKOV, G.; AGREN, H. Principles of phosphorescent organic light emitting devices. **Phys. Chem. Chem. Phys.**, v. 16, n. 5, p. 1719–1758, Feb. 2014.

MIRJANI, F.; RENAUD, N.; GORCZAK, N.; GROZEMA, F. C. Theoretical investigation of singlet fission in molecular dimers: The role of charge transfer states and quantum interference. **J. Phys. Chem. C**, v. 118, n. 26, p. 14192–14199, July 2014.

MIYATA, K.; KURASHIGE, Y.; WATANABE, K.; SUGIMOTO, T.; TAKAHASHI, S.; TANAKA, S.; TAKEYA, J.; YANAI, T.; MATSUMOTO, Y. Coherent singlet fission activated by symmetry breaking. **Nat. Chem.**, v. 9, n. 10, p. 983–989, Oct. 2017.

- MORRISON, A. F.; HERBERT, J. M. Evidence for singlet fission driven by vibronic coherence in crystalline tetracene. **J. Phys. Chem. Lett.**, v. 8, n. 7, p. 1442–1448, Apr. 2017.
- MÜLLER, A. M.; AVLASEVICH, Y. S.; SCHOELLER, W. W.; MÜLLEN, K.; BARDEEN, C. J. Exciton fission and fusion in bis(tetracene) molecules with different covalent linker structures. **J. Am. Chem. Soc.**, v. 129, n. 46, p. 14240–14250, Nov. 2007.
- NAGAMI, T.; MIYAMOTO, H.; YOSHIDA, W.; OKADA, K.; TONAMI, T.; NAKANO, M. Theoretical molecular design of phenanthrenes for singlet fission by Diazadibora-Substitution. **J. Phys. Chem. A**, v. 124, n. 34, p. 6778–6789, Aug. 2020.
- NAKAMURA, S.; SENOH, M.; IWASA, N.; NAGAHAMA, S.-I. N. S.-I. High-Brightness InGaN blue, green and yellow Light-Emitting diodes with quantum well structures. **Jpn. J. Appl. Phys.**, v. 34, n. 7A, p. L797, July 1995.
- NAKAMURA, S.; SENOH, M.; NAGAHAMA, S.-I.; IWASA, N.; YAMADA, T.; MATSUSHITA, T.; KIYOKU, H.; SUGIMOTO, Y. InGaN-Based Multi-Quantum-Well-Structure laser diodes. **Jpn. J. Appl. Phys.**, v. 35, p. L74–L76, Jan. 1996.
- NELSON, C. A.; MONAHAN, N. R.; ZHU, X.-Y. Exceeding the Shockley–Queisser limit in solar energy conversion. **Energy Environ. Sci.**, v. 6, n. 12, p. 3508–3519, Nov. 2013.
- NOBEL FOUNDATION. **The Nobel Prize in Physics 2014**. Stockholm: Nobel Prize Outreach, 2023. Available at: <https://www.nobelprize.org/prizes/physics/2014/>. Accessed: June 6, 2023.
- O'BRIEN, D. F.; BALDO, M. A.; THOMPSON, M. E.; FORREST, S. R. Improved energy transfer in electrophosphorescent devices. **Appl. Phys. Lett.**, v. 74, n. 3, p. 442–444, Jan. 1999.
- PENSACK, R. D.; TILLEY, A. J.; GRIECO, C.; PURDUM, G. E.; OSTROUMOV, E. E.; GRANGER, D. B.; OBLINSKY, D. G.; DEAN, J. C.; DOUCETTE, G. S.; ASBURY, J. B.; LOO, Y.-L.; SEFEROS, D. S.; ANTHONY, J. E.; SCHOLE, G. D. Striking the right balance of intermolecular coupling for high-efficiency singlet fission. **Chem. Sci.**, v. 9, n. 29, p. 6240–6259, Aug. 2018.
- PETERSILKA, M.; GOSSMANN, U. J.; GROSS, E. K. U. Excitation energies from Time-Dependent Density-Functional theory. **Phys. Rev. Lett.**, v. 76, n. 8, p. 1212–1215, Feb. 1996.
- PETERSSON, G. A.; BENNETT, A.; TENSFELDT, T.; AL-LAHAM, M.; SHIRLEY, W.; MANTZARIS, J. A complete basis set model chemistry. i. the total energies of closed-shell atoms and hydrides of the first-row elements. **J. Chem. Phys.**, v. 89, p. 2193–2218, Aug. 1988.
- PILAND, G. B.; BURDETT, J. J.; KURUNTHU, D.; BARDEEN, C. J. Magnetic field effects on singlet fission and fluorescence decay dynamics in amorphous rubrene. **J. Phys. Chem. C**, v. 117, n. 3, p. 1224–1236, Jan. 2013.
- PIMENTEL, J. V. M. **Investigation of singlet fission in B,N-substituted tetracene**. 2023. Monograph - Instituto Tecnológico de Aeronáutica, São José dos Campos, 2023.

- PIMENTEL, J. V. M. **Study of B,N-substituted tetracene derivatives for use in OLED technology**. 2023. Senior thesis (Electronic Engineering) - Instituto Tecnológico de Aeronáutica, São José dos Campos, 2023.
- PIMENTEL, J. V. M.; PINHEIRO JR., M.; AQUINO, A. J. A.; LISCHKA, H.; MACHADO, F. B. C. Exploring thermally activated delayed fluorescence in b,n-substituted tetracene derivatives: Towards enhanced oled materials. In preparation, 2024.
- PINHEIRO, M.; FERRÃO, L. F. A.; BETTANIN, F.; AQUINO, A. J. A.; MACHADO, F. B. C.; LISCHKA, H. How to efficiently tune the biradicaloid nature of acenes by chemical doping with boron and nitrogen. **Phys. Chem. Chem. Phys.**, v. 19, n. 29, p. 19225–19233, July 2017.
- PINHEIRO, M.; MACHADO, F. B. C.; PLASSER, F.; AQUINO, A. J. A.; LISCHKA, H. A systematic analysis of excitonic properties to seek optimal singlet fission: the BN-substitution patterns in tetracene. **J. Mater. Chem. C**, v. 8, n. 23, p. 7793–7804, June 2020.
- PINHEIRO, M.; MACHADO, F. B. C.; PLASSER, F.; AQUINO, A. J. A.; LISCHKA, H. A systematic analysis of excitonic properties to seek optimal singlet fission: the BN-substitution patterns in tetracene. **J. Mater. Chem.**, v. 8, n. 23, p. 7793–7804, June 2020.
- PLASSER, F. TheoDORE: A toolbox for a detailed and automated analysis of electronic excited state computations. **J. Chem. Phys.**, v. 152, n. 8, p. 084108, Feb. 2020.
- RAMANAN, C.; SMEIGH, A. L.; ANTHONY, J. E.; MARKS, T. J.; WASIELEWSKI, M. R. Competition between singlet fission and charge separation in solution-processed blend films of 6,13-bis(triisopropylsilylethynyl)pentacene with sterically-encumbered perylene-3,4:9,10-bis(dicarboximide)s. **J. Am. Chem. Soc.**, v. 134, n. 1, p. 386–397, Jan. 2012.
- RAO, A.; FRIEND, R. H. Harnessing singlet exciton fission to break the Shockley–Queisser limit. **Nature Reviews Materials**, v. 2, n. 11, p. 1–12, Oct. 2017.
- RAO, A.; WILSON, M. W. B.; HODGKISS, J. M.; ALBERT-SEIFRIED, S.; BÄSSLER, H.; FRIEND, R. H. Exciton fission and charge generation via triplet excitons in pentacene/c60 bilayers. **J. Am. Chem. Soc.**, v. 132, n. 36, p. 12698–12703, Sept. 2010.
- RENAUD, N.; GROZEMA, F. C. Intermolecular vibrational modes speed up singlet fission in perylenediimide crystals. **J. Phys. Chem. Lett.**, v. 6, n. 3, p. 360–365, Feb. 2015.
- ROBERTS, S. T.; MCANALLY, R. E.; MASTRON, J. N.; WEBBER, D. H.; WHITED, M. T.; BRUTCHEY, R. L.; THOMPSON, M. E.; BRADFORTH, S. E. Efficient singlet fission discovered in a disordered acene film. **J. Am. Chem. Soc.**, v. 134, n. 14, p. 6388–6400, Apr. 2012.
- ROOS, B. O.; ANDERSSON, K. Multiconfigurational perturbation theory with level shift — the cr2 potential revisited. **Chem. Phys. Lett.**, v. 245, n. 2, p. 215–223, Oct. 1995.

- ROOS, B. O.; ANDERSSON, K.; FÜLSCHER, M. P.; MALMQVIST, P.-Å.; SERRANO-ANDRÉS, L.; PIERLOOT, K.; MERCHÁN, M. Multiconfigurational perturbation theory: Applications in electronic spectroscopy. *In: PRIGOGINE, I.; RICE, S.A. Advances in Chemical Physics*. Hoboken, NJ: John Wiley & Sons, 2007, (Advances in chemical physics). p. 219–331.
- ROOS, B. O.; TAYLOR, P. R.; SIGBAHN, P. E. M. A complete active space SCF method (CASSCF) using a density matrix formulated super-CI approach. **Chem. Phys.**, v. 48, n. 2, p. 157–173, May 1980.
- RUNGE, E.; GROSS, E. K. U. Density-Functional theory for Time-Dependent systems. **Phys. Rev. Lett.**, v. 52, n. 12, p. 997–1000, Mar. 1984.
- SAKAI, H.; INAYA, R.; NAGASHIMA, H.; NAKAMURA, S.; KOBORI, Y.; TKACHENKO, N. V.; HASOBE, T. Multiexciton dynamics depending on intramolecular orientations in pentacene dimers: Recombination and dissociation of correlated triplet pairs. **J. Phys. Chem. Lett.**, v. 9, n. 12, p. 3354–3360, June 2018.
- SANDERS, S. N.; KUMARASAMY, E.; PUN, A. B.; TRINH, M. T.; CHOI, B.; XIA, J.; TAFFET, E. J.; LOW, J. Z.; MILLER, J. R.; ROY, X.; ZHU, X.-Y.; STEIGERWALD, M. L.; SFEIR, M. Y.; CAMPOS, L. M. Quantitative intramolecular singlet fission in bipentacenes. **J. Am. Chem. Soc.**, v. 137, n. 28, p. 8965–8972, July 2015.
- SANDERS, S. N.; PUN, A. B.; PARENTI, K. R.; KUMARASAMY, E.; YABLON, L. M.; SFEIR, M. Y.; CAMPOS, L. M. Understanding the bound Triplet-Pair state in singlet fission. **Chem**, v. 5, n. 8, p. 1988–2005, Aug. 2019.
- SAWAKI, N.; AKASAKI, I.; TOYODA, Y. Metalorganic vapor phase epitaxial growth of a high quality GaN film using an AlN buffer layer. **Appl. Phys. Lett.**, 1986.
- SCHULTZ, J. D.; SHIN, J. Y.; CHEN, M.; O’CONNOR, J. P.; YOUNG, R. M.; RATNER, M. A.; WASIELEWSKI, M. R. Influence of vibronic coupling on ultrafast singlet fission in a linear terrylenediimide dimer. **J. Am. Chem. Soc.**, v. 143, n. 4, p. 2049–2058, Feb. 2021.
- SEMONIN, O. E.; LUTHER, J. M.; BEARD, M. C. Quantum dots for next-generation photovoltaics. **Mater. Today**, v. 15, n. 11, p. 508–515, Nov. 2012.
- SHAH, B. K.; NECKERS, D. C.; SHI, J.; FORSYTHE, E. W.; MORTON, D. Anthanthrene derivatives as blue emitting materials for organic Light-Emitting diode applications. **Chem. Mater.**, v. 18, n. 3, p. 603–608, Feb. 2006.
- SHOCKLEY, W.; QUEISSER, H. J. Detailed balance limit of efficiency of p-n junction solar cells. **J. Appl. Phys.**, v. 32, n. 3, p. 510–519, Mar. 1961.
- SINGH, A.; HUMENIUK, A.; RÖHR, M. I. S. Energetics and optimal molecular packing for singlet fission in BN-doped perylenes: electronic adiabatic state basis screening. **Phys. Chem. Chem. Phys.**, v. 23, n. 31, p. 16525–16536, Aug. 2021.
- SINGH, S.; JONES, W. J.; SIEBRAND, W.; STOICHEFF, B. P.; SCHNEIDER, W. G. Laser generation of excitons and fluorescence in anthracene crystals. **J. Chem. Phys.**, v. 42, n. 1, p. 330–342, Jan. 1965.

- SLYKE, S. A. V.; CHEN, C. H.; TANG, C. W. Organic electroluminescent devices with improved stability. **Appl. Phys. Lett.**, v. 69, n. 15, p. 2160–2162, Oct. 1996.
- SMITH, M. B.; MICHL, J. Singlet fission. **Chem. Rev.**, v. 110, n. 11, p. 6891–6936, Nov. 2010.
- SMITH, M. B.; MICHL, J. Recent advances in singlet fission. **Annu. Rev. Phys. Chem.**, v. 64, p. 361–386, Jan. 2013.
- STERN, H. L.; MUSSER, A. J.; GELINAS, S.; PARKINSON, P.; HERZ, L. M.; BRUZEK, M. J.; ANTHONY, J.; FRIEND, R. H.; WALKER, B. J. Identification of a triplet pair intermediate in singlet exciton fission in solution. **Proc. Natl. Acad. Sci. U. S. A.**, v. 112, n. 25, p. 7656–7661, June 2015.
- STRATMANN, R. E.; SCUSERIA, G. E.; FRISCH, M. J. An efficient implementation of time-dependent density-functional theory for the calculation of excitation energies of large molecules. **J. Chem. Phys.**, v. 109, p. 8218–8224, Nov. 1998.
- SUNDAR, V. C.; ZAUMSEIL, J.; PODZOROV, V.; MENARD, E.; WILLETT, R. L.; SOMEYA, T.; GERSHENSON, M. E.; ROGERS, J. A. Elastomeric transistor stamps: reversible probing of charge transport in organic crystals. **Science**, v. 303, n. 5664, p. 1644–1646, Mar. 2004.
- SURESH, S. M.; DUDA, E.; HALL, D.; YAO, Z.; BAGNICH, S.; SLAWIN, A. M. Z.; BÄSSLER, H.; BELJONNE, D.; BUCK, M.; OLIVIER, Y.; KÖHLER, A.; ZYSMAN-COLMAN, E. A deep blue B,N-Doped heptacene emitter that shows both thermally activated delayed fluorescence and delayed fluorescence by Triplet–Triplet annihilation. **J. Am. Chem. Soc.**, v. 142, n. 14, p. 6588–6599, Apr. 2020.
- SUTTON, C.; TUMMALA, N. R.; BELJONNE, D.; BRÉDAS, J.-L. Singlet fission in rubrene derivatives: Impact of molecular packing. **Chem. Mater.**, v. 29, n. 7, p. 2777–2787, Apr. 2017.
- SZABO, A.; OSTLUND, N. **Modern Quantum Chemistry: Introduction to Advanced Electronic Structure Theory**. [*S.l.*]: Dover Publications, 1996. (Dover Books on Chemistry).
- TAKAHASHI, S.; WATANABE, K.; MATSUMOTO, Y. Singlet fission of amorphous rubrene modulated by polariton formation. **J. Chem. Phys.**, v. 151, n. 7, p. 074703, Aug. 2019.
- TANG, C. W. Two-layer organic photovoltaic cell. **Appl. Phys. Lett.**, v. 48, p. 183–185, Jan. 1986.
- TANG, C. W.; VANSLYKE, S. A. Organic electroluminescent diodes. **Appl. Phys. Lett.**, v. 51, p. 913–915, Sept. 1987.
- TANG, C. W.; VANSLYKE, S. A.; CHEN, C. H. Electroluminescence of doped organic thin films. **J. Appl. Phys.**, v. 65, p. 3610–3616, May 1989.
- TEMPELAAR, R.; REICHMAN, D. R. Vibronic exciton theory of singlet fission. i. linear absorption and the anatomy of the correlated triplet pair state. **J. Chem. Phys.**, v. 146, n. 17, p. 174703, May 2017.

- TEMPELAAR, R.; REICHMAN, D. R. Vibronic exciton theory of singlet fission. II. two-dimensional spectroscopic detection of the correlated triplet pair state. **J. Chem. Phys.**, v. 146, n. 17, p. 174704, May 2017.
- TEMPELAAR, R.; REICHMAN, D. R. Vibronic exciton theory of singlet fission. III. how vibronic coupling and thermodynamics promote rapid triplet generation in pentacene crystals. **J. Chem. Phys.**, v. 148, n. 24, p. 244701, June 2018.
- THOMPSON, N. J.; HONTZ, E.; CHANG, W.; VOORHIS, T. V.; BALDO, M. Magnetic field dependence of singlet fission in solutions of diphenyl tetracene. **Philosophical Transactions of the Royal Society A: Mathematical, Physical and Engineering Sciences**, v. 373, n. 2044, p. 20140323, June 2015.
- THORSMØLLE, V. K.; AVERITT, R. D.; DEMSAR, J.; SMITH, D. L.; TRETIAK, S.; MARTIN, R. L.; CHI, X.; CRONE, B. K.; RAMIREZ, A. P.; TAYLOR, A. J. Morphology effectively controls singlet-triplet exciton relaxation and charge transport in organic semiconductors. **Phys. Rev. Lett.**, v. 102, n. 1, p. 017401, Jan. 2009.
- TOMKIEWICZ, Y.; GROFF, R. P.; AVAKIAN, P. Spectroscopic approach to energetics of exciton fission and fusion in tetracene crystals. **J. Chem. Phys.**, v. 54, n. 10, p. 4504–4507, May 1971.
- UOYAMA, H.; GOUSHI, K.; SHIZU, K.; NOMURA, H.; ADACHI, C. Highly efficient organic light-emitting diodes from delayed fluorescence. **Nature**, v. 492, n. 7428, p. 234–238, Dec. 2012.
- VOLZ, D.; WALLECH, M.; FLÉCHON, C.; DANZ, M.; VERMA, A.; NAVARRO, J. M.; ZINK, D. M.; BRÄSE, S.; BAUMANN, T. From iridium and platinum to copper and carbon: new avenues for more sustainability in organic light-emitting diodes. **Green Chem.**, v. 17, n. 4, p. 1988–2011, Apr. 2015.
- WALIA, R.; YANG, J. Exploring optimal multimode vibronic pathways in singlet fission of azaborine analogues of perylene. **Photochem. Photobiol. Sci.**, v. 21, n. 9, p. 1689–1700, Sept. 2022.
- WALKER, B. J.; MUSSER, A. J.; BELJONNE, D.; FRIEND, R. H. Singlet exciton fission in solution. **Nat. Chem.**, v. 5, n. 12, p. 1019–1024, Dec. 2013.
- WANG, C.; TAUBER, M. J. High-yield singlet fission in a zeaxanthin aggregate observed by picosecond resonance raman spectroscopy. **J. Am. Chem. Soc.**, v. 132, n. 40, p. 13988–13991, Oct. 2010.
- WANG, J.; DURBEEJ, B. How accurate are TD-DFT excited-state geometries compared to DFT ground-state geometries? **J. Comput. Chem.**, v. 41, n. 18, p. 1718–1729, July 2020.
- WANG, R.; ZHANG, C.; ZHANG, B.; LIU, Y.; WANG, X.; XIAO, M. Magnetic dipolar interaction between correlated triplets created by singlet fission in tetracene crystals. **Nat. Commun.**, v. 6, p. 8602, Oct. 2015.
- WANG, X.; TOM, R.; LIU, X.; CONGREVE, D. N.; MAROM, N. An energetics perspective on why there are so few triplet–triplet annihilation emitters. **J. Mater. Chem.**, v. 8, n. 31, p. 10816–10824, Aug. 2020.

- WEIGEND, F.; AHLRICHS, R. Balanced basis sets of split valence, triple zeta valence and quadruple zeta valence quality for H to rn: Design and assessment of accuracy. **Phys. Chem. Chem. Phys.**, v. 7, n. 18, p. 3297–3305, Sept. 2005.
- WERNER, H.-J.; KNOWLES, P. J.; CELANI, P.; GYÖRFFY, W.; HESSELMANN, A.; KATS, D.; KNIZIA, G.; KÖHN, A.; KORONA, T.; KREPLIN, D.; LINDH, R.; MA, Q.; MANBY, F. R.; MITRUSHENKOV, A.; RAUHUT, G.; Schütz, M.; SHAMASUNDAR, K. R.; ADLER, T. B.; AMOS, R. D.; BENNIE, S. J.; BERNHARDSSON, A.; BERNING, A.; BLACK, J. A.; BYGRAVE, P. J.; CIMIRAGLIA, R.; COOPER, D. L.; COUGHTRIE, D.; DEEGAN, M. J. O.; DOBBYN, A. J.; DOLL, K.; DORNBACH, M.; ECKERT, F.; ERFORT, S.; GOLL, E.; HAMPEL, C.; HETZER, G.; HILL, J. G.; HODGES, M.; HRENAR, T.; JANSEN, G.; KÖPPL, C.; KOLLMAR, C.; LEE, S. J. R.; LIU, Y.; LLOYD, A. W.; MATA, R. A.; MAY, A. J.; MUSSARD, B.; MCNICHOLAS, S. J.; MEYER, W.; Miller III, T. F.; MURA, M. E.; NICKLASS, A.; O'NEILL, D. P.; PALMIERI, P.; PENG, D.; PETERSON, K. A.; PFLÜGER, K.; PITZER, R.; POLYAK, I.; REIHER, M.; RICHARDSON, J. O.; ROBINSON, J. B.; SCHRÖDER, B.; SCHWILK, M.; SHIOZAKI, T.; SIBAEV, M.; STOLL, H.; STONE, A. J.; TARRONI, R.; THORSTEINSSON, T.; TOULOUSE, J.; WANG, M.; WELBORN, M.; ZIEGLER, B. **MOLPRO, version , a package of ab initio programs**. Available at: <https://www.molpro.net>. Accessed: June 6, 2023.
- WERNER, H.-J.; KNOWLES, P. J.; KNIZIA, G.; MANBY, F. R.; SCHÜTZ, M. Molpro: a general-purpose quantum chemistry program package. **WIREs Comput Mol Sci**, v. 2, p. 242–253, 2012.
- WILSON, M. W. B.; RAO, A.; CLARK, J.; KUMAR, R. S. S.; BRIDA, D.; CERULLO, G.; FRIEND, R. H. Ultrafast dynamics of exciton fission in polycrystalline pentacene. **J. Am. Chem. Soc.**, v. 133, n. 31, p. 11830–11833, Aug. 2011.
- WONG, M. Y.; ZYSMAN-COLMAN, E. Purely organic thermally activated delayed fluorescence materials for organic Light-Emitting diodes. **Adv. Mater.**, v. 29, n. 22, June 2017.
- WU, T.; NI, W.; GURZADYAN, G. G.; SUN, L. Singlet fission from upper excited singlet states and polaron formation in rubrene film. **RSC Adv.**, v. 11, n. 8, p. 4639–4645, Jan. 2021.
- YANG, Y.; DAVIDSON, E. R.; YANG, W. Nature of ground and electronic excited states of higher acenes. **Proc. Natl. Acad. Sci. U. S. A.**, v. 113, n. 35, p. E5098–107, Aug. 2016.
- YANG, Z.; MAO, Z.; XIE, Z.; ZHANG, Y.; LIU, S.; ZHAO, J.; XU, J.; CHI, Z.; ALDRED, M. P. Recent advances in organic thermally activated delayed fluorescence materials. **Chem. Soc. Rev.**, v. 46, n. 3, p. 915–1016, Feb. 2017.
- ZBOROWSKI, K. K.; ALKORTA, I.; ELGUERO, J.; PRONIEWICZ, L. M. Calculation of the HOMA model parameters for the carbon–boron bond. **Struct. Chem.**, v. 23, n. 2, p. 595–600, Apr. 2012.
- ZENG, T.; ANANTH, N.; HOFFMANN, R. Seeking small molecules for singlet fission: a heteroatom substitution strategy. **J. Am. Chem. Soc.**, v. 136, n. 36, p. 12638–12647, Sept. 2014.

ZENG, T.; MELLERUP, S. K.; YANG, D.; WANG, X.; WANG, S.; STAMPLECOSKIE, K. Identifying (BN)2-pyrenes as a new class of singlet fission chromophores: Significance of azaborine substitution. **J. Phys. Chem. Lett.**, v. 9, n. 11, p. 2919–2927, June 2018.

ZHANG, G.; CHEN, X.-K.; XIAO, J.; CHOW, P. C. Y.; REN, M.; KUPGAN, G.; JIAO, X.; CHAN, C. C. S.; DU, X.; XIA, R.; CHEN, Z.; YUAN, J.; ZHANG, Y.; ZHANG, S.; LIU, Y.; ZOU, Y.; YAN, H.; WONG, K. S.; COROPCEANU, V.; LI, N.; BRABEC, C. J.; BREDAS, J.-L.; YIP, H.-L.; CAO, Y. Delocalization of exciton and electron wavefunction in non-fullerene acceptor molecules enables efficient organic solar cells. **Nat. Commun.**, v. 11, n. 1, p. 3943, Aug. 2020.

ZHANG, Q.; LI, J.; SHIZU, K.; HUANG, S.; HIRATA, S.; MIYAZAKI, H.; ADACHI, C. Design of efficient thermally activated delayed fluorescence materials for pure blue organic light emitting diodes. **J. Am. Chem. Soc.**, v. 134, n. 36, p. 14706–14709, Sept. 2012.

ZHANG, Y.; LEI, Y.; ZHANG, Q.; XIONG, Z. Thermally activated singlet exciton fission observed in rubrene doped organic films. **Org. Electron.**, v. 15, n. 2, p. 577–581, Feb. 2014.

ZIMMERMAN, P. M.; ZHANG, Z.; MUSGRAVE, C. B. Singlet fission in pentacene through multi-exciton quantum states. **Nat. Chem.**, v. 2, n. 8, p. 648–652, Aug. 2010.

# **Appendix A - Additional Theoretical Background**

## 2 Theoretical Background

### 2.1 LEDs and Semiconductor Theory

#### 2.1.1 Introduction to Semiconductors

Semiconductors are materials that have electrical conductivity between conductors (such as metals) and insulators (such as non-metals) (SEDRA *et al.*, 2020). Semiconductors possess an energy band structure consisting of a valence band, which is either filled (at absolute zero) or almost filled ( $T > 0$ ) with electrons, and a conduction band, which is either empty (at absolute zero) or partially filled ( $T > 0$ ).

Electrons in materials obey Fermi-Dirac statistics, which describe the behavior of particles with half-integer spin, fermions, in thermodynamic equilibrium (SAKURAI; NAPOLITANO, 2017). No two fermions can occupy the same quantum state simultaneously, due to the Pauli exclusion principle. This principle restricts the number of electrons that can occupy a particular energy level in a material, creating distinct energy bands. These bands result from the interaction of numerous atoms, on the order of 1 mole, situated in close proximity. As their atomic orbitals overlap, they undergo a splitting, giving rise to an equal number of molecular orbitals, some with greater energy and others with lower energy. However, due to the significant number of atoms involved, and consequently, a multitude of molecular orbitals, the energy spacing between them becomes exceedingly minute, on the order of approximately  $10^{-22}$  eV. Consequently, this leads to the formation of a continuum of energy levels known as a “band”, as shown in Figure 2.1.

The Fermi-Dirac distribution function provides the probability of finding an electron in a given energy state at a specific temperature, forming the foundation for understanding the electronic properties and behavior of materials.

The Fermi level refers to the energy level within a material at which the probability of finding an electron is equal to 50% at absolute zero temperature. In conductors, the Fermi level lies within the conduction band, allowing for the free movement of electrons and high conductivity. In semiconductors and insulators, it lies inside a band gap, and its position relative to the energy bands determines the behavior and conductivity characteristics

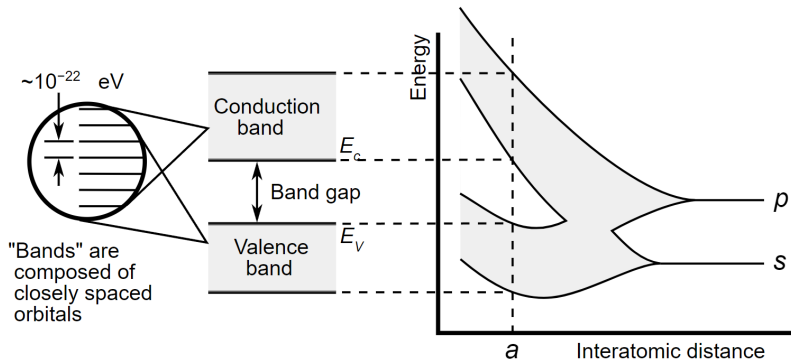


FIGURE 2.1 – Energy levels of a large number of carbon atoms as a function of the interatomic distance. When the atoms are far apart (right side of graph) each atom has discrete energy levels corresponding to the valence atomic orbitals  $2s$  and  $2p$ .  $a$  is the interatomic distance found in a diamond lattice.

of the material. In semiconductors the bands are near to the Fermi level, thus being thermally populated with charge carriers (electrons or holes). Figure 2.2 shows the band structure of some materials.

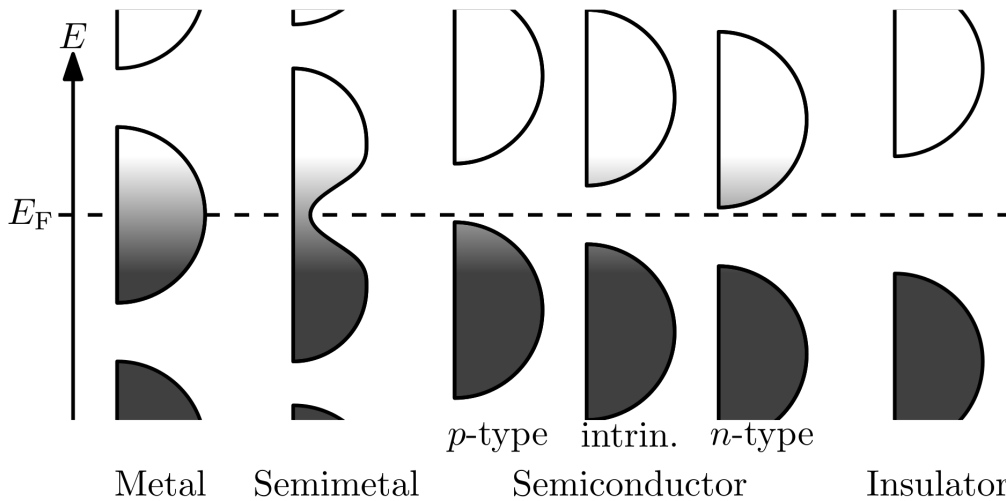


FIGURE 2.2 – Energy distribution of electrons in materials. The width represents the density of available states for a certain energy. The shade follows the Fermi–Dirac distribution (black: completely filled, white: empty).

### 2.1.2 Doping and p–n Junction

The behavior of semiconductors can be modified through a process called doping, in which impurity atoms are intentionally added to alter the concentration of charge carriers. There are  $n$ -type (electron donor) and  $p$ -type (electron acceptor) dopants.

The introduction of an n-type dopant adds extra electrons to the semiconductor lattice, increasing the concentration of negative charge carriers. Conversely, a p-type dopant introduces “holes” or vacancies in the valence band, creating an excess of positive charge carriers.

When a p-type and n-type semiconductor are brought together, they form a p–n junction. At the junction, the excess electrons from the n-side and the holes from the p-side recombine, creating a depletion region with no charge carriers.

### 2.1.3 Diodes

A diode is a two-terminal electronic component that allows the flow of electric current in only one direction. It consists of a p–n junction. When a forward bias voltage is applied to the diode, meaning the positive terminal of the voltage source is connected to the p-side and the negative terminal to the n-side, the diode conducts current. This occurs as the forward bias reduces the width of the depletion region, allowing charge carriers to flow across the junction.

On the other hand, when a reverse bias voltage is applied, meaning the positive terminal of the voltage source is connected to the n-side and the negative terminal to the p-side, the diode blocks current flow. The reverse bias widens the depletion region, preventing charge carriers from crossing the junction (RAZAVI, 2013). Figure 2.3 shows a comparison between these two operating modes.

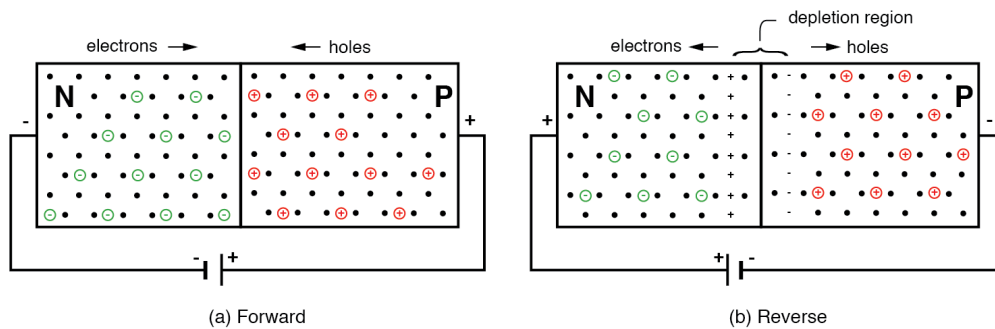


FIGURE 2.3 – Comparison of diode (p–n junction) operation under forward bias (left) and reverse bias (right). *Note.* From [www.allaboutcircuits.com](http://www.allaboutcircuits.com).

### 2.1.4 LED Operation

LEDs are diodes that emit light when an electric current passes through them. They are typically made from semiconductors which have a direct band gap. The direct band

gap allows efficient light emission. That's because in indirect band gap semiconductors (*e.g.* silicon), there occurs dissipation of energy to the surrounding crystal lattice as heat (SEDRA *et al.*, 2020). Figure 2.4 depicts the difference between direct and indirect band gap semiconductors.

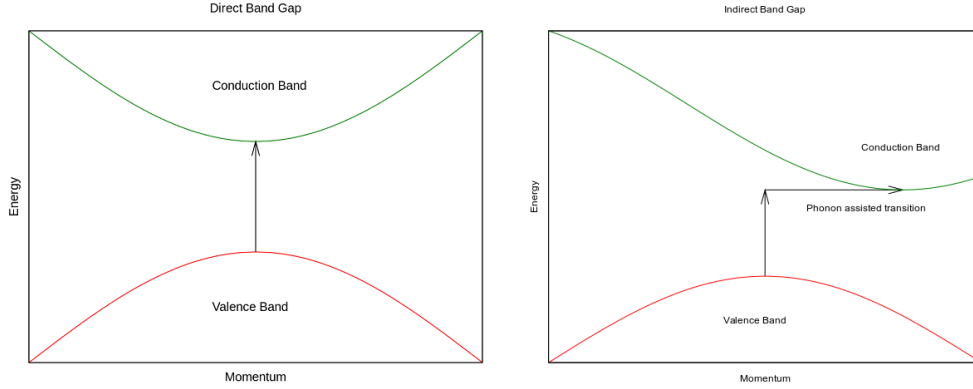


FIGURE 2.4 – Energy vs. crystal momentum in direct (left) and indirect (right) band gap semiconductors.

The crystal momentum, denoted by  $\mathbf{p}$  is associated with the motion of electrons within a crystalline material. It takes into account the periodic nature of the crystal lattice structure. The wave vector, represented by  $\mathbf{k}$ , describes the spatial variation of the wave function that characterizes the electrons in the crystal. It is related to the crystal momentum through the equation:

$$\mathbf{p} = \hbar\mathbf{k}. \quad (2.1)$$

According to Bloch's theorem (SAKURAI; NAPOLITANO, 2017), the wave function of an electron in a crystal can be expressed as the product of a periodic function, known as the Bloch function, and a plane wave. Mathematically, it can be written as:

$$\psi(\mathbf{r}) = e^{i\mathbf{k}\cdot\mathbf{r}}u(\mathbf{r}), \quad (2.2)$$

where  $\psi(\mathbf{r})$  is the wave function,  $\mathbf{k}$  is the wave vector,  $\mathbf{r}$  is the position vector, and  $u(\mathbf{r})$  is a periodic function with the same periodicity as the crystal lattice.

LEDs consist of layers of different semiconductors sandwiched together, forming a heterostructure. The light emission in LEDs is based on the phenomenon of electroluminescence. When a forward voltage is applied to the LED, electrons in the conduction band recombine with holes in the valence band. This occurs in the emissive layer (see Figure 1.1), releasing energy in the form of photons. The energy of the emitted photons is determined by the band gap of the semiconductor material used. Figure 2.5 shows the current–voltage characteristic (I-V curve) of a LED.

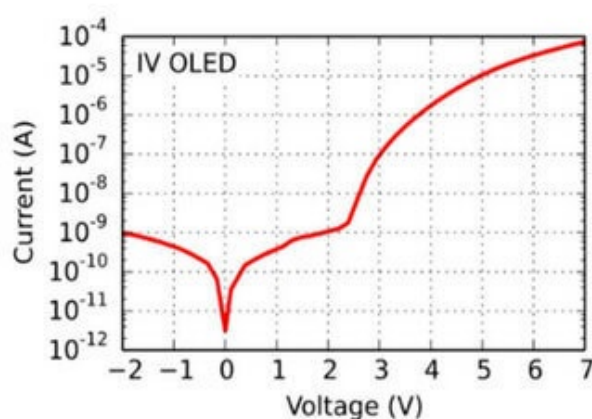


FIGURE 2.5 – Typical current-voltage curve of a LED. *Note.* The vertical axis is the absolute value of the current, in logarithmic scale. From [www.fluxim.com](http://www.fluxim.com).

## 2.2 Clarification: Isolated Molecules vs. Crystalline Solids

In Sections 1.2 and 2.1, we explored theoretical concepts like electronic bands, band gaps, and excitons. It is important to note that our discussion was centered around the implicit assumption of crystalline solids. However, in our current research, we are conducting computational studies on isolated molecules without considering their crystal structure. This approach is valid because these molecules come together to form molecular crystals or amorphous thin films, where their interactions are governed by weak intermolecular forces.

In crystalline solids held together by stronger bonds, the band structure differs significantly from that of these materials. Instead of electronic bands, these solids have discrete energy levels (or more precisely, narrow bands) that result from interactions between individual molecules. Two relevant energy levels are the highest occupied molecular orbital (HOMO) and the lowest unoccupied molecular orbital (LUMO). The energy difference between the HOMO and LUMO levels is analogous to the band gap and is referred to as the HOMO-LUMO gap in this context.

Furthermore, when we discuss excitations in this kind of molecular solids, we encounter localized (or more precisely, less delocalized) excited states as opposed to the delocalized excitons observed in crystalline solids.

## 2.3 Atomic Units and Notation

In this study, we adopt atomic units, which is a system of natural units commonly used in quantum chemistry. Atomic units simplify calculations by setting certain fundamental physical constants to unity, thereby eliminating their explicit appearance in equations. By definition, in atomic units, the following fundamental physical constants are expressed as the numeric value 1:

$$\text{Reduced Planck constant } \hbar = 1 \quad (2.3)$$

$$\text{Elementary charge } e = 1 \quad (2.4)$$

$$\text{Electron mass } m_e = 1 \quad (2.5)$$

$$\text{Coulomb constant } \frac{1}{4\pi\epsilon_0} = 1 \quad (2.6)$$

Throughout this chapter, all mathematical expressions and numerical results will be presented in atomic units unless otherwise stated. By employing dimensional analysis, one can determine the unique exponents for  $\hbar$ ,  $e$ ,  $m_e$ , and  $\frac{1}{4\pi\epsilon_0}$  in order to convert these expressions back into units with dimensions.

## 2.4 The Schrödinger Equation for a Multielectronic Molecule

The time-independent Schrödinger equation describes the quantum mechanical behavior of a system in a stationary state, *i.e.* a state with well defined energy (SAKURAI; NAPOLITANO, 2017; PARR; WEITAO, 1995), not a quantum superposition of energy eigenstates. For a multielectronic molecule, it can be written as:

$$\hat{H}\Psi = E\Psi. \quad (2.7)$$

In this equation,  $\hat{H}$  represents the molecular Hamiltonian operator,  $\Psi$  is the molecular wave function, and  $E$  corresponds to the energy of the system.

The molecular Hamiltonian operator incorporates various physical interactions within the molecule. It can be expanded to explicitly include the kinetic energy of the electrons, as well as the kinetic energy of the nuclei, and the Coulombic interactions:

$$\begin{aligned} \hat{H} = & - \sum_{i=1}^N \frac{1}{2} \nabla_i^2 - \sum_{A=1}^M \frac{1}{2M_A} \nabla_A^2 - \sum_{A=1}^M \sum_{i=1}^N \frac{Z_A}{|\mathbf{r}_i - \mathbf{R}_A|} + \sum_{i=1}^N \sum_{j>i}^N \frac{1}{|\mathbf{r}_i - \mathbf{r}_j|} \\ & + \sum_{A=1}^M \sum_{B>A}^M \frac{Z_A Z_B}{|\mathbf{R}_A - \mathbf{R}_B|}. \end{aligned} \quad (2.8)$$

The terms in the expanded Hamiltonian operator represent specific interactions within the molecule. The  $M$  nuclei are labeled by the index  $A$  (or  $B$ ) and the  $N$  electrons are labeled by the index  $i$  (or  $j$ ). Thus, for example,  $\mathbf{R}_A$  represents the position of the  $A^{\text{th}}$  nucleus and  $\mathbf{r}_i$  represents the position of the  $i^{\text{th}}$  electron.

The first term accounts for the kinetic energy of each electron in the molecule. It considers the Laplacian operator ( $\nabla_i^2$ ), which describes the spatial variation of the wave function for each electron  $i$ .

The second term represents the kinetic energy of the nuclei. It considers the mass of each nucleus ( $M_A$ ), and the Laplacian operator ( $\nabla_A^2$ ), which describes the spatial variation of the wave function for each nucleus.

The third term represents the interaction between each electron and the nuclei of the atoms in the molecule. It considers the attractive electrostatic interaction and is described by the potential generated by the nuclei. The term includes the atomic number of the nucleus ( $Z_A$ ) and the distance between the electron and the nucleus.

The fourth term accounts for the electron-electron repulsion, as described previously.

The fifth term represents the nuclear-nuclear repulsion, as described previously.

The molecular wave function,  $\Psi$ , represents the quantum state of the multielectronic molecule, describing the distribution of electrons and their associated energies in the molecular system. In theory, by solving the Schrödinger equation, researchers could gain insights into the electronic structure and properties of multielectronic molecules, enabling a deeper understanding of their chemical bonding, reactivity, and spectroscopic behavior.

But solving the Schrödinger equation for a multielectronic molecule is a challenging task due to the complexity of the electron-electron interactions involved. Various approximation methods and computational techniques, such as Hartree-Fock (HF) theory, density functional theory (DFT), and many-body perturbation theory, are commonly employed to obtain solutions for the corresponding energy of the molecule without explicitly computing the wave function.

In fact, storing the many-body wave function is an insurmountable challenge. The

wave function depends on  $3N$  spatial dimensions<sup>1</sup> (3 for each electron). Let us give the example of the oxygen atom with 8 electrons. Even if we attempt to simplify the problem by sampling the wave function using just 10 values in each spatial coordinate ( $x$ ,  $y$ , and  $z$ ) for each electron, the sheer magnitude of data required is staggering. This would necessitate storing  $1000^8 = 10^{24}$  floating-point numbers, equivalent to a mind-boggling 4 trillion terabytes of data. Such storage demands are unattainable.

## 2.5 Born-Oppenheimer Approximation

The Born-Oppenheimer approximation is a fundamental concept in quantum chemistry that simplifies the treatment of the electronic and nuclear motions in a multielectronic molecule. The approximation assumes that the electronic motion and the nuclear motion can be separated due to a significant disparity in their masses (SZABO; OSTLUND, 1996). This means that the electronic structure can be treated independently of the nuclear positions. It is assumed that the motion of electrons is much faster compared to the motion of atomic nuclei. Electrons occupy regions around the nuclei, forming an electronic cloud, and their movements are influenced by the electrostatic interaction with the nuclei and other electrons. The nuclear motion, on the other hand, is much slower. The nuclei move in response to the overall electronic distribution but at a significantly slower timescale.

By making these assumptions, the Born-Oppenheimer approximation simplifies the problem by allowing one to treat the electronic structure separately from the nuclear positions.

Equation (2.8) can be split in the following manner:

$$\hat{H} = \underbrace{-\sum_{i=1}^N \frac{1}{2} \nabla_i^2 - \sum_{A=1}^M \sum_{i=1}^N \frac{Z_A}{|\mathbf{r}_i - \mathbf{R}_A|} + \sum_{i=1}^N \sum_{j>i}^N \frac{1}{|\mathbf{r}_i - \mathbf{r}_j|}}_{\hat{H}_{\text{elec}}} - \sum_{A=1}^M \frac{1}{2M_A} \nabla_A^2 + \sum_{A=1}^M \sum_{B>A}^M \frac{Z_A Z_B}{|\mathbf{R}_A - \mathbf{R}_B|}. \quad (2.9)$$

Then, for each fixed<sup>2</sup> set  $\{\mathbf{R}_A\}$  of coordinates of the nuclei, an electronic wave function  $\Phi_{\text{elec}}(\{\mathbf{r}_i\})$  can be found as the solution to

$$\hat{H}_{\text{elec}} \Phi_{\text{elec}} = E_{\text{elec}} \Phi_{\text{elec}}. \quad (2.10)$$

The total energy for fixed nuclei, which also depends parametrically on the positions of

<sup>1</sup>Besides the  $N$  spin coordinates, one for each electron.

<sup>2</sup>As a consequence,  $\Phi_{\text{elec}}$  and  $E_{\text{elec}}$  can be considered *parametrically* dependent on the coordinates  $\{\mathbf{R}_A\}$  of the nuclei. Note that  $\Phi_{\text{elec}}$  depends *explicitly* on the coordinates  $\{\mathbf{r}_i\}$  of the electrons, though.

the nuclei, can be found as

$$E_{\text{tot}}(\{\mathbf{R}_A\}) = E_{\text{elec}}(\{\mathbf{R}_A\}) + \sum_{A=1}^M \sum_{B>A}^M \frac{Z_A Z_B}{|\mathbf{R}_A - \mathbf{R}_B|}. \quad (2.11)$$

Therefore, the positions of the nuclei in the minimum of the potential energy (hyper)surface can be found. This optimization process determines the most stable arrangement of the nuclei in the molecule, corresponding to the equilibrium geometry.

After solving the electronic problem, one can suppose that the nuclei “feel” the average field of the electrons under the assumptions of the Born-Oppenheimer approximation. This gives an approximate hamiltonian:

$$\hat{H}_{\text{nucl}} \approx - \sum_{A=1}^M \frac{1}{2M_A} \nabla_A^2 + E_{\text{tot}}(\{\mathbf{R}_A\}). \quad (2.12)$$

Then, one can solve for the motion of the nuclei, *i.e.* the vibration, rotation and translation of the molecule in the average field of the electrons:

$$\hat{H}_{\text{nucl}} \Phi_{\text{nucl}} = E_{\text{BO}} \Phi_{\text{nucl}}. \quad (2.13)$$

Here, the energy  $E_{\text{BO}}$  does not require fixed nuclei and must not be confused with the previously defined  $E_{\text{tot}}$ . In fact,  $E_{\text{BO}}$  is the Born-Oppenheimer approximation to the energy in Equation (2.7). Similarly, the corresponding Born-Oppenheimer approximation to the molecular wave function in Equation (2.7) is:

$$\Psi_{\text{BO}}(\{\mathbf{r}_i\}, \{\mathbf{R}_A\}) = \Phi_{\text{elec}}(\{\mathbf{r}_i\}) \Phi_{\text{nucl}}(\{\mathbf{R}_A\}). \quad (2.14)$$

## 2.6 Orbitals

An orbital can be defined as a wave function that describes the behavior of an electron. Molecular orbitals represent the wave functions of electrons within a molecule.

A spatial orbital, denoted as  $\psi_i(\mathbf{r})$ , is a function of the position vector  $\mathbf{r} = (x, y, z)$ . It is defined such that  $|\psi_i(\mathbf{r})|^2 d\mathbf{r}$  is the probability of finding the electron in a small volume element<sup>3</sup>  $d\mathbf{r}$  around the position  $\mathbf{r}$ . Figure 2.6 illustrates this concept.

To fully describe an electron, including its spin, spin orbitals denoted as  $\chi_j(\mathbf{x})$  are adopted, where  $\mathbf{x} = (\mathbf{r}, \omega)$  represents both the spatial and spin coordinates. This can be

<sup>3</sup>Here,  $d\mathbf{r} = dx dy dz$ .

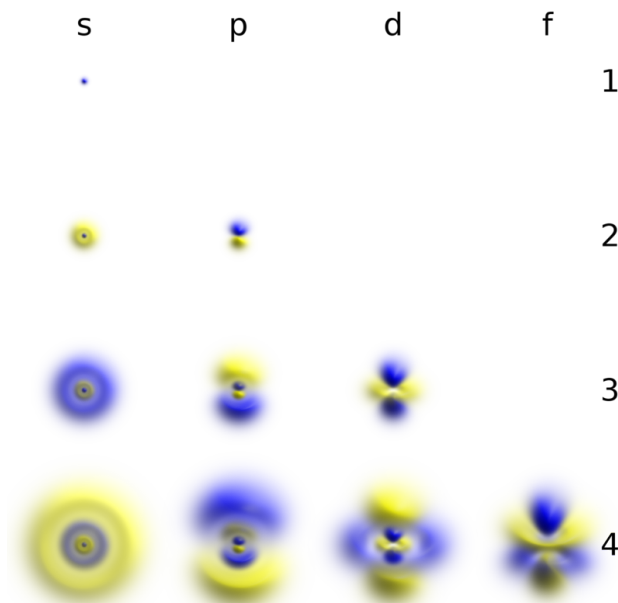


FIGURE 2.6 – Ten orbitals for a hydrogen-like atom are shown. Each column corresponds to a specific angular momentum quantum number  $l$ . The row labels represent the principal quantum number  $n$  values. All the orbitals are aligned along the  $z$ -axis, with the orbital magnetic quantum number  $m_l = 0$ . These images show the probability density per unit volume, where the color represents the phase of the orbital. *Note.* Licensed under [creativecommons.org/licenses/by-sa/4.0](https://creativecommons.org/licenses/by-sa/4.0).

expressed as:

$$\chi_{2i-1}(\mathbf{x}) = \psi_i(\mathbf{r})\alpha(\omega) \text{ or } \chi_{2i}(\mathbf{x}) = \psi_i(\mathbf{r})\beta(\omega), \quad (2.15)$$

where  $\alpha(\omega)$  and  $\beta(\omega)$  indicate the electron's spin state (spin up or spin down). Each spatial orbital  $\psi_i(\mathbf{r})$  can give rise to two distinct spin orbitals.<sup>4</sup>

## 2.7 The HF Approximation

Within the framework of the Born-Oppenheimer approximation, the HF method is commonly employed to determine the electronic wave function of a multielectronic molecule. The HF method makes additional assumptions about the electronic structure to simplify the calculations.

### 2.7.1 Hartree Product

The Hartree product is an early approximation used in quantum chemistry to describe the behavior of many-electron systems. In this method, the wave function of a

<sup>4</sup>For open-shell systems, which will be defined later, this might not exactly be true.

many-electron system is approximated as a product of single-electron wave functions, neglecting electron-electron interactions. The total energy is calculated as the sum of the energies of individual electrons. However, the Hartree method does not take into account the antisymmetry principle, which states that the wave function of a system of indistinguishable fermions must change sign upon the exchange of any two particles. This omission leads to unphysical results and inconsistency.

### 2.7.2 Slater Determinant

The HF method incorporates the antisymmetry principle through the Slater determinant, ensuring that the wave function changes sign upon electron exchange. It provides a self-consistent solution for the wave function of a many-electron system considering the interaction of each electron with the mean-field generated by the other electrons, but ignoring the repulsion between each particular pair of electrons. In the HF method, the wave function is approximated as a single Slater determinant. A Slater determinant is shown in Equation (2.16):

$$\begin{aligned} \Psi(\mathbf{x}_1, \mathbf{x}_2, \dots, \mathbf{x}_N) &= \frac{1}{\sqrt{N!}} \begin{vmatrix} \chi_1(\mathbf{x}_1) & \chi_2(\mathbf{x}_1) & \dots & \chi_N(\mathbf{x}_1) \\ \chi_1(\mathbf{x}_2) & \chi_2(\mathbf{x}_2) & \dots & \chi_N(\mathbf{x}_2) \\ \vdots & \vdots & \ddots & \vdots \\ \chi_1(\mathbf{x}_N) & \chi_2(\mathbf{x}_N) & \dots & \chi_N(\mathbf{x}_N) \end{vmatrix} \\ &= |\chi_1 \chi_2 \dots \chi_N\rangle. \end{aligned} \quad (2.16)$$

In this equation,  $\Psi(\mathbf{x}_1, \mathbf{x}_2, \dots, \mathbf{x}_N)$  represents the molecular wave function, which depends on the coordinates  $\mathbf{x}_1, \mathbf{x}_2, \dots, \mathbf{x}_N$  of the  $N$  electrons in the system.  $\chi_1, \chi_2, \dots, \chi_N$  are the spin orbitals.

In quantum chemistry, *correlation* refers to the interdependence or mutual influence of electron motions in a many-electron system. The probability of locating an electron at a specific region depends on the spatial arrangement of the other electrons. It is important to note that even though a Slater determinant incorporates exchange-correlation effects, which arise due to the indistinguishability of identical particles, thus providing a more accurate description of many-electron systems compared to the Hartree products, it is customary to refer to a single determinantal wave function as an uncorrelated wave function. This is because, within the single Slater determinantal description, only the motion of electrons with parallel spins is correlated. The correlation due to the repulsive Coulomb interactions between individual electrons is not captured by a simple mean-field approximation.

The HF equations can be written as:

$$\hat{F}(\mathbf{x})\chi(\mathbf{x}) = \epsilon\chi(\mathbf{x}). \quad (2.17)$$

Here,  $\hat{F}(\mathbf{x})$  represents the Fock operator for an electron with coordinates  $\mathbf{x}$ ,  $\chi$  is a spin orbital, and  $\epsilon$  is the energy eigenvalue associated with  $\chi$ .

The Fock operator,  $\hat{F}(\mathbf{x})$ , is given by:

$$\hat{F}(\mathbf{x}) = \underbrace{-\frac{1}{2}\nabla^2 - \sum_{A=1}^M \frac{Z_A}{|\mathbf{r} - \mathbf{R}_A|}}_{\hat{h}(\mathbf{r})} + \underbrace{\sum_j [\hat{J}_j(\mathbf{x}) - \hat{K}_j(\mathbf{x})]}_{\hat{v}^{\text{HF}}(\mathbf{x})}. \quad (2.18)$$

The operators in the Fock operator are such that:

$$\hat{J}_j(\mathbf{x})\chi(\mathbf{x}) = \left[ \int \frac{\chi_j^*(\mathbf{x}')\chi_j(\mathbf{x}')}{|\mathbf{x} - \mathbf{x}'|} d\mathbf{x}' \right] \chi(\mathbf{x}), \text{ and} \quad (2.19)$$

$$\hat{K}_j(\mathbf{x})\chi(\mathbf{x}) = \left[ \int \frac{\chi_j^*(\mathbf{x}')\chi(\mathbf{x}')}{|\mathbf{x} - \mathbf{x}'|} d\mathbf{x}' \right] \chi_j(\mathbf{x}). \quad (2.20)$$

In these equations,  $\hat{J}_j(\mathbf{x})$  represents the Coulomb operator, which describes the electron-electron repulsion, and  $\hat{K}_j(\mathbf{x})$  represents the exchange operator, which accounts for the exchange correlation effects.

The exchange operator differs from the Coulomb operator because it is nonlocal. Unlike the Coulomb potential, which can be described by a simple potential function at a specific point in space, the exchange operator's action depends on the electron density throughout all space, not just at a particular point: the result of operating  $\hat{K}_j(\mathbf{x})$  depends on the value of  $\chi$  throughout all space, not just at  $\mathbf{x}$ . The nonlocal nature of the exchange operator arises from the quantum mechanical phenomenon of electron exchange, where electrons with the same spin become correlated even when separated by large distances. This exchange correlation is a fundamental aspect of electronic structure and plays a pivotal role in determining the properties of molecules and materials.

The HF method aims to minimize the electronic energy by self-consistently solving the HF equations. This involves an iterative process where one takes a guess at the spin orbitals, applies the Fock operator to them, gets new spin orbitals, updates the Fock operator with the new orbitals and repeats the process.

To overcome the limitations of the HF method and include electron correlation ef-

fects, more advanced computational methods are employed. Examples include post-HF methods, such as configuration interaction (CI), coupled cluster (CC), and Møller–Plesset perturbation theory, which consider electron correlation beyond the mean-field approximation, albeit at the cost of increased computational complexity.

The difference between the exact (non-relativistic) energy and the HF energy calculated using a complete basis set (the HF limit) is called the *correlation energy*:

$$E_{\text{corr}} = E_{\text{exact}} - E_{\text{HF}}. \quad (2.21)$$

It is worth noting that the HF limit refers to the theoretical limit approached by the HF method as the basis set size (a set of functions used to approximate the wave function) becomes complete. In the HF limit, the HF method provides the best possible mean-field approximation to the true electronic structure of a molecule within the given basis set.

However, even in the HF limit, electron correlation effects are still missing. Achieving accurate descriptions of electronic structure requires the use of advanced methods that go beyond the HF approximation and incorporate electron correlation in a more sophisticated manner.

The energy of an  $N$ -electron system, described by a Slater determinant, can be expressed as the sum of one-electron energies and unique pair-wise interaction energies (SZABO; OSTLUND, 1996). Table 2.1 explains the notations for one- and two-electron integrals, some of which contribute to the energy.  $h_{ij}$  are integrals associated to the core Hamiltonian,  $J_{ij}$  are the Coulomb integrals and  $K_{ij}$  are the exchange integrals. Each occupied spin orbital, denoted as  $\chi_i$ , contributes to the energy through the term  $\langle i | \hat{h} | i \rangle$ , representing the one-electron energy. Furthermore, the interaction energy arises from the interaction between pairs of occupied spin orbitals,  $\chi_i$  and  $\chi_j$ , given by the term  $\langle ij || ij \rangle$ .

### 2.7.3 Multiplicity of a State

While the Hamiltonian will explicitly depend on spin in systems with spin-dependent potentials, spin-orbit coupling, or spin-exchange interactions, this does not usually happen when solving the nonrelativistic Schrödinger equation. Consequently, both the total spin operator squared  $\hat{S}^2$  and the spin operator along the  $z$ -axis  $\hat{S}_z$  commute with the Hamiltonian. As a result, the exact eigenfunctions of the Hamiltonian also serve as eigenfunctions of the two spin operators:

$$\hat{S}^2 \Psi = S(S+1) \Psi, \quad (2.22)$$

$$\hat{S}_z \Psi = M_S \Psi. \quad (2.23)$$

Here,  $S$  and  $M_S$  represent the spin quantum numbers that describe the total spin and its  $z$  component of an  $N$ -electron state  $|\Psi\rangle$ . States with  $S = 0, \frac{1}{2}, 1, \frac{3}{2}, \dots$  have multiplicities of  $2S + 1$ , giving rise to singlets, doublets, triplets, quartets, and so on. While it is true that any single Slater determinant is an eigenfunction of the spin operator  $\hat{S}_z$ , it is not necessarily guaranteed to be an eigenfunction of the spin operator  $\hat{S}^2$ .

Each spatial orbital gives rise to two spin orbitals due to spin degeneracy (see Equation (2.15)). A closed-shell ground state is a system with an even number of electrons, where each occupied spin orbital has its counterpart—associated with the same spatial orbital—also occupied. Hence, it must be a singlet. The HF energy of a closed-shell ground-state is:

$$E_{\text{HF}} = 2 \sum_a h_{aa} + \sum_{a,b} (2J_{ab} - K_{ab}). \quad (2.24)$$

In this equation, the term  $h_{aa}$  represents the one-electron contribution to the energy,  $J_{ab}$  represents the Coulomb (electron-electron repulsion) integral, and  $K_{ab}$  represents the exchange integral. The summation indices  $a$  and  $b$  denote the occupied spatial orbitals in the closed-shell ground state.

TABLE 2.1 – One- and two-electron integrals over spin orbitals ( $\chi$ ) and spatial orbitals ( $\psi$ ). *Note.* From (SZABO; OSTLUND, 1996).

Notation	Meaning	Expanded formula
$\langle i \hat{h} j\rangle$	$\langle \chi_i \hat{h} \chi_j\rangle$	$\int d\mathbf{x} \chi_i^*(\mathbf{x})\hat{h}(\mathbf{r})\chi_j(\mathbf{x})$
$\langle ij kl\rangle$	$\langle \chi_i\chi_j \chi_k\chi_l\rangle$	$\iint d\mathbf{x} d\mathbf{x}' \chi_i^*(\mathbf{x})\chi_j^*(\mathbf{x}') \frac{1}{ \mathbf{r}-\mathbf{r}' } \chi_k(\mathbf{x})\chi_l(\mathbf{x}')$
$\langle ij  kl\rangle$		$\langle ij kl\rangle - \langle ij lk\rangle$
$h_{ij}$	$(\psi_i \hat{h} \psi_j)$	$\int d\mathbf{r} \psi_i^*(\mathbf{r})\hat{h}(\mathbf{r})\psi_j(\mathbf{r})$
$(ij kl)$	$(\psi_i\psi_j \psi_k\psi_l)$	$\iint d\mathbf{r} d\mathbf{r}' \psi_i^*(\mathbf{r})\psi_j(\mathbf{r}) \frac{1}{ \mathbf{r}-\mathbf{r}' } \psi_k^*(\mathbf{r}')\psi_l(\mathbf{r}')$
$J_{ij}$	$(ii jj)$	$\iint d\mathbf{r} d\mathbf{r}' \psi_i^*(\mathbf{r})\psi_i(\mathbf{r}) \frac{1}{ \mathbf{r}-\mathbf{r}' } \psi_j^*(\mathbf{r}')\psi_j(\mathbf{r}')$
$K_{ij}$	$(ij ji)$	$\iint d\mathbf{r} d\mathbf{r}' \psi_i^*(\mathbf{r})\psi_j(\mathbf{r}) \frac{1}{ \mathbf{r}-\mathbf{r}' } \psi_j^*(\mathbf{r}')\psi_i(\mathbf{r}')$

## 2.8 Occupied and Virtual Orbitals

The HF method gives a set of spin orbitals of different energies.

Occupied spin orbitals refer to the spin orbitals that are filled with electrons according to the electronic configuration of the system. These orbitals represent stable, lowest-energy electron configurations and are typically associated with the ground state. On the

other hand, virtual spin orbitals are unoccupied orbitals that can accommodate additional electrons. These orbitals represent higher-energy states that are not currently populated in the system.

An excited Slater determinant corresponds to a state in which one or more electrons have been promoted from occupied spin orbitals to virtual spin orbitals, resulting in an excited electronic configuration.

Mathematically, given a ground state Slater determinant  $\Psi_0 = |\chi_1\chi_2 \dots \chi_{a-1}\chi_a\chi_{a+1} \dots \chi_N\rangle$ , a (singly) excited Slater determinant corresponding to the excitation of an electron in  $\chi_a$  to  $\chi_r$  can be represented using ket notation as  $\Psi_a^r = |\chi_1\chi_2 \dots \chi_{a-1}\chi_r\chi_{a+1} \dots \chi_N\rangle$ . Figure 2.7 depicts both states.

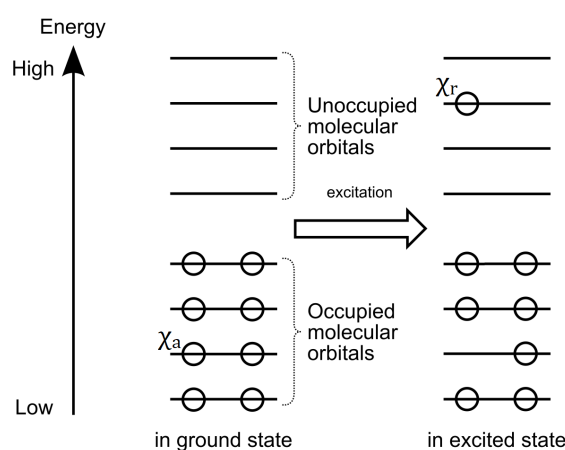


FIGURE 2.7 – Electron distributions in the ground state and after an excitation from spin orbital  $\chi_a$  to  $\chi_r$ . Note that each vertical line corresponds to one spatial orbital, and hence to two spin orbitals.

Similarly, it is also possible to define doubly excited determinants, where two electrons are excited from occupied spin orbitals to virtual spin orbitals, or even higher order excitations involving multiple electrons.

## 2.9 Brillouin's Theorem for Singly Excited Determinants

In quantum chemistry, Brillouin's Theorem states that singly excited determinants do not directly interact with a reference HF determinant. This theorem provides a useful simplification in many electronic structure calculations, allowing for a more efficient treatment of electronic correlation.

Mathematically, Brillouin's Theorem can be expressed as follows:

$$\langle \Psi_0 | \hat{H} | \Psi_a^r \rangle = 0. \quad (2.25)$$

Consequently, the singly excited determinants do not mix with the ground state, except indirectly through higher order excitations.

## 2.10 Roothaan Equations

### 2.10.1 Comparison with HF Equations

The Roothaan equations (ROOTHAAN, 1951; HALL; LENNARD-JONES, 1997) can be seen as an efficient reformulation of the HF equations. While the HF equations directly solve for the spin orbitals, the Roothaan equations solve for the expansion coefficients used to represent the spin orbitals in terms of a set of, say,  $K$  basis functions  $\phi_\nu$ ,  $\nu \in \{1, 2, \dots, K\}$ . This change of variables simplifies the calculations and allows for a more straightforward implementation.

The Roothaan equations can be expressed as follows:

$$\mathbf{FC} = \mathbf{SC}\epsilon, \quad (2.26)$$

where  $\mathbf{F}$  is the Fock matrix,  $\mathbf{C}$  is the coefficient matrix,  $\mathbf{S}$  is the overlap matrix, and  $\epsilon$  is a diagonal matrix of orbital energies.

The Fock matrix,  $\mathbf{F}$ , is defined as:

$$F_{\mu\nu} = H_{\mu\nu}^{\text{core}} + \sum_{\lambda,\sigma} P_{\lambda\sigma} \left[ (\mu\nu|\sigma\lambda) - \frac{1}{2}(\mu\lambda|\sigma\nu) \right], \quad (2.27)$$

where  $H_{\mu\nu}^{\text{core}} = \int \phi_\mu^*(\mathbf{r}) \hat{h}(\mathbf{r}) \phi_\nu(\mathbf{r}) \, d\mathbf{r}$  represents the core Hamiltonian matrix elements,  $P_{\lambda\sigma}$  are elements of the density matrix, which will be defined below, and  $(\mu\nu|\sigma\lambda)$  and  $(\mu\lambda|\sigma\nu)$  are two-electron integrals.

The coefficient matrix,  $\mathbf{C}$ , contains the expansion coefficients of the basis functions. Each column of  $\mathbf{C}$  corresponds to a particular spin orbital:

$$\psi_i = \sum_{\nu=1}^K C_{\nu i} \phi_\nu, \quad \forall i \in \{1, 2, \dots, K\}. \quad (2.28)$$

The electron density  $\rho(\mathbf{r})$  is defined such that  $\rho(\mathbf{r}) \, d\mathbf{r}$  is the sum of probabilities of finding each electron in a volume element  $d\mathbf{r}$  at  $\mathbf{r}$ , so its integral over all space is the total number  $N$  of electrons. For a closed-shell system, the density matrix corresponding to

this function is:

$$P_{\mu\nu} = 2 \sum_{a=1}^{N/2} C_{\mu a}^* C_{\nu a}, \quad (2.29)$$

which has the property

$$\rho(\mathbf{r}) = \sum_{\mu,\nu} P_{\mu\nu} \phi_{\mu}^*(\mathbf{r}) \phi_{\nu}(\mathbf{r}). \quad (2.30)$$

The overlap matrix,  $\mathbf{S}$ , accounts for the overlap between the basis functions and is defined as:

$$S_{\mu\nu} = \int \phi_{\mu}^*(\mathbf{r}) \phi_{\nu}(\mathbf{r}) \, d\mathbf{r}, \quad (2.31)$$

where  $\phi_{\mu}(\mathbf{r})$  and  $\phi_{\nu}(\mathbf{r})$  are the basis functions.

Since  $\mathbf{F}$  depends on  $\mathbf{C}$  and  $\mathbf{C}$  depends on  $\mathbf{F}$ , the process must be done iteratively. This is why the solution of the HF and Roothaan equations is called the self-consistent field (SCF) method.

### 2.10.2 Detailed Explanation of the SCF Method

The SCF method follows a step-by-step procedure as outlined below:

1. Specify a molecule by providing the set of nuclear coordinates  $\{R_A\}$ , atomic numbers  $\{Z_A\}$ , and the number of electrons  $N$ . Additionally, choose an appropriate basis set  $\{\phi_{\nu}\}$  in which the orbitals will be represented.
2. Calculate all the necessary integrals, including the overlap integrals  $S_{\mu\nu}$ , the one-electron Hamiltonian matrix elements  $H_{\mu\nu}^{\text{core}}$ , and the two-electron repulsion integrals  $(\mu\nu|\lambda\sigma)$ . These integrals are computed based on the chosen basis set and the molecular geometry.
3. Diagonalize the overlap matrix  $\mathbf{S}$  to obtain its eigenvectors, and calculate the transformation matrix  $\mathbf{X}$ . The transformation matrix is used to orthogonalize the basis set.
4. Make an initial guess for the density matrix  $\mathbf{P}$ . The density matrix describes the occupation of molecular orbitals by electrons. The initial guess can be constructed in various ways, such as assuming all electrons occupy the lowest-energy orbitals.
5. Calculate the Fock matrix  $\mathbf{F}$  from the calculated integrals and the density matrix. The Fock matrix represents the effective potential experienced by electrons in the presence of other electrons.

## CHAPTER 2. THEORETICAL BACKGROUND

46

6. Transform the Fock matrix  $\mathbf{F}$  using the transformation matrix  $\mathbf{X}$  to obtain the transformed Fock matrix  $\mathbf{F}' = \mathbf{X}^\dagger \mathbf{F} \mathbf{X}$ . The transformation ensures that the Fock matrix is represented in the orthogonalized basis.
7. Diagonalize the transformed Fock matrix  $\mathbf{F}'$  to obtain its eigenvectors and eigenvalues. The eigenvectors give the coefficient matrix, while the eigenvalues represent their corresponding orbital energies.
8. Obtain the new coefficient matrix  $\mathbf{C}$  by multiplying the transformation matrix  $\mathbf{X}$  with the eigenvector matrix from the previous step:  $\mathbf{C} = \mathbf{X} \mathbf{C}'$ . The coefficient matrix  $\mathbf{C}$  contains the expansion coefficients of the molecular orbitals in the atomic orbital basis.
9. Calculate a new density matrix  $\mathbf{P}$  using the coefficients of the molecular orbitals (see Equation (2.29)). This density matrix reflects the occupation of the molecular orbitals by electrons.
10. Determine whether the procedure has converged by comparing the new density matrix with the previous density matrix. If the difference between the two density matrices is sufficiently small within a specified criterion, the self-consistency has been achieved, and the procedure can terminate. Otherwise, return to step 5 with the new density matrix and repeat the iterative process.
11. After convergence, the matrices can be used to calculate various properties of interest.

The flowchart in Figure 2.8 provides a graphical representation of the steps involved in the self-consistent method:

The self-consistent method iteratively improves the wave function and electron density until a self-consistent solution is obtained. This solution represents the electronic structure of the molecule, allowing for accurate calculations of molecular properties and behavior.

It is important to note that the convergence of the self-consistent method depends on the system being studied, the choice of basis set, and the desired level of accuracy. In some cases, achieving convergence may require careful parameter tuning or using more sophisticated algorithms.

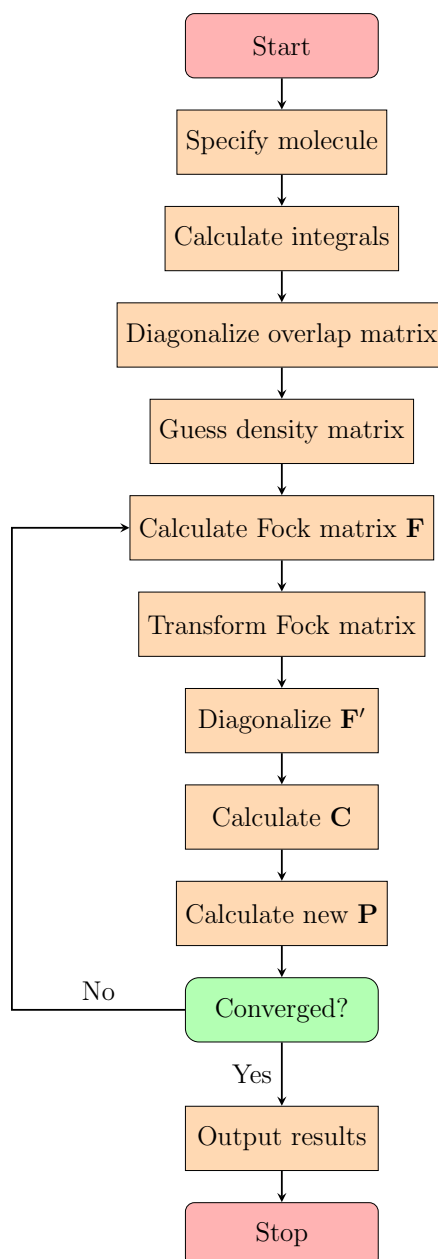


FIGURE 2.8 – Flowchart of the self-consistent method.

## 2.11 Handling Two-Electron Integrals in Large-Scale Calculations

The computation of overlap and one-electron integrals is relatively straightforward compared to the evaluation of two-electron repulsion integrals. This is primarily due to

the small number of one-electron integrals involved. The real challenge in large-scale calculations lies in the efficient handling and evaluation of a substantial number of two-electron integrals.

For systems with a basis of  $K$  functions, the number of distinct two-electron integrals can be estimated to be approximately on the order of  $\frac{K^4}{8}$ . Consequently, even for moderately sized molecules and small basis sets, the total count of two-electron integrals can quickly reach significant magnitudes, sometimes spanning millions.

The sheer magnitude of these integrals presents a computational bottleneck, demanding substantial resources in terms of time and memory. Consequently, devising effective strategies to tackle this challenge is crucial to enable accurate electronic structure calculations for complex systems. Researchers have devised various approaches to address the issue at hand. Approximation techniques and truncation schemes can be employed to reduce the number of integrals that require explicit computation.

## 2.12 Geometry Optimization in Quantum Chemistry

Geometry optimization is a fundamental task in quantum chemistry that involves finding the most stable arrangement of atoms in a molecule. The geometry of a molecule significantly influences its electronic structure, molecular properties, and reactivity. It is used to predict and validate molecular structures, including bond lengths, bond angles, and dihedral angles. The optimized geometries provide valuable information for comparing experimental data, interpreting spectroscopic measurements, and understanding the stability of chemical species.

Various methods are available for performing geometry optimization in quantum chemistry. These methods aim to minimize the total energy of the molecule by iteratively adjusting the atomic positions until a stable configuration is reached.

Gradient-based optimization methods, such as the steepest descent (shown in Figure 2.9) and conjugate gradient methods, are some of the commonly used approaches and rely on the gradient of the energy with respect to the nuclear coordinates. The gradient provides information about the direction and magnitude of the force acting on each atom, allowing for stepwise adjustments of the atomic positions towards the energy minimum.

The energy of a molecule with  $N$  atoms can be expressed as a function of the coordinates of the atoms. The  $3N$  Cartesian coordinates are converted into internal coordinates. This conversion removes the rotational and translational degrees of freedom. For non-linear molecules, the number of internal coordinates is  $3N - 6$ , while for linear molecules, it is  $3N - 5$ . These coordinates can be a set of interatomic distances, angles or other

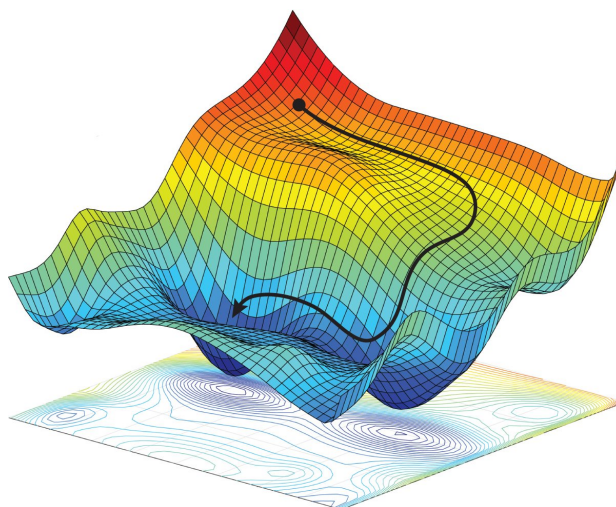


FIGURE 2.9 – Diagram of a potential energy surface and the path taken during gradient descent optimization. The vertical axis corresponds to the energy and the horizontal axes are the internal coordinates of the molecule. Note that in general (when the number of internal coordinates is greater than two) the graph is a hypersurface and cannot be plotted.

relevant geometric quantities that completely determine the geometry of molecule.

The general steps of geometry optimization include:

1. Start with a set of coordinates.
2. Carry out a SCF calculation to obtain the energy, gradient (and optionally the Hessian matrix).
3. Feed the gradient and Hessian matrix into the optimization algorithm, which determines how to vary the coordinates to move towards the energy minimum. This step is known as a *step*.
4. Check if the step is too large. If it is, scale it down (optional).
5. Update the coordinates by taking the step.
6. Update the Hessian matrix.
7. Repeat steps 2-6 until convergence is achieved.

## 2.13 Choice of Bases

Different types of basis sets have been developed to address various computational needs and accuracy requirements.

Polyatomic basis sets are constructed by combining basis functions centered on each atom within the molecule. These basis sets offer a flexible and accurate representation of the electronic wave functions and properties of molecules. By considering the behavior of electrons around atomic nuclei, polyatomic basis sets facilitate quantum chemistry calculations.

In computational quantum chemistry, the choice of basis functions is crucial for accurately describing the behavior of electrons in molecules. While Slater functions<sup>5</sup> give a closer representation of the physical nature of orbitals, their practical use in evaluating two-electron integrals can be computationally challenging. On the other hand, Gaussian functions offer a more convenient approach by simplifying the calculation of these integrals.

A contracted Gaussian function refers to a type of basis function constructed by combining multiple primitive Gaussian functions with different exponents and contraction coefficients. By combining multiple Gaussian functions with different widths and contraction coefficients, it is possible to both get a good approximation of orbitals and make the evaluation of two-electron integrals easy.

Mathematically, a contracted Gaussian function can be represented as:

$$\phi(\mathbf{r}) = \sum_i d_i \cdot \underbrace{Y_{l,m}(\theta, \phi) |\mathbf{r} - \mathbf{R}|^{2n-2-l} e^{-\alpha_i |\mathbf{r} - \mathbf{R}|^2}}_{\text{primitive Gaussian function}}, \quad (2.33)$$

where  $\phi(\mathbf{r})$  is the contracted Gaussian function at position  $\mathbf{r}$ ,  $\alpha_i$  are the exponents that control the width of each primitive Gaussian function,  $\mathbf{R}$  represents the center of the Gaussian function, and  $d_i$  are the contraction coefficients that determine the contribution of each primitive Gaussian function.

The use of contracted Gaussian functions allows for an efficient and accurate representation of the molecular orbitals and electron density in quantum chemical calculations. The contraction coefficients and exponents are typically optimized to reproduce experimental data and accurately describe the electronic behavior of the system under investigation.

It is important to note that the specific details of contracted Gaussian functions can vary depending on the computational chemistry method and basis set used. Different basis

<sup>5</sup>A Slater function is typically expressed as a product of an exponential term and a polynomial term (JENSEN, 2017). Mathematically, a Slater function can be written as:

$$\psi_{\zeta,n,l,m}(\mathbf{r}) = N Y_{l,m}(\theta, \phi) |\mathbf{r} - \mathbf{R}|^{n-1} e^{-\zeta |\mathbf{r} - \mathbf{R}|}, \quad (2.32)$$

where  $\psi(\mathbf{r})$  represents the Slater function at position  $\mathbf{r}$ ,  $\zeta$  is a parameter controlling the decay rate,  $\mathbf{R}$  is the center of the Slater function (the position of the nucleus),  $N$  is the normalization constant,  $n = 1, 2, \dots$  is a natural number that corresponds to the principal quantum number, and  $Y_{l,m}(\theta, \phi)$  is the angular part of the function, a spherical harmonic.

sets may employ different contraction schemes and combinations of primitive Gaussian functions, tailored for specific levels of accuracy and computational efficiency.

### 2.13.1 Minimal Basis Sets

In computational quantum chemistry, a minimal basis set refers to the smallest set of basis functions used in electronic structure calculations. Each atom in the molecule is assigned a single basis function for each orbital in a HF calculation on the free atom. For example, in the second period of the periodic table (Li - Ne), a minimal basis set consists of five functions, including two s functions (1s and 2s) and three p functions (2p). Minimal basis sets, such as the STO-3G basis set (HEHRE *et al.*, 1969), are computationally efficient and serve as a starting point for electronic structure calculations.

### 2.13.2 Double-Zeta Basis Sets

Double-zeta<sup>6</sup> basis sets, such as the 6-31G basis set<sup>7</sup> (DITCHFIELD *et al.*, 1971; HEHRE *et al.*, 1972), provide an improvement over minimal bases by including two functions for each orbital in a HF calculation on the free atom. By incorporating additional functions, double-zeta basis sets are more flexible and enable a better representation of electron density depending on the molecular environment.

### 2.13.3 Polarized Basis Sets

Polarized basis sets, such as the 6-31G\* basis set, go beyond the capabilities of minimal and double-zeta bases. While a minimal basis set can provide an exact description of the gas-phase atom at the SCF level, additional functions are often added to account for electron density polarization in molecules. These additional functions, known as polarization functions, allow for more accurate modeling of chemical bonding. For instance, a simple polarized basis set for hydrogen may include p functions, enabling molecular orbitals involving hydrogen to exhibit greater asymmetry around the nucleus.

In addition to polarization functions, diffuse functions are commonly included in basis sets. Diffuse functions are extended Gaussian basis functions with small exponents that provide flexibility to the outer regions of atomic orbitals, away from the nucleus. By incorporating polarization and diffuse functions, the basis set becomes more versatile and capable of capturing a wider range of chemical properties.

<sup>6</sup>Zeta ( $\zeta$ ) is a reference to the term that appears in the exponential part of the basis functions.

<sup>7</sup>Rigorously, it is a split-valence double-zeta basis set, because only the valence orbitals are described by two functions, while a single function is assigned to the inner orbitals.

## 2.14 Configuration Interaction

Configuration interaction (CI) is a powerful method used to incorporate electron correlation effects into the wave function of a multielectronic molecule. It offers a more accurate description of the electronic structure compared to the mean-field HF method. CI accounts for the fact that the true wave function of a molecule is not a single Slater determinant but rather a linear combination of multiple determinants.

### 2.14.1 CI and Correlation Energy

The name “configuration interaction” stems from the fact that the wave function is expanded as a linear combination of different electronic configurations. An electronic configuration refers to a specific arrangement of electrons in molecular orbitals. The CI method includes multiple configurations to improve the description of the electronic structure.

The CI wave function can be written as:

$$\Phi_{\text{CI}} = c_0 \Psi_0 + \sum_{i,a} c_i^a \Psi_i^a + \sum_{\substack{i<j \\ a<b}} c_{ij}^{ab} \Psi_{ij}^{ab} + \sum_{\substack{i<j<k \\ a<b<c}} c_{ijk}^{abc} \Psi_{ijk}^{abc} + \dots \quad (2.34)$$

Here,  $\Psi_0 = |\chi_1 \chi_2 \dots \chi_N\rangle$  represents the reference configuration, typically the HF determinant, and  $\Psi_{ijk}^{abc}$  represents an excited configuration obtained by promoting electrons from occupied orbitals  $\chi_i, \chi_j, \chi_k$  to virtual orbitals  $\chi_a, \chi_b, \chi_c$ . The coefficients  $c_0, c_i^a, c_{ij}^{ab}$ , etc., determine the contribution of each configuration to the overall wave function.

The CI method aims to find the best set of coefficients that minimizes the electronic energy. By considering multiple configurations and their associated coefficients, CI accounts for a broader range of electron correlation effects, resulting in a more accurate representation of the electronic structure and energetics of the system. However, the computational cost of CI increases rapidly with the number of configurations included, limiting its applicability to larger systems.

Post-HF methods, like CI, can go beyond the HF limit and partially recover some of the electron correlation energy, defined previously in Equation (2.24). In Figure 2.10, the graphical representation of the electron correlation energy is shown.

### 2.14.2 Full CI

In principle, the most accurate treatment of electron correlation would involve including all possible configurations in the CI expansion, of which there is an infinite number.

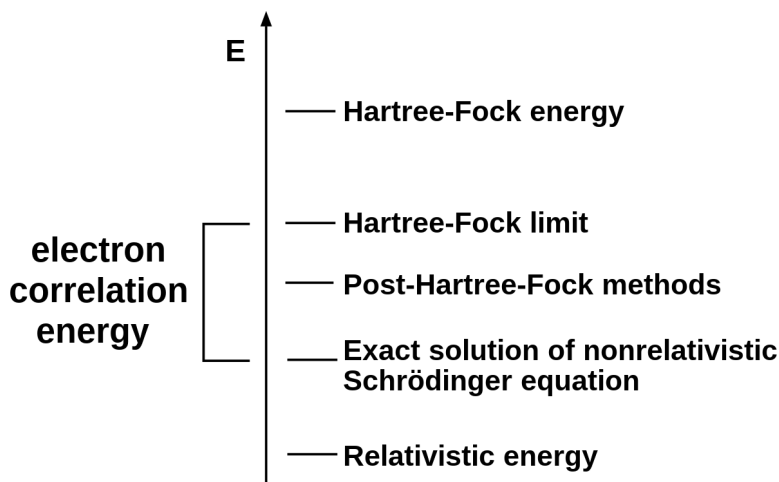


FIGURE 2.10 – Graphical representation of the electron correlation energy.

When working with a finite set of  $2K$  spin orbitals, the  $N$ -electron wave function is constrained to the linear subspace spanned by the  $\binom{2K}{N}$  determinants formed from these spin orbitals, which clearly do not constitute a complete  $N$ -electron basis.<sup>8</sup>

The full configuration interaction (full CI) method involves diagonalizing the finite Hamiltonian matrix formed from this set of determinants, providing solutions that are exact within that subspace.

While full CI calculations theoretically yield the exact solution within a given basis set, they are computationally infeasible for larger systems due to the rapid growth of the configuration space. The number of configurations increases factorially with the number of electrons and molecular orbitals, making full CI calculations practically impossible for systems with more than a few electrons, even when cleverly exploiting Equation (2.25) and the fact that there is no coupling between Slater determinants that differ by more than two spin orbitals, *e.g.*  $\langle \Psi_2 | \hat{H} | \Psi_5 \rangle = 0$  if  $\Psi_2$  is a doubly excited Slater determinant and  $\Psi_5$  is a quintuply excited Slater determinant with respect to some reference configuration  $\Psi_0$ . The full CI matrix can reach, say, dimensions  $10^9 \times 10^9$  for a molecule that is not too big when using a minimal basis set.

To overcome this computational challenge, various CI variants are employed to approximate the full CI wave function and obtain reliable results for moderately sized systems. These variants include truncated CI methods such as configuration interaction singles and doubles (CISD), which include single and double excitations from the reference determinants,<sup>9</sup> and higher order CI methods that incorporate additional excitations.

<sup>8</sup>Just like a spin orbital is expanded as a linear combination of functions in a usual (one-electron) basis set, an  $N$ -electron wave function is expanded in a  $N$ -electron basis.

<sup>9</sup>Which may already represent excited configurations.

While full CI remains a benchmark for accuracy, approximate CI methods provide efficient and reasonably accurate descriptions of electron correlation in molecular systems, enabling the study of larger and more complex systems. A CI method used in this work is CISD, which is limited to single and double excitations from the reference configurations.<sup>10</sup>

### 2.14.3 Size Consistency

A key concept in computational chemistry is *size consistency*. Size consistency refers to the property where the energy of a system composed of two non-interacting fragments is equal to the sum of the energies of the individual fragments. In other words, the total energy of the combined system composed of two non-interacting molecules should be the sum of the energies of the individual molecules.

Among the different types of CI, only full CI is size consistent. Full CI includes all possible excitations from the reference determinant and provides the best solution to the electronic Schrödinger equation within a given basis set.

On the other hand, truncated CI methods such as CISD are not size consistent. When size consistency is violated, the correlation energy per electron, denoted as  $E_{\text{corr}}/N$ , does not approach a constant nonzero value in the limit of an infinitely large system. Instead, it converges to zero. This behavior is undesirable, as it fails to capture the true nature of electron correlation in larger systems. The Pople correction, which will be mentioned later in the Chapter 3 of this work, tries to make the correlation energy size consistent.

Perturbation theory (PT) is a size consistent method, though it is not variational.

## 2.15 Canonical and Natural Orbitals

### 2.15.1 Canonical Orbitals

Canonical orbitals are obtained by solving the eigenvalue equation associated with the HF equations. The set of canonical spin orbitals represents the unique set of spin orbitals that satisfy the eigenvalue equation. They diagonalize the Fock operator and, thus, have well-defined energy. These orbitals are obtained through an iterative self-consistent procedure.

One important property is the invariance of the wave function to arbitrary unitary transformations of the canonical orbitals. In other words, any unitary transformation of the spin orbitals does not change any expectation value.

---

<sup>10</sup>See footnote 9.

The canonical spin orbitals are generally delocalized. This means that the electrons are not localized around specific atoms but are spread out over the entire molecule. Canonical orbitals form a basis for an irreducible representation of the point group of the molecule. By applying a unitary transformation to transform a set of canonical spin orbitals into a set of localized spin orbitals, no information about the wave function is lost. However, this transformation introduces a trade-off, as the transformed orbitals do not have well-defined energies due to being a superposition of canonical orbitals.

### 2.15.2 Natural Orbitals

Natural orbitals (LÖWDIN, 1955) offer an alternative representation. Natural orbitals are obtained by diagonalizing the one-particle reduced density matrix (1-RDM) calculated from the wave function  $\Phi(\mathbf{x}_1, \dots, \mathbf{x}_N)$  of the  $N$ -electron system. To define the 1-RDM, let us first define a *reduced density function*<sup>11</sup> for a single electron:

$$\rho(\mathbf{x}_1) = N \int d\mathbf{x}_2 d\mathbf{x}_3 \cdots d\mathbf{x}_N \Phi(\mathbf{x}_1, \dots, \mathbf{x}_N) \Phi^*(\mathbf{x}_1, \dots, \mathbf{x}_N), \quad (2.35)$$

which has the property

$$\int d\mathbf{x}_1 \rho(\mathbf{x}_1) = N. \quad (2.36)$$

Similarly, the 1-RDM can be defined as:

$$\gamma(\mathbf{x}_1, \mathbf{x}'_1) = N \int d\mathbf{x}_2 d\mathbf{x}_3 \cdots d\mathbf{x}_N \Phi(\mathbf{x}_1, \dots, \mathbf{x}_N) \Phi^*(\mathbf{x}'_1, \dots, \mathbf{x}_N), \quad (2.37)$$

and fulfills

$$\gamma(\mathbf{x}_1, \mathbf{x}_1) = \rho(\mathbf{x}_1). \quad (2.38)$$

$\gamma(\mathbf{x}_1, \mathbf{x}'_1)$  is called a matrix in the sense it can be expanded in a basis, *e.g.* the orthonormal basis of canonical orbitals  $\{\chi_i\}$ :

$$\gamma(\mathbf{x}_1, \mathbf{x}'_1) = \sum_{i,j} \chi_i(\mathbf{x}_1) \gamma_{ij} \chi_j^*(\mathbf{x}'_1), \quad (2.39)$$

and the coefficients

$$\gamma_{ij} = \int d\mathbf{x}_1 d\mathbf{x}'_1 \chi_i^*(\mathbf{x}_1) \gamma(\mathbf{x}_1, \mathbf{x}'_1) \chi_j(\mathbf{x}'_1) \quad (2.40)$$

form a matrix that describes the 1-RDM in the basis of canonical orbitals.

If, instead, it is expanded in the basis of natural orbitals  $\{\eta_i\}$ , in which it is diagonal,

<sup>11</sup>The electron density previously defined in Equations (2.29) and (2.30) is distinct from this new concept, even though both are being represented by  $\rho$ .

one can write:

$$\gamma(\mathbf{x}_1, \mathbf{x}'_1) = \sum_i \lambda_i \eta_i(\mathbf{x}_1) \eta_i^*(\mathbf{x}'_1), \quad (2.41)$$

where the eigenvalue  $\lambda_i$  ( $0 \leq \lambda_i \leq 1$ ) is called the occupation number of  $\eta_i$  in the wave function  $\Phi$ .

Unlike canonical orbitals, natural orbitals are not constrained by the HF equations and do not necessarily correspond to the eigenfunctions of the Fock operator. Instead, natural orbitals represent a different set of orbitals that diagonalize the 1-RDM. These orbitals make the CI expansion converge more rapidly in comparison with canonical HF orbitals, therefore allowing one to obtain equivalent results with a smaller number of configurations (SZABO; OSTLUND, 1996).

## 2.16 Static and Dynamic Correlation

The distinction between static and dynamic correlation refers to the deficiencies of the HF single-determinantal approach in capturing the electronic behavior of a system. The HF approach has two main limitations that give rise to correlation effects.

Firstly, the HF model does not account for the instantaneous interactions between electrons. Instead, each electron interacts with the mean field created by all other electrons. But in reality each electron avoids regions near the instantaneous positions of other electrons. The HF model fails to accurately reproduce this dynamic electron motion, leading to deviations in the correlation energy. This type of correlation is referred to as dynamic correlation as it is directly related to the dynamic behavior of electrons.

Secondly, the HF wave function is constructed as a single Slater determinant, which may not adequately represent certain electronic states. In some cases, an electronic state can only be properly described by a linear combination of multiple nearly degenerate Slater determinants. The HF model's inability to account for this mixing of determinants introduces static correlation. Static correlation arises from the deficiencies in representing the electron configuration in the HF model and is not directly related to electron dynamics.

To address both static and dynamic correlation effects, the HF wave function can be expanded by including additional Slater determinants alongside the reference determinant, as shown in Equation (2.34).

If the method assumes that  $c_0 \approx 1$  and includes a large number of excited determinants with small coefficients, the method primarily treats dynamic correlation. On the other hand, if only a few excited determinants with coefficients comparable to that of the reference determinant are included, the method primarily addresses static correlation. It is important to note that fully separating static and dynamic correlation effects is

challenging since they both arise from the same underlying electron-electron interactions.

## 2.17 Many-Body Perturbation Theory Overview

Many-body perturbation theory involves expanding the Hamiltonian in terms of a perturbation parameter. In the case of Møller-Plesset perturbation theory, the Hamiltonian is written as  $\hat{H} = \hat{H}_0 + \lambda\hat{V}$ , where  $\hat{H}_0$  is the HF Hamiltonian and  $\hat{V}$  is the perturbation, *i.e.* the difference between the exact non-relativistic Hamiltonian and the HF Hamiltonian. As the parameter  $\lambda$  changes continuously from 0 to 1, relevant quantities such as energies vary from the value obtained by the HF method to the real value, and can be expanded as a perturbation series in the parameter  $\lambda$ . For instance,  $E = E^{(0)} + \lambda E^{(1)} + \lambda^2 E^{(2)} + \dots$ . In second order Møller-Plesset perturbation theory (MP2) this expansion is truncated, ignoring terms that depend on  $\lambda^3$  or higher powers of  $\lambda$ .

An important characteristic of perturbation theory is its size consistency. Perturbation theory methods are size consistent, meaning that the energy of a system is additive when it is composed of non-interacting fragments. This property ensures that the energy calculations remain accurate and consistent for both isolated fragments and their assemblies. Size consistency is particularly crucial when studying large (potentially infinite) systems.

Perturbation theory approaches, by including perturbative corrections to the wave function, can effectively account for dynamic correlation in the electron-electron interactions.

## 2.18 Multiconfigurational and Multireference Methods

In quantum chemistry, multiconfigurational and multireference methods play a vital role in addressing strong electron correlation in molecular systems. These methods employ multiple configurations and references to provide a comprehensive treatment of electronic correlation. Let us explore these concepts in more detail.

### 2.18.1 Configurations and References

#### 2.18.1.1 Configurations

A configuration refers to a specific occupation of molecular orbitals, representing the arrangement of electrons within a system. Mathematically, configurations can be described as Slater determinants, which have already been defined as anti-symmetrized products of spin-orbitals. Alternatively, spin-adapted configuration state functions (CSFs) can

be used, which are linear combinations of Slater determinants that satisfy the requirement of the electronic wave function being an eigenfunction of the total spin angular momentum operator squared  $\hat{S}^2$ . It is important to note that the term “configuration” is a general term that encompasses both Slater determinants and CSFs.

### 2.18.1.2 References

In multiconfigurational and multireference methods, a reference configuration is selected as a starting point for generating excitations. In single-reference methods, typically the HF configuration is chosen as the reference. Examples of single-reference methods include configuration interaction with single and double excitations (CISD) and coupled cluster with single and double excitations (CCSD).

In contrast, multireference methods involve more than one reference configuration to account for complex electronic correlation effects. Methods such as full CI and complete active space configuration interaction (CASCI) do not restrict the excitations to specific degrees but include all possible excitations.

To better understand CASCI, let us first define active space. When studying a molecule, spatial orbitals can either hold two electrons, one electron, or be empty. If the occupation number of some orbital is not the same in all configurations considered in a method this orbital is said to be part of the active space. One can choose a particular set of orbitals and a particular number of electrons to be put into them and consider all possible manners (configurations) of putting that number of electrons into those orbitals. In this case, one talks about a complete active space (CAS). If, however, possible configurations are ignored, *i.e.* the configurations are restricted to some rules, a restricted active space (RAS) is being considered.

## 2.18.2 Some Methods

### 2.18.2.1 Multireference Configuration Interaction

Multireference configuration interaction (MRCI) is a method that incorporates multiple reference configurations and treats electron correlation through CI. It allows for a comprehensive description of the electronic structure in systems with strong correlation effects.

MRCISD, for example, which is used in this work, includes single and double excitations from the reference space of configurations.<sup>12,13</sup>

<sup>12</sup>Configurations are represented by Slater determinants or CSFs, which are linear combinations of Slater determinants.

<sup>13</sup>See footnote 9.

### 2.18.2.2 Multiconfigurational Self-Consistent Field

The multiconfigurational self-consistent field (MCSCF) combines CI and SCF methodologies. The MCSCF wave function is:

$$\Psi_{\text{MCSCF}} = \sum_I c_I \Psi_I. \quad (2.42)$$

In addition to variationally optimizing the coefficients  $c_I$  of the Slater determinants<sup>14</sup>  $\Psi_I$  to minimize the energy, which is already done in usual CI calculations, in MCSCF the orthonormal orbitals that make  $\Psi_I$  are themselves optimized (*i.e.* the coefficients of each orbital as a linear combination of the basis functions are optimized). This approach provides a more accurate treatment of static correlation effects.

Complete active space self-consistent field (CASSCF) and restricted active space self-consistent field (RASSCF) are types of MCSCF that can be understood with the earlier definitions of CAS and RAS.

### 2.18.2.3 NEVPT2 Method

Second order n-electron valence state perturbation theory (NEVPT2) is a perturbation theory approach that extends MP2 to CASSCF wave functions. It accounts for both static and dynamic correlation effects beyond the reference wave function up to second order. In NEVPT2, the wave function is expanded as a linear combination of the reference state and excited determinants. The second order energy correction is then obtained by evaluating the perturbation series.

## 2.19 Vertical and Adiabatic Transitions

In quantum chemistry, vertical and adiabatic transitions refer to different types of vibronic transitions within a molecule.

### 2.19.1 Vertical Transitions

Vertical transitions in quantum chemistry involve the excitation of a molecule to an electronic excited state while keeping the nuclear configuration fixed. This means that the positions of the atomic nuclei remain unchanged during the transition. The energy associated with a vertical transition is the vertical excitation energy. Vertical excitation

---

<sup>14</sup>Or CSFs. See footnote 12.

energies are accurate in fast processes where there is not enough time for the nuclear geometry to change.

### 2.19.2 Adiabatic Transitions

Unlike vertical transitions, adiabatic transitions involve changes in a molecule's nuclear configuration, resulting in what we call adiabatic excitation energy. In adiabatic transitions, the positions of atomic nuclei adjust to the new electronic configuration. The adiabatic excitation energy generally differs from the vertical excitation energy because it considers the nuclear reorganization energy associated with this relaxation of nuclear geometry during an electronic state change.

## 2.20 Thermally Activated Delayed Fluorescence

As already stated, TADF is a process observed in certain organic molecules where delayed fluorescence occurs due to the efficient conversion of triplet excitons to emissive singlet excitons. This phenomenon has gained significant attention in the field of OLEDs as it enables the harvesting of both singlet and triplet excitons, leading to enhanced device efficiency. The occurrence of TADF is governed by specific energy criteria that are essential for its manifestation. In this section, the energy criteria necessary for the occurrence of TADF will be discussed.

### 2.20.1 Reverse Intersystem Crossing

RISC (reverse intersystem crossing) refers to a thermally activated process where triplet excitons transition to a singlet state. The transition from the lowest-lying triplet state  $T_1$  to the first excited singlet state  $S_1$  is spin-forbidden, meaning it occurs relatively slowly and is less likely to happen. However, in TADF materials, RISC can be facilitated by the small energy gap between the  $S_1$  and  $T_1$  states.

During RISC, the triplet excitons gain enough thermal energy to convert back to the singlet state. Then, the triplet excitons can radiatively relax to the ground state, resulting in the emission of light with high quantum efficiency. By utilizing RISC, TADF emitters can achieve a theoretical IQE of 100%, making them highly efficient for OLED applications.

### 2.20.2 $T_1$ to $S_1$ Energy Gap

The key requirement for TADF is a small energy difference between the lowest singlet excited state ( $S_1$ ) and the lowest triplet excited state ( $T_1$ ) of the molecule.<sup>15</sup> The small  $\Delta E_{ST}$  allows for efficient RISC. The energy criterion for TADF can be expressed as  $\Delta E_{ST}$  being the same order of magnitude of  $k_B T$ , where  $k_B$  is the Boltzmann constant and  $T$  is the temperature. The small  $\Delta E_{ST}$  ensures that the thermal energy at room temperature is sufficient to facilitate RISC, leading to the population of the singlet excited state and subsequent delayed fluorescence. It is stated in the equations:

$$\Delta E_{ST} = E(S_1) - E(T_1), \quad (2.43)$$

$$\Delta E_{ST} \sim k_B T. \quad (2.44)$$

### 2.20.3 Charge Transfer Character

Molecules with charge transfer (CT) character often exhibit favorable TADF properties (GUO *et al.*, 2023; FROITZHEIM *et al.*, 2022; CHEN *et al.*, 2018; ZHANG *et al.*, 2014). In these systems, the singlet and triplet excited states have different degrees of charge separation, leading to a small  $\Delta E_{ST}$  and efficient RISC. The presence of CT character promotes the mixing of singlet and triplet states, facilitating the conversion of triplets to singlets through molecular reorganization and spin-flip processes.

---

<sup>15</sup>As mentioned in Chapter 1, Aizawa *et al.* and many other authors call this value *singlet-triplet energy gap* but this nomenclature is avoided in this study, since Yang *et al.* use it to designate  $E(T_1)$ .

**Appendix B - “Exploring Thermally  
Activated Delayed Fluorescence in  
B,N-Substituted Tetracene Derivatives:  
Towards Enhanced OLED Materials”**

## Exploring Thermally Activated Delayed Fluorescence in B,N-Substituted Tetracene Derivatives: Towards Enhanced OLED Materials

J. V. M. Pimentel<sup>a</sup>, M. Pinheiro Jr.<sup>a</sup>, A. J. A. Aquino<sup>b</sup>, H. Lischka<sup>c,\*</sup>, F. B. C. Machado<sup>a,\*</sup>

<sup>a</sup>*Departamento de Química, Instituto Tecnológico de Aeronáutica, São José dos Campos, 12228-900, São Paulo, Brazil*

<sup>b</sup>*Department of Mechanical Engineering, Texas Tech University, Lubbock, 79409, Texas, United States of America*

<sup>c</sup>*Department of Chemistry and Biochemistry, Texas Tech University, Lubbock, 79409, Texas, United States of America*

\*Corresponding authors. Emails: hans.lischka@ttu.edu; fmachado@ita.br

### Abstract

Polycyclic aromatic hydrocarbons (PAHs) exhibit intriguing characteristics that position them as promising candidates for advancements in organic semiconductor technologies. Notably, tetracene finds substantial utility in Electronics due to its application in organic light-emitting diodes (OLEDs) and organic field-effect transistors (OFETs). The strategic introduction of an isoelectronic boron-nitrogen (B,N) pair to replace a carbon-carbon pair in acenes introduces polarization, allowing for the controlled modulation of diradical characteristics. Consequently, this B,N substitution enables precise adjustments in chemical, optical, and electronic attributes. In this work, we undertook a systematic exploration of thermally activated delayed fluorescence (TADF) phenomena within a set of 77 B,N-substituted derivatives of tetracene. The primary objective was to identify and select prospective molecules for the fabrication of OLEDs. Employing multiconfigurational methods of computational quantum chemistry, we conducted an extensive investigation to unravel the potential candidates. As a result, we identified twelve molecules that might exhibit the sought-after TADF behavior. This research not only contributes to a deeper understanding of the influence of B,N substitution on acene derivatives but also opens doors for the development of organic electronics by harnessing the properties of these selected molecules.

*Keywords:* Excited states, Polycyclic aromatic hydrocarbons, Acenes, multireference methods

### 1. Introduction

Organic light-emitting diodes (OLEDs) represent a significant advancement in light-emitting diode (LED) technology. Unlike traditional inorganic LEDs, OLEDs employ organic compounds as the emissive layer, enabling applications in various domains. OLEDs offer advantages such as energy efficiency, flexible form factors, and vibrant colors. The development of efficient OLEDs relies on selecting organic materials with desirable photophysical properties, including efficient light emission and charge transport characteristics.<sup>1</sup> In comparison to liquid-crystal displays (LCD) screens, OLED displays provide better contrast, improved color reproduction, faster refresh rates, thinner design, wider viewing angles, energy efficiency, and the potential for flexible and curved displays.<sup>2,3</sup>

Different types of OLEDs have been explored, including fluorescent OLEDs (FOLEDs) and phosphorescent OLEDs (PhOLEDs). First-generation OLEDs, the FOLEDs, utilize organic dyes as emitters. These dyes primarily undergo the transition of singlet excitons to the singlet ground state ( $S_1 \rightarrow S_0$ ) by fluorescence. But LEDs operate via electroluminescence, for which optical selection rules do not apply. As a result, singlet and triplet excitons are produced in a statistical ratio of 1:3. Since the intersystem

crossing (ISC) decay of the triplet excitons to the ground state is spin-forbidden, the efficiency of fluorescence OLEDs is limited to around 25%, resulting in an upper limit of 5% external quantum efficiency (EQE) without additional optical outcoupling.<sup>3</sup>

To harness the triplet excitons, which constitute 75% of the total amount of excitons, and improve OLED efficiency, phosphorescent heavy metal complexes have been developed as emitters for the second generation of OLEDs.<sup>4</sup> These metal-containing complexes enhance spin-orbit coupling, reducing the lifetime of the lowest-lying triplet state  $T_1$ .<sup>5,6</sup> This leads to phosphorescence as  $T_1$  decays to the ground state  $S_0$ , with facilitated intersystem crossing (ISC) from the lowest-lying singlet state  $S_1$  to  $T_1$ . This triplet-based approach enables phosphorescent emitters to achieve internal quantum efficiency (IQE) close to 100%, resulting in high EQEs.<sup>1,7</sup> While PhOLEDs have demonstrated high efficiency due to the utilization of triplet excitons, they often require expensive and scarce heavy metal complexes as emitter materials. As an alternative, thermally activated delayed fluorescence (TADF) has emerged as a promising mechanism for achieving high-efficiency OLEDs without relying on heavy metals.<sup>8,9</sup>

Achieving efficient TADF hinges on the energy gap between the lowest singlet and triplet excited states, denoted as

$$\Delta E_{ST} = E(S_1) - E(T_1), \quad (1)$$

being small enough to facilitate efficient reverse intersystem crossing (RISC). If the triplet excitons ( $T_1$ ) possess a sufficiently long lifetime, thermally activated RISC, though formally spin-forbidden, permits the conversion of triplet excitons into singlet excitons ( $S_1$ ). Subsequent radiative relaxation leads to a theoretical IQE of 100%.<sup>10,11</sup>

The energy criterion for TADF is the following:  $\Delta E_{ST}$  should be of the same order of magnitude as  $k_B T$ , where  $k_B$  is the Boltzmann constant and  $T$  is the temperature. The small  $\Delta E_{ST}$  ensures that the thermal energy at room temperature is sufficient to facilitate RISC, leading to the population of the singlet excited state and subsequent delayed fluorescence.

Polycyclic aromatic hydrocarbons (PAHs) have garnered substantial interest due to their intriguing properties and potential applications in various fields, including optoelectronics. Among PAHs, acenes have emerged as a promising class of compounds for electronic device fabrication. Acenes, characterized by their linear arrangement of fused aromatic rings, possess unique electronic structures that make them attractive for use in organic semiconductor technologies.<sup>12</sup>

Among PAHs of similar size, acenes have the smallest energy gaps between the highest occupied and the lowest unoccupied molecular orbitals (HOMO-LUMO gaps). Larger acenes display open-shell character, being more reactive than many other PAHs.<sup>13</sup> Higher acenes are also more prone to polymerization and photooxidation and difficult to synthesize.

Achieving the desired properties of a compound for a specific application often requires a delicate balance of tradeoffs. Fine-tuning molecular properties without significantly altering the compound's overall structure requires synthesizing a large number of acene derivatives, which can be an arduous and costly endeavor. Theoretical calculations provide a useful tool for fine-tuning the properties of acene derivatives. Through such calculations, we can explore the relatively uncharted chemical space of acene derivatives and identify exceptional molecules without risking resources on potentially underperforming candidates.

The insertion of heteroatoms in acenes is an efficient strategy to change properties such as conjugation, stability and diradicaloid character<sup>14–18</sup> and tune them to a specific application. In recent years, several research groups have reported significant advancements in the synthesis and application of B,N-substituted organic semiconductors as TADF emitters in OLEDs. These materials hold great promise for novel optoelectronic devices. For instance, Matsui et al.<sup>19</sup> demonstrated the synthesis of B,N-doped nanographenes through a one-shot multiple borylation reaction. The researchers employed a B,N-doped nanographene as an emitter in an OLED device, achieving deep pure-blue emission with an external quantum efficiency of 18.3%. Suresh et al.<sup>20</sup> designed and synthesized an easily accessible B,N-doped heptacene with high thermal stability, exhibiting TADF at ambient temperature originating from a multiresonant state. Changes in the optoelectronic properties of the heptacene molecule were predicted by altering the positions of boron and nitrogen atoms. Earlier, Ishibashi et al.<sup>21</sup> were successful in achieving the synthesis of a B,N-substituted tetracene. It displayed distinct characteristics, including a slightly widened HOMO-LUMO gap. Additionally, the HOMO energy level was observed to be positioned at a lower energy compared to the pristine tetracene, contributing to its altered electronic structure. Remarkably, this synthesized compound also exhibited enhanced resistance to photodecomposition when compared with the unmodified tetracene molecule. Theoretical analyses conducted by Ishibashi et al.<sup>21</sup> further predicted variations in the HOMO and LUMO energies based on the positions of the heteroatoms.

These studies contributed to the growing research on TADF-based OLEDs based on B,N-substituted acenes as potential emitters. The present study focuses on exploring the potential of acenes, with a particular focus on tetracene as a representative member of this class. Rubrene, a derivative of tetracene, is known for its impressive hole mobility, making it a well-studied candidate for applications such as OLEDs, organic photovoltaics (OPVs)<sup>22</sup>, organic field effect transistors (OFETs),<sup>23–26</sup> and more. The high charge carrier mobility exhibited by acenes, including rubrene, compared to other organic semiconductors plays a crucial role in enabling efficient charge generation, transport, and electroluminescence in these devices.

In a previous study,<sup>15</sup> our research group identified four promising B,N-substituted tetracene candidates with focus on singlet fission (SF). The findings demonstrated that substitution of a pair of carbon atoms with one boron and one nitrogen atom effectively modulates the diradicaloid nature of B,N-substituted derivatives. This modulation led to significant changes in the excitonic and energetic properties of the molecules. Building on this prior work, the present work aims to extend the investigation to identify promising candidates for TADF, which has significantly distinct energetic criteria from SF. By systematically exploring the all the possible B,N-substitution patterns of tetracene, this study seeks to identify compounds with the potential for efficient TADF behavior and chemical stability. For that purpose, the  $S_1$  and  $T_1$  states were analyzed using high-level multireference (MR) methods based on second-order n-electron valence state perturbation theory (NEVPT2)<sup>27</sup> and multireference configuration interaction with single and double excitations (MR-CISD).<sup>28,29</sup>

## 2. Method and Models

### 2.1. Nomenclature of the B,N-Substituted Tetracene Molecules

Only one B,N pair is used for doping in each B,N-tetracene molecule analyzed in this work. For the positioning of atoms within the tetracene moiety, we have adopted the numbering scheme shown in Figure 1. To characterize each B,N-tetracene isomer, the order of (B atom position),(N atom position) is specified. To classify the positions, a “position class” is defined as a set of positions that are equivalent to one another due to symmetry. Five distinct position classes can be recognized: {1, 4, 10, 13}, {2, 3, 11, 12}, {5, 9, 14, 18}, {6, 8, 15, 17}, and {7, 16}. To address potential ambiguities arising from symmetry, two rules are established: (i) the B atom position should be labeled with the lowest possible number; (ii) once rule (i) is satisfied, the N atom position should be labeled with the lowest possible number.

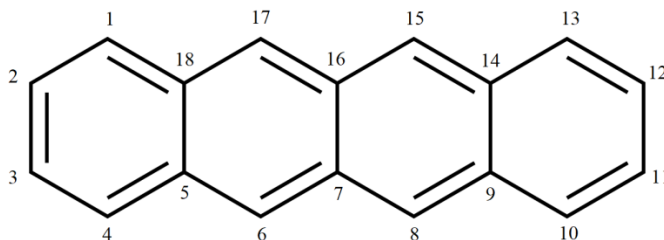


Figure 1: Atom labeling scheme within the structure of tetracene.

Following rule (i) of our nomenclature, it is possible to place the B atom in positions 1, 2, 5, 6, or 7, which represent all five classes. For each of the first four choices, there are 17 distinct positions remaining to place the N atom (excluding the position already occupied by B). If the B atom is positioned at position 7, due to symmetry with respect to the vertical plane containing the 7–16 bond that is orthogonal to the plane of the paper, only 9 non-equivalent positions are available for the N atom. In total, there are  $4 \times 17 + 9 = 77$  possible B,N-tetracene molecules, as enumerated by Chakraborty et al.<sup>30</sup>

## 2.2. Geometries and Overview of the Method

The pristine tetracene exhibits  $D_{2h}$  symmetry, the structure 7,16 has  $C_{2v}$  symmetry, and the 76 remaining structures display  $C_s$  symmetry. Using the geometries of our previous work,<sup>15</sup> tetracene and the other 17 B,N-tetracene structures not previously characterized, were optimized using the same methodology, i.e. the second-order Møller-Plesset perturbation theory and the resolution of identity approximation (RI-MP2)<sup>31</sup> in combination with the def2-TZVP basis set.<sup>32</sup> All the Cartesian coordinates are available in the Supporting Information (SI). At the MP2/def2-TZVP geometries, the excited singlet and triplet states were calculated using NEVPT2<sup>27</sup> and MR-CISD<sup>28,29,33,34</sup> as explained below.

## 2.3. NEVPT2 Calculations

Initially, complete active space self-consistent field (CASSCF)<sup>35</sup> calculations correlating the active space orbitals were performed to construct the reference wave function, which captures the static correlation inherent in singlet open-shell systems. The resulting molecular orbitals and configuration state functions (CSFs) from the CASSCF calculations were then utilized in the subsequent MR calculations. The NEVPT2 calculations were performed using the strongly contracted (SC) approach. The active space for the CASSCF procedure included 12 electrons in 12  $\pi$  orbitals, denoted as CAS(12,12). The MP2 natural orbitals (NOs) were used to generate the initial guess for the CASSCF calculations, which consisted of the six highest occupied and the six lowest unoccupied NOs. For the computation of excited states, a state-averaged

CASSCF scheme was employed, considering five states of equal weight (1/5), the three lowest singlets and the two lowest triplets resulting from  $\pi$ - $\pi^*$  excitations. All calculations were carried out using the def2-TZVP basis set.<sup>32</sup>

#### 2.4. *Multireference configuration interaction considering single and double excitations (MR-CISD) Calculations*

The MR-CISD calculations have been performed using an uncontracted approach.<sup>28</sup> To reduce the computational cost associated with the uncontracted MR-CISD calculations, an active space of eight electrons in eight  $\pi$  orbitals (CAS(8,8)) was employed, for both the CASSCF calculation and the MR-CISD reference space. The initial active orbitals were obtained from a prior Hartree-Fock calculation by selecting the four highest occupied and four lowest unoccupied  $\pi$  orbitals. Like in the CASSCF calculations prior to the NEVPT2 calculations, no orbitals were kept frozen at this level. In the MR-CISD calculations, electron correlation was introduced for all  $\pi$  orbitals and twelve  $\sigma$  orbitals (six doubly occupied in the reference space and six virtual orbitals), while the remaining  $\sigma$  orbitals were frozen. The MR-CISD external configurations encompassed all permissible single and double electron excitations as per the generalized interacting space restrictions<sup>36,37</sup> (see the schematic illustration in Figure S1 in the Supporting Information).

In contrast to NEVPT2, the CASSCF calculations were separately performed for different spin multiplicities. Specifically, three singlet roots of  $A'$  symmetry were computed with equal weights (1/3) in a state-averaged fashion. Separately, three triplet roots of  $A'$  symmetry with equal weights (1/3) underwent a similar procedure. The CAS(8,8)/MR-CISD calculations employed the Pople 6-31G\* basis set.<sup>38</sup> To include size extensivity, excitation energies in the MR-CISD calculations, the Pople correction<sup>28,39</sup> was included, which will be denoted as +P. The MR-CISD calculations for both 7,16 and pristine tetracene were conducted with  $C_s$  symmetry, consistent with the other molecules under investigation.

#### 2.5 *Multireference averaged quadratic coupled-cluster (MR-AQCC) calculations*

To enhance the accuracy of unpaired electron results, we conducted MR-AQCC calculations on the singlet ground state of each identified TADF candidate molecule. This approach was adopted due to the tendency of MR-CISD to underestimate  $N_U$ . The computational procedures closely followed the CAS(8,8)/MR-CISD calculations. The main change is that this time, we only looked at the singlet ground state, unlike before when we considered both the singlet and triplet states. When possible, the active space mirrored that of the CAS(8,8)/MR-CISD calculations. However, for two specific candidates, intruder states with contributions exceeding 1% were included.

The RI-MP2 geometry optimization and NEVPT2 calculations were carried out using the ORCA 4.0 program package.<sup>40,41</sup> The MR-CISD and MR-AQCC calculations utilized the COLUMBUS software, making efficient use of the available parallel algorithm.<sup>42,43</sup>

#### 2.6. *HOMA*

To evaluate and quantify the aromaticity of each ring in each B,N-tetracene structure, the harmonic oscillator model of aromaticity (HOMA)<sup>44,45</sup> was chosen, which is based on bond lengths as given by Equation (2):

$$HOMA = 1 - \frac{1}{n} \sum_{a,b} \alpha(a,b) (R_{opt}(a,b) - R_i(a,b))^2. \quad (2)$$

Here, the sum is taken over all pairs (a, b) of adjacent atoms (i.e., that share a bond) in a ring, where  $n$  is the number of atoms in a ring (6 in this study), and  $R_i(a,b)$  is the bond length of the bond between atoms  $a$  and  $b$ . The empirical parameters  $\alpha(a,b)$  and  $R_{opt}(a,b)$  depend on the atoms and are determined such that the following conditions are satisfied: (i) in an ideal aromatic ring, HOMA should be 1, so  $R_{opt}(a,b)$  is equal to the value  $R_i(a,b)$ ; (ii) in a non-aromatic ring, i.e., that lacks resonance and has marked alternating bond lengths between the single and double bonds, HOMA should be 0.

The values considered for  $R_{opt}$  and  $\alpha$  are provided in Table S1 in the Supporting Information.

### 2.7. Effectively Unpaired Electrons

The theory of effectively unpaired electrons has been developed by Takatsuka et al.<sup>46</sup> It has been shown previously<sup>47</sup> that Head-Gordon’s nonlinear formula<sup>48</sup> provides a useful approach for computing the total number of effectively unpaired electrons in molecules. The formula can be expressed as:

$$N_U = \sum_i n_i^2 (2 - n_i)^2, \quad (3)$$

where  $n_i$  is the occupation number of the  $i^{\text{th}}$  NO and the sum goes over all NOs.

The density of effectively unpaired electrons (or spin density) is defined as

$$\rho_U(\mathbf{r}) = \sum_i n_i^2 (2 - n_i)^2 |\psi_i(\mathbf{r})|^2, \quad (4)$$

where  $\psi_i(\mathbf{r})$  is the normalized  $i^{\text{th}}$  NO.

The number of effectively unpaired electrons provides a quantitative measure of the diradical character of a molecule. Diradical character signifies the extent to which two electrons occupy two nearly degenerate molecular orbitals, implying the manifestation of radical-like or open-shell properties. A significant diradical character suggests the presence of one unpaired electron in each of the two degenerate molecular orbitals. Conversely, a low diradical character indicates the occupation of all occupied molecular orbitals by electron pairs, resulting in a closed-shell configuration.

The unpaired electron density and the effective number of unpaired electrons  $N_U$  were calculated<sup>48</sup> with the TheoDORE program<sup>49-51</sup> using the MR-CISD and MR-AQCC wave functions.

### 2.8. Multicenter bond indices (MCI)

Considering a ring of  $n$  atoms to be represented by the string  $\mathcal{A} = \{A_1, A_2, \dots, A_n\}$ , whose elements are ordered according to the connectivity of the atoms in the ring, MCI<sup>52,53</sup> is defined to be:

$$MCI(\mathcal{A}) = \sum_{P \in \mathcal{P}(\mathcal{A})} \sum_{i_1, i_2, \dots, i_n}^{\text{occ}} S_{i_1 i_2}(P(A_1)) S_{i_2 i_3}(P(A_2)) \dots S_{i_n i_1}(P(A_n)), \quad (5)$$

where  $\mathcal{P}(\mathcal{A})$  is the set of all  $n!$  permutations of the string  $\mathcal{A}$  and  $S_{ij}(A)$  is the overlap of molecular orbitals  $i$  and  $j$  in the atom  $A$ . By taking all permutations into account rather than considering only the original string, one ensures that the Kekulé structure is not the only one to be considered. MCI is greater for aromatic species, as it indicates a greater electron sharing in the ring.

The atomic overlap matrices were calculated using the QTAIM partition with the AIMAll software.<sup>54</sup> MCI values were calculated using the ESI-3D program.<sup>55</sup>

### 2.9. NICS

Nucleus Independent Chemical Shifts (NICS) were calculated to elucidate the aromaticity of the molecules.<sup>56</sup> The NICS values were calculated employing the Gauge-Independent Atomic Orbital (GIAO) method,<sup>57</sup> utilizing the B3LYP functional<sup>58</sup> with the pcS-3 basis set,<sup>59</sup> implemented on Gaussian software.<sup>60</sup> We analyzed the negative of the  $zz$  component of the NICS calculated 1 Å above the geometrical center of each ring:

$$-NICS_{zz}(1) = \sigma_{zz}(1), \quad (6)$$

where  $\sigma(\mathbf{r})$  is the chemical shielding tensor that relates the induced magnetic field to the applied magnetic field.

The visualization of the chemical shielding tensors was accomplished using the Visualization of the Chemical Shielding Tensors (VIST) method,<sup>61</sup> implemented in TheoDORE.<sup>49-51</sup> The VIST method involves diagonalizing the chemical shift tensor and showing a dumbbell along each of its three principal axes, providing a comprehensive visualization of the chemical shielding tensor and insights into aromaticity. The size and length of each dumbbell is proportional to the magnitude of the eigenvalue corresponding to it. Its color is blue if the eigenvalue is positive (indicating shielding/aromaticity), and red if it is negative (indicating deshielding/antiaromaticity). Similarly,  $-NICS_{zz}(1)$  being positive/negative indicates aromaticity/antiaromaticity.

### 2.10. Anisotropy of the Induced Current Density (ACID)

We employed the ACID software by Geuenich et al. to visualize isosurfaces of the ACID scalar field of selected molecules. The ACID plot allows one to see the delocalization of the electron density in a molecule, which is correlated with the aromaticity.<sup>62</sup> Besides the total plot, separate plots were also made for the  $\sigma$  and  $\pi$  contributions alone.

### 2.11. Selection of Candidates for TADF

All energies corresponding to excited states, denoted as  $E(T_n)$  or  $E(S_n)$ , are calculated with respect to the ground singlet state ( $S_0$ ), which serves as the reference energy. Furthermore, for the selection of Thermally Activated Delayed Fluorescence (TADF) candidates, a criterion of

$$\Delta E_{ST} < 0.2 \text{ eV} \quad (5)$$

is applied.<sup>8,62</sup> This criterion ensures that the energy difference between the singlet and triplet states is less than approximately  $8k_B T$  at room temperature ( $T = 300 \text{ K}$ ). By employing it, the TADF candidates thus identified have  $T_1$  triplet excitons capable of undergoing upconversion to the  $S_1$  state by thermal activation.

### 3. Results and discussion

#### 3.1. Method Validation

To validate our computational methods, we compared our results (summarized in Table 1) with prior experimental and calculated tetracene energies. In comparison to experimental data, our SC-NEVPT2(12,12)  $E(S_1)$  value is lower by  $\sim 0.4 \text{ eV}$ . The SC-NEVPT2(12,12)  $E(S_2)$  value surpasses the experimental value by  $\sim 0.2 \text{ eV}$ . DFT/MRCI slightly underestimates both  $E(S_1)$  and  $E(S_2)$  by  $< 0.2 \text{ eV}$ . Our MR-CISD+P(8,8) results match SC-NEVPT2(12,12) for  $E(T_1)$  but overestimate  $E(S_1)$  by  $\sim 0.2 \text{ eV}$  and  $E(S_2)$  by  $\sim 0.4 \text{ eV}$ .

As observed in our previous work,<sup>15</sup> the present MRCISD+P(8,8) calculations exhibit a tendency to slightly overestimate  $E(S_1)$ . Thus, Equ. (5) is fulfilled less frequently in comparison to the SC-NEVPT2 results. This implies that the present MR-CISD indicates a smaller number of potential candidates for TADF than NEVPT2. Given that we were able to include a larger basis set, the correlation of all valence  $\sigma$  orbitals, and a larger active space in NEVPT2 than in MR-CISD, we rely more on the NEVPT2 results for the chemical screening based on energetic criteria for TADF. However, we utilize the MR-CISD results to complement the analysis by providing information on the diradicaloid character of the systems and the multiconfigurational character of the wave functions. Unless specifically mentioned, the reported energy values for all systems will be provided at the SC-NEVPT2(12,12) level of theory.

Table 1: Comparative Analysis of Vertical Energies of Tetracene

Study	Energy	Value (eV)
SC-NEVPT2(12,12)	$E(T_1)$	1.59
	$E(S_1)$	2.46
	$E(T_2)$	2.91
	$E(S_2)$	3.63
MR-CISD+P(8,8)	$E(T_1)$	1.58
	$E(S_1)$	3.04
	$E(T_2)$	2.82
	$E(S_2)$	3.75

pp-RPA@R <sup>63</sup>	E(T <sub>1</sub> )	1.39
	E(S <sub>1</sub> )	2.82
	E(T <sub>2</sub> )	3.11
DFT/MRCI <sup>64</sup>	E(S <sub>1</sub> )	2.74
	E(S <sub>2</sub> )	3.22
Experimental	E(T <sub>1</sub> ) <sup>a</sup>	1.27
	E(S <sub>1</sub> ) <sup>b</sup>	2.88
	E(S <sub>2</sub> ) <sup>b</sup>	3.39
<sup>a</sup> Data from Ref. <sup>63</sup> , citing the original source in Ref. <sup>65</sup>		
<sup>b</sup> Ref. <sup>66</sup> with Grimme and Parac’s correction for solvent effects <sup>67</sup>		

The availability of experimental data for B,N-tetracene molecules is limited, posing a challenge in assessing the accuracy of our methods. However, a relevant study conducted by Ishibashi et al.<sup>21</sup> examined a closely related compound to one of the molecules investigated in this article. Specifically, they provided experimental measurements for the energy associated with the  $S_0 \rightarrow S_1$  transition in 2-nBu-tetracene and 2-nBu-2,1-B,N-tetracene, representing the lowest-energy absorption peaks observed in the UV-vis spectra. The reported values were 2.78 eV for 2-nBu-tetracene, which closely resembles the experimental values obtained for pristine tetracene. This suggests that the presence of the butyl group does not significantly influence the optical properties of the molecule. For 2-nBu-2,1-B,N-tetracene, Ishibashi et al.<sup>21</sup> measured a value of 2.90 eV. In our study, we determined  $E(S_1) = 3.18$  eV for compound 2,1 using the NEVPT2 level of theory, and this result aligns with the finding of Ishibashi et al.<sup>21</sup> This comparison is shown in Table 2.

Table 2: Comparison of Energy Values for Tetracene and Derivatives

Study	Compound	E(S <sub>1</sub> ) (eV)
SC-NEVPT2(12,12)	Tetracene	2.46
	2,1-B,N-tetracene	3.18
MR-CISD+P(8,8)	Tetracene	3.04
	2,1-B,N-tetracene	3.36
Ishibashi et al. <sup>a</sup>	2-nBu-tetracene	2.78
	2-nBu-2,1-B,N-tetracene	2.90
<sup>a</sup> UV-Vis experimental values <sup>21</sup>		

### 3.2. TADF Candidates

The graphical representation of the molecules that fulfill the two criteria for TADF as predicted by the NEVPT2 calculations is shown in Figure 2. The numerical values of  $E(S_1)$  and  $E(T_1)$  are collected in Table S4 of the SI. They are above the dashed line indicating the condition  $\Delta E = 0.2$  eV. Among all the 77 B,N-tetracene molecules, we found twelve TADF candidates highlighted in Figure 2. They are: 1,11; 1,14; 1,15; 2,9; 2,14; 2,16; 5,8; 5,12; 6,1; 6,9; 6,11, and 6,15. It is worth noting that tetracene itself (marked by a cross in Figure 2) does not fulfill the condition to be a candidate for TADF. None of the candidates show a negative  $\Delta E$  value except compound 5,12. In the case of the compound 5,12, our SC-NEVPT2(12,12) calculations yielded  $E(T_1) = 1.53$  eV and  $E(S_1) = 1.48$  eV, which indicates a violation of Hund's rule. However, the calculated difference is -0.05 eV, which is less than the accuracy of the present methodology. Moreover, this inversion is not seen in the MR-CISD+P(8,8).

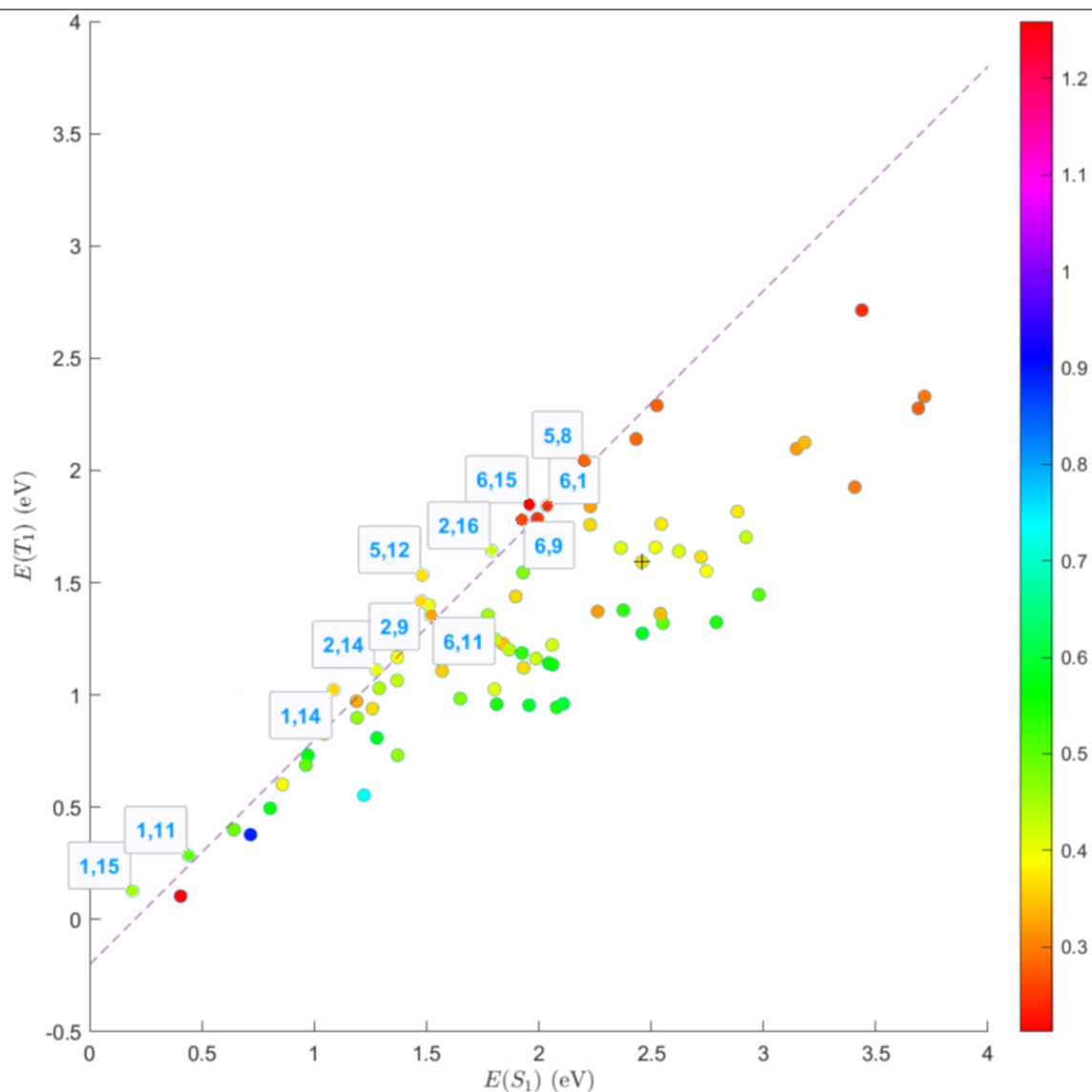


Figure 2: Vertical singlet ( $E(S_1)$ ) and triplet ( $E(T_1)$ ) excitation energies of the 77 BN-doped and pristine tetracene molecules calculated by using the SC-NEVPT2(12,12) method. The dashed line ( $\Delta E_{ST} = 0.2$  eV) indicate the energetic conditions for TADF. The color map represents the total number of effectively unpaired electrons ( $N_U$ ). The names of the twelve optimal B,N-tetracene candidates for TADF are highlighted. The pristine tetracene molecule is marked with a cross.

Figure 2 and Figure S6 show that there are TADF candidates within a wide range of diradicaloid character. In fact, the  $N_U$  values vary from  $0.21e$  (molecule 6,15, the molecule with the lowest  $N_U$  among all B,N-tetracene derivatives) to  $0.50e$  (molecule 1,11) among the TADF candidates, as depicted in Figure S6 and Figure S7. Thus, this analysis shows that there are no TADF candidates with high diradicaloid character. However, the diradicaloid character of the doped tetracene compounds show a remarkable

dependence of the  $N_U$  values on the position of the doping sites. Considering the entire set of 77 B,N-tetracene molecules, the  $N_U$  values can range from as low as  $0.21e$  for 6,15 up to  $1.26e$  for 1,13, representing a six-fold increase. In comparison, pristine tetracene has an  $N_U$  value of  $0.37e$ . Figure 3 shows the  $N_U$  for the TADF candidates calculated with MR-AQCC(8,8) when possible. When intruder states with more than 1% contribution were found, they were removed and the active space was adjusted accordingly. For molecule 1,11, those were  $5a'' \rightarrow 10a''$  and  $9a'' \rightarrow 14a''$ . For molecule 1,15, those were  $5a'' \rightarrow 10a''$  and  $4a'' \rightarrow 10a''$ . Their  $N_U$  values calculated with MR-AQCC fall in the range  $0.4e$  to  $0.7e$  and are significantly higher than the corresponding values calculated with MR-CISD.

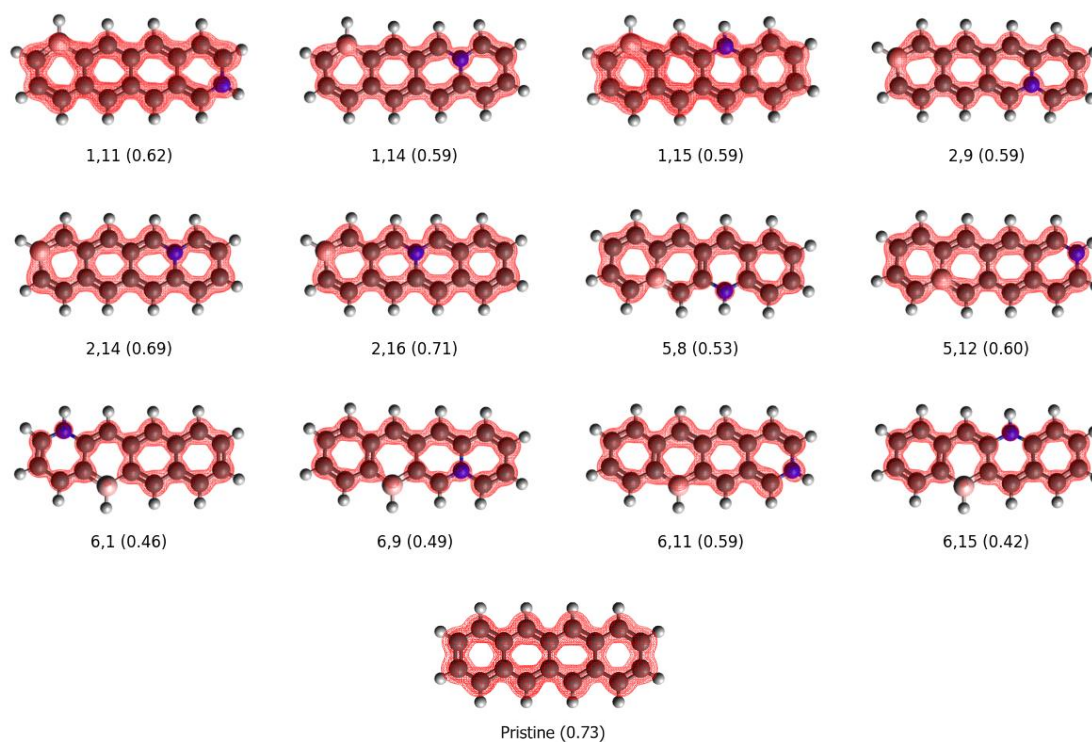


Figure 3: Density of effectively unpaired electron plotted with isovalue  $5 \times 10^{-4} e a_0^{-3}$  and number of effectively unpaired electrons given in parentheses, for each of the TADF candidates.

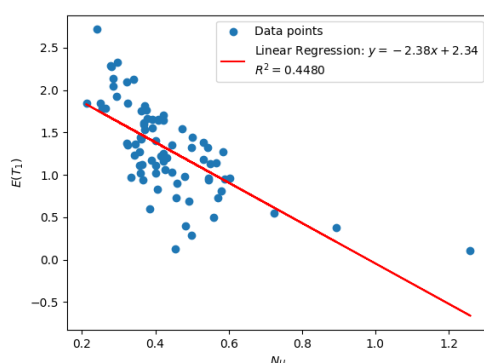


Figure 4: Linear regression analysis of  $E(T_1)$  with respect to the number of unpaired electrons.

Our analysis, though, suggests a correlation between  $E(T_1)$  and  $N_U$  values, as shown in Figure 4. For a more straightforward visualization of the  $E(T_1)$  values, readers may refer to the bar chart provided in Figure S4 in the Supporting Information. Among the ten molecules with the lowest  $E(T_1)$  values, five (1,13; 2,10; 2,8; 1,10; 1,12) also rank among the ten molecules with the highest  $N_U$  values. Conversely, among the ten molecules with the highest  $E(T_1)$  values, seven (6,17; 2,17; 6,5; 6,3; 5,8; 1,4; 6,15) exhibit  $N_U$  values among the ten lowest ones. However, it is important to note that there are exceptions to this trend. For instance, molecule 1,15, which is a TADF candidate that has the second lowest  $E(T_1)$  value of 0.13 eV, displays a relatively low  $N_U$  value of 0.45e. Similarly, molecule 6,12, with an  $E(T_1)$  value of 0.60 eV (the eighth lowest value), exhibits a low  $N_U$  value of 0.39e. Note that this value is similar to the  $N_U$  of pristine tetracene (0.37e).

Among the TADF candidates, 1,11 and 1,15 likely face significant challenges in their synthesis. This arises from their presumably low stability, indicated by their respective  $E(T_1)$  values of 0.29 eV and 0.13 eV. In contrast, the remaining ten TADF candidates present a more promising outlook. All of these exhibit  $E(T_1)$  values exceeding 1.0 eV, with five candidates — 2,16; 5,8; 6,1; 6,9; 6,15 — surpassing the pristine tetracene’s  $E(T_1)$  of 1.59 eV and emitting visible light. This suggests that these five candidates hold the potential for successful synthesis and further exploration.

Figure 5 presents the HOMA index for each ring in the TADF candidates, highlighting the influence of the heteroatoms’ position on the chemical properties of the acene analogues. An interesting trend can be seen: in each molecule, the ring with the highest HOMA value generally contains the nitrogen atom, whereas the ring with the lowest HOMA value contains the boron atom.

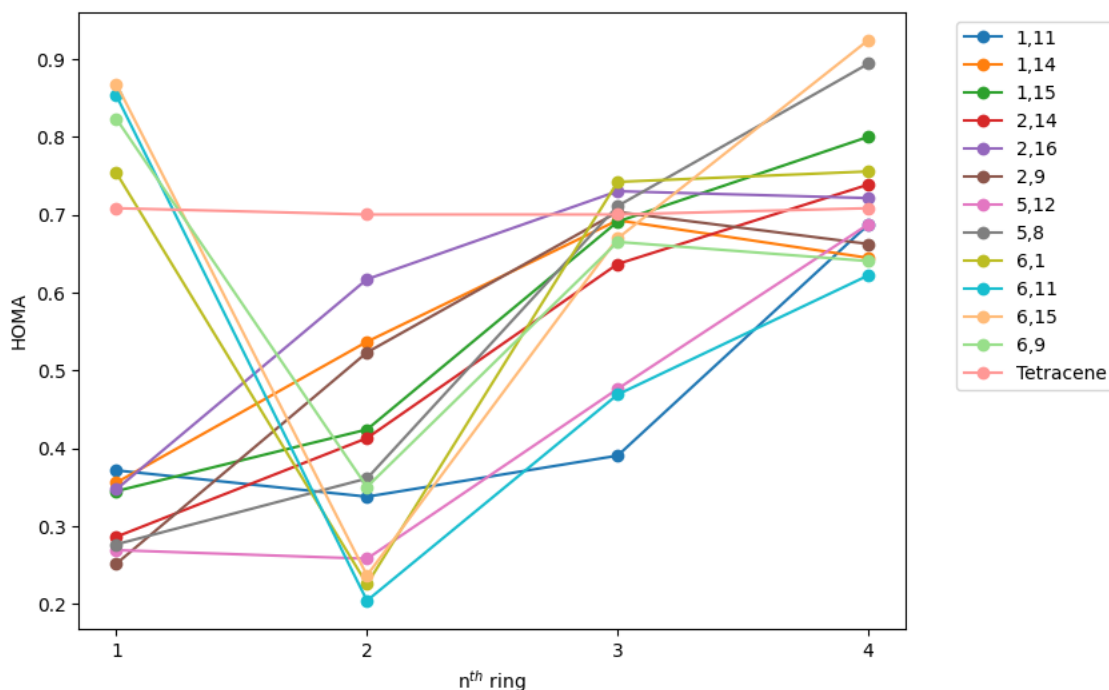


Figure 5: HOMA index of each ring in the TADF candidates and pristine tetracene with the RI-MP2/def2-TZVP optimized geometries.

Overall, our findings demonstrate excellent agreement with the results obtained by Ghosh et al.,<sup>68</sup> with only minor discrepancies observed. The minimum HOMA values in compounds 5,18 and 7,6 show deviations larger than 0.1, indicating some variability in the aromaticity calculations. Figure 6 shows the MCI index for each ring in the TADF candidates, as well as pristine tetracene. The linear regression analysis in Figure 7 reveals a parallel trend between the MCI and HOMA indices of the TADF candidates, suggesting a consistent description of aromaticity. Nevertheless, there are deviations from this general trend, manifested by a number of outliers in the dataset.

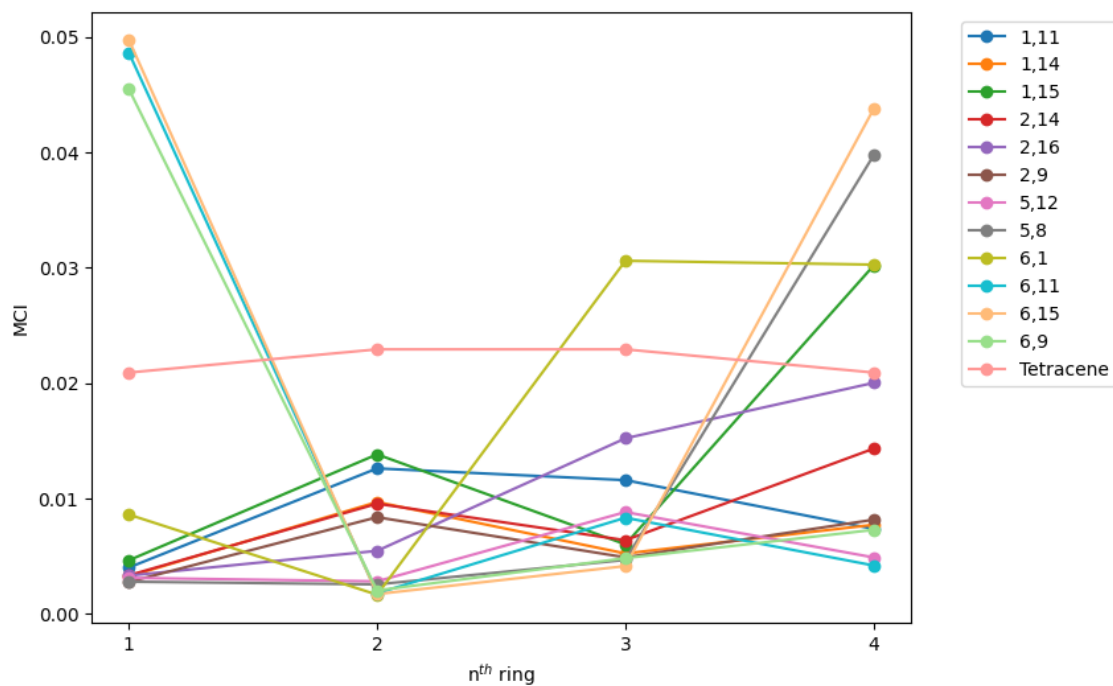


Figure 6: MCI index of each ring in the TADF candidates and pristine tetracene with the RI-MP2/def2-TZVP optimized geometries.

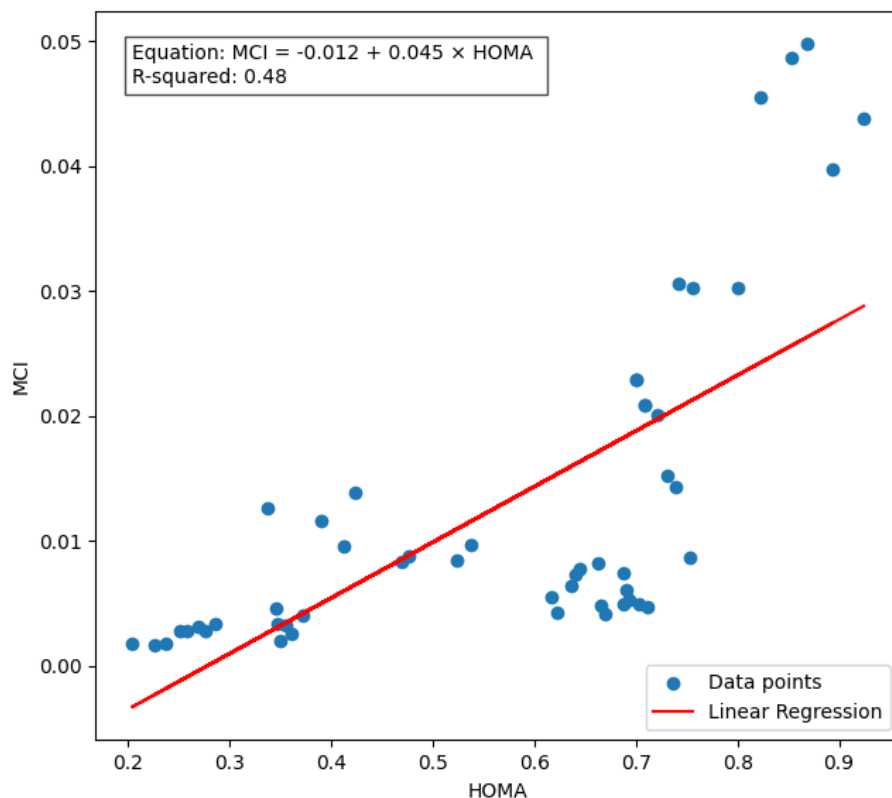


Figure 7: Linear regression analysis of MCI with respect to HOMA for the rings of the TADF candidates.

Figure S5 shows the minimum HOMA value in tetracene and each of its B,N-derivatives. All of the substituted molecules contain at least one ring with a HOMA value lower than 0.70, which is the HOMA value of the four tetracene rings. Hence, none of the analyzed molecules is expected to possess all rings with greater aromaticity or chemical stability than pristine tetracene. Among the TADF candidates, we see that the minimum HOMA varies between 0.20 (compound 6,11) and 0.36 (compound 1,14), which is approximately half of the HOMA of the tetracene rings. Therefore, we can conclude that the minimum HOMA for TADF candidates figures on the the lower side. These molecules have at least one ring significantly less aromatic than tetracene’s rings, even though they may also have a ring that is considerably more aromatic than those of tetracene. Compound 6,15 is an example of that. But that does not mean the TADF candidates cannot be synthesized. In fact, Ishibashi et al.<sup>21</sup> could synthesize a molecule similar to 2,1 even though our analysis suggests the heteroatom-containing ring in 2,1 possesses a relatively low HOMA value of 0.49 (while its other rings exhibit HOMA values 0.74, 0.71, 0.70, close to pristine tetracene).

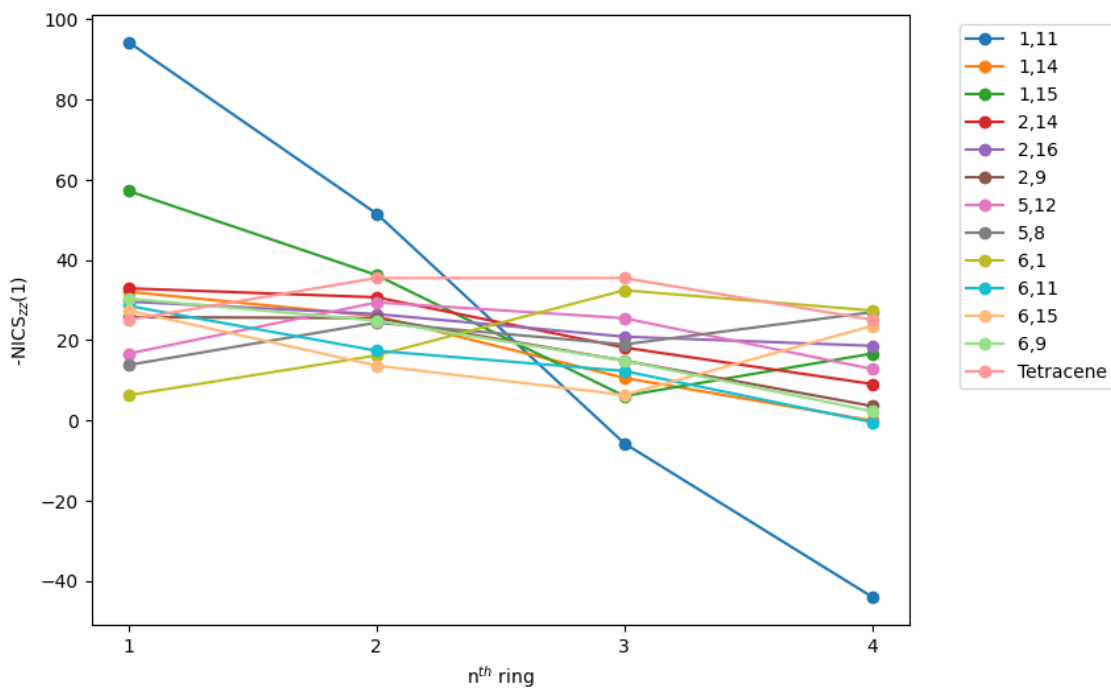


Figure 8:  $-NICS_{zz}(1)$  of each ring in the TADF candidates and pristine tetracene with the RI-MP2/def2-TZVP optimized geometries.

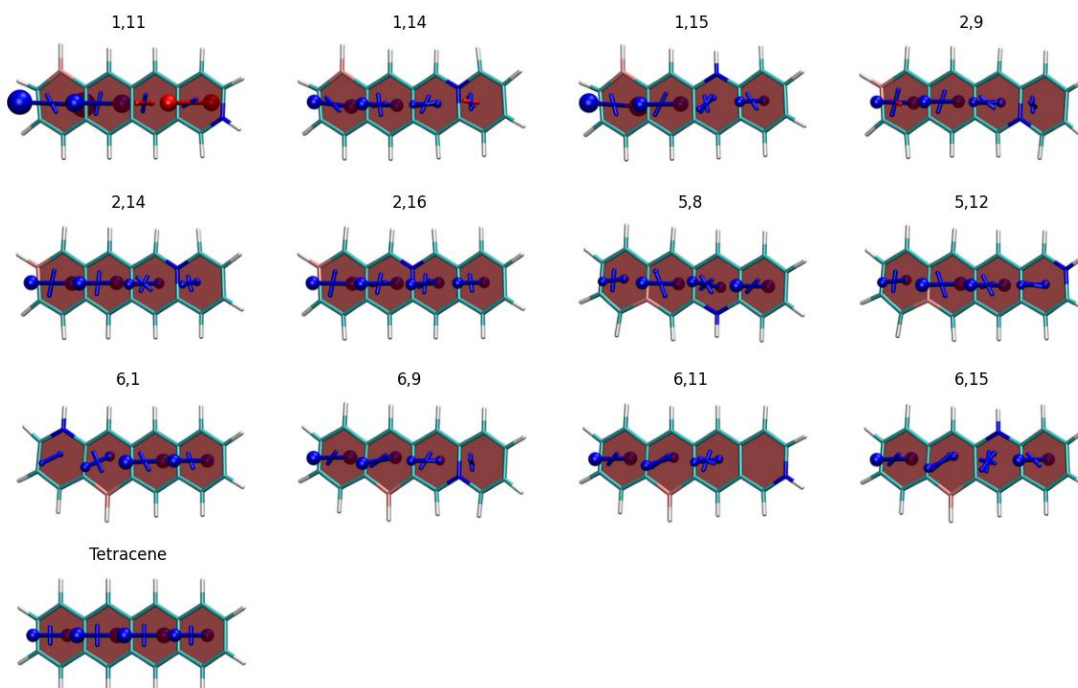


Figure 9: VIST of each ring in the TADF candidates and pristine tetracene with the RI-MP2/def2-TZVP optimized geometries.

The NICS values corresponding to the TADF candidates, alongside pristine tetracene as a reference, are illustrated in Figure 8 and Figure 9. A comparative analysis between Figure 5 and Figure 8 reveals a discrepancy in the quantification of aromaticity between descriptors HOMA and  $-NICS_{zz}(1)$ . This disparity is exemplified by the assessment of the leftmost ring (ring 1) in molecule 1,11. NICS suggests a pronounced aromatic character, whereas the low HOMA and MCI values indicate the opposite interpretation. Molecule 1,11 exhibits in its rings both the highest and the lowest values of  $-NICS_{zz}(1)$  among the candidates, but its HOMA and MCI values are not outstanding.

In Figure S8, the ACID plots are shown for the TADF candidates, as well as tetracene. Particularly interesting are the figures that take into account exclusively the  $\pi$  electrons. We display these plots separately in Figure 10. It can be seen that, for pristine tetracene, there is a diamagnetic ring current along the entire periphery of the molecule, but not in the vertical carbon-carbon bonds, which do not make up the  $\pi$  system. This is expected according to Geuenich et al.<sup>62</sup> In the B,N-substituted molecules, delocalization along the molecule is broken. Furthermore, the  $\pi$  current is stronger next to the nitrogen atom, and weakest next to the boron atom. This corroborates the trend seen in Figure 5 for HOMA: rings containing nitrogen are expected to be the most aromatic and rings containing boron are expected to be the least aromatic.

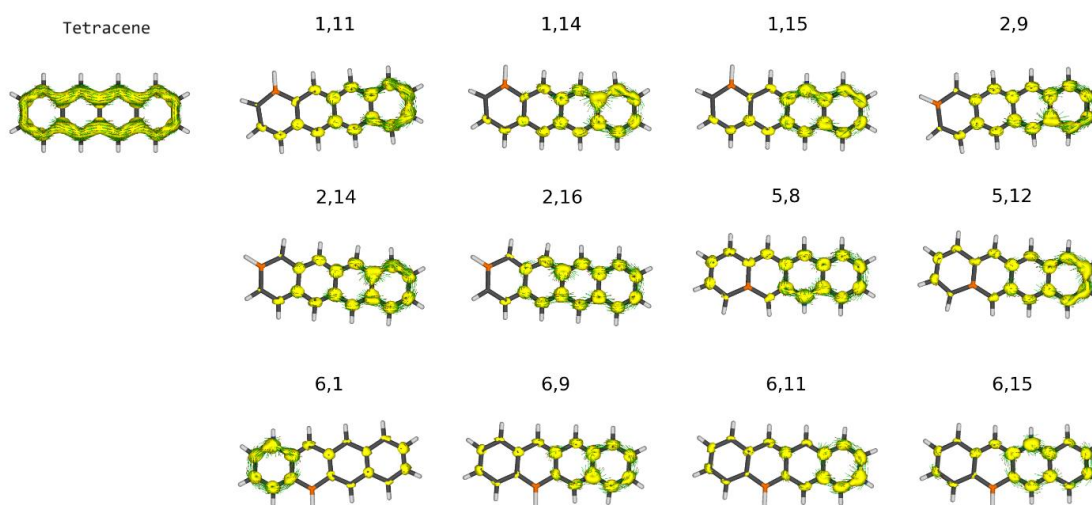


Figure 10: ACID plots relative to the  $\pi$  electrons plotted with isovalue  $5 \times 10^{-2}$  for pristine tetracene and the TADF candidates.

#### 4. Conclusions

In this comprehensive study, we have conducted an in-depth investigation into the potential of B,N-substituted tetracene derivatives for their application in OLEDs based on TADF. By employing multireference methods, we have explored the effects of carbon substitution by nitrogen and boron atoms in tetracene, aiming to find molecules suitable to undergo TADF.

Achieving the delicate balance between modifying molecular properties and preserving the overall structure is crucial for tailoring compounds to specific applications. However, this task poses challenges in terms of synthesizing and evaluating a wide range of molecules, which can be both demanding and costly. The complexity associated with synthesizing acenes further exacerbates these challenges. By employing theoretical calculations, we have unlocked valuable insights in molecular design, enabling us to explore uncharted chemical spaces and identify exceptional molecules without the need to invest resources in unpromising candidates. Our utilization of computational multireference methods has provided a systematic exploration of the effects resulting from carbon substitution by nitrogen and boron atoms in tetracene. This systematic approach has indicated potential efficient B,N-substituted tetracene derivatives.

To validate our computational results, we compared them with available experimental data for similar systems. We found good agreement between the calculated properties and the experimental findings, suggesting the reliability of our computational approach. To understand the relationship between the structural features of B,N-tetracene molecules and their properties, we examined the correlations between molecular descriptors and specific properties, thereby gaining valuable insights into the structure-property relationships in these systems.

Our findings have provided convincing evidence that B,N substitution in tetracene represents a promising approach for achieving molecules with efficiency in undergoing TADF, as the strategic introduction of heteroatoms induces diradicaloid character and polarization, effectively tuning the electronic properties of the resulting derivatives. It is worth noting that none of the B,N-substituted molecules exhibit all rings more aromatic than those observed in pristine tetracene, suggesting that the aromaticity of the tetracene core is significantly affected.

Based on our calculations and analysis, we have successfully identified a set of twelve B,N-tetracene candidates, namely 1,11; 1,14; 1,15; 2,9; 2,14; 2,16; 5,8; 5,12; 6,1; 6,9; 6,11, and 6,15, which exhibit potential for TADF. It was observed that their  $N_U$  values figure on the lower side. This observation suggests that these candidates may possess the necessary stability to be synthesized and effectively employed in TADF-based OLEDs, further bolstering their potential for practical implementation. Specifically, five candidates — 2,16; 5,8; 6,1; 6,9; 6,15 — are likely to emit in the visible range. It is worth noting that two candidates, namely 1,11 and 1,15, have low  $E(T_1)$  (below 0.30 eV), which might translate to instability and difficulty in synthesis.

It is important to acknowledge that our current findings represent a preliminary analysis, serving as a solid foundation for further exploration. With the prior reported synthesis of B,N-tetracene<sup>21</sup> and the confidence instilled by our computational predictions, we anticipate that the identified candidates could be synthesized in the near future and subjected to experimental testing to accurately evaluate their properties, especially those displaying stability indicated by a sufficiently high  $E(T_1)$  and a sufficiently low  $N_U$ , such as values similar to those of pristine tetracene, making them feasible for synthesis.

*Data Availability Statement.* The data that support the findings of this study beyond those provided in the Supporting Information are available from the authors upon reasonable request.

### Acknowledgements

The financial assistance of Brazilian agencies Conselho Nacional de Desenvolvimento Científico e Tecnológico (CNPq) under project No. 307168/2022-0, and Fundação de Amparo à Pesquisa do Estado de São Paulo (FAPESP) under project No. 2022/16385-8 are gratefully acknowledged. H.L. acknowledges support by the U.S. National Science Foundation for this research (Grant No. 2107923).

### References

- (1) Baldo, M. A.; O'Brien, D. F.; You, Y.; Shoustikov, A.; Sibley, S.; Thompson, M. E.; Forrest, S. R. Highly Efficient Phosphorescent Emission from Organic Electroluminescent Devices. *Electrophosphorescent Materials and Devices* **2023**, 1–12.
- (2) Wong, M. Y.; Zysman-Colman, E. Purely Organic Thermally Activated Delayed Fluorescence Materials for Organic Light-Emitting Diodes. *Advanced Materials* **2017**, *29* (22).
- (3) Hong, G.; Gan, X.; Leonhardt, C.; Zhang, Z.; Seibert, J.; Busch, J. M.; Bräse, S. A Brief History of OLEDs—Emitter Development and Industry Milestones. *Advanced Materials* **2021**, *33* (9).
- (4) Baldo, M. A.; Thompson, M. E.; Forrest, S. R. High-Efficiency Fluorescent Organic Light-Emitting Devices Using a Phosphorescent Sensitizer. *Nature* **2000**, *403* (6771), 750–753.
- (5) Baldo, M. A.; Lamansky, S.; Burrows, P. E.; Thompson, M. E.; Forrest, S. R. Very High-Efficiency Green Organic Light-Emitting Devices Based on Electrophosphorescence. *Appl Phys Lett* **1999**, *75* (1), 4–6.
- (6) O'Brien, D. F.; Baldo, M. A.; Thompson, M. E.; Forrest, S. R. Improved Energy Transfer in Electrophosphorescent Devices. *Appl Phys Lett* **1999**, *74* (3), 442–444.
- (7) Minaev, B.; Baryshnikov, G.; Agren, H. Principles of Phosphorescent Organic Light Emitting Devices. *Physical Chemistry Chemical Physics* **2014**, 1719–1758.
- (8) Uoyama, H.; Goushi, K.; Shizu, K.; Nomura, H.; Adachi, C. Highly Efficient Organic Light-Emitting Diodes from Delayed Fluorescence. *Nature* **2012**, *492* (7428), 234–238.
- (9) Volz, D.; Wallesch, M.; Fléchon, C.; Danz, M.; Verma, A.; Navarro, J. M.; Zink, D. M.; Bräse, S.; Baumann, T. From Iridium and Platinum to Copper and Carbon: New Avenues for More Sustainability in Organic Light-Emitting Diodes. *Green Chemistry* **2015**, *17* (4), 1988–2011.
- (10) Yang, Z.; Mao, Z.; Xie, Z.; Zhang, Y.; Liu, S.; Zhao, J.; Xu, J.; Chi, Z.; Aldred, M. P. Recent Advances in Organic Thermally Activated Delayed Fluorescence Materials. *Chem Soc Rev* **2017**, *46* (3), 915–1016.
- (11) Zhang, Q.; Li, J.; Shizu, K.; Huang, S.; Hirata, S.; Miyazaki, H.; Adachi, C. Design of Efficient Thermally Activated Delayed Fluorescence Materials for Pure Blue Organic Light Emitting Diodes. *J Am Chem Soc* **2012**, *134* (36), 14706–14709.
- (12) Anthony, J. E. The Larger Acenes: Versatile Organic Semiconductors. *Angewandte Chemie - International Edition* **2008**, 452–483.

- (13) Tönshoff, C.; Bettinger, H. F. Pushing the Limits of Acene Chemistry: The Recent Surge of Large Acenes. *Chemistry - A European Journal* **2021**, 3193–3212.
- (14) Shi, X.; Chi, C. Different Strategies for the Stabilization of Acenes and Acene Analogues. *Chemical Record* **2016**, 1690–1700.
- (15) Pinheiro, M.; MacHado, F. B. C.; Plasser, F.; Aquino, A. J. A.; Aquino, A. J. A.; Aquino, A. J. A.; Lischka, H.; Lischka, H.; Lischka, H. A Systematic Analysis of Excitonic Properties to Seek Optimal Singlet Fission: The BN-Substitution Patterns in Tetracene. *J Mater Chem C Mater* **2020**, 8 (23), 7793–7804.
- (16) Milanez, B. D.; dos Santos, G. M.; Pinheiro, M.; Ueno, L. T.; Ferrão, L. F. A.; Aquino, A. J. A.; Lischka, H.; Machado, F. B. C. Structural Stability and the Low-Lying Singlet and Triplet States of BN-n-Acenes, n = 1–7. *J Comput Chem* **2023**, 44 (6), 755–765.
- (17) Pinheiro, M.; Das, A.; Aquino, A. J. A.; Lischka, H.; Machado, F. B. C. Interplay between Aromaticity and Radicaloid Character in Nitrogen-Doped Oligoacenes Revealed by High-Level Multireference Methods. *Journal of Physical Chemistry A* **2018**, 122 (49), 9464–9473.
- (18) Pinheiro, M.; Ferrão, L. F. A.; Bettanin, F.; Aquino, A. J. A.; Machado, F. B. C.; Lischka, H. How to Efficiently Tune the Biradicaloid Nature of Acenes by Chemical Doping with Boron and Nitrogen. *Physical Chemistry Chemical Physics* **2017**, 19 (29), 19225–19233.
- (19) Matsui, K.; Oda, S.; Yoshiura, K.; Nakajima, K.; Yasuda, N.; Hatakeyama, T. One-Shot Multiple Borylation toward BN-Doped Nanographenes. *J Am Chem Soc* **2018**, 140 (4), 1195–1198.
- (20) Suresh, S. M.; Duda, E.; Hall, D.; Yao, Z.; Bagnich, S.; Slawin, A. M. Z.; Bäessler, H.; Beljonne, D.; Buck, M.; Olivier, Y.; Köhler, A.; Zysman-Colman, E. A Deep Blue B,N-Doped Heptacene Emitter That Shows Both Thermally Activated Delayed Fluorescence and Delayed Fluorescence by Triplet-Triplet Annihilation. *J Am Chem Soc* **2020**, 142 (14), 6588–6599.
- (21) Ishibashi, J. S. A.; Dargelos, A.; Darrigan, C.; Chrostowska, A.; Liu, S. Y. BN Tetracene: Extending the Reach of BN/CC Isosterism in Acenes. *Organometallics* **2017**, 36 (14), 2494–2497.
- (22) Chan, M. Y.; Lai, S. L.; Fung, M. K.; Lee, C. S.; Lee, S. T. Doping-Induced Efficiency Enhancement in Organic Photovoltaic Devices. *Appl Phys Lett* **2007**, 90 (2).
- (23) Sundar, V. C.; Zaumseil, J.; Podzorov, V.; Menard, E.; Willett, R. L.; Someya, T.; Gershenson, M. E.; Rogers, J. A. Elastomeric Transistor Stamps: Reversible Probing of Charge Transport in Organic Crystals. *Science* **2004**, 303 (5664), 1644–6.
- (24) McGarry, K. A.; Xie, W.; Sutton, C.; Risko, C.; Wu, Y.; Young, V. G.; Brédas, J. L.; Frisbie, C. D.; Douglas, C. J. Rubrene-Based Single-Crystal Organic Semiconductors: Synthesis, Electronic Structure, and Charge-Transport Properties. *Chemistry of Materials* **2013**, 25 (11), 2254–2263.
- (25) Matsuoka, W.; Kawahara, K. P.; Ito, H.; Sarlah, D.; Itami, K.  $\pi$ -Extended Rubrenes via Dearomative Annulative  $\pi$ -Extension Reaction. *J Am Chem Soc* **2023**, 145 (1), 658–666.
- (26) Hasegawa, T.; Takeya, J. Organic Field-Effect Transistors Using Single Crystals. *Sci Technol Adv Mater* **2009**, 10 (2).
- (27) Angeli, C.; Cimiraaglia, R.; Malrieu, J. P. N-Electron Valence State Perturbation Theory: A Spinless Formulation and an Efficient Implementation of the Strongly Contracted and of the Partially Contracted Variants. *Journal of Chemical Physics* **2002**, 117 (20), 9138–9153.

- (28) Szalay, P. G.; Müller, T.; Gidofalvi, G.; Lischka, H.; Shepard, R. Multiconfiguration Self-Consistent Field and Multireference Configuration Interaction Methods and Applications. *Chemical Reviews* **2012**, 108–181.
- (29) Lischka, H.; Nachtigallová, D.; Aquino, A. J. A.; Szalay, P. G.; Plasser, F.; MacHado, F. B. C.; Barbatti, M. Multireference Approaches for Excited States of Molecules. *Chemical Reviews* **2018**, 7293–7361.
- (30) Chakraborty, S.; Kayastha, P.; Ramakrishnan, R. The Chemical Space of B, N-Substituted Polycyclic Aromatic Hydrocarbons: Combinatorial Enumeration and High-Throughput First-Principles Modeling. *Journal of Chemical Physics* **2019**, 150 (11).
- (31) Weigend, F.; Häser, M. RI-MP2: First Derivatives and Global Consistency. *Theor Chem Acc* **1997**, 97 (1–4), 331–340.
- (32) Weigend, F.; Ahlrichs, R. Balanced Basis Sets of Split Valence, Triple Zeta Valence and Quadruple Zeta Valence Quality for H to Rn: Design and Assessment of Accuracy. *Physical Chemistry Chemical Physics* **2005**, 7 (18), 3297–3305.
- (33) Buenker, R. J.; Peyerimhoff, S. D. Individualized Configuration Selection in CI Calculations with Subsequent Energy Extrapolation. *Theoret Chim Acta* **1974**, 35, 33–58.
- (34) Werner, H. J.; Knowles, P. J. An Efficient Internally Contracted Multiconfiguration-Reference Configuration Interaction Method. *J Chem Phys* **1988**, 89 (9), 5803–5814.
- (35) Roos, B. O.; Taylor, P. R.; Sigbahn, P. E. M. A Complete Active Space SCF Method (CASSCF) Using a Density Matrix Formulated Super-CI Approach. *Chem Phys* **1980**, 48 (2), 157–173.
- (36) Liu, B.; Mclean, A. D. Accurate Calculation of the Attractive Interaction of Two Ground State Helium Atoms. *Journal of Chemical Physics* **1973**, 59 (8), 4557–4558.
- (37) Bunge, A. Electronic Wavefunctions for Atoms. III. Partition of Degenerate Spaces and Ground State of C. *J Chem Phys* **1970**, 53 (1), 20–28.
- (38) Francl, M. M.; Pietro, W. J.; Hehre, W. J.; Binkley, J. S.; Gordon, M. S.; DeFrees, D. J.; Pople, J. A. Self-Consistent Molecular Orbital Methods. XXIII. A Polarization-Type Basis Set for Second-Row Elements. *J Chem Phys* **1982**, 77 (7), 3654–3665.
- (39) Pople, J. A.; Seeger, R.; Krishnan, R. Variational Configuration Interaction Methods and Comparison with Perturbation Theory. *Int J Quantum Chem* **1977**, 12 (S11), 149–163.
- (40) Neese, F. Software Update: The ORCA Program System, Version 4.0. *Wiley Interdiscip Rev Comput Mol Sci* **2018**, 8 (1).
- (41) Neese, F. The ORCA Program System. *Wiley Interdiscip Rev Comput Mol Sci* **2012**, 2 (1), 73–78.
- (42) Lischka, H.; Müller, T.; Szalay, P. G.; Shavitt, I.; Pitzer, R. M.; Shepard, R. Columbus-a Program System for Advanced Multireference Theory Calculations. *Wiley Interdiscip Rev Comput Mol Sci* **2011**, 1 (2), 191–199.
- (43) Lischka, H.; Shepard, R.; Pitzer, R. M.; Shavitt, I.; Dallos, M.; Müller, T.; Szalay, P. G.; Seth, M.; Kedziora, G. S.; Yabushita, S.; Zhang, Z. High-Level Multireference Methods in the Quantum-Chemistry Program System COLUMBUS: Analytic MR-CISD and MR-AQCC Gradients and MR-AQCC-LRT for Excited States, GUGA Spin-Orbit CI and Parallel CI Density. *Physical Chemistry Chemical Physics* **2001**, 3 (5), 664–673.

- (44) Krygowski, T. M. Crystallographic Studies of Inter- and Intramolecular Interactions Reflected in Aromatic Character of  $\pi$ -Electron Systems. *J Chem Inf Comput Sci* **1993**, *33* (1), 70–78.
- (45) Kruszewski, J.; Krygowski, T. M. Definition of Aromaticity Basing on the Harmonic Oscillator Model. *Tetrahedron Lett* **1972**, *13* (36), 3839–3842.
- (46) Takatsuka, K.; Fueno, T.; Yamaguchi, K. Distribution of Odd Electrons in Ground-State Molecules. *Theor Chim Acta* **1978**, *48* (3), 175–183.
- (47) Plasser, F.; Pašalić, H.; Gerzabek, M. H.; Libisch, F.; Reiter, R.; Burgdörfer, J.; Müller, T.; Shepard, R.; Lischka, H. The Multiradical Character of One- and Two-Dimensional Graphene Nanoribbons. *Angew Chem Int Ed Engl* **2013**, *52* (9), 2581–2584.
- (48) Head-Gordon, M. Characterizing Unpaired Electrons from the One-Particle Density Matrix. *Chem Phys Lett* **2003**, *372* (3–4), 508–511.
- (49) Plasser, F. TheoDORE: A Toolbox for a Detailed and Automated Analysis of Electronic Excited State Computations. *Journal of Chemical Physics* **2020**, *152* (8).
- (50) Plasser, F.; Lischka, H. Analysis of Excitonic and Charge Transfer Interactions from Quantum Chemical Calculations. *J Chem Theory Comput* **2012**, *8* (8), 2777–2789.
- (51) Plasser, F.; Wormit, M.; Dreuw, A. New Tools for the Systematic Analysis and Visualization of Electronic Excitations. I. Formalism. *Journal of Chemical Physics* **2014**, *141* (2).
- (52) Bultinck, P.; Ponec, R.; Van Damme, S. Multicenter Bond Indices as a New Measure of Aromaticity in Polycyclic Aromatic Hydrocarbons. *J Phys Org Chem* **2005**, *18* (8), 706–718.
- (53) Bultinck, P.; Rafat, M.; Ponec, R.; Van Gheluwe, B.; Carbó-Dorca, R.; Popelier, P. Electron Delocalization and Aromaticity in Linear Polyacenes: Atoms in Molecules Multicenter Delocalization Index. *Journal of Physical Chemistry A* **2006**, *110* (24), 7642–7648.
- (54) AIMAll (Version 19.10.12), Todd A. Keith, TK Gristmill Software, Overland Park KS, USA, 2019 (aim.tkgristmill.com).
- (55) E. Matito, ESI-3D: Electron Sharing Indices Program for 3D Molecular Space Partitioning; Institute of Computational Chemistry and Catalysis (IQCC), University of Girona, Catalonia, Spain, 2006; <http://iqc.udg.es/eduard/ESI>, 2014.
- (56) Schleyer, P. V. R.; Maerker, C.; Dransfeld, A.; Jiao, H.; Van Eikema Hommes, N. J. R. Nucleus-Independent Chemical Shifts: A Simple and Efficient Aromaticity Probe. *J Am Chem Soc* **1996**, *118* (26), 6317–6318.
- (57) Wolinski, K.; Hinton, J. F.; Pulay, P. Efficient Implementation of the Gauge-Independent Atomic Orbital Method for NMR Chemical Shift Calculations. *J Am Chem Soc* **1990**, *112* (23), 8251–8260.
- (58) Lee, C.; Yang, W.; Parr, R. G. Development of the Colle-Salvetti Correlation-Energy Formula into a Functional of the Electron Density. *Phys Rev B Condens Matter* **1988**, *37* (2), 785–789.
- (59) Jensen, F. Basis Set Convergence of Nuclear Magnetic Shielding Constants Calculated by Density Functional Methods. *J Chem Theory Comput* **2008**, *4* (5), 719–727.
- (60) Gaussian 09, Revision A.02, M. J. Frisch, G. W. Trucks, H. B. Schlegel, G. E. Scuseria, M. A. Robb, J. R. Cheeseman, G. Scalmani, V. Barone, G. A. Petersson, H. Nakatsuji, X. Li, M. Caricato, A. Marenich, J. Bloino, B. G. Janesko, R. Gomperts, B. Mennucci, H. P. Hratchian, J. V. Ortiz, A. F. Izmaylov, J. L. Sonnenberg, D. Williams-Young, F. Ding, F. Lipparini, F. Egidi, J. Goings, B. Peng, A. Petrone, T. Henderson, D. Ranasinghe, V. G. Zakrzewski, J.

- Gao, N. Rega, G. Zheng, W. Liang, M. Hada, M. Ehara, K. Toyota, R. Fukuda, J. Hasegawa, M. Ishida, T. Nakajima, Y. Honda, O. Kitao, H. Nakai, T. Vreven, K. Throssell, J. A. Montgomery, Jr., J. E. Peralta, F. Ogliaro, M. Bearpark, J. J. Heyd, E. Brothers, K. N. Kudin, V. N. Staroverov, T. Keith, R. Kobayashi, J. Normand, K. Raghavachari, A. Rendell, J. C. Burant, S. S. Iyengar, J. Tomasi, M. Cossi, J. M. Millam, M. Klene, C. Adamo, R. Cammi, J. W. Ochterski, R. L. Martin, K. Morokuma, O. Farkas, J. B. Foresman, and D. J. Fox, Gaussian, Inc., Wallingford CT, 2016.
- (61) Plasser, F.; Glöckhofer, F. Visualisation of Chemical Shielding Tensors (VIST) to Elucidate Aromaticity and Antiaromaticity\*\*. *European J Org Chem* **2021**, 2021 (17), 2529–2539.
- (62) Geuenich, D.; Hess, K.; Köhler, F.; Herges, R. Anisotropy of the Induced Current Density (ACID), a General Method to Quantify and Visualize Electronic Delocalization. *Chem Rev* **2005**, 105 (10), 3758–3772.
- (63) Mamada, M.; Inada, K.; Komino, T.; Potscavage, W. J.; Nakanotani, H.; Adachi, C. Highly Efficient Thermally Activated Delayed Fluorescence from an Excited-State Intramolecular Proton Transfer System. *ACS Cent Sci* **2017**, 3 (7), 769–777.
- (64) Yang, Y.; Davidson, E. R.; Yang, W. Nature of Ground and Electronic Excited States of Higher Acenes. *Proc Natl Acad Sci USA* **2016**, 113 (35), E5098–E5107.
- (65) Marian, C. M.; Gilka, N. Performance of the Density Functional Theory/Multireference Configuration Interaction Method on Electronic Excitation of Extended  $\pi$ -Systems. *J Chem Theory Comput* **2008**, 4 (9), 1501–1515.
- (66) Sabbatini, N.; Indelli, M. T.; Gandolfi, M. T.; Balzani, V. Quenching of Singlet and Triplet Excited States of Aromatic Molecules by Europium Ions. *Journal of Physical Chemistry* **1982**, 86 (18), 3585–3591.
- (67) Biermann, B.; Biermann, D.; Schmidt, W. Diels-Alder Reactivity of Polycyclic Aromatic Hydrocarbons. 1. Acenes and Benzologs. *J Am Chem Soc* **1980**, 102 (9), 3163–3173.
- (68) Grimme, S.; Parac, M. Substantial Errors from Time-Dependent Density Functional Theory for the Calculation of Excited States of Large  $\pi$  Systems. *ChemPhysChem* **2003**, 4 (3), 292–295.
- (69) Ghosh, D.; Periyasamy, G.; Pati, S. K. Density Functional Theoretical Investigation of the Aromatic Nature of BN Substituted Benzene and Four Ring Polyaromatic Hydrocarbons. *Physical Chemistry Chemical Physics* **2011**, 13 (46), 20627–20636.

# **Appendix C - Cartesian Coordinates for the wB97XD Optimized Geometries**

---

**pristine\_dpt.xyz**

50

C	-3.209651	1.397874	0.000000
C	-4.375365	0.712521	0.000000
C	-4.375365	-0.712521	0.000000
C	-3.209651	-1.397874	0.000000
C	-1.945071	-0.719950	0.000000
C	-0.744500	-1.416875	0.000000
C	0.483749	-0.718430	0.000000
C	1.716886	-1.392771	0.000000
C	2.920296	-0.717265	0.000000
C	4.177446	-1.401957	0.000000
C	5.342635	-0.714155	0.000000
C	5.342635	0.714155	0.000000
C	4.177446	1.401957	0.000000
C	2.920296	0.717265	0.000000
C	1.716886	1.392771	0.000000
C	0.483749	0.718430	0.000000
C	-0.744500	1.416875	0.000000
C	-1.945071	0.719950	0.000000
H	-5.318002	1.245133	0.000000
H	-5.318002	-1.245133	0.000000
H	-3.215204	2.479629	0.000000
H	-3.215204	-2.479629	0.000000
H	1.724181	2.475467	0.000000
H	1.724181	-2.475467	0.000000
H	6.287588	1.242624	0.000000
H	4.173953	2.485665	0.000000
H	4.173953	-2.485665	0.000000
H	6.287588	-1.242624	0.000000
C	-0.739097	-2.905887	0.000000
C	-0.733204	-3.612992	1.197934
C	-0.723435	-4.999511	1.198851
C	-0.718415	-5.696134	0.000000
C	-0.723435	-4.999511	-1.198851
C	-0.733204	-3.612992	-1.197934
C	-0.739097	2.905887	0.000000
C	-0.733204	3.612992	-1.197934
C	-0.723435	4.999511	-1.198851
C	-0.718415	5.696134	0.000000
C	-0.723435	4.999511	1.198851
C	-0.733204	3.612992	1.197934
H	-0.736533	3.068035	-2.134161
H	-0.719764	5.536134	-2.139326
H	-0.710587	6.778825	0.000000
H	-0.719764	5.536134	2.139326
H	-0.736533	3.068035	2.134161
H	-0.736533	-3.068035	2.134161
H	-0.719764	-5.536134	2.139326
H	-0.710587	-6.778825	0.000000
H	-0.719764	-5.536134	-2.139326
H	-0.736533	-3.068035	-2.134161

**1\_10\_leftdpt.xyz**

50

B -3.344593 1.502870 0.000000  
C -4.579614 0.639242 0.000000  
C -4.424555 -0.719546 0.000000  
C -3.168512 -1.383208 0.000000  
C -1.967330 -0.714564 0.000000  
C -0.714653 -1.422542 0.000000  
C 0.474850 -0.749963 0.000000  
C 1.749083 -1.417158 0.000000  
C 2.905761 -0.717024 0.000000  
N 4.153114 -1.332232 0.000000  
C 5.318327 -0.658026 0.000000  
C 5.348937 0.702669 0.000000  
C 4.121308 1.397740 0.000000  
C 2.924713 0.728962 0.000000  
C 1.665417 1.389602 0.000000  
C 0.483150 0.710281 0.000000  
C -0.783263 1.419489 0.000000  
C -1.973891 0.751700 0.000000  
H -5.590979 1.032465 0.000000  
H -5.300750 -1.364806 0.000000  
H -3.384089 2.698530 0.000000  
H -3.168837 -2.465199 0.000000  
H 1.664899 2.472099 0.000000  
H 1.771138 -2.499753 0.000000  
H 6.294985 1.220923 0.000000  
H 4.115811 2.481406 0.000000  
H 4.171445 -2.338064 0.000000  
H 6.214318 -1.263109 0.000000  
C -0.719256 -2.910941 0.000000  
C -0.716076 -3.621242 1.196785  
C -0.700570 -5.008033 1.198671  
C -0.690953 -5.705456 0.000000  
C -0.700570 -5.008033 -1.198671  
C -0.716076 -3.621242 -1.196785  
C -0.727578 2.909125 0.000000  
C -0.689322 3.612562 -1.197831  
C -0.623392 4.997191 -1.198577  
C -0.589572 5.693365 0.000000  
C -0.623392 4.997191 1.198577  
C -0.689322 3.612562 1.197831  
H -0.725737 3.068598 -2.133830  
H -0.605696 5.533260 -2.139251  
H -0.543232 6.775124 0.000000  
H -0.605696 5.533260 2.139251  
H -0.725737 3.068598 2.133830  
H -0.728451 -3.075442 2.132568  
H -0.698795 -5.544752 2.139395  
H -0.679573 -6.788283 0.000000  
H -0.698795 -5.544752 -2.139395  
H -0.728451 -3.075442 -2.132568

**1\_10\_rightdpt.xyz**

50

C 4.179792 1.331605 0.000000  
C 5.418850 0.635934 0.000000  
C 5.547892 -0.729647 0.000000  
B 4.294354 -1.568016 0.000000  
C 2.955712 -0.778282 0.000000  
C 1.756724 -1.413772 0.000000  
C 0.493569 -0.721549 0.000000  
C -0.689253 -1.413242 0.000000  
C -1.940416 -0.711939 0.000000  
C -3.158189 -1.347463 0.000000  
C -4.369939 -0.628279 0.000000  
C -4.311165 0.731227 0.000000  
N -3.132831 1.375134 0.000000  
C -1.896862 0.736117 0.000000  
C -0.736905 1.441465 0.000000  
C 0.522713 0.740442 0.000000  
C 1.725632 1.381308 0.000000  
C 2.970224 0.681278 0.000000  
H -5.192157 1.358154 0.000000  
H -5.324668 -1.130239 0.000000  
H -3.119021 2.383203 0.000000  
H -3.183757 -2.429572 0.000000  
H 1.751530 2.464721 0.000000  
H 1.740312 -2.497297 0.000000  
H 6.311999 1.257860 0.000000  
H 4.194225 2.415875 0.000000  
H 4.271733 -2.769495 0.000000  
H 6.553742 -1.137011 0.000000  
C -0.719664 -2.901752 0.000000  
C -0.740232 -3.605434 1.199196  
C -0.776007 -4.991315 1.199184  
C -0.794536 -5.686807 0.000000  
C -0.776007 -4.991315 -1.199184  
C -0.740232 -3.605434 -1.199196  
C -0.774622 2.927658 0.000000  
C -0.801507 3.637257 -1.198562  
C -0.860884 5.022940 -1.199451  
C -0.892509 5.718115 0.000000  
C -0.860884 5.022940 1.199451  
C -0.801507 3.637257 1.198562  
H -0.766176 3.092508 -2.134373  
H -0.878270 5.559939 -2.139484  
H -0.938239 6.799816 0.000000  
H -0.878270 5.559939 2.139484  
H -0.766176 3.092508 2.134373  
H -0.717155 -3.061079 2.135398  
H -0.783125 -5.528025 2.139340  
H -0.817612 -6.769132 0.000000  
H -0.783125 -5.528025 -2.139340  
H -0.717155 -3.061079 -2.135398

**1\_11\_leftdpt.xyz**

50

B -3.339030 1.494887 0.000000  
C -4.553230 0.639279 0.000000  
C -4.414967 -0.745712 0.000000  
C -3.195464 -1.411040 0.000000  
C -1.973224 -0.723921 0.000000  
C -0.748773 -1.418972 0.000000  
C 0.463695 -0.727379 0.000000  
C 1.697265 -1.393343 0.000000  
C 2.894896 -0.695282 0.000000  
C 4.119894 -1.355833 0.000000  
N 5.258732 -0.684562 0.000000  
C 5.319621 0.698879 0.000000  
C 4.167775 1.403729 0.000000  
C 2.906455 0.753564 0.000000  
C 1.696780 1.414599 0.000000  
C 0.475362 0.732177 0.000000  
C -0.762726 1.419453 0.000000  
C -1.972953 0.744738 0.000000  
H -5.565440 1.032696 0.000000  
H -5.306093 -1.371179 0.000000  
H -3.373953 2.693783 0.000000  
H -3.188701 -2.492550 0.000000  
H 1.691932 2.497120 0.000000  
H 1.716185 -2.476320 0.000000  
H 6.306980 1.131131 0.000000  
H 4.212337 2.484880 0.000000  
H 4.187401 -2.436271 0.000000  
H 6.123420 -1.200174 0.000000  
C -0.729213 -2.907256 0.000000  
C -0.714520 -3.616921 1.197040  
C -0.675776 -5.003242 1.198695  
C -0.653877 -5.700322 0.000000  
C -0.675776 -5.003242 -1.198695  
C -0.714520 -3.616921 -1.197040  
C -0.722802 2.910960 0.000000  
C -0.689506 3.616500 -1.196842  
C -0.626246 5.001387 -1.198390  
C -0.592419 5.698138 0.000000  
C -0.626246 5.001387 1.198390  
C -0.689506 3.616500 1.196842  
H -0.730378 3.072448 -2.132670  
H -0.611563 5.537552 -2.139254  
H -0.547124 6.780056 0.000000  
H -0.611563 5.537552 2.139254  
H -0.730378 3.072448 2.132670  
H -0.742934 -3.071270 2.132535  
H -0.669336 -5.539965 2.139389  
H -0.628276 -6.782932 0.000000  
H -0.669336 -5.539965 -2.139389  
H -0.742934 -3.071270 -2.132535

**1\_11\_rightdpt.xyz**

50

B 4.278337 -1.523670 0.000000  
C 5.504238 -0.683430 0.000000  
C 5.382698 0.708331 0.000000  
C 4.175027 1.394437 0.000000  
C 2.949410 0.715599 0.000000  
C 1.728179 1.396785 0.000000  
C 0.504411 0.733795 0.000000  
C -0.719236 1.428881 0.000000  
C -1.918409 0.714102 0.000000  
C -3.146141 1.375283 0.000000  
N -4.288362 0.712153 0.000000  
C -4.355858 -0.669236 0.000000  
C -3.207996 -1.377365 0.000000  
C -1.936643 -0.738875 0.000000  
C -0.734062 -1.428262 0.000000  
C 0.484286 -0.726835 0.000000  
C 1.722758 -1.394026 0.000000  
C 2.938082 -0.745706 0.000000  
H -5.148215 1.235584 0.000000  
H -5.344121 -1.099582 0.000000  
H -3.208938 2.455167 0.000000  
H -3.261513 -2.457132 0.000000  
H 1.738173 2.480024 0.000000  
H 1.724424 -2.477575 0.000000  
H 6.285488 1.316986 0.000000  
H 4.170843 2.478612 0.000000  
H 4.258352 -2.729035 0.000000  
H 6.514285 -1.082876 0.000000  
C -0.745477 -2.917221 0.000000  
C -0.755641 -3.621470 1.198923  
C -0.780519 -5.007660 1.199172  
C -0.794773 -5.703310 0.000000  
C -0.780519 -5.007660 -1.199172  
C -0.755641 -3.621470 -1.198923  
C -0.746070 2.915989 0.000000  
C -0.760340 3.620515 -1.199552  
C -0.798410 5.006653 -1.199435  
C -0.819803 5.701981 0.000000  
C -0.798410 5.006653 1.199435  
C -0.760340 3.620515 1.199552  
H -0.728281 3.075942 -2.135456  
H -0.803632 5.543607 -2.139480  
H -0.844452 6.784269 0.000000  
H -0.803632 5.543607 2.139480  
H -0.728281 3.075942 2.135456  
H -0.731665 -3.077076 2.135108  
H -0.781180 -5.544538 2.139288  
H -0.809640 -6.785787 0.000000  
H -0.781180 -5.544538 -2.139288  
H -0.731665 -3.077076 -2.135108

**1\_13\_leftdpt.xyz**

50

```
B -3.339102 1.503888 0.000000
C -4.562005 0.655294 0.000000
C -4.421601 -0.722452 0.000000
C -3.195889 -1.396628 0.000000
C -1.974277 -0.726241 0.000000
C -0.743872 -1.429137 0.000000
C 0.464835 -0.750810 0.000000
C 1.714483 -1.417317 0.000000
C 2.908380 -0.733773 0.000000
C 4.182178 -1.355027 0.000000
C 5.338719 -0.622639 0.000000
C 5.263757 0.771911 0.000000
N 4.081378 1.365236 0.000000
C 2.882985 0.704174 0.000000
C 1.684560 1.390966 0.000000
C 0.476455 0.707534 0.000000
C -0.767987 1.410057 0.000000
C -1.970428 0.742518 0.000000
H -5.572705 1.051577 0.000000
H -5.310851 -1.350600 0.000000
H -3.361849 2.702800 0.000000
H -3.199601 -2.478227 0.000000
H 1.683026 2.474693 0.000000
H 1.735193 -2.499372 0.000000
H 6.132293 1.413520 0.000000
H 4.043693 2.374633 0.000000
H 4.227964 -2.437690 0.000000
H 6.308558 -1.097072 0.000000
C -0.738238 -2.917493 0.000000
C -0.729901 -3.628179 1.198580
C -0.702483 -5.014765 1.198586
C -0.686152 -5.712143 0.000000
C -0.702483 -5.014765 -1.198586
C -0.729901 -3.628179 -1.198580
C -0.710190 2.900861 0.000000
C -0.666189 3.606172 -1.197054
C -0.585187 4.990295 -1.198518
C -0.542624 5.686569 0.000000
C -0.585187 4.990295 1.198518
C -0.666189 3.606172 1.197054
H -0.714945 3.062513 -2.132799
H -0.566630 5.526491 -2.139293
H -0.488001 6.768061 0.000000
H -0.566630 5.526491 2.139293
H -0.714945 3.062513 2.132799
H -0.751123 -3.082529 2.132290
H -0.697447 -5.551408 2.139367
H -0.665328 -6.794847 0.000000
H -0.697447 -5.551408 -2.139367
H -0.751123 -3.082529 -2.132290
```

**1\_13\_rightdpt.xyz**

50

```
B 4.300811 1.523687 0.000000
C 5.533339 0.687485 0.000000
C 5.404194 -0.696122 0.000000
C 4.188288 -1.387742 0.000000
C 2.965156 -0.723245 0.000000
C 1.735448 -1.409347 0.000000
C 0.518485 -0.754628 0.000000
C -0.725496 -1.446117 0.000000
C -1.917336 -0.743750 0.000000
C -3.200129 -1.353922 0.000000
C -4.353170 -0.617795 0.000000
C -4.272741 0.776093 0.000000
N -3.088627 1.359023 0.000000
C -1.890728 0.696444 0.000000
C -0.697038 1.408502 0.000000
C 0.504706 0.705707 0.000000
C 1.750736 1.384346 0.000000
C 2.955831 0.738599 0.000000
H -5.137151 1.423483 0.000000
H -5.323867 -1.090443 0.000000
H -3.031278 2.370719 0.000000
H -3.254238 -2.435291 0.000000
H 1.745458 2.468471 0.000000
H 1.750281 -2.492328 0.000000
H 6.542789 1.087184 0.000000
H 4.272548 2.728613 0.000000
H 4.194168 -2.471889 0.000000
H 6.303627 -1.309957 0.000000
C -0.749042 -2.932839 0.000000
C -0.759388 -3.639046 1.198541
C -0.790826 -5.025266 1.199163
C -0.808551 -5.721074 0.000000
C -0.790826 -5.025266 -1.199163
C -0.759388 -3.639046 -1.198541
C -0.750056 2.896758 0.000000
C -0.789576 3.601327 -1.200402
C -0.865765 4.985933 -1.199873
C -0.905571 5.679635 0.000000
C -0.865765 4.985933 1.199873
C -0.789576 3.601327 1.200402
H -0.740705 3.058030 -2.136312
H -0.884478 5.522912 -2.139556
H -0.960065 6.760723 0.000000
H -0.884478 5.522912 2.139556
H -0.740705 3.058030 2.136312
H -0.733589 -3.094426 2.134627
H -0.796177 -5.562192 2.139352
H -0.829827 -6.803528 0.000000
H -0.796177 -5.562192 -2.139352
H -0.733589 -3.094426 -2.134627
```

**1\_14\_leftdpt.xyz**

50

B -3.334641 1.506895 0.000000  
C -4.570714 0.657424 0.000000  
C -4.432826 -0.709307 0.000000  
C -3.193892 -1.387761 0.000000  
C -1.982780 -0.727568 0.000000  
C -0.741869 -1.447079 0.000000  
C 0.449074 -0.773673 0.000000  
C 1.729647 -1.406744 0.000000  
C 2.894468 -0.710220 0.000000  
C 4.195620 -1.324229 0.000000  
C 5.323645 -0.594683 0.000000  
C 5.239460 0.838308 0.000000  
C 4.038609 1.429875 0.000000  
N 2.860823 0.693622 0.000000  
C 1.661954 1.333104 0.000000  
C 0.467102 0.678220 0.000000  
C -0.774896 1.404286 0.000000  
C -1.973583 0.741974 0.000000  
H -5.578910 1.059113 0.000000  
H -5.319505 -1.340207 0.000000  
H -3.357219 2.704068 0.000000  
H -3.202684 -2.469531 0.000000  
H 1.712044 2.412752 0.000000  
H 1.788912 -2.486219 0.000000  
H 6.129181 1.450234 0.000000  
H 3.903294 2.501588 0.000000  
H 4.221869 -2.405409 0.000000  
H 6.291734 -1.076506 0.000000  
C -0.743108 -2.934932 0.000000  
C -0.736591 -3.644150 1.197213  
C -0.713719 -5.030735 1.198793  
C -0.700205 -5.727641 0.000000  
C -0.713719 -5.030735 -1.198793  
C -0.736591 -3.644150 -1.197213  
C -0.696596 2.892943 0.000000  
C -0.643744 3.595493 -1.198174  
C -0.548505 4.978579 -1.198797  
C -0.499711 5.673595 0.000000  
C -0.548505 4.978579 1.198797  
C -0.643744 3.595493 1.198174  
H -0.695955 3.052545 -2.134082  
H -0.521450 5.514431 -2.139309  
H -0.432030 6.754180 0.000000  
H -0.521450 5.514431 2.139309  
H -0.695955 3.052545 2.134082  
H -0.752906 -3.098873 2.133199  
H -0.707613 -5.567384 2.139400  
H -0.681351 -6.810282 0.000000  
H -0.707613 -5.567384 -2.139400  
H -0.752906 -3.098873 -2.133199

**1\_14\_rightdpt.xyz**

50

B 4.258761 -1.567056 0.000000  
C 5.511420 -0.741315 0.000000  
C 5.396794 0.632112 0.000000  
C 4.174320 1.339238 0.000000  
C 2.955585 0.695044 0.000000  
C 1.721108 1.402992 0.000000  
C 0.516539 0.759216 0.000000  
C -0.750335 1.428544 0.000000  
C -1.921174 0.727246 0.000000  
C -3.213549 1.365544 0.000000  
C -4.360162 0.667464 0.000000  
C -4.304989 -0.762357 0.000000  
C -3.118172 -1.381077 0.000000  
N -1.910802 -0.684421 0.000000  
C -0.716091 -1.363223 0.000000  
C 0.478574 -0.692550 0.000000  
C 1.722410 -1.398769 0.000000  
C 2.928014 -0.766556 0.000000  
H -5.315053 1.174831 0.000000  
H -5.205300 -1.358965 0.000000  
H -3.218462 2.445436 0.000000  
H -3.026967 -2.453602 0.000000  
H 1.746843 2.485678 0.000000  
H 1.704065 -2.481863 0.000000  
H 6.299049 1.240992 0.000000  
H 4.196028 2.423130 0.000000  
H 4.221649 -2.769564 0.000000  
H 6.514596 -1.155643 0.000000  
C -0.762688 -2.850015 0.000000  
C -0.769125 -3.548357 1.201728  
C -0.787113 -4.934050 1.200406  
C -0.797878 -5.627812 0.000000  
C -0.787113 -4.934050 -1.200406  
C -0.769125 -3.548357 -1.201728  
C -0.779797 2.915414 0.000000  
C -0.780735 3.620133 -1.198864  
C -0.797458 5.006441 -1.199353  
C -0.807758 5.702095 0.000000  
C -0.797458 5.006441 1.199353  
C -0.780735 3.620133 1.198864  
H -0.765515 3.075037 -2.134819  
H -0.799760 5.543433 -2.139446  
H -0.820283 6.784665 0.000000  
H -0.799760 5.543433 2.139446  
H -0.765515 3.075037 2.134819  
H -0.747578 -3.003322 2.137336  
H -0.783158 -5.471631 2.139719  
H -0.805464 -6.710220 0.000000  
H -0.783158 -5.471631 -2.139719  
H -0.747578 -3.003322 -2.137336

**1\_15\_leftdpt.xyz**

50

```
B -3.340923 1.484560 0.000000
C -4.550925 0.633993 0.000000
C -4.435679 -0.766365 0.000000
C -3.235050 -1.435087 0.000000
C -1.998363 -0.739117 0.000000
C -0.793223 -1.439814 0.000000
C 0.436590 -0.744708 0.000000
C 1.667721 -1.380884 0.000000
C 2.876481 -0.677842 0.000000
C 4.142045 -1.318059 0.000000
C 5.290645 -0.588089 0.000000
C 5.226889 0.825183 0.000000
C 4.032463 1.482470 0.000000
C 2.832778 0.737448 0.000000
N 1.633867 1.341915 0.000000
C 0.424419 0.695067 0.000000
C -0.764512 1.403041 0.000000
C -1.993791 0.728429 0.000000
H -5.561291 1.033464 0.000000
H -5.336423 -1.376422 0.000000
H -3.366213 2.685206 0.000000
H -3.223305 -2.516081 0.000000
H 1.594518 2.353194 0.000000
H 1.698217 -2.464352 0.000000
H 6.146104 1.397090 0.000000
H 3.989755 2.564682 0.000000
H 4.171877 -2.400736 0.000000
H 6.253435 -1.080480 0.000000
C -0.760920 -2.927563 0.000000
C -0.737454 -3.633389 1.198455
C -0.682518 -5.018927 1.199080
C -0.652280 -5.714648 0.000000
C -0.682518 -5.018927 -1.199080
C -0.737454 -3.633389 -1.198455
C -0.679246 2.891404 0.000000
C -0.616564 3.595687 -1.198483
C -0.502287 4.977553 -1.199173
C -0.444106 5.671281 0.000000
C -0.502287 4.977553 1.199173
C -0.616564 3.595687 1.198483
H -0.681728 3.053441 -2.134021
H -0.469549 5.513600 -2.139359
H -0.362678 6.750932 0.000000
H -0.469549 5.513600 2.139359
H -0.681728 3.053441 2.134021
H -0.772413 -3.089051 2.134325
H -0.666704 -5.555213 2.139556
H -0.610495 -6.796517 0.000000
H -0.666704 -5.555213 -2.139556
H -0.772413 -3.089051 -2.134325
```

**1\_15\_rightdpt.xyz**

50

```
B 4.231189 -1.551951 0.000000
C 5.451616 -0.713987 0.000000
C 5.354428 0.693235 0.000000
C 4.163902 1.377288 0.000000
C 2.926295 0.684247 0.000000
C 1.725739 1.367498 0.000000
C 0.482272 0.706698 0.000000
C -0.723974 1.395797 0.000000
C -1.948051 0.694763 0.000000
C -3.199087 1.364786 0.000000
C -4.371575 0.674124 0.000000
C -4.345585 -0.734859 0.000000
C -3.168116 -1.423329 0.000000
C -1.937349 -0.724734 0.000000
N -0.752774 -1.387692 0.000000
C 0.471281 -0.738001 0.000000
C 1.668472 -1.423452 0.000000
C 2.904881 -0.773784 0.000000
H -5.317494 1.198155 0.000000
H -5.277449 -1.286085 0.000000
H -3.201013 2.446212 0.000000
H -3.171441 -2.502925 0.000000
H 1.730377 2.450300 0.000000
H 1.672933 -2.505101 0.000000
H 6.266435 1.286460 0.000000
H 4.149526 2.460980 0.000000
H 4.213337 -2.757994 0.000000
H 6.458911 -1.121704 0.000000
C -0.754235 -2.826308 0.000000
C -0.748651 -3.504985 1.205654
C -0.745614 -4.890717 1.201921
C -0.745086 -5.582500 0.000000
C -0.745614 -4.890717 -1.201921
C -0.748651 -3.504985 -1.205654
C -0.736233 2.882219 0.000000
C -0.742472 3.580987 -1.201230
C -0.755886 4.966997 -1.199637
C -0.763466 5.661818 0.000000
C -0.755886 4.966997 1.199637
C -0.742472 3.580987 1.201230
H -0.729004 3.036738 -2.137452
H -0.755713 5.503802 -2.139540
H -0.771046 6.744231 0.000000
H -0.755713 5.503802 2.139540
H -0.729004 3.036738 2.137452
H -0.736986 -2.948497 2.133869
H -0.736139 -5.429155 2.140401
H -0.736743 -6.664744 0.000000
H -0.736139 -5.429155 -2.140401
H -0.736986 -2.948497 -2.133869
```

**2\_3\_leftdpt.xyz**

50

C -3.215159 1.419502 0.000000  
B -4.486060 0.670620 0.000000  
N -4.328829 -0.777417 0.000000  
C -3.159512 -1.399748 0.000000  
C -1.950263 -0.698474 0.000000  
C -0.731884 -1.408559 0.000000  
C 0.475889 -0.716447 0.000000  
C 1.721027 -1.393947 0.000000  
C 2.915001 -0.721974 0.000000  
C 4.178056 -1.405791 0.000000  
C 5.339379 -0.718278 0.000000  
C 5.336679 0.715905 0.000000  
C 4.175602 1.404081 0.000000  
C 2.911236 0.721260 0.000000  
C 1.719294 1.398669 0.000000  
C 0.467560 0.730365 0.000000  
C -0.737555 1.431540 0.000000  
C -1.978515 0.751712 0.000000  
H -5.602807 1.095126 0.000000  
H -5.139813 -1.376209 0.000000  
H -3.184218 2.501861 0.000000  
H -3.165889 -2.481775 0.000000  
H 1.730870 2.480989 0.000000  
H 1.726603 -2.476749 0.000000  
H 6.282177 1.243566 0.000000  
H 4.173096 2.487679 0.000000  
H 4.174937 -2.489582 0.000000  
H 6.285818 -1.243859 0.000000  
C -0.738390 -2.897488 0.000000  
C -0.740433 -3.604040 1.198558  
C -0.745340 -4.990692 1.199054  
C -0.748322 -5.687075 0.000000  
C -0.745340 -4.990692 -1.199054  
C -0.740433 -3.604040 -1.198558  
C -0.723507 2.919687 0.000000  
C -0.714823 3.627509 -1.197423  
C -0.693847 5.013808 -1.198714  
C -0.682523 5.710568 0.000000  
C -0.693847 5.013808 1.198714  
C -0.714823 3.627509 1.197423  
H -0.725812 3.082597 -2.133608  
H -0.687228 5.550395 -2.139278  
H -0.666321 6.793233 0.000000  
H -0.687228 5.550395 2.139278  
H -0.725812 3.082597 2.133608  
H -0.734136 -3.058830 2.134642  
H -0.744781 -5.527384 2.139416  
H -0.750910 -6.769722 0.000000  
H -0.744781 -5.527384 -2.139416  
H -0.734136 -3.058830 -2.134642

**2\_3\_rightdpt.xyz**

50

C 4.122940 1.395896 0.000000  
N 5.291924 0.771328 0.000000  
B 5.448897 -0.681062 0.000000  
C 4.179305 -1.434515 0.000000  
C 2.949556 -0.757918 0.000000  
C 1.706264 -1.413693 0.000000  
C 0.495831 -0.735064 0.000000  
C -0.752393 -1.426306 0.000000  
C -1.939985 -0.725251 0.000000  
C -3.213330 -1.398897 0.000000  
C -4.373773 -0.711195 0.000000  
C -4.374180 0.719449 0.000000  
C -3.211068 1.402693 0.000000  
C -1.941624 0.723632 0.000000  
C -0.749724 1.415328 0.000000  
C 0.489018 0.711306 0.000000  
C 1.704153 1.376815 0.000000  
C 2.922106 0.686997 0.000000  
H -5.317198 1.251116 0.000000  
H -5.317914 -1.241372 0.000000  
H -3.216173 2.484495 0.000000  
H -3.221957 -2.480443 0.000000  
H 1.718163 2.459880 0.000000  
H 1.705165 -2.495815 0.000000  
H 6.106452 1.365249 0.000000  
H 4.120251 2.479930 0.000000  
H 4.134974 -2.518550 0.000000  
H 6.568165 -1.099190 0.000000  
C -0.753370 -2.914960 0.000000  
C -0.749695 -3.622063 1.197866  
C -0.746294 -5.008545 1.198838  
C -0.744612 -5.705136 0.000000  
C -0.746294 -5.008545 -1.198838  
C -0.749695 -3.622063 -1.197866  
C -0.733366 2.903834 0.000000  
C -0.720161 3.610757 -1.198094  
C -0.697736 4.997213 -1.198923  
C -0.686247 5.693756 0.000000  
C -0.697736 4.997213 1.198923  
C -0.720161 3.610757 1.198094  
H -0.729983 3.065654 -2.134194  
H -0.691029 5.533838 -2.139387  
H -0.670658 6.776365 0.000000  
H -0.691029 5.533838 2.139387  
H -0.729983 3.065654 2.134194  
H -0.749146 -3.077126 2.134094  
H -0.743796 -5.545161 2.139309  
H -0.739966 -6.787835 0.000000  
H -0.743796 -5.545161 -2.139309  
H -0.749146 -3.077126 -2.134094

**2\_9\_leftdpt.xyz**

50

```
C -3.216656 1.425377 0.000000
B -4.525455 0.682062 0.000000
C -4.431579 -0.858464 0.000000
C -3.224048 -1.454411 0.000000
C -1.976807 -0.710734 0.000000
C -0.787969 -1.386605 0.000000
C 0.454652 -0.667402 0.000000
C 1.646905 -1.325573 0.000000
N 2.848997 -0.688371 0.000000
C 4.024160 -1.426756 0.000000
C 5.227117 -0.838068 0.000000
C 5.313895 0.593682 0.000000
C 4.186434 1.325171 0.000000
C 2.885093 0.713255 0.000000
C 1.720725 1.412785 0.000000
C 0.439022 0.784212 0.000000
C -0.749908 1.461214 0.000000
C -2.007912 0.763580 0.000000
H -5.585834 1.246525 0.000000
H -5.302851 -1.508050 0.000000
H -3.173624 2.509095 0.000000
H -3.139098 -2.535530 0.000000
H 1.783233 2.491891 0.000000
H 1.696933 -2.405069 0.000000
H 6.282623 1.074167 0.000000
H 4.214470 2.406295 0.000000
H 3.886696 -2.498216 0.000000
H 6.115467 -1.452009 0.000000
C -0.726079 -2.875848 0.000000
C -0.681466 -3.580457 1.198612
C -0.598004 -4.964593 1.199101
C -0.554975 -5.659664 0.000000
C -0.598004 -4.964593 -1.199101
C -0.681466 -3.580457 -1.198612
C -0.736874 2.949286 0.000000
C -0.720013 3.658224 -1.197003
C -0.677404 5.044231 -1.198710
C -0.653715 5.740915 0.000000
C -0.677404 5.044231 1.198710
C -0.720013 3.658224 1.197003
H -0.745796 3.113407 -2.133022
H -0.665095 5.580749 -2.139344
H -0.620315 6.823220 0.000000
H -0.665095 5.580749 2.139344
H -0.745796 3.113407 2.133022
H -0.724178 -3.036559 2.134494
H -0.572457 -5.500683 2.139454
H -0.493954 -6.740600 0.000000
H -0.572457 -5.500683 -2.139454
H -0.724178 -3.036559 -2.134494
```

**2\_9\_rightdpt.xyz**

50

```
C 4.183053 -1.402140 0.000000
B 5.481667 -0.640426 0.000000
C 5.373319 0.904209 0.000000
C 4.160848 1.490594 0.000000
C 2.931880 0.724421 0.000000
C 1.738205 1.373737 0.000000
C 0.489826 0.679761 0.000000
C -0.699701 1.357266 0.000000
N -1.900432 0.684795 0.000000
C -3.102361 1.387842 0.000000
C -4.293838 0.776604 0.000000
C -4.356757 -0.652074 0.000000
C -3.213538 -1.356318 0.000000
C -1.918354 -0.724790 0.000000
C -0.750688 -1.432974 0.000000
C 0.519500 -0.771455 0.000000
C 1.719381 -1.421914 0.000000
C 2.974312 -0.741884 0.000000
H -5.190577 1.378464 0.000000
H -5.314614 -1.153994 0.000000
H -3.005916 2.459898 0.000000
H -3.223477 -2.436114 0.000000
H 1.731850 2.456591 0.000000
H 1.739241 -2.504176 0.000000
H 6.241731 1.557693 0.000000
H 4.047382 2.572566 0.000000
H 4.135292 -2.488423 0.000000
H 6.551288 -1.188138 0.000000
C -0.787869 -2.919713 0.000000
C -0.790834 -3.624517 1.198798
C -0.809408 -5.010765 1.199328
C -0.820119 -5.706399 0.000000
C -0.809408 -5.010765 -1.199328
C -0.790834 -3.624517 -1.198798
C -0.737173 2.844328 0.000000
C -0.739644 3.543559 -1.201511
C -0.751888 4.929501 -1.200421
C -0.760206 5.623512 0.000000
C -0.751888 4.929501 1.200421
C -0.739644 3.543559 1.201511
H -0.722499 2.998283 -2.137102
H -0.748517 5.467034 -2.139824
H -0.767602 6.705938 0.000000
H -0.748517 5.467034 2.139824
H -0.722499 2.998283 2.137102
H -0.773833 -3.079518 2.134786
H -0.810898 -5.547734 2.139419
H -0.830561 -6.788973 0.000000
H -0.810898 -5.547734 -2.139419
H -0.773833 -3.079518 -2.134786
```

**2\_14\_leftdpt.xyz**

50

```
C -3.214152 1.439381 0.000000
B -4.520737 0.719438 0.000000
C -4.434549 -0.822354 0.000000
C -3.233759 -1.442011 0.000000
C -1.984607 -0.720126 0.000000
C -0.794472 -1.420299 0.000000
C 0.444520 -0.735840 0.000000
C 1.668699 -1.384906 0.000000
C 2.876700 -0.710874 0.000000
C 4.139421 -1.358316 0.000000
C 5.300311 -0.664604 0.000000
C 5.235896 0.757338 0.000000
C 4.051724 1.389742 0.000000
N 2.846169 0.685053 0.000000
C 1.685325 1.349106 0.000000
C 0.439540 0.713025 0.000000
C -0.751272 1.425179 0.000000
C -2.003291 0.754754 0.000000
H -5.580170 1.287983 0.000000
H -5.311828 -1.465070 0.000000
H -3.150741 2.522346 0.000000
H -3.167757 -2.524180 0.000000
H 1.761191 2.426665 0.000000
H 1.705300 -2.465949 0.000000
H 6.137481 1.353600 0.000000
H 3.947035 2.464009 0.000000
H 4.129942 -2.440180 0.000000
H 6.255341 -1.169383 0.000000
C -0.763562 -2.910734 0.000000
C -0.731866 -3.616602 1.198085
C -0.669940 -5.001841 1.198954
C -0.637090 -5.697692 0.000000
C -0.669940 -5.001841 -1.198954
C -0.731866 -3.616602 -1.198085
C -0.700039 2.912037 0.000000
C -0.665287 3.620468 -1.197383
C -0.588199 5.005093 -1.198848
C -0.546963 5.700813 0.000000
C -0.588199 5.005093 1.198848
C -0.665287 3.620468 1.197383
H -0.710889 3.076337 -2.133099
H -0.567173 5.541571 -2.139326
H -0.491201 6.782190 0.000000
H -0.567173 5.541571 2.139326
H -0.710889 3.076337 2.133099
H -0.765352 -3.072427 2.134166
H -0.650755 -5.538010 2.139461
H -0.589540 -6.779322 0.000000
H -0.650755 -5.538010 -2.139461
H -0.765352 -3.072427 -2.134166
```

**2\_14\_rightdpt.xyz**

50

```
C 4.167127 -1.457819 0.000000
B 5.468884 -0.728231 0.000000
C 5.379172 0.818532 0.000000
C 4.177224 1.436027 0.000000
C 2.940929 0.699649 0.000000
C 1.749240 1.377758 0.000000
C 0.504052 0.720069 0.000000
C -0.711337 1.395845 0.000000
C -1.919586 0.702942 0.000000
C -3.181627 1.356543 0.000000
C -4.351673 0.679878 0.000000
C -4.299079 -0.737836 0.000000
C -3.121076 -1.382039 0.000000
N -1.896337 -0.701140 0.000000
C -0.735681 -1.390340 0.000000
C 0.505917 -0.728525 0.000000
C 1.707185 -1.415898 0.000000
C 2.960521 -0.767735 0.000000
H -5.299151 1.198767 0.000000
H -5.203273 -1.330446 0.000000
H -3.165752 2.436626 0.000000
H -3.045740 -2.455071 0.000000
H 1.764391 2.460803 0.000000
H 1.702062 -2.497863 0.000000
H 6.258829 1.458145 0.000000
H 4.090200 2.520232 0.000000
H 4.090193 -2.542819 0.000000
H 6.534344 -1.286676 0.000000
C -0.787848 -2.873678 0.000000
C -0.790874 -3.572483 1.201811
C -0.811759 -4.958155 1.200540
C -0.824725 -5.651791 0.000000
C -0.811759 -4.958155 -1.200540
C -0.790874 -3.572483 -1.201811
C -0.737034 2.884543 0.000000
C -0.740601 3.586887 -1.199708
C -0.753680 4.973164 -1.199540
C -0.761620 5.668440 0.000000
C -0.753680 4.973164 1.199540
C -0.740601 3.586887 1.199708
H -0.726361 3.042091 -2.135785
H -0.753531 5.510111 -2.139508
H -0.770407 6.750934 0.000000
H -0.753531 5.510111 2.139508
H -0.726361 3.042091 2.135785
H -0.766184 -3.027516 2.137419
H -0.808755 -5.495910 2.139793
H -0.834889 -6.734205 0.000000
H -0.808755 -5.495910 -2.139793
H -0.766184 -3.027516 -2.137419
```

**2\_16\_leftdpt.xyz**

50

C -3.197932 1.447678 0.000000  
B -4.509430 0.738087 0.000000  
C -4.436863 -0.802135 0.000000  
C -3.242643 -1.438891 0.000000  
C -1.995766 -0.724370 0.000000  
C -0.793523 -1.395260 0.000000  
C 0.439820 -0.707852 0.000000  
C 1.668213 -1.368670 0.000000  
C 2.876827 -0.708617 0.000000  
C 4.140024 -1.371983 0.000000  
C 5.289078 -0.655620 0.000000  
C 5.252432 0.773306 0.000000  
C 4.076887 1.441905 0.000000  
C 2.839458 0.718863 0.000000  
C 1.632862 1.362388 0.000000  
N 0.425708 0.696536 0.000000  
C -0.747813 1.383507 0.000000  
C -1.998766 0.735525 0.000000  
H -5.562181 1.317406 0.000000  
H -5.321744 -1.434109 0.000000  
H -3.120747 2.528848 0.000000  
H -3.185087 -2.521386 0.000000  
H 1.570146 2.436817 0.000000  
H 1.648159 -2.449140 0.000000  
H 6.185547 1.322303 0.000000  
H 4.050729 2.524614 0.000000  
H 4.158671 -2.455104 0.000000  
H 6.246383 -1.160014 0.000000  
C -0.747280 -2.885166 0.000000  
C -0.722863 -3.588405 1.199007  
C -0.671991 -4.973840 1.199314  
C -0.644687 -5.669198 0.000000  
C -0.671991 -4.973840 -1.199314  
C -0.722863 -3.588405 -1.199007  
C -0.673078 2.865779 0.000000  
C -0.648482 3.567503 -1.200235  
C -0.587539 4.952109 -1.200129  
C -0.553947 5.645971 0.000000  
C -0.587539 4.952109 1.200129  
C -0.648482 3.567503 1.200235  
H -0.688668 3.022780 -2.135524  
H -0.574557 5.489672 -2.139676  
H -0.510969 6.727762 0.000000  
H -0.574557 5.489672 2.139676  
H -0.688668 3.022780 2.135524  
H -0.751039 -3.043886 2.134941  
H -0.656617 -5.510293 2.139551  
H -0.605033 -6.751060 0.000000  
H -0.656617 -5.510293 -2.139551  
H -0.751039 -3.043886 -2.134941

**2\_16\_rightdpt.xyz**

50

C 4.069819 -1.496054 0.000000  
B 5.386091 -0.794108 0.000000  
C 5.329147 0.752684 0.000000  
C 4.143589 1.406730 0.000000  
C 2.900344 0.696087 0.000000  
C 1.700957 1.354249 0.000000  
C 0.455835 0.706808 0.000000  
C -0.760053 1.404067 0.000000  
C -1.970417 0.730101 0.000000  
C -3.232213 1.402768 0.000000  
C -4.391151 0.704898 0.000000  
C -4.371605 -0.721174 0.000000  
C -3.203553 -1.401682 0.000000  
C -1.948176 -0.703115 0.000000  
C -0.751810 -1.383474 0.000000  
N 0.455841 -0.697699 0.000000  
C 1.630442 -1.366009 0.000000  
C 2.888831 -0.757890 0.000000  
H -5.340465 1.224289 0.000000  
H -5.308657 -1.263351 0.000000  
H -3.241529 2.484401 0.000000  
H -3.200679 -2.482792 0.000000  
H 1.690996 2.435428 0.000000  
H 1.556806 -2.440033 0.000000  
H 6.226125 1.367494 0.000000  
H 4.083443 2.492319 0.000000  
H 3.960382 -2.577756 0.000000  
H 6.438494 -1.374287 0.000000  
C -0.703116 -2.866479 0.000000  
C -0.690504 -3.567967 1.200907  
C -0.665461 -4.953631 1.200384  
C -0.651944 -5.647525 0.000000  
C -0.665461 -4.953631 -1.200384  
C -0.690504 -3.567967 -1.200907  
C -0.728539 2.892229 0.000000  
C -0.718626 3.594648 -1.199709  
C -0.697095 4.980776 -1.199508  
C -0.685785 5.676035 0.000000  
C -0.697095 4.980776 1.199508  
C -0.718626 3.594648 1.199709  
H -0.724922 3.049931 -2.135917  
H -0.687137 5.517571 -2.139510  
H -0.665980 6.758382 0.000000  
H -0.687137 5.517571 2.139510  
H -0.724922 3.049931 2.135917  
H -0.700147 -3.022938 2.136863  
H -0.656442 -5.491240 2.139759  
H -0.630856 -6.729838 0.000000  
H -0.656442 -5.491240 -2.139759  
H -0.700147 -3.022938 -2.136863

**5\_2\_leftdpt.xyz**

50

C -3.177138 1.440612 0.000000  
N -4.350002 0.800141 0.000000  
C -4.503272 -0.571848 0.000000  
C -3.432399 -1.392909 0.000000  
B -2.032307 -0.781753 0.000000  
C -0.715625 -1.509893 0.000000  
C 0.462651 -0.764235 0.000000  
C 1.736789 -1.403675 0.000000  
C 2.919386 -0.716314 0.000000  
C 4.194380 -1.382103 0.000000  
C 5.345481 -0.678434 0.000000  
C 5.328458 0.757299 0.000000  
C 4.158281 1.428512 0.000000  
C 2.903482 0.727397 0.000000  
C 1.702102 1.381122 0.000000  
C 0.452502 0.701039 0.000000  
C -0.735757 1.431416 0.000000  
C -1.976423 0.750337 0.000000  
H -5.185639 1.359340 0.000000  
H -5.536489 -0.895447 0.000000  
H -3.246879 2.523003 0.000000  
H -3.631605 -2.459018 0.000000  
H 1.702164 2.463923 0.000000  
H 1.762861 -2.486245 0.000000  
H 6.267983 1.295398 0.000000  
H 4.140094 2.512304 0.000000  
H 4.206569 -2.465758 0.000000  
H 6.298295 -1.192957 0.000000  
C -0.664572 -2.994817 0.000000  
C -0.660723 -3.710212 1.195686  
C -0.648133 -5.096986 1.197311  
C -0.641266 -5.796322 0.000000  
C -0.648133 -5.096986 -1.197311  
C -0.660723 -3.710212 -1.195686  
C -0.711145 2.921545 0.000000  
C -0.713382 3.630894 -1.197650  
C -0.714465 5.017780 -1.198674  
C -0.715230 5.714944 0.000000  
C -0.714465 5.017780 1.198674  
C -0.713382 3.630894 1.197650  
H -0.706406 3.085642 -2.133829  
H -0.711317 5.554355 -2.139294  
H -0.713464 6.797680 0.000000  
H -0.711317 5.554355 2.139294  
H -0.706406 3.085642 2.133829  
H -0.666548 -3.166482 2.132861  
H -0.644224 -5.632564 2.138878  
H -0.631922 -6.879139 0.000000  
H -0.644224 -5.632564 -2.138878  
H -0.666548 -3.166482 -2.132861

**5\_2\_rightdpt.xyz**

50

C 4.134038 1.448650 0.000000  
N 5.319499 0.829979 0.000000  
C 5.491303 -0.541107 0.000000  
C 4.436832 -1.384492 0.000000  
B 3.022933 -0.800139 0.000000  
C 1.698861 -1.506695 0.000000  
C 0.511839 -0.783597 0.000000  
C -0.763096 -1.446327 0.000000  
C -1.941588 -0.736296 0.000000  
C -3.225384 -1.395347 0.000000  
C -4.377439 -0.695283 0.000000  
C -4.361655 0.736557 0.000000  
C -3.191290 1.405969 0.000000  
C -1.927257 0.712907 0.000000  
C -0.728626 1.387791 0.000000  
C 0.515941 0.679968 0.000000  
C 1.709906 1.386271 0.000000  
C 2.953814 0.731018 0.000000  
H -5.298232 1.279690 0.000000  
H -5.327501 -1.215115 0.000000  
H -3.186482 2.487622 0.000000  
H -3.247290 -2.476558 0.000000  
H 1.672466 2.470488 0.000000  
H 1.611269 -2.587491 0.000000  
H 6.147607 1.400091 0.000000  
H 4.176357 2.533742 0.000000  
H 4.667696 -2.444372 0.000000  
H 6.530120 -0.846601 0.000000  
C -0.796345 -2.935245 0.000000  
C -0.812511 -3.643182 1.197164  
C -0.846980 -5.029250 1.198573  
C -0.864204 -5.726264 0.000000  
C -0.846980 -5.029250 -1.198573  
C -0.812511 -3.643182 -1.197164  
C -0.715673 2.877481 0.000000  
C -0.710722 3.585471 -1.197494  
C -0.705042 4.972134 -1.198715  
C -0.702313 5.669309 0.000000  
C -0.705042 4.972134 1.198715  
C -0.710722 3.585471 1.197494  
H -0.714193 3.039846 -2.133312  
H -0.706463 5.508526 -2.139454  
H -0.702445 6.752090 0.000000  
H -0.706463 5.508526 2.139454  
H -0.714193 3.039846 2.133312  
H -0.796664 -3.097977 2.133077  
H -0.859613 -5.565520 2.139332  
H -0.889336 -6.808790 0.000000  
H -0.859613 -5.565520 -2.139332  
H -0.796664 -3.097977 -2.133077

**5\_4\_leftdpt.xyz**

50

```
C -3.215059 1.434205 0.000000
C -4.410453 0.730002 0.000000
C -4.426512 -0.656961 0.000000
N -3.302647 -1.365761 0.000000
B -1.988832 -0.746753 0.000000
C -0.704557 -1.503944 0.000000
C 0.475726 -0.756301 0.000000
C 1.746380 -1.394444 0.000000
C 2.929770 -0.703441 0.000000
C 4.205833 -1.364255 0.000000
C 5.355122 -0.655453 0.000000
C 5.332809 0.778347 0.000000
C 4.158375 1.444215 0.000000
C 2.908493 0.737522 0.000000
C 1.701939 1.388139 0.000000
C 0.457545 0.707093 0.000000
C -0.738528 1.441537 0.000000
C -1.977988 0.774245 0.000000
H -5.356228 1.253018 0.000000
H -5.363831 -1.200182 0.000000
H -3.259564 2.519413 0.000000
H -3.389742 -2.371858 0.000000
H 1.698964 2.470799 0.000000
H 1.775071 -2.477277 0.000000
H 6.269895 1.320658 0.000000
H 4.134591 2.527866 0.000000
H 4.223582 -2.447880 0.000000
H 6.309434 -1.167241 0.000000
C -0.682179 -2.989024 0.000000
C -0.699375 -3.705516 1.196306
C -0.727496 -5.092342 1.197675
C -0.741886 -5.791061 0.000000
C -0.727496 -5.092342 -1.197675
C -0.699375 -3.705516 -1.196306
C -0.704792 2.931561 0.000000
C -0.700743 3.640193 -1.197530
C -0.689604 5.026864 -1.198595
C -0.683823 5.723966 0.000000
C -0.689604 5.026864 1.198595
C -0.700743 3.640193 1.197530
H -0.701533 3.095167 -2.133793
H -0.684272 5.563353 -2.139245
H -0.674613 6.806676 0.000000
H -0.684272 5.563353 2.139245
H -0.701533 3.095167 2.133793
H -0.684533 -3.161503 2.133290
H -0.736897 -5.628117 2.138978
H -0.763447 -6.873622 0.000000
H -0.736897 -5.628117 -2.138978
H -0.684533 -3.161503 -2.133290
```

**5\_4\_rightdpt.xyz**

50

```
C 4.172263 1.470276 0.000000
C 5.387218 0.798846 0.000000
C 5.435093 -0.586912 0.000000
N 4.330889 -1.330697 0.000000
B 2.997328 -0.749366 0.000000
C 1.709256 -1.495306 0.000000
C 0.516737 -0.773935 0.000000
C -0.751375 -1.441254 0.000000
C -1.934874 -0.735768 0.000000
C -3.214609 -1.399336 0.000000
C -4.369810 -0.702777 0.000000
C -4.358572 0.727638 0.000000
C -3.188937 1.400275 0.000000
C -1.924927 0.710815 0.000000
C -0.725092 1.389550 0.000000
C 0.518636 0.688021 0.000000
C 1.714857 1.405003 0.000000
C 2.961577 0.771030 0.000000
H -5.296724 1.267974 0.000000
H -5.318086 -1.225856 0.000000
H -3.186446 2.481971 0.000000
H -3.233587 -2.480700 0.000000
H 1.668150 2.488567 0.000000
H 1.631057 -2.576991 0.000000
H 6.321527 1.342249 0.000000
H 4.176384 2.557847 0.000000
H 4.460154 -2.330572 0.000000
H 6.386226 -1.105529 0.000000
C -0.777936 -2.930278 0.000000
C -0.790552 -3.638866 1.197079
C -0.818568 -5.025198 1.198600
C -0.832528 -5.722405 0.000000
C -0.818568 -5.025198 -1.198600
C -0.790552 -3.638866 -1.197079
C -0.719813 2.879528 0.000000
C -0.719119 3.587277 -1.197524
C -0.720547 4.973872 -1.198689
C -0.721298 5.670957 0.000000
C -0.720547 4.973872 1.198689
C -0.719119 3.587277 1.197524
H -0.718851 3.041784 -2.133420
H -0.723103 5.510327 -2.139361
H -0.725343 6.753713 0.000000
H -0.723103 5.510327 2.139361
H -0.718851 3.041784 2.133420
H -0.779254 -3.093403 2.132959
H -0.831099 -5.561573 2.139350
H -0.855258 -6.805017 0.000000
H -0.831099 -5.561573 -2.139350
H -0.779254 -3.093403 -2.132959
```

**5\_8\_leftdpt.xyz**

50

```
C -3.283644 1.509892 0.000000
C -4.454722 0.840876 0.000000
C -4.541244 -0.604825 0.000000
C -3.451123 -1.402797 0.000000
B -2.056991 -0.751411 0.000000
C -0.738461 -1.489436 0.000000
C 0.410330 -0.743108 0.000000
N 1.647042 -1.354642 0.000000
C 2.848719 -0.726259 0.000000
C 4.053809 -1.446162 0.000000
C 5.245765 -0.767727 0.000000
C 5.282069 0.635810 0.000000
C 4.108695 1.342541 0.000000
C 2.868557 0.678945 0.000000
C 1.625694 1.361069 0.000000
C 0.419648 0.718595 0.000000
C -0.823184 1.458535 0.000000
C -2.022279 0.800795 0.000000
H -5.382976 1.400992 0.000000
H -5.541197 -1.030548 0.000000
H -3.293655 2.594559 0.000000
H -3.605123 -2.478426 0.000000
H 1.644809 2.444377 0.000000
H 1.635185 -2.364013 0.000000
H 6.233291 1.150464 0.000000
H 4.115934 2.426057 0.000000
H 4.032341 -2.529351 0.000000
H 6.173465 -1.325800 0.000000
C -0.633976 -2.972865 0.000000
C -0.583725 -3.688033 1.196430
C -0.484574 -5.071616 1.197930
C -0.432849 -5.768131 0.000000
C -0.484574 -5.071616 -1.197930
C -0.583725 -3.688033 -1.196430
C -0.744910 2.948035 0.000000
C -0.712241 3.654876 -1.197850
C -0.645429 5.039944 -1.198742
C -0.610349 5.735942 0.000000
C -0.645429 5.039944 1.198742
C -0.712241 3.654876 1.197850
H -0.745249 3.110795 -2.134065
H -0.624092 5.576119 -2.139285
H -0.559884 6.817492 0.000000
H -0.624092 5.576119 2.139285
H -0.745249 3.110795 2.134065
H -0.633626 -3.146147 2.133412
H -0.451862 -5.606559 2.139093
H -0.357246 -6.848229 0.000000
H -0.451862 -5.606559 -2.139093
H -0.633626 -3.146147 -2.133412
```

**5\_8\_rightdpt.xyz**

50

```
C 4.200418 -1.478749 0.000000
C 5.379661 -0.825285 0.000000
C 5.475942 0.622104 0.000000
C 4.397065 1.437332 0.000000
B 2.993248 0.802940 0.000000
C 1.663657 1.517431 0.000000
C 0.500862 0.797817 0.000000
N -0.749745 1.418733 0.000000
C -1.941101 0.738536 0.000000
C -3.172749 1.419863 0.000000
C -4.351344 0.717598 0.000000
C -4.358487 -0.680996 0.000000
C -3.166807 -1.355411 0.000000
C -1.936298 -0.670524 0.000000
C -0.681367 -1.357287 0.000000
C 0.503270 -0.667840 0.000000
C 1.755755 -1.375366 0.000000
C 2.957775 -0.744292 0.000000
H -5.287498 1.261619 0.000000
H -5.294811 -1.222410 0.000000
H -3.192274 2.499360 0.000000
H -3.156447 -2.436842 0.000000
H 1.593865 2.598207 0.000000
H 1.702246 -2.459489 0.000000
H 6.480893 1.036547 0.000000
H 4.573308 2.509824 0.000000
H 4.181133 -2.565507 0.000000
H 6.304625 -1.390850 0.000000
C -0.701109 -2.846261 0.000000
C -0.720446 -3.547836 1.199712
C -0.753287 -4.933670 1.199215
C -0.770114 -5.629271 0.000000
C -0.753287 -4.933670 -1.199215
C -0.720446 -3.547836 -1.199712
C -0.785743 2.852028 0.000000
C -0.804916 3.535692 -1.203743
C -0.852236 4.920734 -1.201363
C -0.877256 5.613335 0.000000
C -0.852236 4.920734 1.201363
C -0.804916 3.535692 1.203743
H -0.777133 2.979485 -2.131809
H -0.867207 5.458801 -2.140294
H -0.914408 6.695154 0.000000
H -0.867207 5.458801 2.140294
H -0.777133 2.979485 2.131809
H -0.703015 -3.003222 2.135754
H -0.762843 -5.470221 2.139432
H -0.794051 -6.711573 0.000000
H -0.762843 -5.470221 -2.139432
H -0.703015 -3.003222 -2.135754
```

**5\_12\_leftdpt.xyz**

50

C -3.251102 1.494413 0.000000  
C -4.424859 0.828617 0.000000  
C -4.515465 -0.615708 0.000000  
C -3.425756 -1.415561 0.000000  
B -2.029395 -0.768129 0.000000  
C -0.708493 -1.507870 0.000000  
C 0.467295 -0.789227 0.000000  
C 1.750781 -1.433021 0.000000  
C 2.921564 -0.747964 0.000000  
C 4.225713 -1.358873 0.000000  
C 5.340626 -0.612023 0.000000  
N 5.257401 0.768241 0.000000  
C 4.070603 1.399328 0.000000  
C 2.894123 0.702411 0.000000  
C 1.643183 1.363492 0.000000  
C 0.453454 0.686011 0.000000  
C -0.788351 1.430233 0.000000  
C -1.993107 0.780585 0.000000  
H -5.351459 1.391897 0.000000  
H -5.516423 -1.039465 0.000000  
H -3.259394 2.579264 0.000000  
H -3.581148 -2.490994 0.000000  
H 1.640977 2.446761 0.000000  
H 1.773606 -2.515430 0.000000  
H 6.102771 1.309272 0.000000  
H 4.096633 2.481350 0.000000  
H 4.310898 -2.437063 0.000000  
H 6.338770 -1.023131 0.000000  
C -0.667729 -2.994521 0.000000  
C -0.663378 -3.711174 1.195008  
C -0.644044 -5.097973 1.197197  
C -0.632022 -5.797664 0.000000  
C -0.644044 -5.097973 -1.197197  
C -0.663378 -3.711174 -1.195008  
C -0.716887 2.920734 0.000000  
C -0.690352 3.629178 -1.197295  
C -0.634901 5.014875 -1.198547  
C -0.605346 5.711750 0.000000  
C -0.634901 5.014875 1.198547  
C -0.690352 3.629178 1.197295  
H -0.720507 3.084376 -2.133212  
H -0.620426 5.551179 -2.139321  
H -0.566153 6.793874 0.000000  
H -0.620426 5.551179 2.139321  
H -0.720507 3.084376 2.133212  
H -0.678299 -3.167424 2.132162  
H -0.641675 -5.633574 2.138895  
H -0.618200 -6.880514 0.000000  
H -0.641675 -5.633574 -2.138895  
H -0.678299 -3.167424 -2.132162

**5\_12\_rightdpt.xyz**

50

C 4.204625 -1.529623 0.000000  
C 5.393213 -0.891537 0.000000  
C 5.509219 0.553383 0.000000  
C 4.439535 1.381728 0.000000  
B 3.027132 0.766502 0.000000  
C 1.701204 1.489044 0.000000  
C 0.514330 0.796433 0.000000  
C -0.765239 1.467337 0.000000  
C -1.934039 0.766718 0.000000  
C -3.240022 1.382382 0.000000  
C -4.360791 0.646668 0.000000  
N -4.287087 -0.731687 0.000000  
C -3.105435 -1.369186 0.000000  
C -1.916734 -0.687701 0.000000  
C -0.667882 -1.378471 0.000000  
C 0.516285 -0.679451 0.000000  
C 1.761149 -1.399611 0.000000  
C 2.971758 -0.780004 0.000000  
H -5.354486 1.068463 0.000000  
H -5.133839 -1.270464 0.000000  
H -3.321475 2.459723 0.000000  
H -3.144555 -2.449530 0.000000  
H 1.634896 2.572390 0.000000  
H 1.704978 -2.484325 0.000000  
H 6.519603 0.954802 0.000000  
H 4.628599 2.452155 0.000000  
H 4.172161 -2.616393 0.000000  
H 6.310432 -1.469973 0.000000  
C -0.695546 -2.868542 0.000000  
C -0.720331 -3.573389 1.198891  
C -0.766071 -4.959275 1.199150  
C -0.790086 -5.655124 0.000000  
C -0.766071 -4.959275 -1.199150  
C -0.720331 -3.573389 -1.198891  
C -0.803021 2.955281 0.000000  
C -0.827650 3.662963 -1.197322  
C -0.886591 5.048335 -1.198763  
C -0.918323 5.744538 0.000000  
C -0.886591 5.048335 1.198763  
C -0.827650 3.662963 1.197322  
H -0.794218 3.118507 -2.133270  
H -0.905105 5.584701 -2.139326  
H -0.964523 6.826334 0.000000  
H -0.905105 5.584701 2.139326  
H -0.794218 3.118507 2.133270  
H -0.690671 -3.028431 2.134631  
H -0.776677 -5.495888 2.139457  
H -0.821467 -6.737304 0.000000  
H -0.776677 -5.495888 -2.139457  
H -0.690671 -3.028431 -2.134631

**6\_1\_leftdpt.xyz**

50

```
N -3.110818 1.444538 0.000000
C -4.317647 0.857957 0.000000
C -4.450369 -0.495993 0.000000
C -3.267040 -1.266414 0.000000
C -2.016619 -0.701810 0.000000
B -0.723200 -1.525950 0.000000
C 0.584003 -0.722674 0.000000
C 1.814042 -1.356845 0.000000
C 3.027661 -0.656645 0.000000
C 4.286423 -1.312012 0.000000
C 5.444735 -0.596629 0.000000
C 5.402222 0.819265 0.000000
C 4.211366 1.478892 0.000000
C 2.982767 0.763831 0.000000
C 1.742486 1.416111 0.000000
C 0.545348 0.717184 0.000000
C -0.720041 1.422673 0.000000
C -1.903615 0.745750 0.000000
H -5.165137 1.530576 0.000000
H -5.429975 -0.947996 0.000000
H -3.055212 2.451152 0.000000
H -3.342475 -2.348546 0.000000
H 1.735881 2.499527 0.000000
H 1.842916 -2.441939 0.000000
H 6.330314 1.377773 0.000000
H 4.182023 2.562360 0.000000
H 4.307274 -2.395872 0.000000
H 6.401283 -1.103370 0.000000
C -0.755782 -3.100431 0.000000
C -0.771132 -3.825025 1.193595
C -0.801638 -5.212134 1.197428
C -0.817491 -5.910774 0.000000
C -0.801638 -5.212134 -1.197428
C -0.771132 -3.825025 -1.193595
C -0.737982 2.912032 0.000000
C -0.757211 3.626266 -1.197048
C -0.796621 5.012899 -1.198970
C -0.817420 5.709446 0.000000
C -0.796621 5.012899 1.198970
C -0.757211 3.626266 1.197048
H -0.733558 3.080929 -2.133060
H -0.808405 5.549765 -2.139375
H -0.848196 6.791779 0.000000
H -0.808405 5.549765 2.139375
H -0.733558 3.080929 2.133060
H -0.755616 -3.296101 2.140532
H -0.811531 -5.748302 2.138713
H -0.840351 -6.993539 0.000000
H -0.811531 -5.748302 -2.138713
H -0.755616 -3.296101 -2.140532
```

**6\_1\_rightdpt.xyz**

50

```
N 4.135313 -1.459769 0.000000
C 5.354347 -0.894798 0.000000
C 5.511566 0.456750 0.000000
C 4.342939 1.252228 0.000000
C 3.084216 0.708815 0.000000
B 1.805777 1.546179 0.000000
C 0.469949 0.786545 0.000000
C -0.754943 1.448261 0.000000
C -1.973129 0.735718 0.000000
C -3.233733 1.394862 0.000000
C -4.398348 0.691669 0.000000
C -4.367999 -0.721259 0.000000
C -3.182094 -1.388136 0.000000
C -1.941455 -0.688291 0.000000
C -0.706710 -1.367050 0.000000
C 0.491316 -0.655856 0.000000
C 1.746213 -1.365061 0.000000
C 2.945741 -0.733123 0.000000
H -5.348514 1.210344 0.000000
H -5.298174 -1.276235 0.000000
H -3.254924 2.476509 0.000000
H -3.171549 -2.469885 0.000000
H 1.885591 2.738613 0.000000
H 1.721738 -2.447523 0.000000
H 6.500282 0.888667 0.000000
H 4.438607 2.332512 0.000000
H 4.065252 -2.463558 0.000000
H 6.190227 -1.581657 0.000000
C -0.697310 -2.857022 0.000000
C -0.692030 -3.567057 1.196799
C -0.681188 -4.953821 1.198583
C -0.675330 -5.651354 0.000000
C -0.681188 -4.953821 -1.198583
C -0.692030 -3.567057 -1.196799
C -0.802132 2.938427 0.000000
C -0.830380 3.644196 -1.197039
C -0.877389 5.029728 -1.198353
C -0.900491 5.726764 0.000000
C -0.877389 5.029728 1.198353
C -0.830380 3.644196 1.197039
H -0.809948 3.099626 -2.133271
H -0.894701 5.565783 -2.139164
H -0.937209 6.808945 0.000000
H -0.894701 5.565783 2.139164
H -0.809948 3.099626 2.133271
H -0.697216 -3.021551 2.132804
H -0.679909 -5.490412 2.139345
H -0.669560 -6.734212 0.000000
H -0.679909 -5.490412 -2.139345
H -0.697216 -3.021551 -2.132804
```

**6\_9\_leftdpt.xyz**

50

```
C -3.202318 1.461961 0.000000
C -4.413842 0.815984 0.000000
C -4.484317 -0.581086 0.000000
C -3.316660 -1.303337 0.000000
C -2.052579 -0.681542 0.000000
B -0.766388 -1.497037 0.000000
C 0.529031 -0.671990 0.000000
C 1.738886 -1.286894 0.000000
N 2.929100 -0.623476 0.000000
C 4.123318 -1.329538 0.000000
C 5.309818 -0.709884 0.000000
C 5.355084 0.725859 0.000000
C 4.209080 1.426879 0.000000
C 2.922452 0.780898 0.000000
C 1.741791 1.450506 0.000000
C 0.472853 0.785819 0.000000
C -0.727113 1.448884 0.000000
C -1.987580 0.741082 0.000000
H -5.326964 1.399925 0.000000
H -5.444799 -1.080395 0.000000
H -3.179678 2.543629 0.000000
H -3.355667 -2.387076 0.000000
H 1.785350 2.531023 0.000000
H 1.818282 -2.367311 0.000000
H 6.310520 1.232520 0.000000
H 4.209178 2.508513 0.000000
H 4.012403 -2.404297 0.000000
H 6.216003 -1.297101 0.000000
C -0.730282 -3.073601 0.000000
C -0.706731 -3.799088 1.193373
C -0.660486 -5.185950 1.197389
C -0.636164 -5.884589 0.000000
C -0.660486 -5.185950 -1.197389
C -0.706731 -3.799088 -1.193373
C -0.732328 2.939560 0.000000
C -0.728161 3.652530 -1.195961
C -0.715376 5.039413 -1.198404
C -0.708085 5.737113 0.000000
C -0.715376 5.039413 1.198404
C -0.728161 3.652530 1.195961
H -0.735862 3.107423 -2.132354
H -0.711466 5.575943 -2.139241
H -0.697312 6.819931 0.000000
H -0.711466 5.575943 2.139241
H -0.735862 3.107423 2.132354
H -0.730003 -3.270183 2.140222
H -0.646388 -5.722017 2.138731
H -0.602180 -6.967075 0.000000
H -0.646388 -5.722017 -2.138731
H -0.730003 -3.270183 -2.140222
```

**6\_9\_rightdpt.xyz**

50

```
C 4.180603 -1.458531 0.000000
C 5.408829 -0.847506 0.000000
C 5.513633 0.550753 0.000000
C 4.367843 1.307853 0.000000
C 3.087275 0.719452 0.000000
B 1.813750 1.546780 0.000000
C 0.484048 0.766705 0.000000
C -0.726649 1.403183 0.000000
N -1.920061 0.711571 0.000000
C -3.137546 1.389540 0.000000
C -4.316110 0.755773 0.000000
C -4.350258 -0.675705 0.000000
C -3.194261 -1.356993 0.000000
C -1.909784 -0.699590 0.000000
C -0.730610 -1.382575 0.000000
C 0.530258 -0.693305 0.000000
C 1.724608 -1.356548 0.000000
C 2.993077 -0.696596 0.000000
H -5.224862 1.339377 0.000000
H -5.297928 -1.196859 0.000000
H -3.063489 2.463108 0.000000
H -3.184695 -2.436794 0.000000
H 1.852784 2.742567 0.000000
H 1.726092 -2.439094 0.000000
H 6.488415 1.021847 0.000000
H 4.436527 2.390315 0.000000
H 4.112122 -2.540626 0.000000
H 6.308659 -1.451793 0.000000
C -0.745081 -2.869960 0.000000
C -0.739102 -3.576021 1.198233
C -0.741183 -4.962500 1.199147
C -0.743729 -5.658733 0.000000
C -0.741183 -4.962500 -1.199147
C -0.739102 -3.576021 -1.198233
C -0.817727 2.890209 0.000000
C -0.850679 3.588024 -1.200343
C -0.916993 4.972182 -1.199833
C -0.952038 5.666179 0.000000
C -0.916993 4.972182 1.199833
C -0.850679 3.588024 1.200343
H -0.809484 3.043797 -2.135729
H -0.933105 5.509178 -2.139574
H -1.000573 6.747642 0.000000
H -0.933105 5.509178 2.139574
H -0.809484 3.043797 2.135729
H -0.730093 -3.030340 2.133956
H -0.738678 -5.499411 2.139424
H -0.744542 -6.741466 0.000000
H -0.738678 -5.499411 -2.139424
H -0.730093 -3.030340 -2.133956
```

**6\_11\_leftdpt.xyz**

50

```
C -3.178988 1.457131 0.000000
C -4.399532 0.821178 0.000000
C -4.482322 -0.571819 0.000000
C -3.317719 -1.304881 0.000000
C -2.053165 -0.692545 0.000000
B -0.763978 -1.510934 0.000000
C 0.551180 -0.703713 0.000000
C 1.754266 -1.338086 0.000000
C 2.992414 -0.630656 0.000000
C 4.189092 -1.278215 0.000000
N 5.358763 -0.600303 0.000000
C 5.378487 0.781706 0.000000
C 4.237279 1.484713 0.000000
C 2.951124 0.824013 0.000000
C 1.761568 1.469788 0.000000
C 0.502569 0.763382 0.000000
C -0.699047 1.421212 0.000000
C -1.974672 0.725902 0.000000
H -5.306788 1.414214 0.000000
H -5.446762 -1.063527 0.000000
H -3.148791 2.538471 0.000000
H -3.365272 -2.388298 0.000000
H 1.753138 2.552346 0.000000
H 1.782685 -2.423747 0.000000
H 6.357595 1.237202 0.000000
H 4.282865 2.565339 0.000000
H 4.257082 -2.358344 0.000000
H 6.224948 -1.105649 0.000000
C -0.755550 -3.087135 0.000000
C -0.750350 -3.812613 1.193266
C -0.739204 -5.200125 1.197276
C -0.732919 -5.899383 0.000000
C -0.739204 -5.200125 -1.197276
C -0.750350 -3.812613 -1.193266
C -0.714015 2.912605 0.000000
C -0.719344 3.625313 -1.195812
C -0.725473 5.012164 -1.198277
C -0.728156 5.710157 0.000000
C -0.725473 5.012164 1.198277
C -0.719344 3.625313 1.195812
H -0.717961 3.079900 -2.132015
H -0.728710 5.548617 -2.139229
H -0.733655 6.793076 0.000000
H -0.728710 5.548617 2.139229
H -0.717961 3.079900 2.132015
H -0.758935 -3.283363 2.140136
H -0.738462 -5.736269 2.138756
H -0.726899 -6.982447 0.000000
H -0.738462 -5.736269 -2.138756
H -0.758935 -3.283363 -2.140136
```

**6\_11\_rightdpt.xyz**

50

```
C 4.166065 -1.477003 0.000000
C 5.406841 -0.883399 0.000000
C 5.532824 0.509418 0.000000
C 4.395264 1.284743 0.000000
C 3.111169 0.713711 0.000000
B 1.839333 1.550712 0.000000
C 0.490385 0.792080 0.000000
C -0.707785 1.451268 0.000000
C -1.950956 0.725773 0.000000
C -3.150803 1.374418 0.000000
N -4.323537 0.706148 0.000000
C -4.354443 -0.673665 0.000000
C -3.217886 -1.381601 0.000000
C -1.922518 -0.731719 0.000000
C -0.741025 -1.401303 0.000000
C 0.516551 -0.679008 0.000000
C 1.709213 -1.339684 0.000000
C 2.994829 -0.697670 0.000000
H -5.183845 1.221497 0.000000
H -5.335632 -1.124686 0.000000
H -3.216763 2.453328 0.000000
H -3.273854 -2.460572 0.000000
H 1.889785 2.746336 0.000000
H 1.707712 -2.422742 0.000000
H 6.514077 0.966888 0.000000
H 4.479459 2.366133 0.000000
H 4.081936 -2.558009 0.000000
H 6.296627 -1.502420 0.000000
C -0.727297 -2.889073 0.000000
C -0.721122 -3.598257 1.197175
C -0.719163 -4.984996 1.198769
C -0.719368 -5.682025 0.000000
C -0.719163 -4.984996 -1.198769
C -0.721122 -3.598257 -1.197175
C -0.784358 2.939806 0.000000
C -0.835009 3.642557 -1.198167
C -0.925657 5.026050 -1.198789
C -0.972163 5.721247 0.000000
C -0.925657 5.026050 1.198789
C -0.835009 3.642557 1.198167
H -0.787115 3.099251 -2.134098
H -0.953214 5.561833 -2.139326
H -1.039879 6.801801 0.000000
H -0.953214 5.561833 2.139326
H -0.787115 3.099251 2.134098
H -0.714715 -3.052557 2.133050
H -0.715570 -5.521816 2.139310
H -0.716883 -6.764858 0.000000
H -0.715570 -5.521816 -2.139310
H -0.714715 -3.052557 -2.133050
```

**6\_15\_leftdpt.xyz**

50

C -3.190623 1.453044 0.000000  
C -4.414670 0.822456 0.000000  
C -4.505141 -0.569995 0.000000  
C -3.344898 -1.308945 0.000000  
C -2.076313 -0.704141 0.000000  
B -0.795430 -1.534684 0.000000  
C 0.525333 -0.737332 0.000000  
C 1.742513 -1.342426 0.000000  
C 2.972211 -0.615346 0.000000  
C 4.229544 -1.233459 0.000000  
C 5.383177 -0.486865 0.000000  
C 5.295054 0.909314 0.000000  
C 4.076342 1.546423 0.000000  
C 2.897574 0.788737 0.000000  
N 1.674119 1.387208 0.000000  
C 0.462082 0.715939 0.000000  
C -0.715447 1.403780 0.000000  
C -1.992655 0.714666 0.000000  
H -5.318607 1.420268 0.000000  
H -5.472681 -1.055377 0.000000  
H -3.154725 2.534707 0.000000  
H -3.396117 -2.392111 0.000000  
H 1.639856 2.394468 0.000000  
H 1.789811 -2.427078 0.000000  
H 6.200522 1.503252 0.000000  
H 4.019073 2.628395 0.000000  
H 4.273903 -2.316202 0.000000  
H 6.350413 -0.970624 0.000000  
C -0.782634 -3.109158 0.000000  
C -0.771208 -3.833400 1.193787  
C -0.746143 -5.220621 1.197480  
C -0.732243 -5.919220 0.000000  
C -0.746143 -5.220621 -1.197480  
C -0.771208 -3.833400 -1.193787  
C -0.678326 2.893257 0.000000  
C -0.649637 3.606450 -1.197093  
C -0.598586 4.992600 -1.198939  
C -0.573317 5.688985 0.000000  
C -0.598586 4.992600 1.198939  
C -0.649637 3.606450 1.197093  
H -0.674979 3.061435 -2.133213  
H -0.582078 5.529233 -2.139381  
H -0.537446 6.771152 0.000000  
H -0.582078 5.529233 2.139381  
H -0.674979 3.061435 2.133213  
H -0.784462 -3.304618 2.140805  
H -0.737433 -5.756638 2.138814  
H -0.711255 -7.001971 0.000000  
H -0.737433 -5.756638 -2.138814  
H -0.784462 -3.304618 -2.140805

**6\_15\_rightdpt.xyz**

50

C 4.133347 -1.520640 0.000000  
C 5.378737 -0.936015 0.000000  
C 5.517227 0.455169 0.000000  
C 4.385784 1.238466 0.000000  
C 3.097103 0.676940 0.000000  
B 1.834443 1.523400 0.000000  
C 0.479172 0.777165 0.000000  
C -0.720841 1.428601 0.000000  
C -1.967701 0.704162 0.000000  
C -3.212282 1.352466 0.000000  
C -4.389559 0.645221 0.000000  
C -4.341687 -0.748627 0.000000  
C -3.140824 -1.418408 0.000000  
C -1.931362 -0.704404 0.000000  
N -0.720883 -1.357062 0.000000  
C 0.505311 -0.683407 0.000000  
C 1.679233 -1.370086 0.000000  
C 2.968610 -0.732456 0.000000  
H -5.339729 1.161689 0.000000  
H -5.261564 -1.320149 0.000000  
H -3.230756 2.433978 0.000000  
H -3.129908 -2.498228 0.000000  
H 1.885363 2.717237 0.000000  
H 1.671325 -2.450826 0.000000  
H 6.501992 0.904620 0.000000  
H 4.477207 2.319130 0.000000  
H 4.042801 -2.601115 0.000000  
H 6.262854 -1.563058 0.000000  
C -0.711191 -2.787770 0.000000  
C -0.704112 -3.473760 1.203467  
C -0.698760 -4.859736 1.201372  
C -0.696858 -5.552904 0.000000  
C -0.698760 -4.859736 -1.201372  
C -0.704112 -3.473760 -1.203467  
C -0.790052 2.916048 0.000000  
C -0.833616 3.616231 -1.198910  
C -0.908743 5.000248 -1.198831  
C -0.946597 5.695529 0.000000  
C -0.908743 5.000248 1.198831  
C -0.833616 3.616231 1.198910  
H -0.797352 3.072895 -2.135166  
H -0.933318 5.536110 -2.139274  
H -1.003794 6.776626 0.000000  
H -0.933318 5.536110 2.139274  
H -0.797352 3.072895 2.135166  
H -0.700548 -2.916750 2.131568  
H -0.694858 -5.398179 2.140278  
H -0.692360 -6.635412 0.000000  
H -0.694858 -5.398179 -2.140278  
H -0.700548 -2.916750 -2.131568

# **Appendix D - Supporting Information: Tables and Figures**

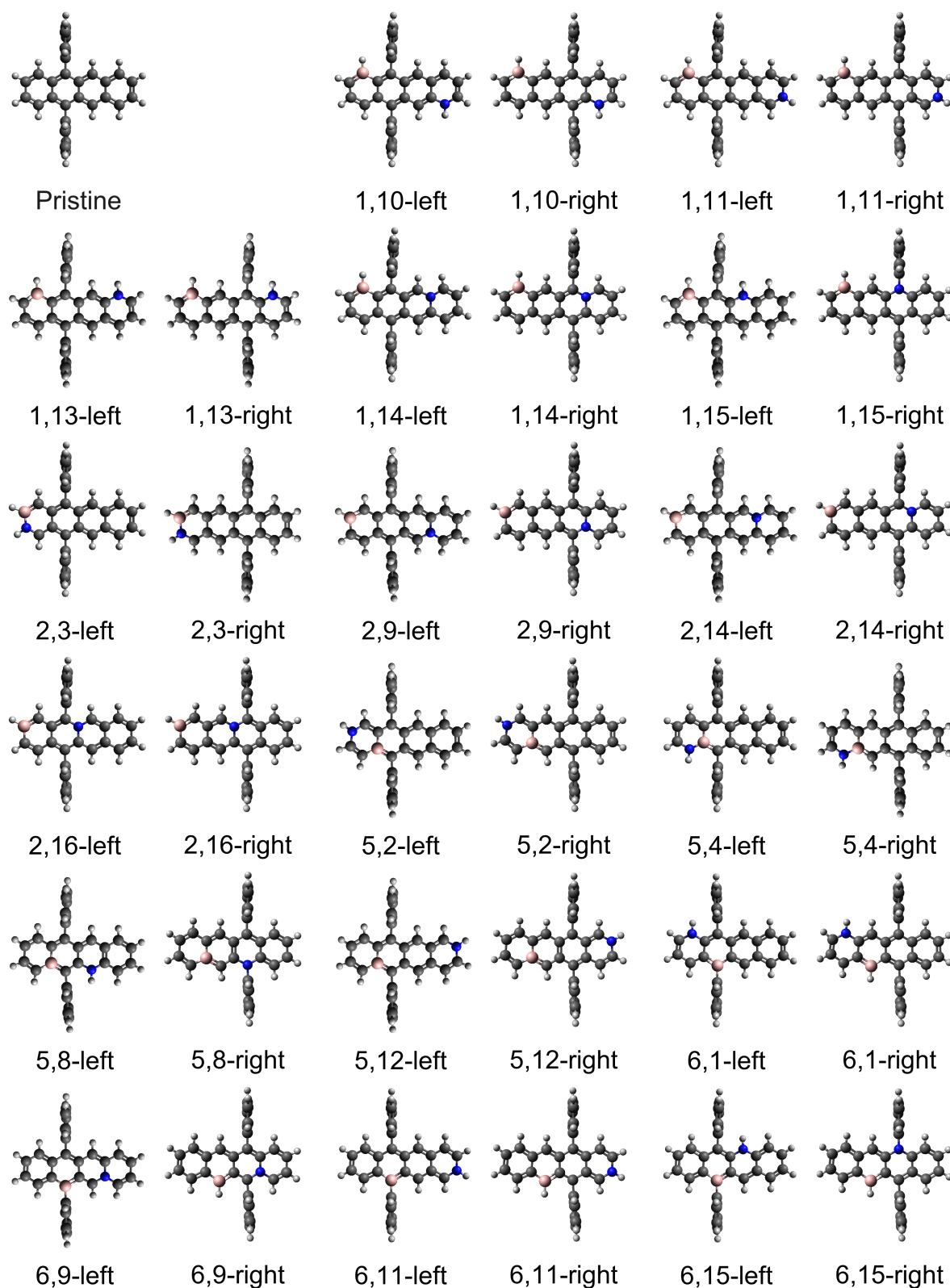


FIGURE D.1 – wB97XD/def2-TZVP optimized geometries of pristine DPT and the 34 B,N-DPT precandidates for SF and TADF.

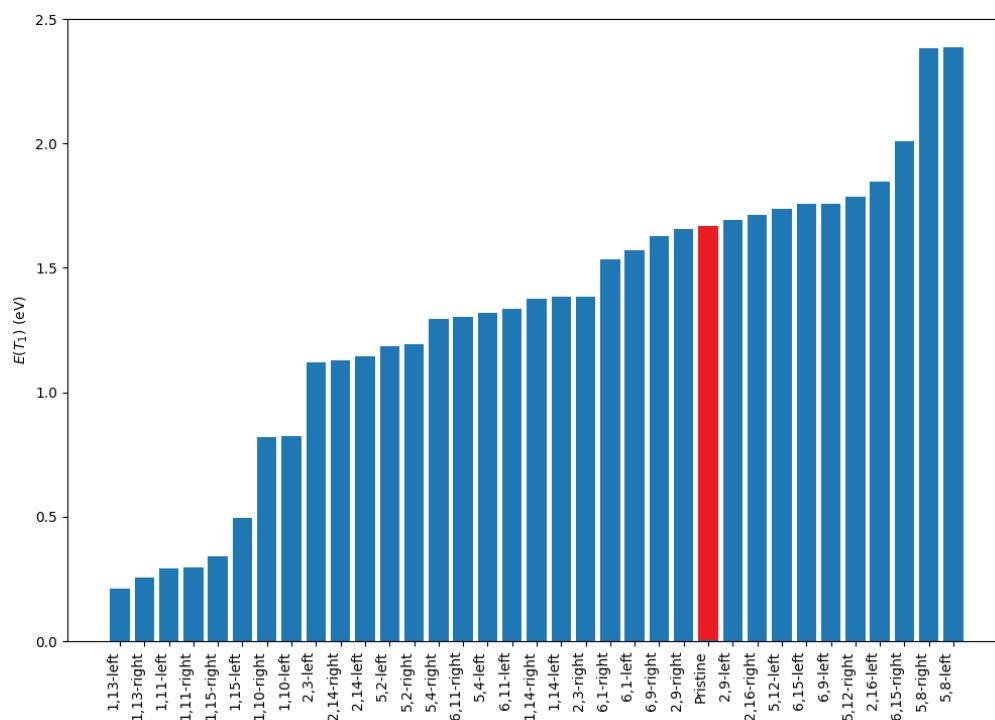


FIGURE D.2 – Vertical  $E(T_1)$  of pristine DPT and the 34 B,N-doped molecules calculated by using the CASPT2(8,8)/6-31G\* method.

TABLE D.1 –  $E(S_1)$ ,  $E(T_1)$  and  $\Delta E_{ST} = E(S_1) - E(T_1)$  for each of the 34 B,N-doped (10 SF precandidates and 24 TADF precandidates) and pristine DPT molecules calculated with the CASPT2(8,8) method. TADF candidates are highlighted in red.

Molecule	$E(S_1)$ (eV)	$E(T_1)$ (eV)	$\Delta E_{ST}$ (eV)
Pristine	2.84	1.67	1.18
1,10-left	1.18	0.82	0.35
1,10-right	1.16	0.82	0.34
1,11-left	0.36	0.29	0.07
1,11-right	0.40	0.30	0.10
1,13-left	0.31	0.21	0.09
1,13-right	0.32	0.26	0.06
1,14-left	1.32	1.38	-0.06
1,14-right	1.28	1.37	-0.09
1,15-left	0.54	0.49	0.05
1,15-right	0.41	0.34	0.07
2,3-left	2.01	1.12	0.89
2,3-right	1.92	1.38	0.54
2,9-left	1.72	1.69	0.03
2,9-right	1.65	1.66	-0.00
2,14-left	1.31	1.14	0.17
2,14-right	1.27	1.13	0.14
2,16-left	1.64	1.85	-0.21
2,16-right	1.62	1.71	-0.09
5,2-left	2.07	1.19	0.89
5,2-right	2.11	1.19	0.92
5,4-left	2.04	1.32	0.72
5,4-right	2.04	1.29	0.75
5,8-left	2.23	2.39	-0.15
5,8-right	2.23	2.38	-0.16
5,12-left	1.66	1.74	-0.07
5,12-right	1.69	1.78	-0.09
6,1-left	1.82	1.57	0.25
6,1-right	1.81	1.53	0.27
6,9-left	1.91	1.76	0.16
6,9-right	1.79	1.63	0.16
6,11-left	1.70	1.33	0.37
6,11-right	1.69	1.30	0.39
6,15-left	1.99	1.76	0.23
6,15-right	1.82	2.01	-0.18

TABLE D.2 – HOMA values for each ring of the 34 B,N-doped (10 SF precandidates and 24 TADF precandidates) and pristine DPT molecules calculated at the wb97XD optimized geometries. TADF candidates are highlighted in red.

Molecule	HOMA <sub>1</sub>	HOMA <sub>2</sub>	HOMA <sub>3</sub>	HOMA <sub>4</sub>
Pristine	0.53	0.73	0.77	0.57
1,10-left	0.21	0.19	0.39	0.74
1,10-right	0.29	0.29	0.34	0.73
1,11-left	0.33	0.45	0.60	0.70
1,11-right	0.41	0.52	0.56	0.66
1,13-left	0.28	0.39	0.64	0.82
1,13-right	0.37	0.46	0.60	0.79
1,14-left	0.24	0.30	0.60	0.48
1,14-right	0.34	0.41	0.58	0.45
1,15-left	0.36	0.58	0.82	0.81
1,15-right	0.43	0.62	0.75	0.81
2,3-left	0.73	0.63	0.62	0.45
2,3-right	0.76	0.69	0.56	0.40
2,9-left	0.06	0.26	0.61	0.50
2,9-right	0.11	0.36	0.59	0.47
2,14-left	0.15	0.44	0.77	0.64
2,14-right	0.20	0.52	0.74	0.62
2,16-left	0.30	0.64	0.80	0.60
2,16-right	0.33	0.70	0.77	0.56
5,2-left	0.50	0.38	0.46	0.42
5,2-right	0.50	0.43	0.40	0.37
5,4-left	0.79	0.48	0.52	0.46
5,4-right	0.80	0.52	0.45	0.41
5,8-left	0.05	0.16	0.66	0.92
5,8-right	0.07	0.18	0.55	0.92
5,12-left	0.07	0.08	0.32	0.57
5,12-right	0.08	0.12	0.24	0.53
6,1-left	0.70	0.10	0.82	0.77
6,1-right	0.71	0.13	0.77	0.74
6,9-left	0.88	0.18	0.53	0.47
6,9-right	0.89	0.23	0.50	0.44
6,11-left	0.91	0.05	0.25	0.49
6,11-right	0.92	0.10	0.16	0.46
6,15-left	0.91	0.13	0.64	0.95
6,15-right	0.92	0.17	0.51	0.94

TABLE D.3 – Summary of energy values obtained by various methods for tetracene.

Method	$E(S_1, B_{2u})$ symmetry) (eV)	$E(S_2, B_{3u})$ symmetry) (eV)	$E(T_1, B_{2u})$ symmetry) (eV)	$E(T_2, B_{1g})$ symmetry) (eV)
NEVPT2(12,12)/def2-TZVP <sup>a</sup>	2.46	3.63	1.59	2.91
NEVPT2(12,12)/6-31G <sup>*a</sup>	2.78	3.74	1.65	2.96
TD-DFT wB97XD/def2-TZVP 3 singlets and 3 triplets	2.88	3.57	1.10	2.60
TD-DFT wB97/def2-TZVP 3 sin- glets and 3 triplets	3.16	3.59	0.54	2.45
CASPT2(8,8)/6-31G <sup>*†</sup>	2.68	2.77	1.27	2.61
CASPT2(8,8)/6-31G <sup>*†</sup> without shift <sup>b</sup>	2.61	2.59	1.20	2.51
CASPT2(8,8)/6-31G <sup>*</sup>	2.65	2.79	1.29	2.61
CASPT2(10,10)/6-31G <sup>*†</sup>	2.79	2.73	1.29	2.45
CASPT2(12,12)/6-31G <sup>*†</sup>	2.86	3.10	1.58	2.57
CASPT2/6-31G <sup>*</sup> with CAS(8,8)/RAS(6,6) <sup>†</sup>	2.89	3.20	1.58	2.65
CASPT2/6-31G <sup>*</sup> with CAS(8,8)/RAS(6,6) <sup>†</sup> with 10 $\sigma$ orbitals added to the core (besides the 1s orbitals)	2.99	3.36	1.65	2.77
Yang and Davidson (Experimen- tal) (YANG <i>et al.</i> , 2016)	2.88	N/A	1.27	N/A
Casanova (Theoretical) (CASANOVA, 2014)	N/A	N/A	1.44 (verti- cal)	N/A
Casanova (Theoretical, wB97XD/6-31G <sup>*</sup> , cluster with 7 molecules) (CASANOVA, 2014)	3.02	N/A	1.58	N/A
Sutton (Theoretical, wB97/cc- pVDZ) (SUTTON <i>et al.</i> , 2017)	2.75 (verti- cal)	N/A	1.29 (adia- batic)	N/A
Sutton (Experimental) (SUTTON <i>et al.</i> , 2017)	2.63	N/A	1.28-1.30 and 1.35 (solution) and 1.25 (thin film)	N/A
Vertical excitation energy (BET- TANIN <i>et al.</i> , 2017; GRIMME; PARAC, 2003; BIERMANN; SCHMIDT, 1980)	2.88	3.39	N/A	N/A

<sup>a</sup> The geometry optimized with MP2 was used for the NEVPT2 calculations. For the other calculations, the geometry optimized with DFT using the wB97XD functional was employed.

<sup>†</sup> indicates that the calculations are done separately: one state-average calculation for the three singlet states (including the ground state) and another for the two triplet states. If not marked with this symbol, the calculation is performed as a state-average considering three singlet states and two triplet states together.

<sup>b</sup> The default shift used in the other CASPT2 calculations is 0.20.

TABLE D.4 – Summary of energy values obtained by various methods for DPT.

<b>Method</b>	$E(S_1, B_1)$ symmetry) (eV)	$E(S_2, A_1)$ symmetry) (eV)	$E(T_1, B_1)$ symmetry) (eV)	$E(T_2, B_1)$ symmetry) (eV)
NEVPT2(6,6)/def2-TZVP	2.53	3.17	1.49	3.60
NEVPT2(6,6)/def2-TZVP <sup>a</sup>	2.20	4.42	1.56	3.41
TD-DFT wB97XD/def2-TZVP 3 singlets and 3 triplets	2.80	3.50	1.05	2.57
TD-DFT wB97/def2-TZVP 3 sin- glets and 3 triplets	3.07	3.51	0.44	2.42
CASPT2(6,6)/def2-TZVP <sup>†</sup>	2.41	3.24	1.59	3.13
CASPT2(6,6)/6-31G <sup>*†</sup>	2.72	3.48	1.68	3.27
CASPT2(6,6)/6-31G <sup>*</sup>	2.81	3.31	1.48	3.00
CASPT2(8,8)/6-31G <sup>*†‡</sup>	2.72	3.38	1.62	2.99
CASPT2(8,8)/6-31G <sup>*‡</sup>	2.62	3.12	1.45	2.75
CASPT2(8,8)/6-31G <sup>*†</sup>	2.84	3.59	1.67	2.87
CASPT2(10,10)/6-31G <sup>*†‡</sup>	2.99	3.37	1.62	2.90
CASPT2(10,10)/6-31G <sup>*†</sup>	3.06	3.32	1.61	2.60
CASPT2/6-31G <sup>*</sup> with CAS(8,8)/RAS(6,6) <sup>†</sup>	2.87	3.29	1.60	2.81
Casanova (Theoretical) (CASANOVA, 2014)	N/A	N/A	1.40 (verti- cal)	N/A
Casanova (Theoretical, wB97XD/6-31G <sup>*</sup> , cluster with 7 molecules) (CASANOVA, 2014)	2.91	N/A	1.38	N/A
Sutton (Theoretical, wB97/cc- pVDZ) (SUTTON <i>et al.</i> , 2017)	2.54 (verti- cal)	N/A	1.23 (adia- batic)	N/A
Sutton (Experimental) (SUTTON <i>et al.</i> , 2017)	2.40 (thin film)	N/A	N/A	N/A

<sup>a</sup> indicates that the geometry optimized with MP2 was used for the calculation. If not marked with this symbol, the geometry optimized with DFT using the wB97XD functional was employed.

<sup>†</sup> indicates that the calculations are done separately: one state-average calculation for the three singlet states (including the ground state) and another for the two triplet states. If not marked with this symbol, the calculation is performed as a state-average considering three singlet states and two triplet states together.

<sup>‡</sup> indicates that no reordering of the orbitals was done and at least one orbital on the phenyl rings attached to the tetracene core was included in the active space. If not marked with this symbol, either no reordering was needed, or the appropriate reordering was done to include only orbitals on the tetracene core in the active space.

## FOLHA DE REGISTRO DO DOCUMENTO

1. CLASSIFICAÇÃO/TIPO DM	2. DATA 11 de junho de 2024	3. DOCUMENTO Nº DCTA/ITA/DM-034/2024	4. Nº DE PÁGINAS 155
5. TÍTULO E SUBTÍTULO: Assessing prospective singlet fission and thermally activated delayed fluorescence candidates in B,N-substituted 5,12-diphenyltetracene			
6. AUTOR(ES): <b>João Víctor Moreira Pimentel</b>			
7. INSTITUIÇÃO(ÕES)/ÓRGÃO(S) INTERNO(S)/DIVISÃO(ÕES): Instituto Tecnológico de Aeronáutica – ITA			
8. PALAVRAS-CHAVE SUGERIDAS PELO AUTOR: Excited states; Acenes; Polycyclic aromatic hydrocarbons; Multireference methods.			
9. PALAVRAS-CHAVE RESULTANTES DE INDEXAÇÃO: Estrutura eletrônica; Fluorescência; Hidrocarbonetos; Estados excitados; Química quântica; Físico-Química; Química.			
10. APRESENTAÇÃO: <span style="float: right;"><input checked="" type="checkbox"/> Nacional    <input type="checkbox"/> Internacional</span> ITA, São José dos Campos. Curso de Mestrado. Programa de Pós-Graduação em Física. Área de Física Atômica e Molecular. Orientador: Prof. Dr. Francisco Bolivar Correto Machado. Defesa em 10/06/2024. Publicada em 2024.			
11. RESUMO: In acenes, substituting a pair of carbon atoms with a boron-nitrogen isoelectronic pair allows for the modulation of the diradical character of the B,N-substituted acene, enabling fine-tuning of chemical, optical, and electronic properties. This theoretical study investigated the singlet fission (SF) and thermally activated delayed fluorescence (TADF) properties of 34 specific B,N-substituted 5,12-diphenyltetracene (DPT) molecules, identified as promising candidates through a previous systematic computational search in tetracene derivatives. Using computational quantum chemistry methods, we analyzed the electronic structure and excitonic properties of these B,N-substituted DPT molecules to understand their potential for application in organic solar cell (OSC) and organic light-emitting diode (OLED) technology. 22 molecules likely to undergo TADF were found. DPT was chosen for its similarity with rubrene, which has more interesting properties, such as enhanced hole mobility, compared to pristine tetracene.			
12. GRAU DE SIGILO: <input checked="" type="checkbox"/> OSTENSIVO <input type="checkbox"/> RESERVADO <input type="checkbox"/> SECRETO			